Bio-Inspired Iron and Manganese Complexes with N2Py2 Ligands

Towards Their Practical Use in Catalytic Oxidations

Bio-geïnspireerde IJzer- en Mangaancomplexen met N2Py2-liganden

Praktische Toepassingen in Katalytische Oxidaties

(met een samenvatting in het Nederlands)

Proefschrift

ter verkrijging van de graad van doctor aan de Universiteit Utrecht
op gezag van de rector magnificus, prof.dr. H.R.B.M. Kummeling
ingevolge het besluit van het college voor promoties
in het openbaar te verdedigen
op woensdag 16 januari 2019 des middags te 4.15 uur

door

Jianming Chen

geboren op 18 juni 1989 te Fujian, China

Promotor: Prof. dr. R.J.M. Klein Gebbink

Copromotor: Dr. M. Otte

The work described in this Ph.D. thesis was financially supported by the China Scholarship Council (CSC).

Bio-Inspired Iron and Manganese Complexes with N2Py2 Ligands

Towards Their Practical Use in Catalytic Oxidations

Dedicated to my family

献给我的家人

Chen, Jianming

Bio-Inspired Iron and Manganese Complexes with N2Py2 Ligands
Towards Their Practical Use in Catalytic Oxidations

ISBN: 978-90-393-7075-9

The work described in this PhD thesis was carried out at:
Organic Chemistry and Catalysis, Debye Institute for Nanomaterials Science,
Faculty of Science, Utrecht University, Utrecht, The Netherlands

Front cover: Sunflowers, Vincent van Gogh (1853 - 1890), Arles, January 1889.
Credits: Van Gogh Museum, Amsterdam (Vincent van Gogh Foundation).
Back cover: Periodic table of elements with highlights of manganese and iron.
Illustration: Jianming Chen.

Table of Contents

Chapter 1

Non-Heme Iron Oxidation Chemistry and Biochemistry

Abstract

The last two decades have witnessed the development of a vast number of synthetic non-heme iron complexes, inspired by the active sites in iron-containing enzymes. These biomimetic iron complexes have been widely used in catalytic oxidative transformations, e.g., aliphatic C−H oxidations and alkene epoxidations. This chapter aims at providing a background on the biochemistry and chemistry of non-heme iron enzymes and synthetic non-heme iron complexes. First, three typical iron-containing enzymes together with some reported synthetic iron complexes mimicking these enzymes are described, revealing their importance to the development of this field. Then, typical features of synthetic non-heme iron coordination chemistry are described, followed by a discussion of different oxygenated intermediates that have been identified in enyzmes and model systems. Finally, some selected catalytic examples using non-heme iron oxidation catalysts are briefly presented in view of the aim of this thesis.

1.1 Introduction

Next to the heme iron enzymes, comprizing an iron ion within a typical exogenous porphyrin type coordination setting in the active site, the past decades have witnissed a lot of interest in the (bio)chemistry of so-called non-heme iron enzymes, in which the mono-nuclear or di-nuclear iron active site is typically ligated by endogenous nitrogen and oxygen donors. The easy identification of heme type enzymes due to their distinct optical properties, including their color, is contrasted by the initial difficulties in the identification of non-heme type enzymes. The latter is largely due to the non-distinctiveness of the high-spin Fe(II) ion typically found in these enzymes, *i.e.* the difficulties often faced in the spectroscopic characterization of such ions. With the advancement of analytical techniques, the number of known and identified non-heme iron enzymes has vastly increased over the past decades.[1]

Amongst the many functions of enzymes containing a non-heme iron active site, their role in oxidative reactions, making uses of O_2 as the oxidant, stand out.[2,3] The number of oxidative transformations carried out by non-heme iron enzymes is very large and rivals those known for heme iron enzymes. Many of these transformations are unprecedented in synthetic chemistry and some of these, such as the oxidation of methane to methanol, are amongst synthetic chemistry's 'dream reactions'.[4,5] It is therefore not surprizing that a lot of effort is being spend on understanding the mechanisms by which these enzymes operate. Next to investigations on the enzymes themselves, these efforts also include the development of model systems that aim to mimic the structure and action of the enzymes. The latter efforts are aimed at an increased understanding of the chemical reactivity of the enyzmes, as well as at the development of catalysts for chemical synthesis.

This chapter is aimed at providing the reader with a background on the biochemistry and chemistry of non-heme iron enzymes and synthetic non-heme iron complexes. It starts with the description of three enzymes that have been of importance to the development of the field and that highlight the power of non-heme enzymes as oxidation catalysts. Accordingly, mono-nuclear Rieskes dioxygenases and α-ketoglutarate-dependent enzymes, as well as soluble methane mono-oxygenase are descibed in some detail, together with some efforts in modelling these enzymes. Due to the large number of enzymes currently being identified to contain a non-heme iron active site, these examples are meant to illustrate typical active site topologies and reactivity patterns. The chapter then continues with a description of typical features of synthetic non-heme iron coordination chemistry and with a section that describes the different oxygenated intermediates that have been identified in enyzmes and model systems. Finally, a

selection of examples of synthetic non-heme iron oxidation catalysts is presented, followed by an outline of the aim and scope of this thesis.

1.2 Typical Non-heme Iron Enzymes

1.2.1 Rieske dioxygenases

The *cis*-dihydroxylation of arenes is regarded as the initial step in the biological degradation of aromatic substrates. This is believed to be a challenging process since the substrates are dearomatized in these transformations. Non-heme iron enzymes from bacterial sources, called Rieske dioxygenases, are known to catalyze the *cis*-dihydroxylation in an enantioselective manner.[3,6] They are the only known examples among both heme and non-heme iron enzymes that are able to catalyze this reaction (Scheme 1).[7] Next to *cis*-dihydroxylation, enzymes from the larger family of Rieske dioxygenases also catalyze other oxidations such as desaturation, sulfoxidation, and O- (and N-)dealkylation.[8] To date, more than 50 different Rieske dioxygenases have been identified,[9] among them naphthalene 1,2-dioxygenase (NDO, Figure 1) is one of the best studied examples. NDO catalyzes the *cis*-dihydroxylation of naphthalene to generate *cis*-(*1R*, *2S*)-1,2-naphthalenediol.

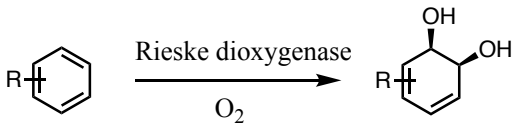

Scheme 1. Rieske dioxygenase-catalyzed *cis*-dihydroxylation of arenes.

NDO is an $\alpha_3\beta_3$ hexamer[10] consisting of three components: a reductase component (a NADH-dependent flavoprotein),[11] a ferredoxin component containing a Rieske-type [2Fe:2S] cluster, and an oxygenase component in which O_2 activation and substrate oxidation takes place (Figure 1).[10] Electrons are transferred from NADH to the Rieske ferredoxin cluster *via* the flavoprotein reductase. The ferredoxin [2Fe:2S] cluster connects to the protein *via* two sulfur linkages of cysteinate residues and two histidine side chains. The α subunit contains this Rieske-type [2Fe:2S] cluster and a mononuclear non-heme iron(II) center, in which the metal center is coordinated by two histidines (His) and an aspartic acid (Asp) residue in a facial manner (Figure 1). The latter structural motif is typical for a so-called 2-His-1-Carboxylate facial triad found in a large number of mononuclear non-heme iron enzymes.[6] Within one α subunit, the Rieske cluster is positioned about 44 Å away from the mononuclear iron center, which prevents electron transfer within the same protein subunit. However, the distance between the Rieske

cluster and the mononuclear iron center from a nearby α subunit is much smaller (12 Å), allowing electron transfer between two neighbouring subunits.[10]

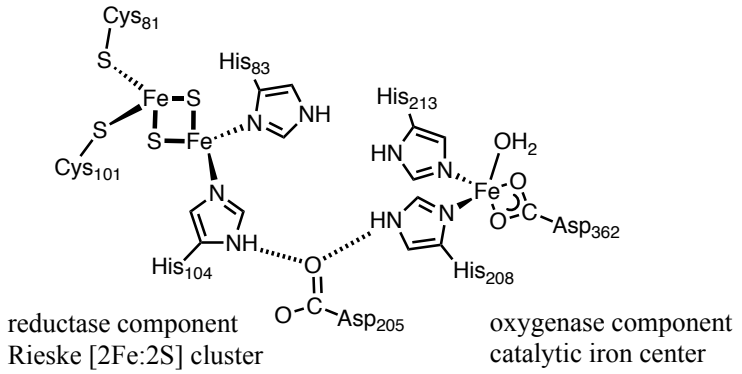

Figure 1. Active site structure of NDO, showing the oxygenase (mononuclear iron) and reductase ([2Fe:2S] cluster) components from two different protein subunits in close proximity.[10]

The actual mechanism by which NDO and other Rieske dioxygenases operate is not completely clear. Based on the crystal structure of oxygenated NDO, in which dioxygen is bound as a side-on peroxo ligand to iron(III) in the presence of an indole substrate with similar polarization of the Fe-O bonds and orientation to the substrate, it was proposed that both oxygens could be engaged in a concerted attack on the substrate, thereby explaining the *cis*-product outcome.[12] More recent studies seem to favor the initial protonation of the iron-peroxo intermediate prior to the electrophilic oxidation of the substrate. These studies include the crystal structure of another oxygen-bound Rieske dioxygenase (carbazole 1,9a-dioxygenase) in which an end-on binding mode of the (hydro)peroxo ligand was observed,[13] and single turnover studies on NDO in which radical intermediates have been observed.[14] Whether it is an Fe(III) hydroperoxo intermediate that attacks the substrate, as is suggested by computational studies,[15] or whether this species first isomerizes to a high-valent HO–Fe(V)═O intermediate before oxygen-transfer takes place is not clear at this moment (Scheme 2). Both pathways seem to involve a subsequent Fe(IV) intermediate that carries out the second and *cis*-selective attack on the substrate.

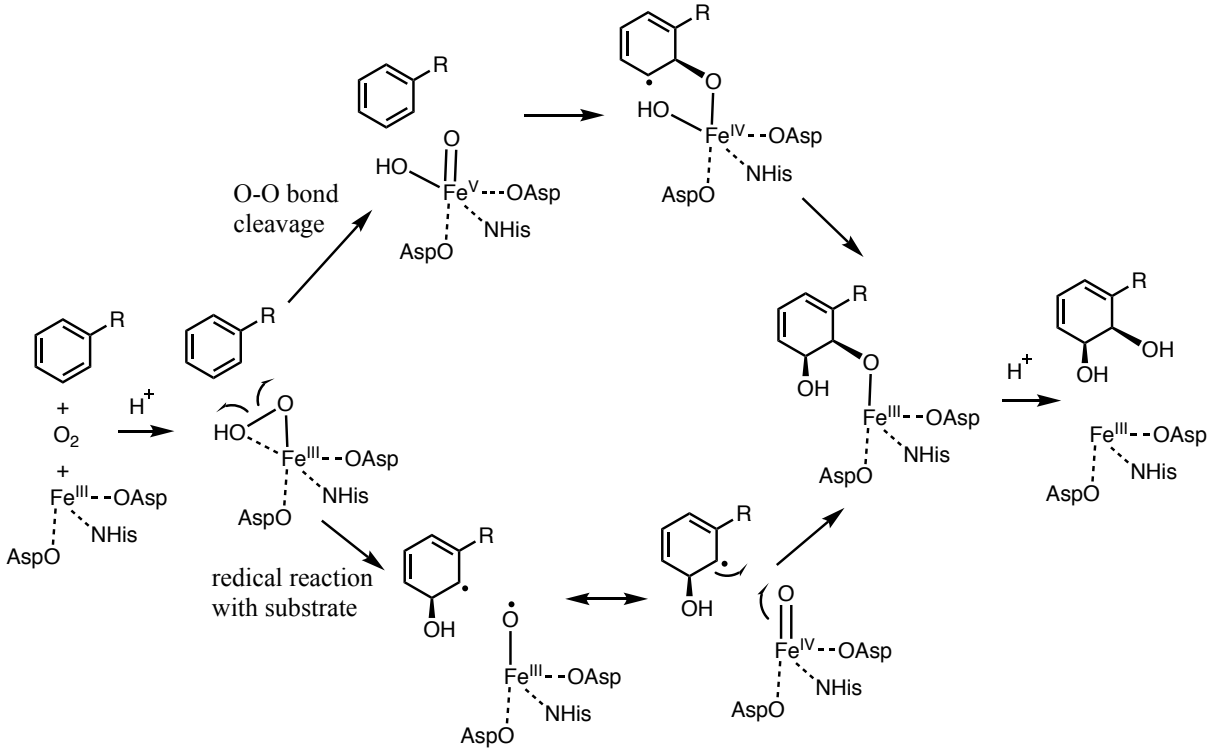

Scheme 2. Postulated mechanisms for Rieske dioxygenases.

In 2005, Que and co-workers described the iron(II) complex $[(Ph\text{-}dpah)_2Fe](CF_3SO_3)_2$ (where Ph-dpah = (di-(2-pyridyl)methyl)benzamide, Figure 2, left) with the bio-inspired N,N,O-ligand Ph-dpah mimicking the facial N,N,O site of the mononuclear iron center in Rieske dioxygenases. This complex is able to perform the *cis*-dihydroxylation of alkenes in a highly selective manner (with diol:epoxide ratios up to >100:1).[16] Three years later, Klein Gebbink and co-workers reported iron complexes that are capable of catalyzing both the epoxidation and the *cis*-dihydroxylation of alkenes (Figure 2, right). In this case, the bio-relevant tripodal N,N,O-ligand PrL1 (propyl 3,3-bis(1-methylimidazol-2-yl)propionate) was employed.[17]

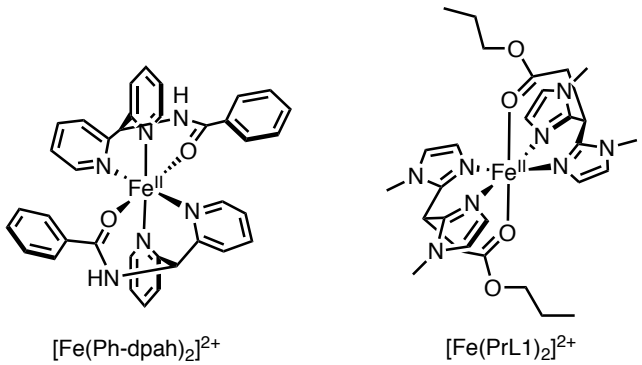

Figure 2. Biomimetic iron complexes with a facial N,N,O-ligand system.

1.2.2 α-Ketoglutarate-dependent enzymes

Iron(II) α-ketoglutarate-(α-KG)-dependent enzymes encompass a large subfamily of non-heme iron enzymes, which catalyze a variety of oxidative transformations, including hydroxylation, epoxidation, desaturation, ring closure, ring expansion, and others.[18] This subfamily of enzymes plays a versatile role in the hydroxylation of structural proteins, synthesis of antibiotics, degradation of selected lipids, and repair of alkylated DNA/RNA.[19-22] Taurine/α-KG dioxygenase (TauD, taurine = 2-aminoethane-1-sulfonic acid) is the most widely studied and prototypical example of this enzyme family.[23] TauD catalyzes the hydroxylation of taurine, followed by the elimination of sulfite (can serve as a nutritional source of sulfur), and eventually leading to the formation of aminoacetaldehyde (Scheme 3).[24] In doing so, one equivalent of α-KG is converted to succinic acid and CO_2.

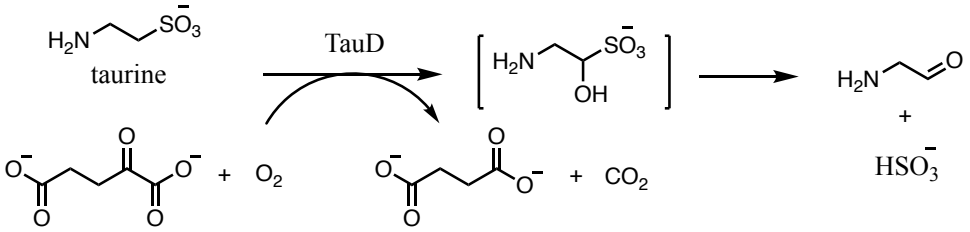

Scheme 3. TauD-catalyzed hydroxylation of taurine.

The non-heme iron active site in TauD is a typical example of a 2-His-1-Carboxylate facial triad active site (see above) (Figure 3).[18,25] In addition to the three endogenous donors, in substrate and co-factor bound enzyme the C1-carboxylate and C2-keto group of α-KG bind to the iron(II) center in a bidentate way. Taurine is not directly bound to the iron(II) center, but instead binds to Arg_{270} and His_{70} *via* its sulfonate group. The observation that the primary substrate does not directly bind to the iron center is a typical feature for both heme and non-heme enzymes involved in oxidation reactions.

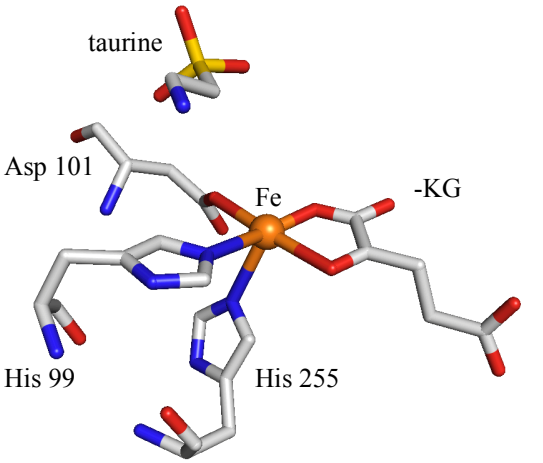

Figure 3. Active site structure of TauD (1OS7 pdb file).

The first step in the catalytic cycle of TauD-catalyzed taurine hydroxylation is believed to be the displacement of two iron-bound water molecules through bidentate α-KG coordination, forming an iron(II)-α-KG complex (Scheme 4). Upon binding of the taurine substrate in close proximity to the iron center, a third aquo ligand is lost to form a five-coordinated iron(II) species that is now set up to react with O_2. Binding of dioxygen to the ferrous ion is proposed to give rise to an superoxo iron(III)-α-KG-taurine complex.[26] Decarboxylation of the resulting intermediate through a cyclic intermediate formed after attack of the superoxo on the α-KG moiety leads to cleavage of the O–O bond, the formation of carbon dioxide, succinate, and a high-valent iron(IV)═O intermediate **J**. The latter is considered to be the key species that carries out substrate oxidation through a typical rebound mechanism, in which C–H bond cleavage to form an Fe(III)–OH intermediate and an organic (carbon-based) radical is followed by recombination (‘rebound’) of the hydroxyl moiety with the radical to form the initial hydroxylated product and the reduced, succinate-coordinated Fe(II) enzyme.

Mechanistical studies revealed the configuration of the short-lived intermediate **J** as a high-spin (S = 2) species using Mössbauer and EPR spectroscopic techniques.[27] To date, an increasing number of (transient) spectroscopic studies support the asignment of **J** as an iron(IV)−oxo intermediate, including Raman spectroscopic studies.[28] Intermediate **J** represents the first observation of an iron(IV)-oxo species in mononuclear non-heme enzymes. Such iron(IV)−oxo species were later also observed in prolyl hydroxylase,[29] α-KG-dependent halogenases,[30-32] and pterin-dependent hydrolases.[33,34]

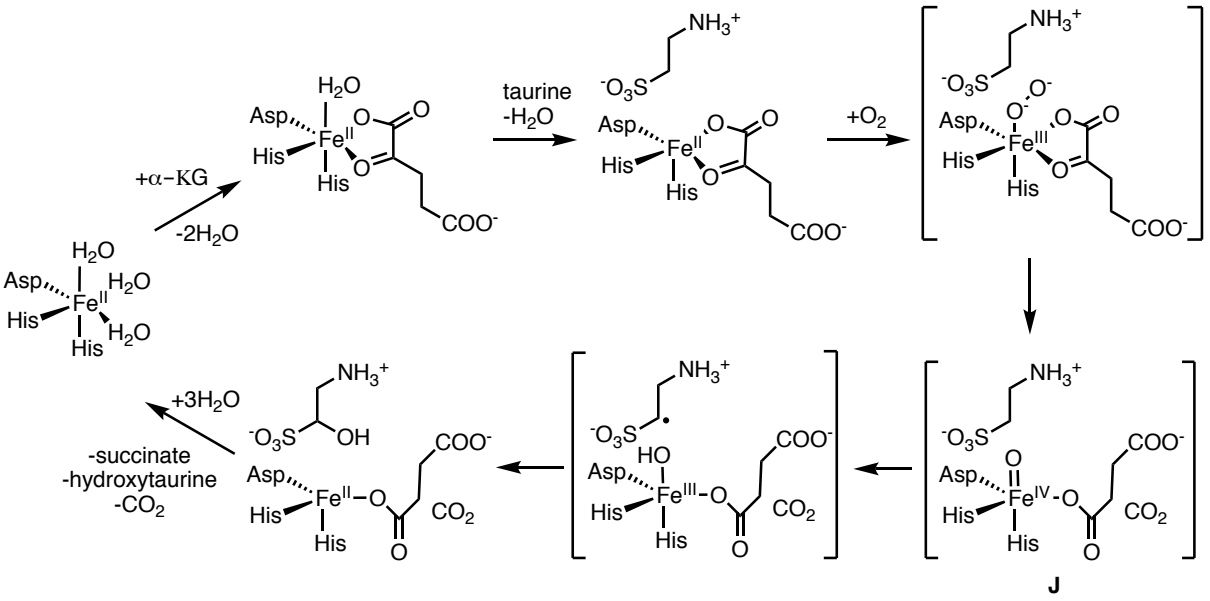

Scheme 4. Consensus mechanism for the hydroxylation of taurine catalyzed by TauD.[23,25]

High-spin iron(IV)−oxo moieties like TauD intermediate **J** are of particular interest because of their ability to oxidize strong C−H bonds.[35] More than sixty synthetic iron(IV)−oxo complexes have been characterized in the past decade,[36] however, most of these were found to have a low-spin (S = 1) electronic configuration.[37] Que and co-workers have reported on a limited number of high-spin iron(IV)-oxo complexes.[37-40] Very recently, they reported on a well-defined high-spin (S = 2) Fe^{IV}═O complex mimicking intermediate **J** of TauD, $[Fe(IV)(O)(TQA)(NCMe)]^{2+}$ (TQA = tris(2-quinolylmethyl)amine) (Figure 4).[37] Replacement of all three pyridine donors in the proto-typical TPA (tris(2-pyridylmethyl)amine) ligand with quinolines weakens the ligand field around the Fe^{IV}═O unit to the extend that $[Fe^{IV}(O)(TQA)(NCMe)]^{2+}$ is a high-spin S = 2 complex.[41] This latter non-heme oxoiron(IV) complex shows a comparable rate for the oxidation of cyclohexane to that of the oxidation of taurine catalyzed by TauD (after proper adjustment for the different reaction conditions). Compared to other reported S = 2 iron(IV)-oxo complexes, $[Fe^{IV}(O)(TQA)(NCMe)]^{2+}$ shows the closest spectroscopic similarity to intermediate **J** and highest hydrogen atom transfer reactivity. Interestingly, this compound is one of few Fe(IV)-oxo complexes with the proven ability to epoxidize olefins and does so at similar rates at which it abstracts C–H bonds.

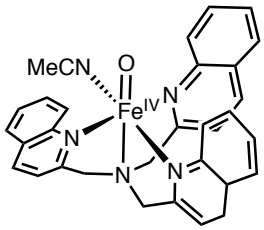

Figure 4. High-spin iron(IV)oxo complex $[Fe^{IV}(O)(TQA)(NCMe)]^{2+}$.

1.2.3 Soluble methane monooxygenase

Bacterial multicomponent monooxygenases (BMMs) are a subfamily of non-heme iron enzymes containing a carboxylate-bridged diiron center. These catalyze the biological oxidation of hydrocarbons. Based on the substrates oxidized, BMMs are classified into soluble methane monooxygenase (sMMO),[42] toluene/*o*-xylene monooxygenase (ToMO),[43] and phenol hydroxylase (PH).[44] Among them, sMMO catalyzes the challenging oxidation of methane to methanol. Considering the importance of methanol for a bio-based econnomy and that methane is a greenhouse gas, this conversion of a hydrocarbon into an alcohol is of great interest.[45] Consequently, a lot of effort has gone into studying the structure and action of sMMO.[46]

sMMO is a three-component enzyme system consisting of a 251 kDa hydroxylase (MMOH), a 38.5 kDa reductase (MMOR), and a 15.9 kDa regulatory protein (MMOB) (Figure 5A). MMOH is a heart-shape $(\alpha\beta\gamma)_2$ heterodimer with a 2-fold axis of symmetry[47,48] and is the central catalytic component of this enzyme system, in which O_2 activation and C–H bond functionalization take place. MMOR contains a bound flavin adenine dinucleotide (FAD) and a N-terminal [2Fe:2S]-ferredoxin (Fd)[49], that transfer electrons to MMOH with consumption of NADH.[45] MMOB docks onto the MMOH α-subunit,[48] forming a specific MMOH-MMOB complex, and plays an important role in structural changes in MMOH required for reactivity. Figure 5B shows the diiron active site of sMMO, which is located in each α-subunit in the $(\alpha\beta\gamma)_2$ heterodimer. Fe1 (left) is coordinated by His147, Glu114, and a water molecule, and Fe2 (right) is coordinated by His246, Glu243, and Glu209.[48,50] The iron ions are linked to each other by a bridging glutamate (Glu144) and two bridging hydroxides.

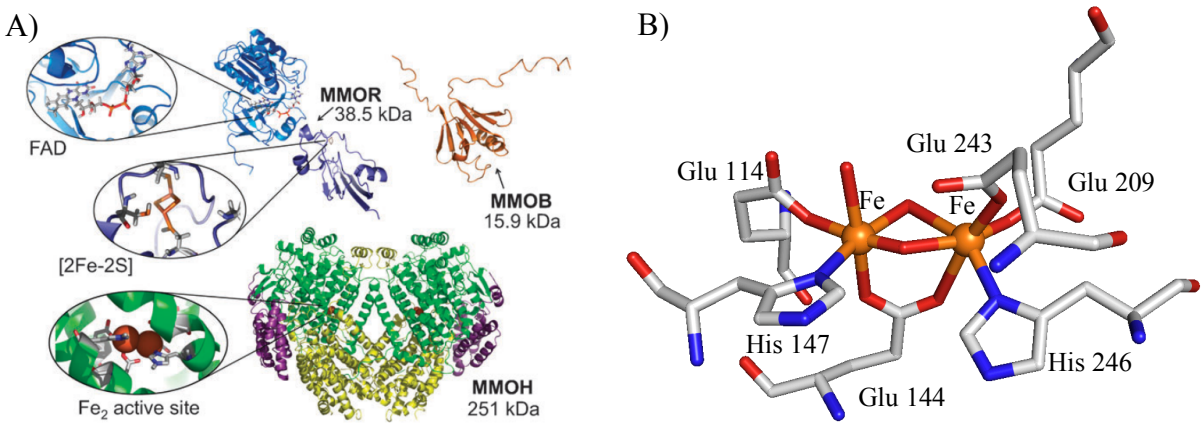

Figure 5. (A) Enzyme architecture of sMMO from *Methylococcus capsultus* (Bath). Reprinted with permission from ref. 46. Copyright 2010 Royal Society of Chemistry. (B) Oxidized diiron center of sMMO (1MTY pdb file).

A proposed mechanism for O_2 activation and methane hydroxylation by sMMO is illustrated in Scheme 5. First, the oxidized diiron(III) center ($MMOH_{ox}$) is activated by MMOR *via* two-electron reduction, resulting in the reduced diiron(II) center ($MMOH_{red}$), which reacts with O_2 in the presence of MMOB. Via a putative superoxodiiron(II, III) species, a peroxo diiron(III) intermediate **P*** is formed,[51] which in turn is transformed into a singly carboxylate bridged, peroxodiiron(III) species ($MMOH_{peroxo}$) upon proton transfer. This species is able to carry out the nucleophilic oxidation of organic substrates (*e.g.* diethyl ether), but not of methane.[52,53] On the other hand, $MMOH_{peroxo}$ serves as the precursor to the dioxo diiron(IV) intermediate **Q** upon proton coupled electron transfer (PCET) induced O−O bond cleavage. Intermediate **Q**, featuring a $Fe^{IV}_2(\mu\text{-}O)_2$ diamond core, is able of electrophilic oxidation and either involved in methane hydroxylation, or decays to an inactive intermediate Q* in the absence of methane, then eventually to the starting diferric state $MMOH_{ox}$. For the actual methane oxidation step both radical rebound and concerted mechanisms have been proposed.[46]

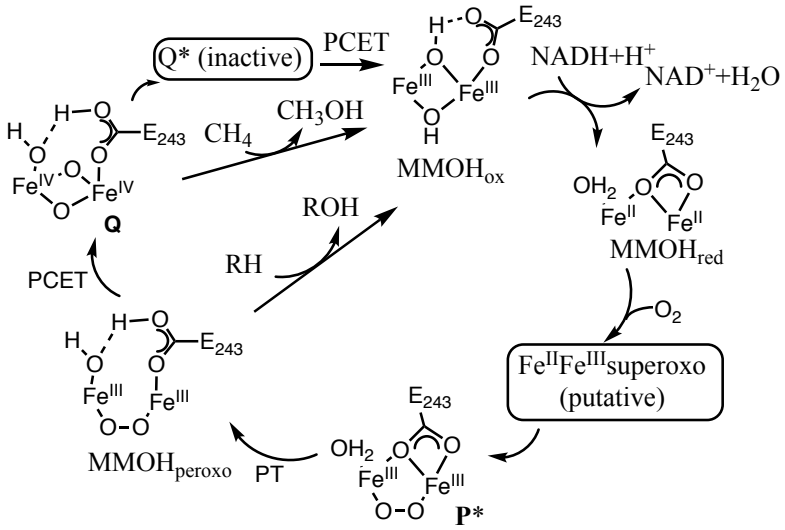

Scheme 5. Catalytic cycle of sMMO (PT = proton transfer, PCET = proton coupled electron transfer; a bridging glutamate (E144) found in each intermediate is not shown for clarity).[46]

In the past decade, many efforts have been spent to synthesize and characterize dinuclear oxoiron(IV) complexes by amongst other the groups of Que and Lippard. Next to the purpose of preparing low molcular weight synthetic models of **Q** that would facilitate the study of this diamond core species, one of the aims was to understand whether or not the reactivity of active dioxo-diiron(IV) intermediates depends on the iron spin state.[54] Based on the fact that intermediate **Q** has an oxygen-rich ligand set and on DFT calculations,[55-57] the iron centers of this diiron(IV) species are proposed to be in a high-spin state.[54] However, no access to models containing an diiron(IV) core in the same (S = 2) spin state as intermediate **Q** of sMMO had been achieved for a long time. In 2012, Kodera and co-workers reported on the reaction of the dinuclear Fe(III)-aquo complex **1** derived from the bis-TPA ligand 6-hpa with hydrogen peroxide (Scheme 6).[58] The resulting μ-oxo-diiron complex was found to exist as an equilibrium mixture of the (μ-oxo)peroxodiiron(III) species (**2a**) and the (μ-oxo)dioxodiiron(IV) species (**2b**). Not only does this system nicely show the (equilibrium) transformation of peroxo-diiron species to dioxo-diiron species, dioxo species **2b** also turned out to be the first example of a synthetic S = 2 diiron(IV) complex. It was found that **2a**/**2b** can be trapped by olefins to form the corresponding epoxides,[58] and that **1** catalyzes the epoxidation and *cis*-dihydroxylation of olefins in combination with H_2O_2.[59] More recently, **1** has been reported to be capable of the activation of strong C−H bonds as well.[60]

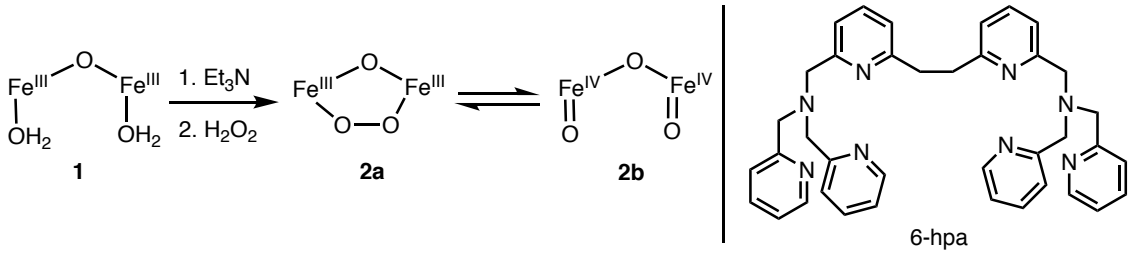

Scheme 6. Synthesis of an oxodiiron(IV) complex mimicking intermediate **Q**.[58]

1.3 The Coordination Chemistry of Non-heme Iron Complexes

The synthetic coordination chemistry of iron is very rich and for a full account of its characteristics a chapter like this one is not appropriately fit. Yet, in order to picture typical coordination chemistry features one may encounter in studying synthetic non-heme iron complexes, a number of these are discussed in brief in this section.

1.3.1 Typical ligands and ligand topologies

Ligands used to synthesize iron complexes aimed at mimicking either structural and/or functional aspects of mono-nuclear non-heme iron enzymes typically constitute nitrogen and oxygen donor atoms. Historically, the focus has for a long time been more on the use of all-nitrogen ligands, while more recently mixed N,O ligands are also more widely studied. The denticity of these ligands varies from 2 to 6, *i.e.* these ligands contain from 2 up to 6 donor atoms that can coordinate to a single iron center. Bidentate ligands like bipyridine (bpy) and phenanthroline (phen) have been used to some extent. The difficulty with such bidentate ligands is that they easily lead to an increased speciation of iron upon dissolution of well-defined solid complexes, which may make further studies more complicated.

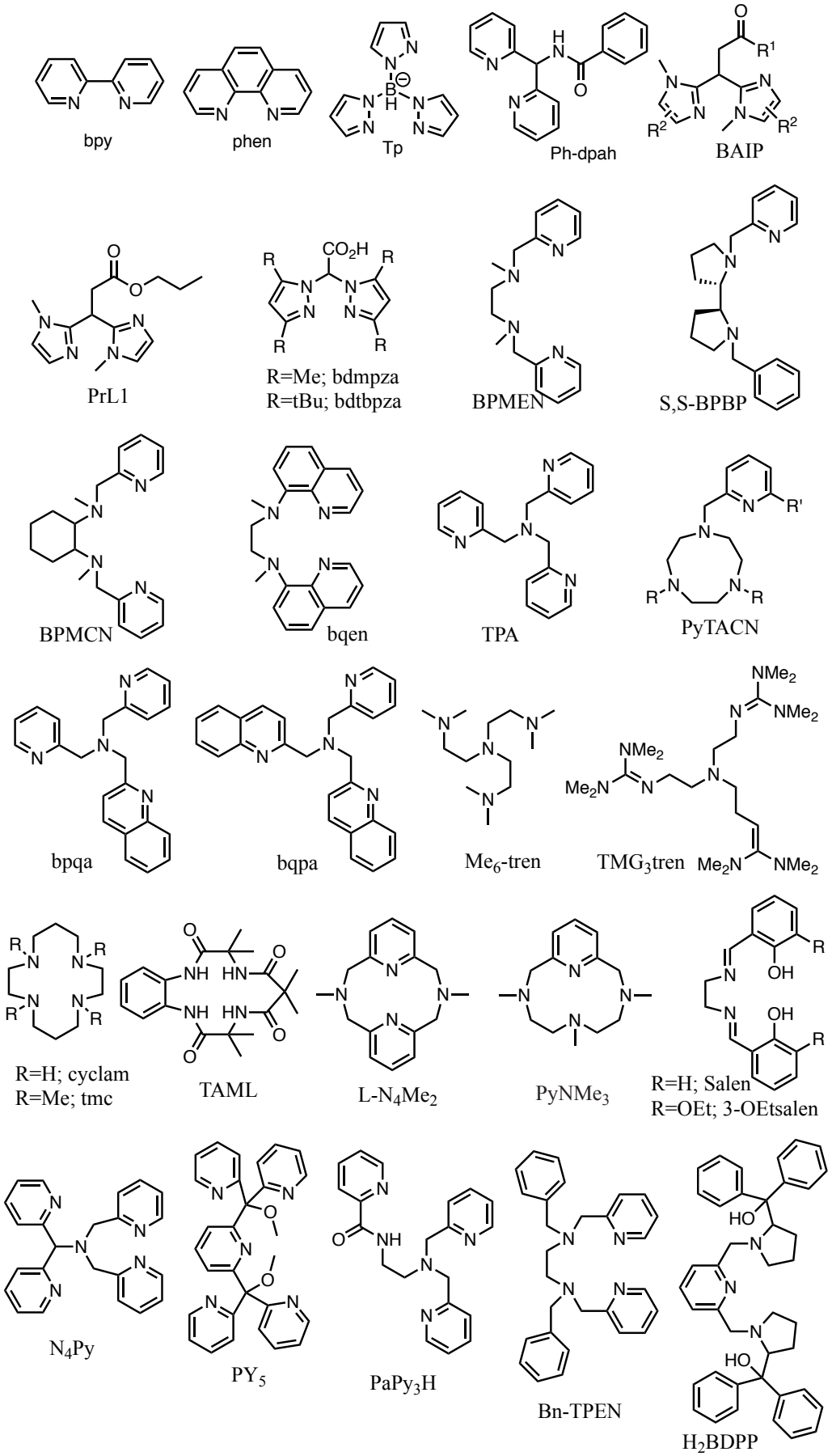

Figure 6. Typical ligands for non-heme iron complexes.

Tridentate ligands come in many variations and some of the successes in non-heme iron chemistry have been achieved using such ligands. Depending on the ligand backbone, tridentate ligands either coordinate in a meridonal or a facial manner to iron and depending on their steric demands only one or instead two tridentate ligands can bind to a single iron center. Some typical tridentate ligands are shown in Figure 6. The trispyrazolylborate (Tp) ligands have a long history in the coordination chemistry of iron. Their use in biomimetic chemistry has amongst others been explored by Kitajima,[61] Que,[62-65] and more recently Limberg.[66] Sterically encumbered Tp ligands tend to form 1:1 complexes with iron provided that sufficiently strong co-ligands are used. The use of biologically relevant (bidentate) co-ligands has been very fruitfull in providing structural as well functional models of non-heme iron enzymes. Mixed N,O tridentate ligands were recently studied by Que,[16] Klein Gebbink,[17,67-70] and others.[71,72] In case of the Ph-dpah and BAIP ligands this has led to Fe(II) complexes that are able to catalyze the epoxidation and *cis*-dihydroxylation of olefins (vide infra). Solid state structures of the complexes employed in catalysis showed coordinatively saturated 2:1 (ligand:iron) complexes, clearly pointing out that the catalytically competent species were formed after complete dissociation of one of the ligands or partial dissociation of both ligands, respectively. These examples point out that care should be taken in translating solid state to solution state structures and that predictions on catalytic (in)activity based on coordinative saturation in the solid state may be misleading (vide infra).

Further extention of the number of donor atoms leads to tetra- and pentadentate ligands, for which even more imaginative structures are possible. A small selection of such ligands is shown in Figure 6. The advantage in the use of these ligands is that the increased number of donor atoms leads to the formation of discrete 1:1 ligand complexes. These ligands are typically comprised of four nitrogen donors (N4). In the case of tetradentate ligands with a linear structure, this may still lead to the formation of different complexes though. Depending on the way a linear tetradentate ligand 'wraps' itself around the iron, either *cis* complexes with two *cis*-positioned open coordination sites are formed, or *trans* complexes are formed in which these open coordination sites are positioned *trans* with respect to each other (Scheme 7a). In the *cis* topologies, two possible configurations can be formed, *i.e.*, *cis*-α or *cis*-β. Two labile sites are *trans* to the N1 or N2 donor in a *cis*-α coordination topology, causing them to be chemically equivalent. Whereas, one of the two labile sites is *cis* to N1 and the other one is *trans* to N2 in the *cis*-β topology (Scheme 7a). Amongst these N4 ligands, bis-alkylamine-bis-pyridine (N2Py2) ligands in a *cis*-α topological configuration have been shown to be the most effective.[73] This ligand platform has two pyridine moieties linked to a bis-alkylamine backbone (Scheme 7b), which allows versatile modifications on both bis-amine and pyridine

fragments. Typical N2Py2 ligands like BPMEN, BPBP, BPMCN and bqen (Figure 6) have already been widely used for the synthesis of non-heme iron oxidation catalysts.

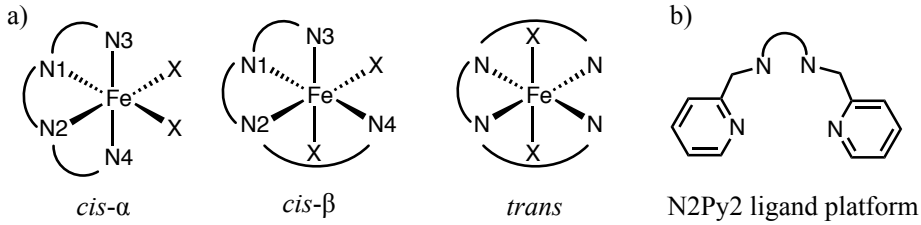

Scheme 7. a) Different topologies for Fe complexes with linear N4 ligands. X is the open coordination site. b) Generic structure of the N2Py2 ligand platform.

Branched all-nitrogen tetradentate ligands like TPA, PyTACN, bpqa, and bqpa form iron complexes in which the *cis*-positioning of open coordination sites is guaranteed. This feature is part of the succes of these ligands, as it seems to result in catalytically active iron complexes for both linear and branched tetradentate ligands (vide infra). Increasing the steric bulk of these ligands may result in the formation of 5-coordinate instead of 6-coordinate complexes, such as in the case of TMG_3tren.[74] The use of cyclic tetradentate all-nitrogen ligands also results in complexes with either *cis* or *trans* postioned open sites. Use of cyclam, TMC, TAML, and related ligands results in complexes with *trans* open sites and complexes of this type have been widely explored for the generation and study of high-valent iron-oxo species (vide infra). In contrast, the cyclic ligands $L\text{-}N_4Me_2$[75,76] and $PyNMe_3$[77,78] enforce the formation of complexes with *cis*-positioned open sites. Mixed N,O tetradentate ligands have also been used for synthesizing iron complexes, most of them are derived from the N_2O_2 coordinating salen ligand.

For pentadentate ligands the speciation and topology of iron complexes seems pretty obvious, as these ligands leave only one open site for further chemistry upon coordination to a single iron center. These pentadentate ligands are typically of the 'branched' type, as the use of linear pentadentate ligands holds the risk of (ill-defined) coordination polymer formation. Typical all-nitrogen pentadentate ligands include N4Py, PY5, and $PaPy_3H$ (Figure 6). Extending the tmc ligand or replacing one nitrogen donor in N4Py provides access to mixed N,O ligands.[35,79-82] Due to the well-defined and rigid topology of these pentadentate ligands they have been used to generate and study high-valent iron intermediates of biological relevance and also to study catalytic radical processes such as those related to lipoxygenase activity and oxidative DNA cleavage. One example is the use of the mixed N,O pentadentate ligand BDPP for the generation of an Fe(III)-superoxo complex (vide infra).

Finally, hexadentate ligands have not been widely studies within the realm of non-heme iron chemistry due to their anticipated inreactivity as a result of the saturated coordination environment brought about by such ligands. There are however exceptions to this general assumption, as will be discussed later.

The above examples examplify the importance of ligand design in mono-nuclear non-heme iron chemistry and show the richness of this chemistry. Similar considerations in ligand design as those mentioned for mono-nuclear systems also apply for the design and development of dinucleating ligands aimed at bio-inspired dinuclear non-heme iron complexes. A selection of prototypical ligands used in dinuclear non-heme iron chemistry is shown in Figure 7. In view of the overall length of this chapter, these examples are not discussed in detail here and the interested reader is referred to reviews by Lippard[46] and others[83]. One important consideration in the design of dinuclear complexes is the use of so-called 'unsupported' bridging carboxylate ligands, which can be used to bring together two formally mono-nuclear complexes to arrive at biomimetic, carboylate-bridged dinuclear structures. The use of bridging carboxylate ligands arises from the bridging carboyxlate moieties found in sMMO. Examples of this approach can be found amongst others in the work of Lippard[84-86] and Tolman.[87,88] Dinuclear complexes may also form through the reaction of mononuclear complexes with appropriate oxidants or water to form hydroxo and/or oxo bridged complexes. The prototypical example in this case is found in the work of Que and co-workers on dinuclear Fe-TPA complexes (vide infra).

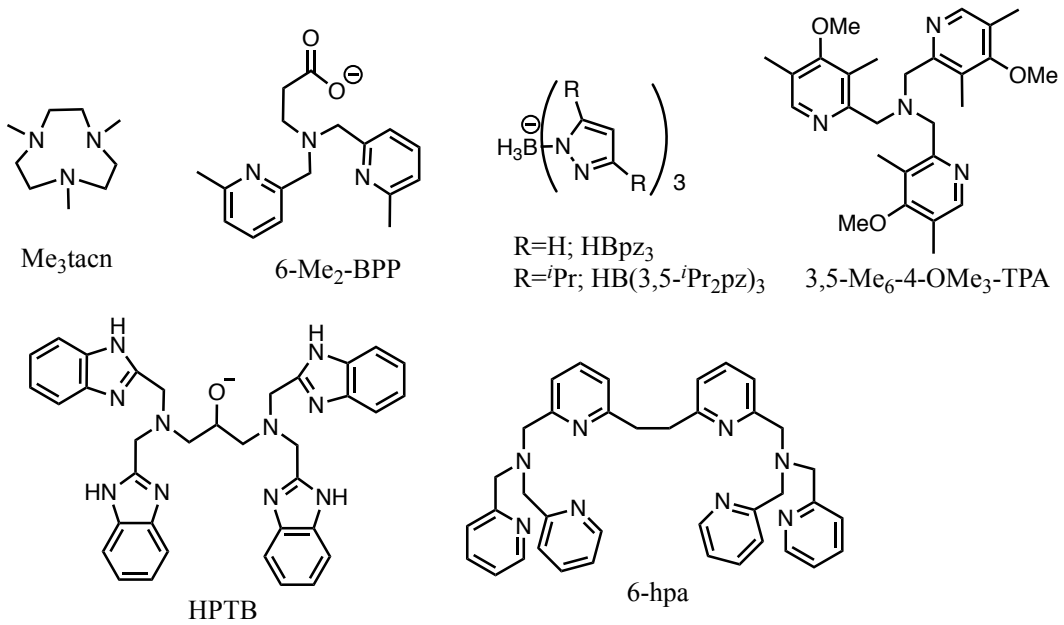

Figure 7. Typical ligands used for the synthesis of dinuclear non-heme iron complexes.

1.3.2 Spin states

Spin states of coordination compounds play an important role in influencing molecular structure, bonding, and reactivity, which is also reflected in non-heme iron chemistry.[44] Whether a certain complex is high-spin state or low-spin state depends on both the *d*-orbital energy gap (or splitting of *d*-orbitals Δ) and the pairing energy. The magnitude of the *d*-orbital energy gap is determinded by a number of factors, including the position of the metal in the periodic table, the oxidation state of the metal ion, the field strength of the ligand(s), and the coordination geometry. The *d*-orbital energy gap will increase with the charge of the metal center and upon descending a periodic group. The field strength of the ligands relies on the orbital interaction between the metal and the donor atoms of the ligands, and it has a determinative effect on the size of the energy gap.[89] The pairing energy refers to the electron repulsion associated with paired electrons sharing the same orbital. Thus, when the *d*-orbital energy gap is larger than the pairing energy, electrons tend to fill up the lower energy orbitals to pair up with electrons in these orbitals before they start to fill the higher energy orbitals, resulting in low-spin state complexes. On the other hand, if the pairing energy is larger than the *d*-orbital energy gap, it is energetically more favorable for the electrons to occupy the empty orbitals first, regardless of the energy of the orbitals. As a result, high-spin state complexes are obtained. For the typical ions encountered in non-heme iron chemistry (Fe(II), d^6; Fe(III), d^5; Fe(IV), d^4) both low and high spin configurations are possible within each of the typical coordination geometries encountered. The electronic configuration of non-heme iron complexes is therefore largely determined by the employed multidentate ligand.

Typical for iron complexes is that high-spin state and low-spin state configurations can in many cases be switched by changes in external conditions, such as temperature, pressure or irradiation with light, and is commonly associated with a color change. This phenomenon of spin crossover in iron(II) compounds leads to greater structural differences between the spin states than for other coordination compounds.[90] Spin state switching is accompanied by changes of magnetic and optical properties, which indicates potential applications of spin crossover compounds in switching sensors and devices.[91]

1.3.3 Two state reactivity

A consequence of dealing with the reactivity of enzymes and metal complexes in with the active iron center has a particular spin state is that reaction intermediates and products, but also the transition states that lead to these, will have spin states features of their own which may have

consequences for the overall energetics of the reaction pathway that is followed. Considerations about the relation between spin state and energy of reaction intermediates in organometallic chemistry have prompted Schröder, Shaik, and Schwarz to propose the so-called model of 'two state reactivity'.[92] In this model, the reaction partner in its lower energy spin state does not necessarily follow the energetically most favorable reaction pathway, *i.e.* of lowest activation energy, when compared to the reaction partner in its higher energy spin state. Accordingly, a change in spin state (spin crossing) along the reaction coordinate may enable the system to follow a different energy pathway. When such a spin crossing takes place in the rate limiting step of a reaction, it may affect the overall rate of the reaction. Initially being proposed as a general concept in organometallic chemistry, the concept of two-state reactivity was more recently demonstrated to have important implications on the reactivity of both heme and non-heme iron enzymes and model systems.[93]

1.4 Reactive Intermediates

A key feature in non-heme iron oxidation chemistry is the formation of reactive intermediates in the reaction of low-valent Fe(II) and Fe(III) complexes with external oxidants. These intermediates are not only of interest from a biomimetic point of view, as these offer the possibility of studying transient oxygenated intermediates found to form in non-heme iron enzymes in greater detail, but are also of interest within the realm of catalyst development. In this section a number of typically encountered reactive intermediates in non-heme iron chemistry are discussed in more detail.

1.4.1 Iron(III) superoxo, hydroperoxo and peroxo species

The initial reaction of O_2 with the low-valent Fe(II) state of non-heme iron enzymes leads to intermediate species in which the O–O bond is still (partially) intact and in which iron is oxidized to the Fe(III) state.

Ferric hydroperoxo species are often suggested as a "second electrophilic oxidant" in many biological oxidation reactions,[94] such as alkene epoxidation and alkane hydroxylation. Activated bleomycin (ABLM) is one of most extensively studied ferric hydroperoxo intermediates. Bleomycin (BLM) is a natural glycopeptide antibiotic with anti-cancer activity that is able to oxidatively cleave single- and double-stranded DNA.[95] ABLM is believed to be a BLM−Fe^{III}−OOH complex based on electrospray mass spectrometry.[96] EPR spectroscopy revealed the presence of a low-spin (S = 1/2) iron center,[97] which is coordinated by five *N*-

donor atoms of BLM and an end-on hydroperoxo ligand (Figure 8). To date, it is generally accepted that BLM−Fe^{III}−OOH acts as the active species responsible for abstraction of the C-4′ hydrogen atom from a backbone deoxyribose sugar (Figure 8), rather than a high-valent iron−oxo species formed *via* heterolytic or homolytic O−O cleavage of the iron(III)−hydroperoxo species. The evidences mainly come from studies of Solomon and co-workers, who have used circular dichroism kinetics to demonstrate that the ABLM + DNA reaction is appreciably faster and has a lower Arrhenius activation energy than does ABLM decay.[98] This is consistent with their previous theoretical studies on the reaction of ABLM with DNA, which revealed that the iron(III)−hydroperoxo species is thermodynamically and kinetically competent of direct hydrogen atom abstraction.[99]

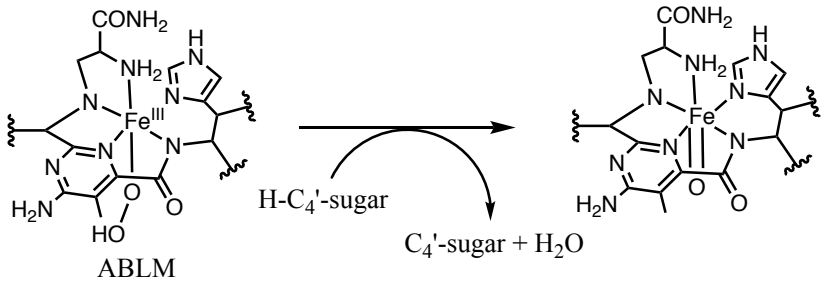

Figure 8. Direct hydrogen atom abstraction by ABLM.[36]

Although ferric hydroperoxo intermediates exhibit oxidizing capability in some biological reactions, biomimetic ferric hydroperoxo complexes are mainly found to be sluggish oxidants. Recently, a well-characterized high-spin ferric hydroperoxo complex, $[Fe^{III}(TMC)(OOH)]^{2+}$ (TMC = 1,4,8,11-tetramethyl-1,4,8,11-tetraazacyclotetradecane, Figure 9), which is generated upon protonation of peroxo complex $[Fe^{III}(TMC)(OO)]^{+}$, was reported by Valentine, Solomon, Nam, and co-workers.[100] In this study, the electrophilic reactivity of $[Fe^{III}(TMC)(OOH)]^{2+}$ was investigated in the oxidation of alkylaromatic compounds with weak C−H bonds such as xanthene (BDE_{C-H} = 75.5 kcal/mol) and 9,10-dihydroanthracene (DHA, BDE_{C-H} = 77 kcal/mol). The results showed that $[Fe^{III}(TMC)(OOH)]^{2+}$ is indeed capable of hydrogen atom abstraction from weak C−H bonds. $[Fe^{III}(TMC)(OOH)]^{2+}$ turned out to be more reactive than the corresponding iron(III)−peroxo complex in a number of oxidation reactions.[100,101]

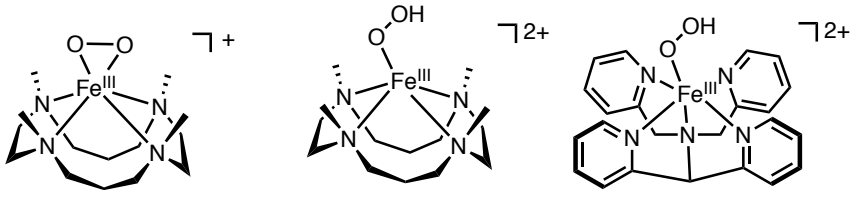

$[Fe^{III}(TMC)(OO)]^{+}$ $[Fe^{III}(TMC)(OOH)]^{2+}$ $[Fe^{III}(N4Py)(OOH)]^{2+}$

Figure 9. Biomimetic ferric peroxo and hydroperoxo complexes.

In order to understand parallels and differences between high-spin Fe^{III}–OOH species and low-spin Fe^{III}–OOH species in electrophilic hydrogen atom abstraction reactions and mechanisms of O−O bond homolysis, Nam, Solomon, and co-workers compared theoretical and experimental results of C−H bond activation of xanthene by the high-spin $[Fe^{III}(TMC)(OOH)]^{2+}$ and low-spin $[Fe^{III}(N4Py)(OOH)]^{2+}$ complexes (Figure 9), concluding that both complexes are able to carry out hydrogen atom abstraction, and that the high-spin $[Fe^{III}(TMC)(OOH)]^{2+}$ is slightly more reactive than the low-spin $[Fe^{III}(N4Py)(OOH)]^{2+}$.[102] However, the reaction coordinates were found to be very different and the reduction potential of high-spin Fe^{III}–OOH is higher than that of low-spin Fe^{III}–OOH. As a result, low-spin Fe^{III}–OOH complexes should be more reactive toward substrates with strong C−H bonds as in ABLM, while high-spin Fe^{III}–OOH complexes should be more reactive toward substrates with low ionization potentials and weak C−H bonds.[102] However, to date, there are no synthetic examples of ferric hydroperoxo complexes capable of activating relatively strong C−H bonds directly,[23] in contrast to ABLM, which contains a low-spin Fe^{III}–OOH core and is able to abstract strong C−H bonds (92 kcal/mol).

It is important to note that biological Fe(III)-hydroperoxo intermediates form after initial reaction of an Fe(II) site with O_2, resulting a transient Fe(III)-superoxo intermediate, followed by single electron transfer to form an Fe(III)-peroxo intermediate, and by subsequent protonation. Superoxo intermediates play important roles themselves as the reactive intermediates in enzymes like isopenicillin-*N*-synthase (IPNS; C–H bond activation) and homoprotocatechuate-2,3-dioxygenase (2,3-HPCD; aromatic ring cleavage). A few synthetic mononuclear Fe(III)-superoxo complexes have also been reported. In a study by Lee and co-workers, use of the dianionic, mixed N,O pentadentate ligand BDPP results in the formation of a Fe(III)-superoxo complex upon reaction of the Fe(II) precursor with O_2 at –80 ºC.[103] This complex was found to have a high-spin configuration, through exchange coupling between Fe(III) and the superoxo ligand, and is able to abstract relatively weak C–H bonds like to ones in DHA.

Dinuclear iron-superoxo complexes have also been reported, amongst others by Que[104] and Lippard.[105] In 2005, Que and Shan reported the reaction of $[Fe_2(\mu\text{-}OH)_2(6\text{-}Me_3\text{-}TPA)_2]^{2+}$ (6-Me3-TPA = tris(6-methyl-2-pyridylmethyl)amine) with O_2 in CH_2Cl_2 at −80 °C, giving rise to two intermediates, a diiron(II, III) complex **4** and a diiron(III)-hydroperoxide complex **5** **(**Scheme 8**)**.[104] Based on Raman experiments intermediate **4** was assigned to be a diiron superoxo species with an end-on bound superoxide. The reactivity of **4** has been evaluated in the reaction with 2,4-di-*tert*-butylphenol (DTBP). Compared to the final oxygenated product,

the diiron-peroxo complex **6**, which shows no reaction with DTBP at −60 °C, **4** is capable of oxidizing this substrate to give 3,3',5,5'-*tetra*-tert-butyl-2,2'-biphenol as product at −80 °C.

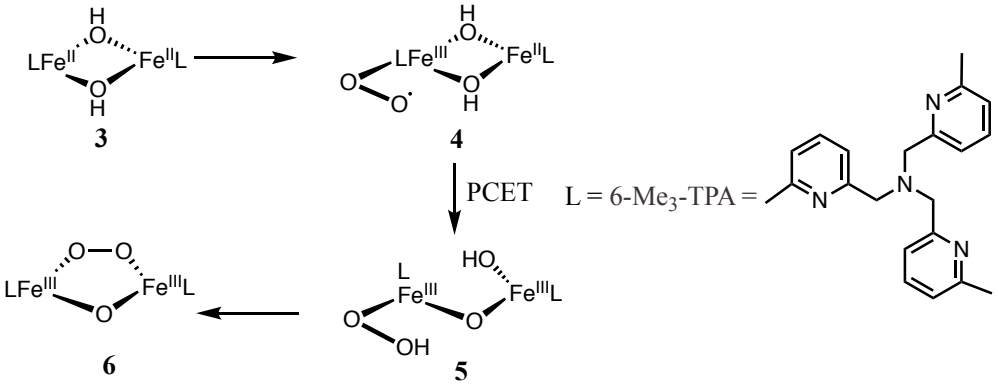

Scheme 8. Diiron-superoxo species and diiron-hydroperoxide species in the oxygenation of $[Fe_2(\mu\text{-}OH)_2(6\text{-}Me_3\text{-}TPA)_2]^{2+}$.

Fe(III)-peroxo intermediates were found to play a role in the activity of enzmyes like sMMO (diiron-peroxo) and NDO (mono-iron-peroxo) (vide supra). These intermediates can be formed upon one-electron reduction of their preceding Fe(III)-superoxo intermediates and can be engaged in both electrophilic and nucleophilic reactions. A number of synthetic iron peroxo species have been synthetized. These include dinuclear iron peroxo complexes like the one reported by Kodera (vide supra) and mononuclear complexes such as the one reported by Nam and Valentine (vide supra).

1.4.2 Iron(IV) and iron(V)–oxo species

Oxygen activation may ultimately lead to the formation of high-valent iron-oxo intermediates upon full cleavage of the O–O bond in enzymes and similar species have been proposed and observed in synthetic non-heme iron chemistry. In general, these species are considered as strong oxidants due to their high-valent nature and the presence of a 'bare' oxo moiety. Since the first kinetic and spectroscopic evidence for a non-heme iron(IV)–oxo intermediate (**J**) in the reaction of TauD,[27] more evidence has been provided to support the involvement of such species in biological oxidative transformations (vide supra).

The distinguished oxidative abilities shown in biological reactions encouraged chemists to investigate the formation and nature, and pursue the use in oxidation reactions of synthetic iron(IV)–oxo complexes. The first biomimetic non-heme iron(IV)–oxo complex $[Fe^{IV}(O)(cyclam\text{-}CH_2CO_2)]^+$ (Figure 10, left) was reported by Wieghardt and co-workers in

2000, where they used Mössbauer spectroscopy to assign it as a low-spin ($S = 1$) complex.[106] Three years later, a crystal structure of the low-spin ($S = 1$) iron(IV)–oxo complex $[Fe^{IV}(O)(TMC)(NCCH_3)]^{2+}$ (Figure 10, right) was reported, which was synthesized through the reaction of $[Fe^{II}(TMC)(OTf)_2]$ with iodosylbenzene (PhIO) in high yield (> 90%), allowing for the complete characterization of an iron(IV)–oxo species for the first time.[107] Since then, over 60 additional iron(IV)–oxo complexes have been generated and spectroscopically characterized.[36] Most of the synthetic iron(IV)–oxo complexes are in a low-spin ($S = 1$) ground state, in contrast to the iron(IV)–oxo species in non-heme enzymes that have a high-spin ($S = 2$) state.

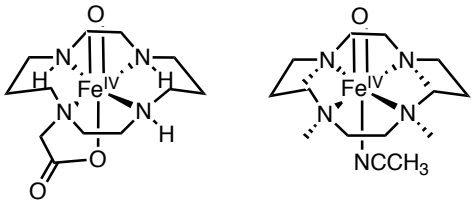

$[Fe^{IV}(cyclam\text{-}CH_2CO_2)]^+$ $[Fe^{IV}(O)(TMC)(NCCH_3)]^{2+}$

Figure 10. Synthetic $S = 1$ iron(IV)–oxo complexes.

One reason that low-spin state iron(IV)–oxo complexes dominate the synthetic examples in the literature is because of the use of relatively strong-field ligands, tertiary amines and pyridines, and the six-coordinate pseudo-octahedral geometry these complexes adopt.[108] The combination of these two factors makes the electrons preferentially fill up the lower energy orbitals, resulting in a low-spin state. In this regard, one strategy toward a high-spin state is employing tripodal tetradentate ligands, which can give rise to a C_3-symmetric trigonal-bipyramidal geometry, instead of the six-coordinate pseudo-octahedral geometry (Figure 11).

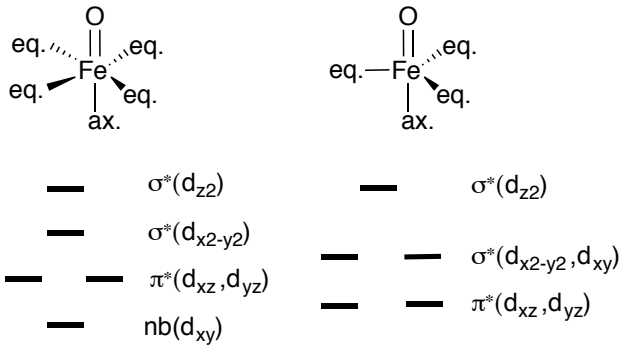

Figure 11. Splitting patterns for *d*-orbitals of iron(IV)–oxo complexes in pseudo-octahedral (left) and trigonal-bipyramidal (right) geometries.[108]

Based on this strategy, an $S = 2$ iron(IV)–oxo complex, $[Fe^{IV}(O)(TMG_3tren)]^{2+}$ (TMG_3tren = 1,1,1-tris{2-[N2-(1,1,3,3-tetramethylguanidino)]ethyl}amine, Figure 12, left), was prepared through reaction of $[Fe^{II}(TMG_3tren)(OTf)](OTf)$ with 2-(tert-butylsulfonyl)-iodosylbenzene (tBuSO$_2$C$_6$H$_4$IO) and fully characterized by Que and co-workers in 2009.[74] The very bulky TMG_3tren ligand contributed in stabilizing the iron(IV)–oxo moiety, and furthermore, enforced a trigonal-bipyramidal geometry at the iron center.[74] Spectroscopic studies of $[Fe^{IV}(O)(TMG_3tren)]^{2+}$ revealed that it shares several similarities with TauD-**J**. For example, like TauD-**J**, $[Fe^{IV}(O)(TMG_3tren)]^{2+}$ exhibits a near-UV charge-transfer band that is likely to be associated with an oxo-to-iron(IV) charge-transfer transition and, as a result, resonance-enhanced Fe═O vibrations were observed.[74]

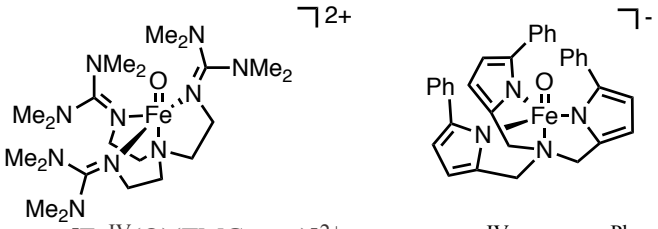

$[Fe^{IV}(O)(TMG_3tren)]^{2+}$ $[Fe^{IV}(O)(TPA^{Ph})]^{-}$

Figure 12. Synthetic $S = 2$ iron(IV)–oxo complexes.

More recently, Britt, Chang and co-workers reported another iron(IV)−oxo complex supported by a trigonal ligand platform, which was obtained upon treatment of the $[Fe^{II}(TPA^{Ph})]^{-}$ complex, in which TPA^{Ph} is a bulky tri-anionic trispyrrolide ligand, with trimethylamine *N*-oxide in acetonitrile solution.[109] It was concluded to be a high-spin ($S = 2$) $[Fe^{IV}(O)(TPA^{Ph})]^{-}$ complex (Figure 12, right) by a number of spectroscopic techniques, including Mössbauer, XAS, FTIR, UV−Vis, and parallel-mode EPR. Its reactivity with organic substrates showed this complex is capable of mediating intermolecular C−H oxidation as well as oxygen atom transfer reactions .

Although some synthetic iron(IV)−oxo complexes have been demonstrated to be able to perform the oxidation of substrates containing strong C−H bonds, such as cyclohexane,[110,111] they are relatively poor oxidants, compared to the iron(IV)−oxo intermediates in enzymes. Moreover, the factors that determine the reactivity of the iron(IV)−oxo complexes remain unclear. To date, all of the theoretical studies predicted that iron(IV) species are better oxidants in a high-spin ($S = 2$) state than in a low-spin ($S = 1$) state.[112-114] The recent observation by Que and co-workers of the high reactivity of a (pseudo)octahedral iron(IV)-oxo species with S = 2 spin state (vide supra) may shed further light on this matter.

As discussed in the Rieske dioxygenases section, a HO−Fe(V)═O species is postulated as a key intermediate in the catalytic cycle of these enzymes (mechanism B, Scheme 2). Direct evidence for the involvement of such a species in synthetic non-heme iron chemistry was revealed by isotope-labeling experiments reported by Que and co-workers. In this study, all of the alcohol products were detected to incorporate some ^{18}O from added $H_2{}^{18}O$, which indicated a stepwise mechanism involving an oxidant that allowed participation of water in the catalytic cycle (the alcohol products do not themselves exchange with solvent $H_2{}^{18}O$ based on control experiments).[115] Based on these results a HO−Fe(V)═O species was proposed as the actual oxidant rather than a Fe^{III}–OOH species, where the Fe(V) species would derive from the Fe^{III}–OOH intermediate *via* water-assisted O−O bond cleavage.

In 2011, evidence for a HO−Fe(V)═O intermediate was reported by Cronin and Costas using variable-temperature mass spectrometry (VT-MS).[116] In their investigation on the reaction of $[Fe^{II}(^{Me,H}PyTACN)(OTf)_2]$ ($^{Me,H}PyTACN$ = 1-(2′-pyridylmethyl)-4,7-dimethyl-1,4,7-triazacyclononane) with H_2O_2 at temperatures between 20 and −40 °C, two possible active intermediates, $[Fe^{III}(OOH)(^{Me,H}PyTACN)(OTf)]^+$ and $[Fe^{V}(O)(OH)(^{Me,H}PyTACN)(OTf)]^+$ (Figure 13), were postulated. The alternative Fe^{III}–OOH species was excluded on the basis of isotopic labeling experiments with $H_2{}^{18}O$, as oxygen exchange between H_2O_2 and water did not happen readily. Subsequent EPR spectroscopic studies assigned this HO−Fe(V)═O species as a low-spin (S = 1/2) complex.[117]

The first synthesis of an iron(V)–oxo complex was reported in 2007. The reaction of $[PPh_4][Fe^{III}(TAML)(H_2O)]$ (where TAML is a tetra-anionic, tetraamido macrocyclic ligand) with *m*CPBA (*m*CPBA = *meta*-chloroperoxybenzoic acid) in *n*-butyronitrile at −60 °C resulted in a long-lived intermediate (several hours at −60 °C), which was identified as $[Fe^{V}(O)(TAML)]^-$ (Figure 13) by various spectroscopies, including ESI-MS, Mössbauer, EPR and EXAFS.[118] This complex exhibits a low-spin state (S = 1/2) with g values of about 1.99, 1.97, and 1.74. Notably, EXAFS analysis showed an O scatterer at 1.58 Å, which was assigned to the oxo atom of an Fe–O unit. Reactivity studies showed that this iron(V)–oxo complex is competent in oxidizing a variety of substrates, including thioanisole, styrene, cyclooctene, ethylbenzene, and DHA.

More recently, a room temperature stable iron(V)–oxo complex, $[Fe^{V}(O)(TAML\text{-}NMe)]^-$ (see Figure 13), has been synthesized from equimolar solutions of $(Et_4N)_2[Fe^{III}(Cl)(biuret\text{-}amide)]$ and *m*CPBA in CH_3CN at room temperature (where the biuret-amide ligand is an amide analogue of the TAML ligand).[119] Thanks to the higher stability, reactivity studies with alkanes

at room temperature showed that this iron(V)–oxo complex is able to oxidize a series of alkanes containing strong C−H bonds, such as those in cyclohexane (with a C−H bond dissociation energy (BDE) of 99.3 kcal/mol).

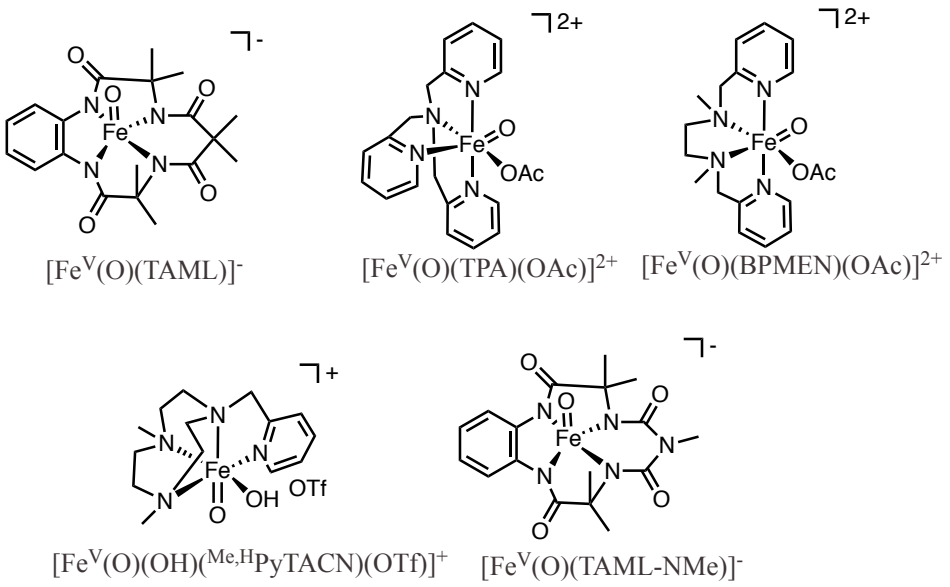

Figure 13. Selected examples of spectroscopically characterized iron(V)–oxo complexes.

Subsequently, inspired by this study, Talsi and co-workers reported spectroscopic evidences for two new iron(V)–oxo complexes. In their study on the catalyst systems $[Fe^{II}(TPA)(CH_3CN)_2]$/peroxide and $[Fe^{II}(BPMEN)(CH_3CN)_2]$/peroxide (peroxide = *m*CPBA, CH_3CO_3H, or H_2O_2), EPR spectra were tentatively assigned to $(TPA)Fe^{V}{=}O$ and $(BPMEN)Fe^{V}{=}O$ species (Figure 13), respectively.[120] Notably, compared to the EPR spectrum for $[Fe^{V}(O)(TAML)]^{-}$, the EPR spectra for these two new $Fe^{V}{=}O$ species displayed distinct differences, which were proposed to be caused by the different ligand fields. That the assignment of these high-valent species is not a trivial exercise was later shown by Shaik and co-workers, who showed that the Fe(V)oxo-acetate species initially proposed as the active oxidant for Fe(BPBP) catalysts in combination with H_2O_2 and acetic acid is more likely to be an cyclic Fe(III)peracetate complex that transforms into a Fe(IV)–oxo–AcO· radical species as the actual oxidant.[121] These findings do not only underscore the difficulties in pinning down the true identity of the highly reactive and transient oxidized species involved in non-heme iron chemistry, they also show the richness of different species that may form depending on the ligand framework, the employed sacrificial oxidant, and any sort of additive such as acetic acid that is used.

As mentioned earlier, many different sacrificial oxidants are used in non-heme iron catalysis and for the generation of reactive intermediates. Starting from O_2 and H_2O_2, also oxidants like peracetic acid, *m*CPBA, and alkylhydroperoxides are used. Each of these may form unique types of intermediates (vide infra). Within this context it is worthwhile to mention that adducts of iodosylbenzene, a popular single oxygen-transfer reagent, have been reported by McKenzie[122] and Nam[123], and of hypochlorite, another single oxygen transfer agent, by De Visser.[124] In each of these cases the oxygen transfer reagent is intact and coordinates to Fe(III) through its terminal oxygen atom. Interestingly, the complex reported by McKenzie constitutes a seven-coordinated iron center formed from the reaction of iodosylbenzene with a six-coordinated iron complex.

Besides mononuclear high-valent iron-oxo species, a number of dinuclear iron complexes with high-valent unites have also been reported. The first example of a synthetic complex comprizing a dinuclear $Fe^{IV}_2(\mu\text{-}O)_2$ core was prepared and characterized by Que and co-workers, providing a biomimetic precedent for intermediate **Q** of sMMO.[125] One-electron oxidation of its $Fe^{III}Fe^{IV}$ precursor **7** (Scheme 9) at –40 °C gave rise to $[Fe^{IV}_2(\mu\text{-}O)_2L_2]^{4+}$ (**8** in Scheme 9; L is an electron-rich TPA variant), which is capable of oxidizing weak C–H bonds such as those in DHA, yet revealing a 100-fold lower reactivity than its corresponding mononuclear Fe^{IV}═O analogue ($[Fe^{IV}(O)(L)(NCMe)]^{2+}$). On the other hand, the addition of water or methanol to complex **7**, which is sluggish in the oxidation of C–H bonds, resulted in much more reactive complexes with an open-core structure $[(X)(L)Fe^{III}–O–Fe^{IV}═O(L)]^{2+}$ (**9a** and **9b**, Scheme 9).[126] The significant improvement of reactivity was proven by DHA oxidation experiments using **9b** as the oxidant, which has a second-order rate constant that is 3.6×10^7-fold larger than that for complex **8**. In addition, **9b** is capable of cleaving C–H bonds as strong as 96 kcal/mol.[126,127] Notably, the fact that **9a** and **9b**, which contain a high-spin Fe^{IV}═O unit, are much more reactive than the corresponding diiron(IV) complex (**11** in Scheme 9) with a $S = 1$ Fe^{IV}═O moiety, shows that the spin state of the Fe^{IV}═O unit significantly influences the overall reactivity.[126] However, despite of the reported dinuclear iron species having strong oxidizing capability, to date, there is still no example of a carboxylate- or oxygen-bridged diiron structural model of sMMO capable of selective methane oxidation.[23,126]

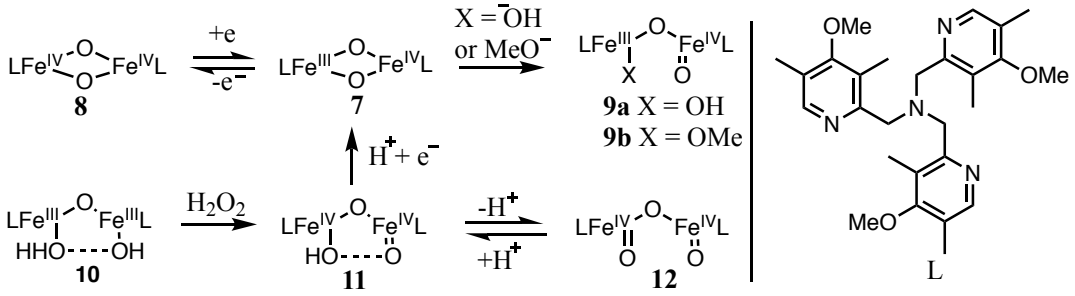

Scheme 9. Diiron complexes with high-valent iron unit based on ligand L.

Very recently, a species with a novel O═Fe^{IV}–O–Fe^{IV}═O core was reported by Bominaar, Que, Münck, and co-workers.[54] The treatment of **11**, containing a HO–Fe^{IV}–O–Fe^{IV}═O core, with strong base at −80 °C gives rise to its conjugate base **12** (Scheme 9). Depending on the solvent used, complex **12** exhibits two spectral forms, that is **12a** and **12b**, which have been extensively characterized by Mössbauer and parallel mode EPR spectroscopy. **12a** has two antiferromagnetically coupled high-spin (S_{loc} = 2) sites, resulting in a cluster S_t = 0 state. **12b** , on the other hand, has an S_t = 3 state, based on Mössbauer and EPR data, resulting from two ferromagnetically coupled local sites (S_{loc1} = 1 and S_{loc2} = 2). DFT calculations showed that complex **12** has six spin multiplets within an energy range of ca. 1000 cm^{-1}, which is in sharp contrast to intermediate **Q** (has no low-lying excited spin states).

1.5 Some Catalytic Examples

Next to the development of synthetic non-heme iron complexes for the purpose of biomimicry, many of the complexes discussed above have been used as synthetic catalysts for organic transformations in their own right. This section provides a short overview of the accomplishments in non-heme iron catalysis, with some emphasis on oxidative transformations.

1.5.1 Mononuclear iron species

1.5.1.1 Selective C–H oxidations catalyzed by mononuclear iron complexes

Oxidation of alkane hydrocarbons is of fundamental interest in both industry and organic synthetic chemistry, due to the extensive presence of oxidized alkane frameworks in industrial products and biological molecules. In the past decades, a large number of bioinspired mononuclear iron complexes have been reported that are able to achieve selective C–H oxidations. However, selective oxidation of alkyl C–H bonds in an environmentally friendly

manner still remains as a challenge for organic chemists.[128] A selected number of examples are presented here.

In 1997, highly stereospecific oxidations of *cis*- and *trans*-1,2-dimethylcyclohexane with >99% retention of stereochemistry were described by Que and co-workers employing the iron complex $[Fe(TPA)(CH_3CN)_2](ClO_4)_2$ as catalyst and hydrogen peroxide as the oxidant.[129] This is the first example of a non-heme iron complex capable of stereospecific alkane hydroxylation. Later, they studied the reactivity of various TPA-based iron(II) complexes with differently substituted pyridine moieties (Figure 14), concluding that the 5-Me_3-TPA-based iron complex is a more efficient catalyst than $[Fe(TPA)(CH_3CN)_2](ClO_4)_2$, while the introduction of either two or three 6-Me substituents decreases the reactivity.[130,115]

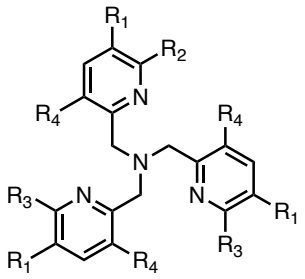

5-Me_3-tpa: R1=Me, R_2=R_3=R_4=H

6-Me-tpa: R_1=R_3=R_4=H, R_2=Me

6-Me_2-tpa: R_1=R_2=R_4=H, R_3=Me

6-Me_3-tpa: R_1=R_4=H, R_2=R_3=Me

6-Me-tpa: R_1=R_2=R_3=H, R_4=Me

Figure 14. TPA-based ligands used for the preparation of iron(II) complexes.

In 2007, Chen and White introduced a remarkably predictable and selective C–H oxidation protocol for the synthesis of complex molecules *via* so-called late stage functionalization.[131] By employing iron catalyst $[Fe(BPBP)(CH_3CN)_2](SbF_6)_2$ (BPBP = *N*,*N*'-bis(2-pyridylmethyl)-2,2'-bipyrrolidine, Scheme 10) and H_2O_2 as the oxidant, predictable and selective C–H bond oxidations were achieved on the basis of the electronic and steric properties of the different C–H bonds present within the same substrate. That is, oxidation of C–H bonds preferentially occurs at the most electron-rich or the less hindered tertiary C–H bond. Interestingly, when considering the electronic and steric effects in a single substrate, steric effects can override electronic effects in site selectivities. Moreover, selective aliphatic C–H oxidation of complex natural products can be achieved utilizing this strategy, showing the functional group tolerance of the catalyst (Scheme 10). Later, the same group studied the combined effects (*i.e.*, electronic, steric, and stereoelectronic factors) on selective secondary C–H bond oxidation using the same iron catalyst.[132] In this case, predictable and highly selective methylene C–H oxidations in a number of natural products were obtained. The reliability and activity of this and related catalyst systems are such that the C–H bond can itself be put forward as a functional group in organic synthesis.

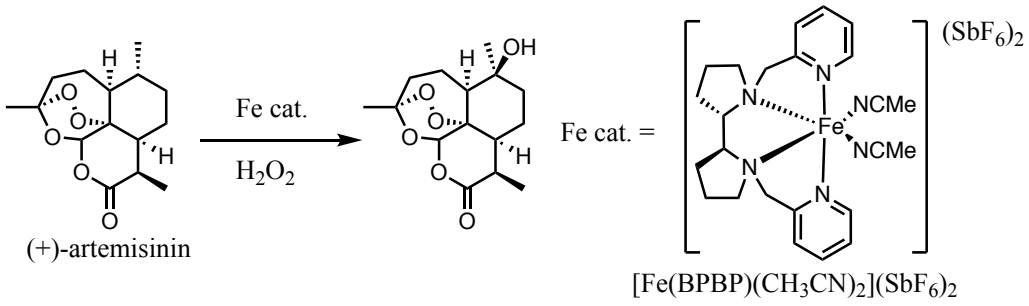

Scheme 10. Predictable selective aliphatic C–H oxidation by $[Fe(BPBP)(CH_3CN)_2](SbF_6)_2$.

Another interesting ligand is BPMCN (or mcp, *i.e. N*,*N*'-dimethyl-*N*,*N*'-bis(2-pyridylmethyl)-cyclohexane-trans-1,2-diamine), which is based on the cyclohexyldiamine backbone. While this catalyst has been studied for some time, a very recent report by Costas and co-workers shows the ability of the iron catalyst $[Fe(OTf)_2(BPMCN)]$ (Scheme 11) to perform selective oxidation of methylenic sites in alkanes.[133] Similar to $[Fe(BPBP)(CH_3CN)_2](SbF_6)_2$, this selectivity is dependent on the electronic and stereoelectronic environments of the C–H bonds. In some cases though, $[Fe(OTf)_2(BPMCN)]$ appears to be an even more sterically sensitive catalyst than the BPBP-based catalyst in distinguishing between multiple methylene C–H bonds within a single substrate. A remarkable example is the oxidation of *trans*-decalin; the former catalyst preferentially oxidizes at the least hindered methylene site C-3 (the ratio of C-3 oxidation to C-2 oxidation is 1.5:1), while $[Fe(OTf)_2(BPBP)]$ yields a 1:1 ratio of products (Scheme 11).

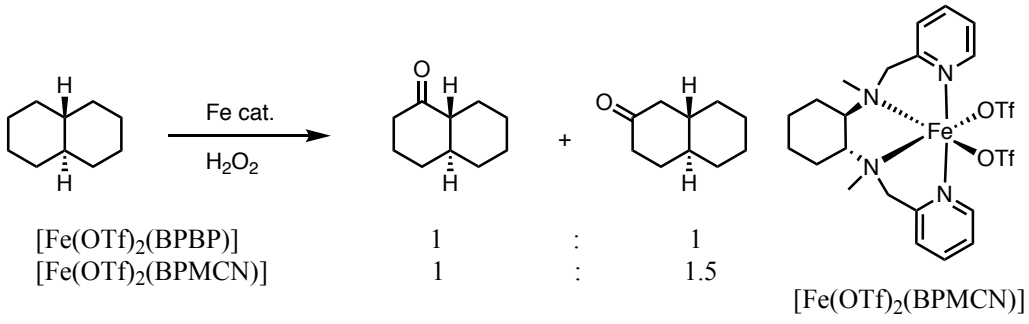

Scheme 11. Methylene oxidation by $[Fe(OTf)_2(BPBP)]$ and $[Fe(OTf)_2(BPMCN)]$.

Substitution of the pyridine rings, especially at the β-position, has been shown to affect the site-selectivity in C–H oxidations. For instance, in 2013, White *et al.* proposed to introduce electron-withdrawing, rotationally blocked aryl rings to the β-positions on the pyridines of the BPBP ligand ($Fe(CF_3$-BPBP), Figure 15).[134] These bulky aryl rings restrict the cone of possible trajectories by which substrate approach the metal center, resulting in improved methylene site-selectivity. More recently, a similar but simpler strategy was adopted by Klein Gebbink and Costas, in which a bulky triisopropylsilyl (TIPS) group is positioned at the β-pyridine position

(Fe(^{TIPS}BPBP) and Fe(^{TIPS}BPMCN), Figure 15).[135] This ligand modification led to even more enhanced selectivity for secondary C–H bond oxidation, and allowed for the site-selective oxidation of steroidal substrates. Notably, the preferentially oxidized sites in steroids were switched by the opposite catalyst enantiomers.

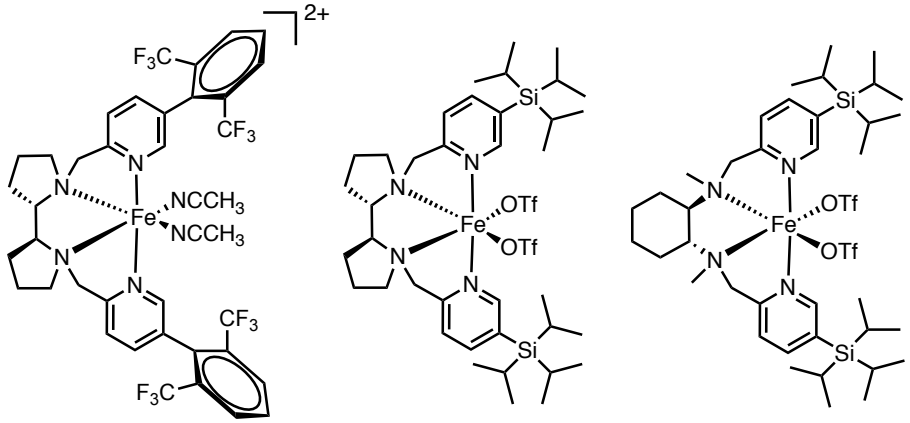

$[Fe(CH_3CN)_2(CF_3\text{-BPBP})]^{2+}$ $[Fe(OTf)_2(^{TIPS}BPBP)]$ $[Fe(OTf)_2(^{TIPS}BPMCN)]$

Figure 15. Structures of $[Fe(CH_3CN)_2(CF_3\text{-BPBP})]^{2+}$, $[Fe(OTf)_2(^{TIPS}BPBP)]$, and $[Fe(OTf)_2(^{TIPS}BPMCN)]$.

1.5.1.2 Alkene oxidations catalyzed by mononuclear iron complexes

Stereoselective epoxidation and *cis*-dihydroxylation are useful transformations in organic chemistry. They are valuable strategies for the formation of new C–X bonds, thus generating building blocks for organic bulk and fine chemicals. The requirement for chemo- and enantioselective alkene oxidations with H_2O_2 on a technical scale in modern chemistry stimulates researchers to develop more efficient, selective, and green alkene oxidation protocols.[136]

A practical iron-catalyzed alkene epoxidation procedure at room temperature and under aerobic conditions was developed by Beller and co-workers.[137] In this work, a combination of commercially available $FeCl_3 \cdot 6H_2O$, pyridine-2,6-dicarboxylic acid, and an organic base (such as pyrrolidine, benzylamines, or methylimidazole derivatives) yields the iron catalyst *in situ*, which activates H_2O_2 to perform the epoxidation of a variety of substrates (such as 1,2-disubstituted aromatic olefins and 1,3-dienes) in a chemo- and stereoselective manner (Scheme 12, left). By replacing the organic bases with a chiral 1,2-diphenyl-ethylene-1,2-diamine derivative (Scheme 12, right), the asymmetric version of this reaction was achieved, which allows for the epoxidation of trans-stilbene derivatives with 40-94% yield and 10-97% *ee*.[138]

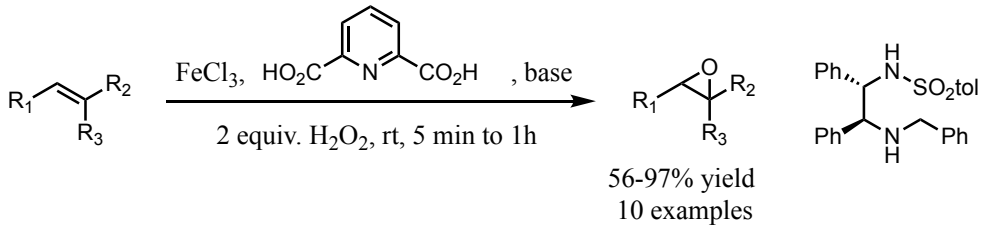

Scheme 12. A practical protocol for the epoxidation of alkenes.

More recently, Costas and co-workers investigated electronic ligand effects on the catalytic epoxidation activities of the iron BPBP family of complexes with the general formula [Fe(OTf)$_2$(^{X}BPBP)] (Figure 16). Using *cis*-*β*-methylstyrene as a model substrate, they concluded that the enantioselectivity of the epoxidation reactions improves with the increase of the electron-donating properties of the BPBP ligand.[139] Like with many other non-heme iron-catalyzed epoxidation reactions using H_2O_2, catalytic amounts of carboxylic acids such as acetic acid were utilized as additives/co-ligands to promote O−O cleavage. In this case though, the authors have introduced chiral carboxylic acids to improve the enantioselectivity. Using chiral amino acids, they were also able to extend the substrate scope of these systems to more challenging terminal olefins obtaining the desired epoxides with high enantioselectivity.[140]

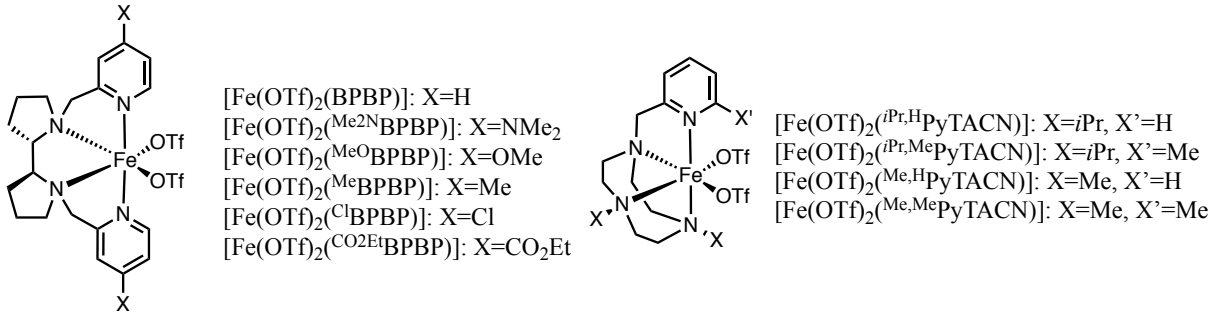

Figure 16. Structures of [Fe(OTf)$_2$ (*S*,*S*-^{X}BPBP)] and [Fe(OTf)$_2$(^{X}PyTACN)].

In 2008, Costas and co-workers developed a family of bioinspired non-heme iron complexes [Fe(OTf)$_2$(^{X}PyTACN)] (Figure 16), which are based on a pyridinyl-derivatized triazacyclononane (TACN) backbone, and have studied their catalytic properties in both epoxidation and *cis*-dihydroxylation of alkenes.[141] These iron catalysts exhibit high efficiency by yielding the corresponding epoxides and *cis*-diol with high turnover numbers (up to 252). Notably, it was concluded that substituents on the N atoms of the triazamacrocycle and on the pyridine ring play a key role in the selectivity of the corresponding iron complexes.

1.5.1.3 Catalytic transformations beyond C–H/C=C oxidations catalyzed by mononuclear iron complexes

In addition to aliphatic C–H oxidation and alkene oxidation, mononuclear iron complexes are used for other catalytic oxidative transformations as well. Halfen and co-workers reported on non-heme iron complexes that are able to perform catalytic alkene aziridinations with N-tosyliminophenyliodinane (PhINTs).[142] By employing the linear triamine ligand 1,1,4,7,7-pentamethyldiethylenetriamine (Me_5dien) supported iron(II) complex [(Me_5dien)Fe($OTf)_2$] and the related macrocyclic ligand 1,4,7-triisopropyl-1,4,7-triazacyclononane ($i$$Pr_3$TACN) supported iron(II) complex [($i$$Pr_3$TACN)Fe($OTf)_2$], both styrene and 1-hexene can be converted to the corresponding aziridine products with 26% to 95% yield (Scheme 13). Like in the case of many non-heme epoxidation and *cis*-dihydroxylation catalysts, *cis* labile coordination sites on the iron center are required for efficient reactivity. In a subsequent mechanistic study, an imidoiron(IV) species (Figure 17) was proposed as an intermediate for the alkene aziridination based on experimental and computational studies.[143]

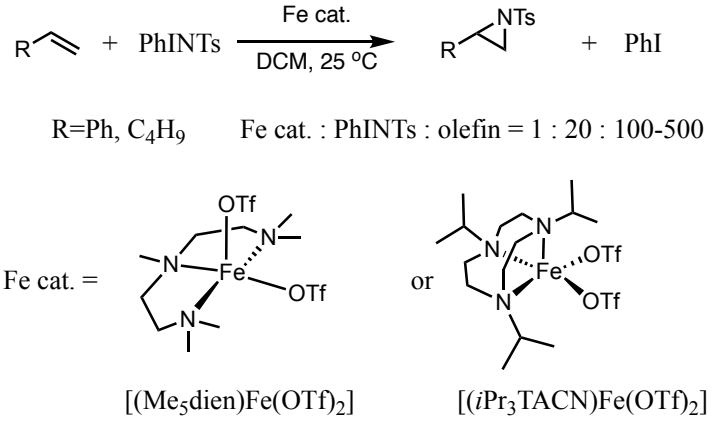

Scheme 13. Alkene aziridination catalyzed by mononuclear iron(II) complexes.

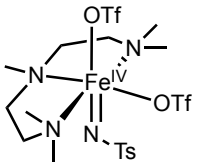

Figure 17. Imidoiron(IV) intermediate proposed in the catalytic cycle of alkene aziridination.

Sulfoxidation reactions catalyzed by mononuclear iron complexes using a variety of different sacrificial oxidants have also been studied. Very recently, high-spin iron(III) iodosylarene intermediates bearing an N-methylated cyclam ligand were synthesized by Latour, Nam, and co-workers from the reaction of [Fe^{II}(13-TMC)($OTf)_2$] (13-TMC = 1,4,7,10-tetramethyl-1,4,7,10-tetraazacyclotridecane) with iodosylarenes at −40 °C. Two intermediates, [Fe^{III}(OIPh)(13-TMC)]$^{3+}$ and [Fe^{III}($OIPhF_5$)(13-TMC)]$^{3+}$ formed, depending on the iodosylarenes used (PhIO or pentafluoroiodosylbenzene (F_5PhIO), respectively).[123] These two

intermediates were characterized by various spectroscopic methods, such as coldspray ionization time-of-flight mass spectrometry (CSI-TOF MS), UV/Vis absorption, EPR, Mössbauer, and resonance Raman (rRaman) spectroscopies. They were found to be highly reactive oxidants not only capable of alkane hydroxylation, but also sulfoxidation reactions. It was also concluded that the iron(III) iodosylarene intermediates are much more reactive than the corresponding iron(IV)-oxo complex $[Fe^{IV}(O)(13\text{-TMC})]^{2+}$.

1.5.2 Dinuclear iron species

The use of non-heme dinuclear iron complexes as catalysts has been inspired by the reactivity of the BMMs. In particular, their potential to oxidize methane to methanol has motivated numerous groups to investigate the catalytic potential of sMMO reactive site mimics in various oxidative reactions. Although, to the best of our knowledge, a mimic that is able to oxidize methane to methanol has not been described yet, dinuclear non-heme iron complexes have proven to be active catalysts for several transformations such as epoxidations, aziridinations and sulfoxidations.

1.5.2.1 Alkene oxidations catalyzed by dinuclear iron complexes

In 1986 Que and co-workers reported the use of $(Me_4N)(Fe^{III}_2(\mu\text{-L})(\mu\text{-}CH_3CO_2)_2$ (Figure 18) as a catalyst for the epoxidation of cyclohexene, *cis*-stilbene, and styrene with turnover numbers between 1.6 and 3.2.[144] The reactions were performed in DMF using H_2O_2 as the oxidant. Although the TON and chemoselectivity of this system are low, it can be seen as the first synthetic dinuclear non-heme iron complex able to catalyze epoxidation reactions.

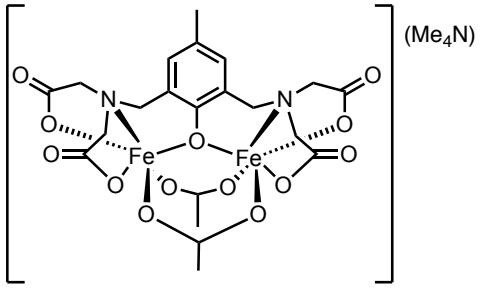

Figure 18. Que's epoxidation catalyst $(Me_4N)(Fe^{III}_2(\mu\text{-L})(\mu\text{-}CH_3CO_2)_2$.

Jacobsen and co-workers reported in 2001 a self-assembled MMO mimic suitable for the catalytic epoxidation of olefins.[145] Compared to previously reported systems their catalyst ($[Fe_2(\mu\text{-O})(\mu\text{-}CH_3CO_2)(BPMEN)_2]$, Scheme 14) was shown to be more active in epoxidation

reactions, being able to perform at low loadings (3 mol%) at 4 °C in MeCN using aqueous H_2O_2 as the oxidant and yielding the desired epoxides in a range between 61 and 90%. This corresponds to TONs between 20 and 30. The system described by Jacobsen can be seen as the first MMO model system applicable in preparative oxidation chemistry. A similar system ($[((phen)_2(H_2O)Fe^{III})_2(\mu\text{-}O)](ClO_4)_4$) has been developed by Stack.[146]

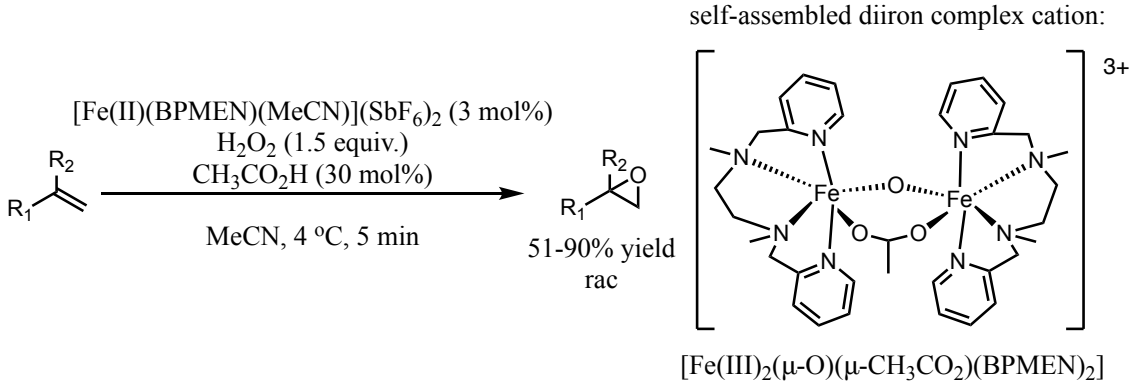

Scheme 14. Olefin epoxidation catalyzed by $[Fe_2(\mu\text{-}O)(\mu\text{-}CH_3CO_2)(BPMEN)_2]$.

The first enantioselective epoxidation catalyzed by a dinuclear non-heme iron catalyst has been described by Jin and co-workers.[147] PhIO (iodosobenzene) has been employed as the oxidant. The catalyst gave only poor yields with moderate enantiomeric excess. More recently, the groups of Ménage[148] and Kwong[149] have reported diiron catalysts that are able to epoxidize olefins with high yields and moderate to good enantiomeric excess (Scheme 15 and 16). Both reports focus mainly on styrenes as substrates. The catalyst described by Ménage is an oxygen-bridged dimer able to reach enatiomeric excess up to 63%. Kwong's catalyst is based on a sexipyridine as ligand and also comprises a bridging oxo-moiety.

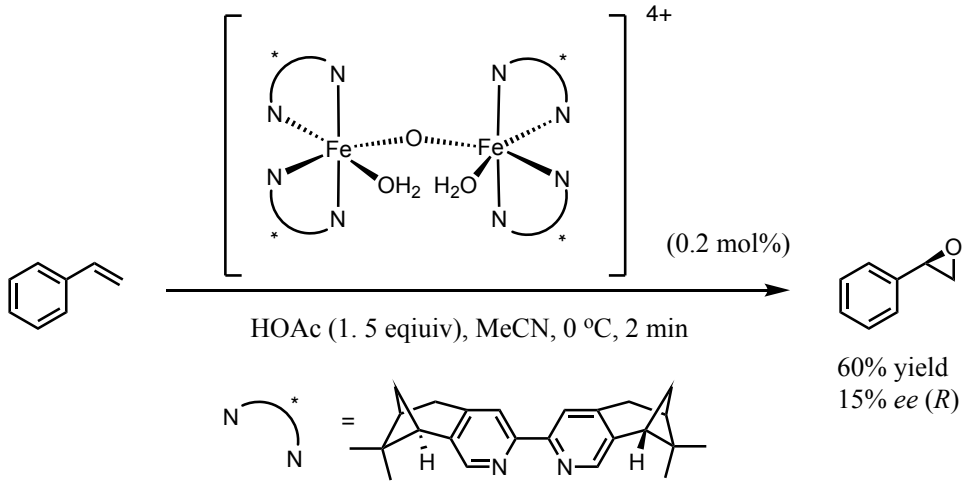

Scheme 15. Ménage's catalyst for enantioselective epoxidation.

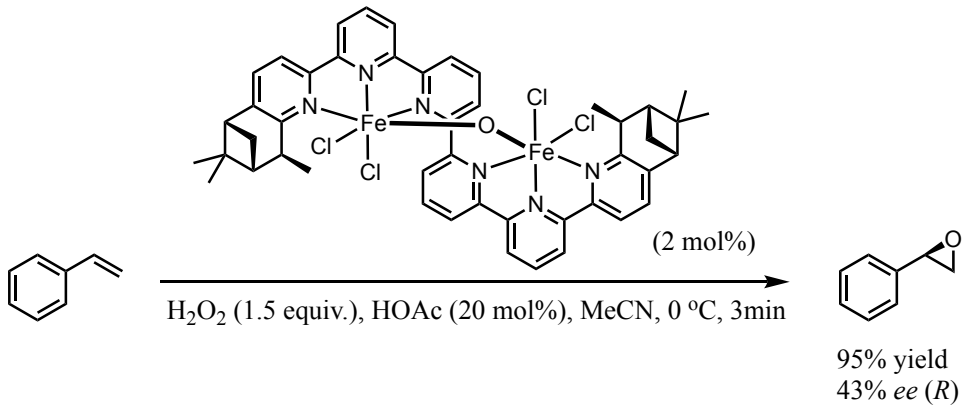

Scheme 16. Kwong's catalyst for enantioselective epoxidation.

Dinuclear iron complexes have not only been found to be able to epoxidize olefins. They were also shown to be suitable catalysts for the oxidation of C–H bonds in alkanes. Examples have been reported by Nordlander and co-workers using a monocarboxylate-briged diiron(III) μ-oxido complex and hydrogen peroxide as the oxidant.[150] The described catalyst is able to oxidize cyclohexane to a mixture of cyclohexanol and cyclohexanon (1.2/1.0) yielding a TON of 19. More recent studies by Norlander and Repo described a novel diiron complex that features lithium ions in its structure (Figure 19).[151] This complex is able to catalyze the oxidation of various alkanes and alkenes. A TON of 51 was found for the oxidation of cyclohexane to cyclohexanol and cyclohexanon, yielding the same ratio as for the earlier reported system. Olefinic substrates such as cyclohexene yield mixtures of the corresponding epoxide, allyl alcohol, and allyl ketone.

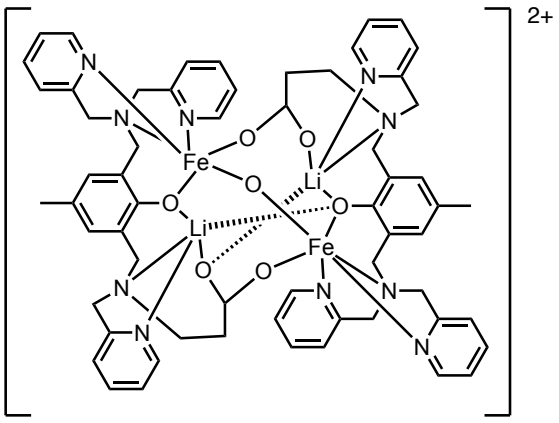

Figure 19. Structure of $[Fe_2(\mu\text{-}O)(LiDPCPMPP)_2]^{2+}$.

1.5.2.2 Catalytic transformations beyond C=C oxidations catalyzed by dinuclear iron complexes

Besides epoxidations and alkane oxidations, dinuclear non-heme iron complexes have also been shown to transform olefines into aziridines. An example is the system of Latour that is shown in Scheme 17.[152] Styrene, cyclooctene, and 1-hexene have been converted in yields between 50 and 69% to the corresponding aziridination products. The reactions proceed at room temperature using acetonitrile as solvent and iodosylbenzene/tosylamine as the oxidizing reagent mixture. Recent studies provided evidence for the involvement of an $Fe^{III}Fe^{IV}$=NTosyl intermediate.[153] Furthermore, Latour and co-workers have shown that their catalyst is able to catalyze the amidation of thioanisole.[152]

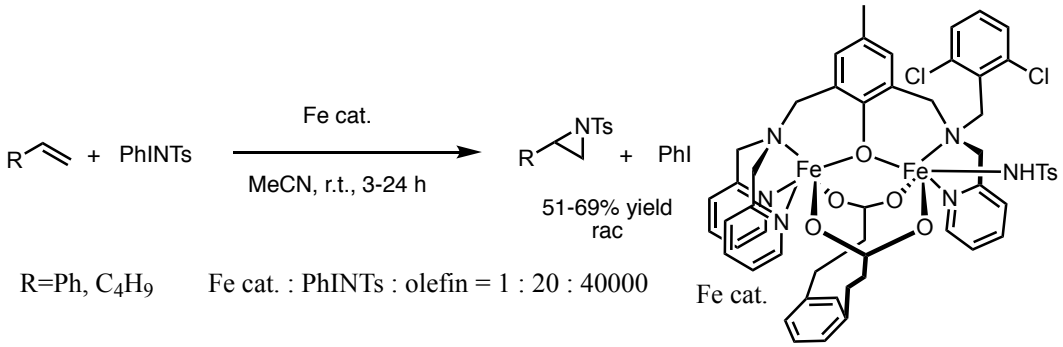

Scheme 17. Alkene aziridination catalyzed by dinuclear iron(II) complexes.

Bryliakov and co-workers demonstrated the iron-catalyzed oxidation of thioethers with iodosylarenes (Scheme 18).[154] The catalyst used is a chiral, oxygen bridged diiron-salen complex. The reactions proceed under mild conditions with the use of different iodosylarenes such as PhIO or MesIO as sacrificial oxidant. Beside the shown dimers also monomeric iron-salen complexes have been shown by the authors to be suitable catalysts for this transformation. Interestingly, the product *ee's* obtained by the dinuclear catalysts are gerenally higher than for the tested mononuclear catalysts. The desired sulfoxides have been obtained in high yields and moderate to good enantiomeric excess (up to 84%). Mahy and co-workers reported recently on the oxidation of dibenzothiophene, a typical fuel contaminant, and thioanisole using hydrogen peroxide as the oxidant.[155]

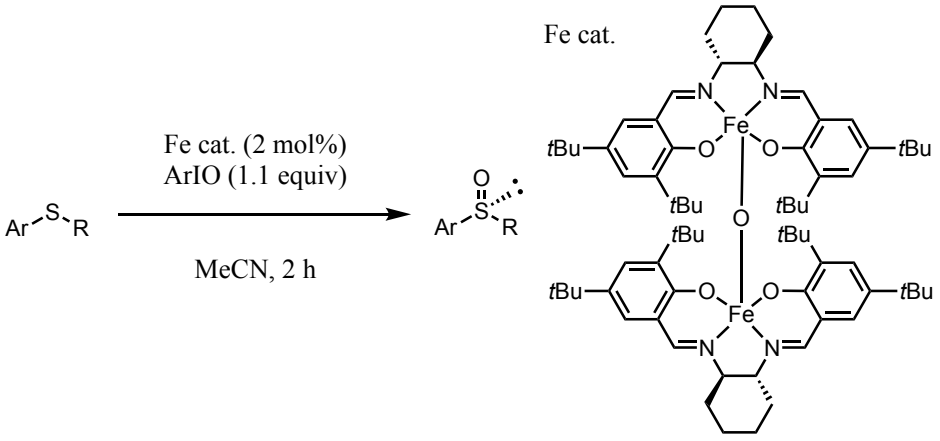

Scheme 18. Sulfoxidation reactions catalyzed by dinuclear iron complexes.

1.6 Aim and Scope of this Thesis

As an introductory text, this chapter has aimed to provide the reader with an entry into the exciting and flourishing field of non-heme iron chemistry and biochemistry. Inspired by enzymes containing either a mono- or a dinuclear non-heme iron active site, an impressive set of iron coordination compounds have been developed over the years. While some of these compounds have been illustrative with respect to the intricate reactivity of the enzymes and putative reaction intermediates involved in their chemistry, others have been turned in to useful catalysts with impressive activity and selectivity. Parallel to the realization of the widespread involvement of non-heme iron enzymes in biology, the field has by now established the richness of non-heme iron systems in synthetic chemistry, which forms the basis of the research described in this thesis.

The general aim of this thesis fucoses on bio-inspired iron oxidation catalysts based on the bis-alkylamine-bis-pyridine (N2Py2) ligand platform. Where Chapters 2-4 solely focus on iron complexes, in Chapter 5 manganese complexes with the N2Py2 ligand platform are also studied. Through the development of modified N2Py2 ligand platforms, the practical use of the corresponding iron (and manganese) complexes in selective catalytic oxidations have been studied in this thesis.

In **Chapter 2**, a new N2Py2 ligand, *N,N*′-bis(2-picolyl)-2,2′-bis-isoindoline (BPBI), has been developed, which has a further rigidified bis-alkylamine backbone based on the well-known BPBP ligand. This ligand modification follows the principle of improving the rigidity of bis-alkylamine moiety of the N2Py2 ligand platform, with the aim of achieving enhanced C–H oxidation selectivities.[131] Next to the parent BPBI ligand, a derivative ^{TIPS}BPBP with bulky

tris-(isopropyl)silyl groups at the 5-position of the pyridine moieties has also been synthesized. The corresponding iron complexes are applied to selective C−H oxidations with several benchmark alkane substrates to test their catalytic performance, with a particular focus on site-selectivity. Additionally, site-selective oxidations of steroidal compounds are also investigated using these Fe(BPBI) complexes.

Chapter 3 describes the practical use of Fe(N2Py2) complexes (including Fe(BPBI) ones developed in **Chapter 2**) in the selective epoxidation of poly-unsaturated fatty acid esters, using methyl linoleate (ML, C18:2) as a model substrate, with a specific attention on the selectivity between partial and full epoxidation. The corresponding partial and full epoxide products are industrially interesting products that can be used in different domains, as their physicochemical properties are different. The influence of various reaction parameters on the outcome of the catalytic epoxidation, including iron catalyst, solvent, temperature, and loading of reagents, have been studied. Slow addition protocols for H_2O_2 oxidant or iron catalysts are used to obtain insight into their influences on the catalytic outcomes *via* tracking of the reactions over time. Finally, the selectivity of O-distribution to mono- or di-epoxides for different catalysts are explored as well.

Although Fe(N2Py2) complexes have been widely used in oxidation reactions (e.g. C–H and C═C bond oxidations), the stability of these catalysts under the oxidizing conditions still remains a problem and attracts much less attention. Therefore, **Chapter 4** focuses on catalyst deactivation and aims to extend the lifetimes of the Fe(N2Py2) catalysts. Based on the findings of dedicated catalyst deactivation experiments, a N2Py2-D_4 ligand platform with fully deuterated 2-pyridinylmethyl positions in N2Py2 ligand is proposed. A series of N2Py2-D_4 ligands with variations on both the alkylamine and pyridine fragments are synthesized, derived from the known BPBP, BPMCN, and BPMEN ligands. The catalytic performances of the corresponding iron complexes are examined by employing them in both aliphatic C–H oxidations and alkene epoxidations with several benchmark substrates. The life-times and reactivities of these Fe(N2Py2-D_4) complexes are investigated through kinetic studies, in comparison with the parent Fe(N2Py2) complexes. Additionally, the lifetimes of the active intermediates generated under the oxidizing conditions are studied.

Compared to the dominating role of non-heme iron complexes in the field of catalytic oxidative transformations, so far, the structurally related manganese complexes are much less investigated.[156] Mn-catalyzed C–H and C═C bond oxidations have been proposed to undergo very similar reaction mechanisms to those mediated by iron complexes. Furthermore, Mn

catalysts can represent higher (even much higher) reactivities as compared to their structural Fe analogs in oxidation reactions.[157-159] Based on this, **Chapter 5** describes the use of Mn(N2Py2) type complexes in combination with H_2O_2 and acetic acid for the catalytic epoxidation of vegetable oils and their derivatives. The study is initiated by optimization of the reaction conditions for the epoxidation of a model substrate, oleic acid, using Mn(N2Py2)/H_2O_2/AcOH catalytic systems. Subsequently, the optimized reaction conditions are applied to the epoxidation of different unsaturated fatty acids and esters. Next, the attention is turned to the epoxidation of vegetable oils, using sunflower oil as model oil for the optimization of reaction conditions, with a particular focus on avoiding using MeCN as the solvent. Finally, one-pot oxidative cleavage of unsaturated fatty acids and esters into industrially interesting aldehyde products is explored, utilizing the Mn-catalyzed epoxidation as the first and key step.

1.7 References

[1] S. P. de Visser, D. Kumar, in *Iron-Containing Enzymes: Versatile Catalysts of Hydroxylation Reactions in Nature* (eds. S. P. de Visser, D. Kumar), RSC publishing, Cambridge, UK **2011**, pp. 1–4.

[2] E. I. Solomon, T. C. Brunold, M. I. Davis, J. N. Kemsley, S.- K. Lee, N. Lehnert, F. Neese, A. J. Skulan, Y.-S. Yang, J. Zhou, *Chem. Rev.* **2000**, *100*, 235–349.

[3] M. Costas, M. P. Mehn, M. P. Jensen, L. Que, Jr., *Chem. Rev.* **2004**, *104*, 939–986.

[4] B. Conley, W. J. Tenn, K. J. H. Young, S. Ganesh, S. Meier, J. Oxgaard, J. Gonzales, W. A. Goddard, R. A. Periana, in *Activation of Small Molecules: Organometallic and Bioinorganic Perspectives* (ed. W. B. Tolman), Wiley-VCH, Weinheim, Germany **2006**, pp. 235–285.

[5] L. Que, Jr., W. B. Tolman, *Nature* **2008**, *455*, 333–340.

[6] P. C. A. Bruijnincx, G. van Koten, R. J. M. Klein Gebbink, *Chem. Soc. Rev.* **2008**, *12*, 2716–2744.

[7] A. Company, L. Gómez, M. Costas, in *Iron-Containing Enzymes: Versatile Catalysts of Hydroxylation Reactions in Nature* (eds. S. P. de Visser, D. Kumar), RSC publishing, Cambridge, UK **2011**, pp. 148–208.

[8] D. T. Gibson, S. M. Resnick, K. Lee, J. M. Brand, D. S. Torok, L. P. Wackett, M. J. Schocken, B. E. Haigler, *J. Bacteriol.* **1995**, *177*, 2615–2621.

[9] L. P. Wackett, *Enzyme Microb. Technol.* **2002**, *31*, 577–587.

[10] B. Kauppi, K. Lee, E. Carredano, R. E. Parales, D. T. Gibson, H. Eklund, S. Ramaswamy, *Structure* **1998**, *6*, 571–586.

[11] B. E. Haigler, D. T. Gibson, *J. Bacteriol.* **1990**, *172*, 457–464.

[12] A. Karlsson, J. V. Parales, R. E. Parales, D. T. Gibson, H. Eklund, S. Ramaswamy, *Science* **2003**, *299*, 1039–1042.

[13] Y. Ashikawa, Z. Fujimoto, Y. Usami, K. Inoue, H. Noguchi, H. Yamane, H. Nojiri, *BMC Struct. Biol.* **2012**, 12:15.

[14] S. Chakrabarty, R. N. Austin, D. Deng, J. T. Groves, J. D. Lipscomb, *J. Am. Chem. Soc.* **2007**, *129*, 3514–3515.

[15] A. Bassan, M. R. Blomberg, P. E. Siegbahn, *J. Biol. Inorg. Chem.* **2004**, *9*, 439–452.

[16] P. D. Oldenburg, A. A. Shteinman, L. Que, Jr., *J. Am. Chem. Soc.* **2005**, *127*, 15672–15673.

[17] P. C. A. Bruijnincx, I. L. Buurmans, S. Gosiewska, M. A. H. Moelands, M. Lutz, A. L. Spek, G. van Koten, R. J. M. Klein Gebbink, *Chem. Eur. J.* **2008**, *14*, 1228–1237.

[18] *2-Oxoglutarate-Dependent Oxygenases*; C. J. Schofield, R. P. Hausinger, Eds.; RSC Metallobiology series No. 3, 2015.

[19] R. P. Hausinger, *Crit. Rev. Biochem. Mol. Biol.* **2004**, *39*, 21–68.

[20] V. Purpero, G. R. Moran, *J. Biol. Inorg. Chem.* **2007**, *12*, 587–601.

[21] C. Loenarz, C. J. Schofield, *Trends Biochem. Sci.* **2011**, *36*, 7–18.

[22] J. M. Simmons, T. A. Müller, R. P. Hausinger, *Dalton Trans.* **2008**, *38*, 5132–5142.

[23] K. P. Bryliakov, E. P. Talsi, *Coord. Chem. Rev.* **2014**, *276*, 73–96.

[24] E. Eichhorn, J. R. van der Ploeg, M. A. Kertesz, T. Leisinger, *J. Biol. Chem.* **1997**, *272*, 23031–23036.

[25] S. Ye, C. Riplinger, A. Hansen, C. Krebs, J. M. Bollinger, Jr., F. Neese, *Chem. Eur. J.* **2012**, *18*, 6555–6567.

[26] G. Schenk, M. Y. Pau, E. I. Solomon, *J. Am. Chem. Soc.* **2004**, *126*, 505–515.

[27] J. C. Price, E. W. Barr, B. Tirupati, J. M. Bollinger, Jr., C. Krebs, *Biochemistry* **2003**, *42*, 7497–7508.

[28] D. A. Proshlyakov, T. F. Henshaw, G. R. Monterosso, M. J. Ryle, R. P. Hausinger, *J. Am. Chem. Soc.* **2004**, *126*, 1022–1023.

[29] L. M. Hoffart, E. W. Barr, R. B. Guyer, J. M. Bollinger, Jr., C. Krebs, *Proc. Natl. Acad. Sci. USA* **2006**, *103*, 14738–14743.

[30] M. L. Matthews, C. M. Krest, E. W. Barr, F. H. Vaillancourt, C. T. Walsh, M. T. Green, C. Krebs, J. M. Bollinger, Jr., *Biochemistry* **2009**, *48*, 4331–4343.

[31] D. P. Galonić, E. W. Barr, C. T. Walsh, J. M. Bollinger, Jr., C. Krebs, *Nat. Chem. Biol.* **2007**, *3*, 113–116.

[32] D. G. Fujimori, E. W. Barr, M. L. Matthews, G. M. Koch, J. R. Yonce, C. T. Walsh, J. M. Bollinger, Jr., C. Krebs, P. J. Riggs-Gelasco, *J. Am. Chem. Soc.* **2007**, *129*, 13408–13409.

[33] B. E. Eser, E. W. Barr, P. A. Frantom, L. Saleh, J. M. Bollinger, Jr., C. Krebs, P. F. Fitzpatrick, *J. Am. Chem. Soc.* **2007**, *129*, 11334–11335.

[34] A. J. Panay, M. Lee, C. Krebs, J. M. Bollinger, Jr., P. F. Fitzpatrick, *Biochemistry* **2011**, *50*, 1928–1933.

[35] A. R. McDonald, Y. Guo, V. V. Vu, E. L. Bominaar, E. Münck, L. Que, Jr., *Chem. Sci.* **2012**, *3*, 1680–1693.

[36] K. Ray, F. F. Pfaff, B. Wang, W. Nam, *J. Am. Chem. Soc.* **2014**, *136*, 13942–13958.

[37] A. N. Biswas, M. Puri, K. K. Meier, W. N. Oloo, G. T. Rohde, E. L. Bominaar, E. Münck, L. Que, Jr., *J. Am. Chem. Soc.* **2015**, *137*, 2428–2431.

[38] O. Pestovsky, S. Stoian, E. L. Bominaar, X. Shan, E. Münck, L. Que, Jr., A. Bakac, *Angew. Chem. Int. Ed.* **2005**, *44*, 6871–6874.

[39] J. England, Y. Guo, E. R. Farquhar, V. G. Young, Jr., E. Münck, L. Que, Jr., *J. Am. Chem. Soc.* **2010**, *132*, 8635–8644.

[40] J. England, Y. Guo, K. M. van Heuvelen, M. A. Cranswick, G. T. Rohde, E. L. Bominaar, E. Münck, L. Que, Jr., *J. Am. Chem. Soc.* **2011**, *133*, 11880–11883.

[41] Y. Zang, J. Kim, Y. Dong, E. C. Wilkinson, E. H. Appelman, L. Que, Jr., *J. Am. Chem. Soc.* **1997**, *119*, 4197–4205.

[42] I. Siewert, C. Limberg, *Chem. Eur. J.* **2009**, *15*, 10316–10328.

[43] M. H. Sazinsky, J. Bard, A. DiDonato, S. J. Lippard, *J. Biol. Chem.* **2004**, *279*, 30600–30610.

[44] M. H. Sazinsky, P. W. Dunten, M. S. McCormick, A. DiDonato, S. J. Lippard, *Biochemistry* **2006**, *45*, 15392–15404.

[45] M. H. Sazinsky, S. J. Lippard, in *Sustaining Life on Planet Earth: Metalloenzymes Mastering Dioxygen and Other Chewy Gases* (eds. P. M. H. Kroneck, M. E. Sosa Torres), Met. Ions Life Sci. **2015**, *15*, pp. 205–256.

[46] S. Friedle, E. Reisner, S. J. Lippard, *Chem. Soc. Rev.* **2010**, *39*, 2768–2779.

[47] N. Elango, R. Radhakrishnan, W. A. Froland, B. J. Wallar, C. A. Earhart, J. D. Lipscomb, D. H. Ohlendorf, *Protein Sci.* **1997**, *6*, 556–568.

[48] A. C. Rosenzweig, C. A. Frederick, S. J. Lippard, P. Nordlund, *Nature* **1993**, *366*, 537–543.

[49] M. Merkx, D. A. Kopp, M. H. Sazinsky, J. L. Blazyk, J. Müller, S. J. Lippard, *Angew. Chem. Int. Ed.* **2001**, *40*, 2782–2807.

[50] S. Sirajuddin, A. C. Sirajuddin, *Biochemistry* **2015**, *54*, 2283–2294.

[51] C. E. Tinberg, S. J. Lippard, *Biochemistry* **2009**, *48*, 12145–12158.

[52] A. M. Valentine, S. S. Stahl, S. J. Lippard, *J. Am. Chem. Soc.* **1999**, *121*, 3876–3887.

[53] L. G. Beauvais, S. J. Lippard, *J. Am. Chem. Soc.* **2005**, *127*, 7370–7378.

[54] S. A. Stoian, G. Xue, E. L. Bominaar, L. Que, Jr., E. Münck, *J. Am. Chem. Soc.* **2014**, *136*, 1545–1558.

[55] P. E. M. Siegbahn, *Inorg. Chem.* **1999**, *38*, 2880–2889.

[56] B. F. Gherman, B. D. Dunietz, D. A. Whittington, S. J. Lippard, R. A. Friesner, *J. Am. Chem. Soc.* **2001**, *123*, 3836–3837.

[57] W.-G. Han, L. Noodleman, *Inorg. Chim. Acta* **2008**, *361*, 973– 986.

[58] M. Kodera, Y. Kawahara, Y. Hitomi, T. Nomura, T. Ogura, Y. Kobayashi, *J. Am. Chem. Soc.* **2012**, *134*, 13236–13239.

[59] M. Kodera, M. Itoh, K. Kano, T. Funabiki, M. Reglier, *Angew. Chem. Int. Ed.* **2005**, *44*, 7104–7106.

[60] M. Kodera, S. Ishiga, T. Tsuji, K. Sakurai, Y. Hitomi, Y. Shiota, P. K. Sajith, K. Yoshizawa, K. Mieda, T. Ogura, *Chem. Eur. J.* **2016**, *22*, 5924–5936.

[61] N. Kitajima, H. Amagai, N. Tamura, M. Ito, Y. Moro-oka, K. Heerwegh, A. Pénicaud, R. Mathur, C. A. Reed, P. D. W. Boyd, *Inorg. Chem.* **1993**, *32*, 3583–3584.

[62] R. Y. N. Ho, M. P. Mehn, E. L. Hegg, A. Liu, M. J. Ryle, R. P. Hausinger, L. Que, Jr., *J. Am. Chem. Soc.* **2001**, *123*, 5022–5029.

[63] M. P. Mehn, K. Fujisawa, E. L. Hegg, L. Que, Jr., *J. Am. Chem. Soc.* **2003**, *125*, 7828–7842.

[64] X. Shan, J.-U. Rohde, K. D. Koehntop, Y. Zhou, M. R, Bukowski, M. Costas, K. Fujisawa, L. Que, Jr., *Inorg. Chem.* **2007**, *46*, 8410–8417.

[65] A. Mukherjee, M. Martinho, E. L. Bominaar, E. Münck, L. Que, Jr., *Angew. Chem. Int. Ed.* **2009**, *48*, 1780 –1783.

[66] M. Sallmann, C. Limberg, *Acc. Chem. Res.* **2015**, *48*, 2734–2743.

[67] P. C. A. Bruijnincx, M. Lutz, A. L. Spek, W. R. Hagen, B. M. Weckhuysen, G. van Koten, R. J. M. Klein Gebbink, *J. Am. Chem. Soc.* **2007**, *129*, 2275–2286.

[68] M. A. H. Moelands, S. Nijsse, E. Folkertsma, B. de Bruin, M. Lutz, A. L. Spek, R. J. M. Klein Gebbink, *Inorg. Chem.* **2013**, *52*, 7394–7410.

[69] M. A. H. Moelands, S D. J. Chamhart, E. Folkertsma, M. Lutz, A. L. Spek, R. J. M. Klein Gebbink, *Dalton Trans.* **2014**, *43*, 6769–6785.

[70] E. Folkertsma, E. F. de Waard, G. Korpershoek, A. J. van Schaik, N. Solozabal Mirón, M. Borrmann, S. Nijsse, M. A. H. Moelands, M. Lutz, M. Otte, M.-E. Moret, R. J. M. Klein Gebbink, *Eur. J. Inorg. Chem.* **2016**, *2016*, 1319–1332.

[71] A. Beck, B. Weibert, N. Burzlaff, *Eur. J. Inorg. Chem.* **2001**, 521–527,

[72] A. Beck, A. Barth, E. Hubner, N. Burzlaff, *Inorg. Chem.* **2003**, *42*, 7182–7188.

[73] G. Olivo, O. Cussó, M. Costas, *Chem. Asian J.* **2016**, *11*, 3148–3158.

[74] J. England, M. Martinho, E. R. Farquhar, J. R. Frisch, E. L. Bominaar, E. Münck, L. Que, Jr., *Angew. Chem. Int. Ed.* **2009**, *48*, 3622–3626.

[75] W. O. Koch, V. Schünemann, M. Gerdan, A. X. Trautwein, H.-J. Krüger, *Chem. Eur. J.* **1998**, *4*, 686–691.

[76] W. O. Koch, V. Schünemann, M. Gerdan, A. X. Trautwein, H.-J. Krüger, *Chem. Eur. J.* **1998**, *4*, 1255–1265.

[77] J. Serrano-Plana, F. Acuña-Parés, V. Dantignana, W. N. Oloo, E. Castillo, A. Draksharapu, C. J. Whiteoak, V. Martin-Diaconescu, M. G. Basallote, J. M. Luis, L. Que, Jr., M. Costas, A. Company, *Chem. Eur. J.* **2018**, *24*, 5331–5340.

[78] J. Serrano-Plana, W. N. Oloo, L. Acosta-Rueda, K. K. Meier, B. Verdejo, E. García-España, M. G. Basallote, E. Münck, L. Que, A. Company, M. Costas,, *J. Am. Chem. Soc.* **2015**, *137*, 15833–15842.

[79] J. F. Berry, E. Bill, E. Bothe, T. Weyhermüller, K. Wieghardt, *J. Am. Chem. Soc.* **2005**, *127*, 11550–11551.

[80] J. F. Berry, E. Bill, R. García-Serres, F. Neese, T. Weyhermüller, K. Wieghardt, *Inorg. Chem.* **2006**, *45,* 2027–2037.

[81] J. F. Berry, E. Bill, E. Bothe, S. D. George, B. Mienert, F. Neese, K. Wieghardt, *Science* **2006,** *312.* 1937–1941.

[82] J. F. Berry, E. Bill, E. Bothe, F. Neese, K. Wieghardt, *J. Am. Chem. Soc.* **2006**, *128,* 13515–13528.

[83] A. Trehoux, J.-P. Mahy, F. Avenier, *Coord. Chem. Rev.* **2016**, *322*, 142–158.

[84] L. H. Do, S. J. Lippard, *J. Inorg. Biochem.* **2011,** *105*, 1774–1785.

[85] L. H. Do, S. J. Lippard, *J. Am. Chem. Soc.* **2011**, *133*, 10568–10581.

[86] Y. Li, C. M. M. Soe, J. J. Wilson, S. L. Tuang, U.-P. Apfel, S. J. Lippard, *Eur. J. Inorg. Chem.* **2013**, 2011–2019.

[87] S. J. Friese, B. E. Kucera, V. G. Young, Jr. L. Que, Jr., W. B. Tolman, *Inorg. Chem.* **2008**, *47*, 1324–1331.

[88] S. V. Kryatov, F. A. Chavez, A. M. Reynolds, E. V. Rybak-Akimova, L. Que, Jr., W. B. Tolman, *Inorg. Chem.* **2004**, *43*, 2141–2150.

[89] S. Alvarez, J. Cirera, *Angew. Chem. Int. Ed.* **2006**, *45*, 3012–3020.

[90] M. A. Halcrow, *Chem. Commun.* **2013**, *49*, 10890–10892.

[91] P. Gütlich, A. B. Gaspar, Y. Garcia, *Beilstein J. Org. Chem.* **2013**, *9*, 342–391.

[92] D. Schröder, S. Shaik, H. Schwarz, *Acc. Chem. Res.* **2000**, *33*, 139–145.

[93] D. Usharani, B. Wang, D. A. Sharon, S. Shaik, in *Spin States in Biochemistry and Inorganic Chemistry: Influence on Structure and Reactivity* (eds. M. Swart, M. Costas), Wiley, New Jersey, USA **2015**, pp. 131–156.

[94] M. Newcomb, P. H. Toy, *Acc. Chem. Res.* **2000**, *33*, 449–455.

[95] R. M. Burger, *Chem. Rev.* **1998**, *98*, 1153–1169.

[96] J. W. Sam, X. Y. Tang, J. Peisach, *J. Am. Chem. Soc.* **1994**, *116*, 5250–5256.

[97] R. M. Burger, J. Peisach, S. B. Horwitz, *J. Biol. Chem.* **1981**, *256*, 11636–11644.

[98] M. S. Chow, L. V. Liu, E. I. Solomon, *Proc. Natl. Acad. Sci. USA* **2008**, *105*, 13241– 13245.

[99] A. Decker, M. S. Chow, J. N. Kemsley, N. Lehnert, E. I. Solomon, *J. Am. Chem. Soc.* **2006**, *128*, 4719–4733.

[100] J. Cho, S. Jeon, S. A. Wilson, L. V. Liu, E. A. Kang, J. J. Braymer, M. H.Lim, B. Hedman, K. O. Hodgson, J. S. Valentine, E. I. Solomon, W. Nam, *Nature* **2011**, *478*, 502–505.

[101] Y. M. Kim, K.-B. Cho, J. Cho, B. Wang, C. Li, S. Shaik, W. Nam, *J. Am. Chem. Soc.* **2013**, *135*, 8838–8841.

[102] L. V. Liu, S. Hong, J. Cho, W. Nam, E. I. Solomon, *J. Am. Chem. Soc.* **2013**, *135*, 3286 –3299.

[103] C.-W. Chiang, S. T. Kleespies, H. D. Stout, K. K. Meier, P.-Y. Li, E. L. Bominaar, L. Que, Jr., E. Münck, W.-Z. Lee, *J. Am. Chem. Soc.* **2014**, *136*, 10846–10849.

[104] X. Shan, L. Que, Jr., *Proc. Natl. Acad. Sci. USA* **2005**, *102*, 5340–5345.

[105] M. Zhao, B. Helms, E. Slonkina, S. Friedle, D. Lee, J. DuBois, B. Hedman, K. O.Hodgson, J. M. J. Fréchet, S. J. Lippard, *J. Am. Chem. Soc.* **2008**, *130*, 4352–4363.

[106] C. A. Grapperhaus, B. Mienert, E. Bill, T. Weyhermüller, K. Wieghardt, *Inorg. Chem.* **2000**, *39*, 5306–5317.

[107] J.-U. Rohde, J.-H. In, M. H. Lim, W. W. Brennessel1, M. R. Bukowski, A. Stubna, E. Münck, W. Nam, L. Que Jr., *Science* **2003**, *299*, 1037–1039.

[108] M. Puri, L. Que, Jr., *Acc. Chem. Res.* **2015**, *48*, 2443–2452.

[109] J. P. Bigi, W. H. Harman, B. Lassalle-Kaiser, D. M. Robles, T. A. Stich, J. Yano, R. D. Britt, C. J. Chang, *J. Am. Chem. Soc.* **2012**, *134*, 1536–1542.

[110] D. Wang, K. Ray, M. J. Collins, E. R. Farquhar, J. R. Frisch, L. Gómez, T. A. Jackson, M. Kerscher, A. Waleska, P. Comba, M.Costas, L. Que, Jr., *Chem. Sci.* **2013**, *4*, 282–291.

[111] J. Kaizer, E. J. Klinker, N. Y. Oh, J.-U. Rohde, W. J. Song, A. Stubna, J. Kim, E. Münck, W. Nam, L. Que, Jr., *J. Am. Chem. Soc.* **2004**, *126*, 472–473.

[112] S. Ye, F. Neese, *Proc. Natl. Acad. Sci. USA* **2011**, *108*, 1228–1233.

[113] S. Shaik, H. Hirao, D. Kumar, *Acc. Chem. Res.* **2007**, *40*, 532–542.

[114] K.-B. Cho, S. Shaik, W. Nam, *Chem. Commun.* **2010**, *46*, 4511–4513.

[115] K. Chen, L. Que, Jr., *J. Am. Chem. Soc.* **2001**,*123*, 6327–6337.

[116] I. Prat, J. S. Mathieson, M. Güell, X. Ribas, J. M. Luis, L. Cronin, M. Costas, *Nat. Chem.* **2011**, *3*, 788–793.

[117] O. Y. Lyakin, I. Prat, K. P. Bryliakov, M. Costas, E. P. Talsi, *Catal. Commun.* **2012**, *29*, 105–108.

[118] F. T. de Oliveira, A. Chanda, D. Banerjee, X. Shan, S. Mondal, L. Que, Jr., E. L. Bominaar, E. Münck, T. J. Collins, *Science* **2007**, *315*, 835–838.

[119] M. Ghosh, K. K. Singh, C. Pand, A. C. Weitz, M. P. Hendrich, T. J. Collins, B. B. Dhar, S. S. Gupta, *J. Am. Chem. Soc.* **2014**, *136*, 9524–9527.

[120] O. Y. Lyakin, K. P. Bryliakov, G. J. P. Britovsek, E. P. Talsi, *J. Am. Chem. Soc.* **2009**, *131*, 10798–10799.

[121] Y. Wang, D. Janardanan, D. Usharani, K. Han, L. Que, Jr., S. Shaik, *ACS Cat.* **2013**, *3*, 1334–1341

[122] A. Lennartson, C. J. McKenzie, *Angew. Chem. Int. Ed.* **2012**, *51*, 6767–6770.

[123] S. Hong, B. Wang, M. S. Seo, Y.–M.Lee, M. J. Kim, H. R.Kim, T. Ogura, R. Garcia-Serres, M. Clémancey, J.-M. Latour, W. Nam, *Angew. Chem. Int. Ed.* **2014**, *53*, 6388–6392.

[124] A. Draksharapu, D. Angelone, M. G. Quesne, S. K. Padamati, L. Gõmez, R. Hage, M. Costas, W. R. Browne, S. P. de Visser, *Angew. Chem. Int. Ed.* **2015**, *54*, 4357–4361

[125] G. Xue, D. Wang, R. de Hont, A. T. Fiedler, X. Shan, E. Münck, L. Que, Jr., *Proc. Natl. Acad. Sci. USA* **2007**, *104*, 20713–20718.

[126] G. Xue, A. Pokutsa, L. Que, Jr., *J. Am. Chem. Soc.* **2011**,*133*, 16657–16667.

[127] G. Xue, R. de Hont, E. L. Münck, L. Que, Jr., *Nat. Chem.* **2010**, *2*, 400–405.

[128] M. Canta, M. Rodríguez, M. Costas, *Top Curr Chem.* **2016**, *372*, 27–54.

[129] C. Kim, K. Chen, J. Kim, L. Que, Jr., *J. Am. Chem. Soc.* **1997**, *119*, 5964–5965.

[130] K. Chen, M. Costas, L. Que, Jr., *J. Chem. Soc. Dalton Trans*. **2002**, 672–679.

[131] M. S. Chen, M. C. White, *Science* **2007**, *318*, 783–787.

[132] M. S. Chen, M. C.White, *Science* **2010**, *327*, 566–571.

[133] M. Canta, D. Font, L. Gomez, X. Ribas, M. Costas, *Adv. Synth. Catal.* **2014**, *356*, 818–830.

[134] P. E. Gormisky, M. C. White, *J. Am. Chem. Soc.* **2013**, *135*, 14052–14055.

[135] D. Font, M. Canta, M. Milan, O. Cussó, X. Ribas, R. J. M. Klein Gebbink, M. Costas, *Angew. Chem. Int. Ed.* **2016**, *55*, 5776–5779.

[136] E. P. Talsi, K. P. Bryliakov, *Coord. Chem. Rev.* **2012**, *256*, 1418–1434.

[137] G. Anilkumar, B. Bitterlich, F. G. Gelalcha, M. K. Tse, M. Beller, *Chem. Commun.* **2007**, 289–291.

[138] F. G. Gelalcha, B. Bitterlich, G. Anilkumar, M. K. Tse, M. Beller, *Angew. Chem. Int. Ed.* **2007**, 47, 7293–7296.

[139] O. Cussó, I. Garcia-Bosch, X. Ribas, J. Lloret-Fillol, M. Costas, *J. Am. Chem. Soc.* **2013**, *135*, 14871–14878.

[140] O. Cussó, X. Ribas, J. Lloret-Fillol, M. Costas, *Angew. Chem. Int. Ed.* **2015**, *54*, 2729–2733.

[141] A. Company, L. Gómez, X. Fontrodona, X. Ribas, M. Costas, *Chem. Eur. J.* **2008**, *14*, 5727–5731.

[142] K. L. Klotz, L. M. Slominski, A. V. Hull, V. M. Gottsacker, R. Mas-Balleste, L. Que, Jr., J. A. Halfen, *Chem. Commun.* **2007**, 2063–2065.

[143] K. L. Klotz, L. M. Slominski, M. E. Riemer, J. A. Phillips, J. A. Halfen, *Inorg. Chem.* **2009**, *48*, 801–803.

[144] B. P. Murch, F. C. Bradley, L. Que, Jr., *J. Am. Chem. Soc.* **1986**, *108*, 5027–5028.

[145] M. C. White, A. G. Doyle, E. N. Jacobsen, *J. Am. Chem. Soc.* **2001**, *123*, 7194–7195.

[146] G. Dubois, A. Murphy, T. D. P. Stack, *Org. Lett.* **2003**, *5*, 2469–2472.

[147] J. F. Wie, X. D. Yu, D. S. Jin, *Chin. Chem. Lett.* **1996**, *7*, 962–964.

[148] C. Marchi-Delapierre, A. Jorge-Robin, A. Thibon, S. Ménage, *Chem. Commun.* **2007**, 1166–1168.

[149] H.-L. Yeung, K.-C. Sham, C.-S. Tsang, T.-C. Lau, H.-L. Kwong, *Chem. Commun.* **2008**, 3801–3803.

[150] M. Jarenmark, E. A. Turitsyna, M. Haukka, A. A. Shteinman, E. Norlander, *New. J. Chem.* **2010**, *34*, 2118–2121.

[151] B. Das, A. Al-Hunaiti, M. Haukka, S. Demeshko, S. Meyer, A. A. Shteinmann, F. Meyer, T. Repo, E. Nordlander, *Eur. J. Inorg. Chem.* **2015**, 3590–3601.

[152] F. Avenier, J.-M. Latour, *Chem. Commun.* **2004**, 1544–1545.

[153] E. Gouré, F. Avenier, P. Dubourdeaux, O. Sénèque, F. Albrieux, C. Lebrun, M. Clémancey, P. Maldivi, J.-M. Latour, *Angew. Chem. Int. Ed.* **2014**, *53*, 1580–1584.

[154] K. P. Bryliakov, E. P. Talsi, *Chem. Eur. J.* **2007**, *13*, 8045–8050.

[155] A. Trehoux, Y. Roux, R. Guillot, J.-P. Mahy, F. Avenier, *J. Mol. Catal. A-Chem.* **2015**, *396*, 40–46.

[156] R. V. Ottenbacher, E. P. Talsi, K. P. Bryliakov, *Molecules* **2016**, *21*, 1454.

[157] D. Shen, C. Miao, D. Xu, C. Xia, W. Sun, *Org. Lett.* **2015**, *17*, 54–57.

[158] R. V. Ottenbacher, D. G. Samsonenko, E. P. Talsi, K. P. Bryliakov, *Org. Lett.* **2012**, *14*, 4310–4313.

[159] O. Y. Lyakin, R. V. Ottenbacher, K. P. Bryliakov, E. P. Talsi, *ACS Catal.* **2012**, *2*, 1196–1202.

Chapter 2

Non-Heme Iron Catalysts with a Rigid Bis-Isoindoline Backbone and Their Use in Selective Aliphatic C–H Oxidation

Abstract

Iron complexes derived from a bis-isoindoline-bis-pyridine ligand platform based on the BPBP ligand (BPBP = *N,N*′-bis(2-picolyl)-2,2′-bis-pyrrolidine) have been synthesized and applied in selective aliphatic C–H oxidation with hydrogen peroxide under mild conditions. The introduction of benzene moieties on the bis-pyrrolidine backbone leads to an increased preference of tertiary over secondary C–H bond oxidation (3°/2° ratio up to 33). On the other hand, substituting the meta-position of the pyridines with bulky silyl groups affords enhanced secondary C–H oxidation selectivity and generally leads to higher product yields and mass balances.

This chapter is based on:

J. Chen, M. Lutz, M. Milan, M. Costas, M. Otte, R. J. M. Klein Gebbink, *Adv. Synth. Catal.* **2017**, *359*, 2590–2595.

2.1 Introduction

Oxidation of aliphatic C–H groups is of particular interest in organic synthesis due to the large abundance of aliphatic moieties in natural products and petrochemical platform molecules, as well as the added value of their corresponding hydroxyl and carbonyl compounds.[1–5] To date, a vast number of iron-containing enzymes, such as methane monooxygenase (MMO) and α-ketoglutarate-(α-KG)-dependent dioxygenases (see Chapter 1 of this thesis), have been revealed to perform biological C–H oxidations through the activation of dioxygen in a selective manner.[6,7] Inspired by these enzymes, the past decades have witnessed the development of a variety of biomimetic non-heme iron catalysts.[8–10] In 1997,[11] a synthetic Fe coordination complex was firstly demonstrated to be capable of stereospecific alkane hydroxylation by Que and co-workers, where the tetradentate N-donor ligand TPA (tris(2-pyridylmethyl)amine) was employed and H_2O_2 was used as terminal oxidant. Since then, several Fe complexes based on tetradentate N4 ligands have been developed.[12–18] Amongst them, iron complexes featuring bis-alkylamine-bis-pyridine (N2Py2) ligands have been proven to be the most effective.[19] However, modifications of this ligand platform often ended up with lower efficiency.[19] These studies were mainly done under large excess of substrate and had limited interest from a synthetic perspective. However, in 2007,[20] White and co-workers described catalytic oxidations under substrate limiting conditions. In this work, a ligand modification strategy was introduced that rigidifies the bis-alkylamine backbone by incorporating the alkylamines into pyrrolidines, forming the BPBP ligand (BPBP = *N,N*′-bis(2-picolyl)-2,2′-bis-pyrrolidine; Figure 1, left), which translated into improved product selectivities.[20] A similar strategy was adopted by Rybak-Akimova and co-workers, where they rigidified the alkylamine moiety into 6-membered piperidine rings.[21] Many efforts have been spent on the modification of the pyridine moieties as well.[22–26] It has recently been reported that the introduction of bulky TIPS (*tris*-(isopropyl)silyl) groups at the meta-position of the pyridine rings will lead to increased secondary C–H oxidation and improved mass balance.[27] Through this modification, site-selective methylene oxidation of steroidal substrates has also been achieved.

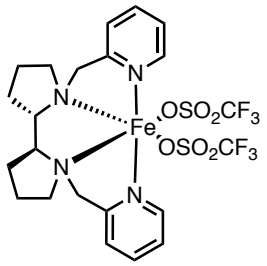

[Fe(OTf)$_2$(*S,S*-BPBP)]
1

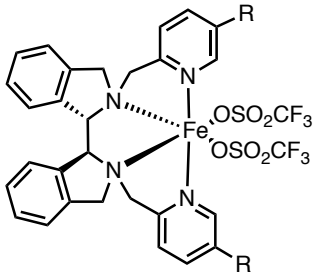

[Fe(OTf)$_2$(*S,S*-^{R}BPBI)]
2: R = H
3: R = TIPS

Figure 1. Complexes **1**-**3** studied in this chapter.

With the goal of achieving enhanced C–H oxidation selectivities, iron complex [Fe(OTf)$_2$(*S,S*-BPBI)] (**2**) (BPBI = (*N,N*′-bis(2-picolyl)-2,2′-bis-isoindoline) and its TIPS substituted analogue [Fe(OTf)$_2$(*S,S*-^{TIPS}BPBI)] **3** (Figure 1), which bear a further rigidified bis-isoindoline backbone compared to the bis-pyrrolidine in the BPBP ligand, are developed in this chapter. BPBI complex **2** is found to give rise to higher tertiary over secondary C–H oxidation selectivities than the parent complex [Fe(OTf)$_2$(*S,S*-BPBP)] (**1**). On the other hand, **3** exhibits enhanced secondary C–H oxidation ability and increased product yields.

2.2 Results and Discussion

2.2.1 Synthesis and characterization of iron complexes

The chiral (*S,S*)-bis-isoindoline backbone of the BPBI ligand was prepared according to a previously reported procedure.[28] It was readily converted into target complexes **2** and **3** by alkylation with 2-picolyl chloride derivatives and subsequent complexation with Fe(OTf)$_2$·2CH$_3$CN (see Experimental Section). Figure 2a shows the X-ray crystal structures of complexes **2** and **3**. The absolute structure of the two complexes was proven by the Flack parameter (see Experimental Section) and similarly to **1**, they also feature a *cis*-α coordination topology, which has been shown a crucial factor for good catalytic efficiency in previous studies.[29–31] In complex **3**, the installation of bulky TIPS groups on the two pyridines leads to a crowded envelope-like configuration around the *cis* labile positions of the iron center[27] (Figure 2a, right, also see Figure 2b), where the plausible reactive Fe-oxo species that is responsible for site selective C–H oxidation is generated.[32] In this sense, the bulky nature may result in modulated regioselectivity.

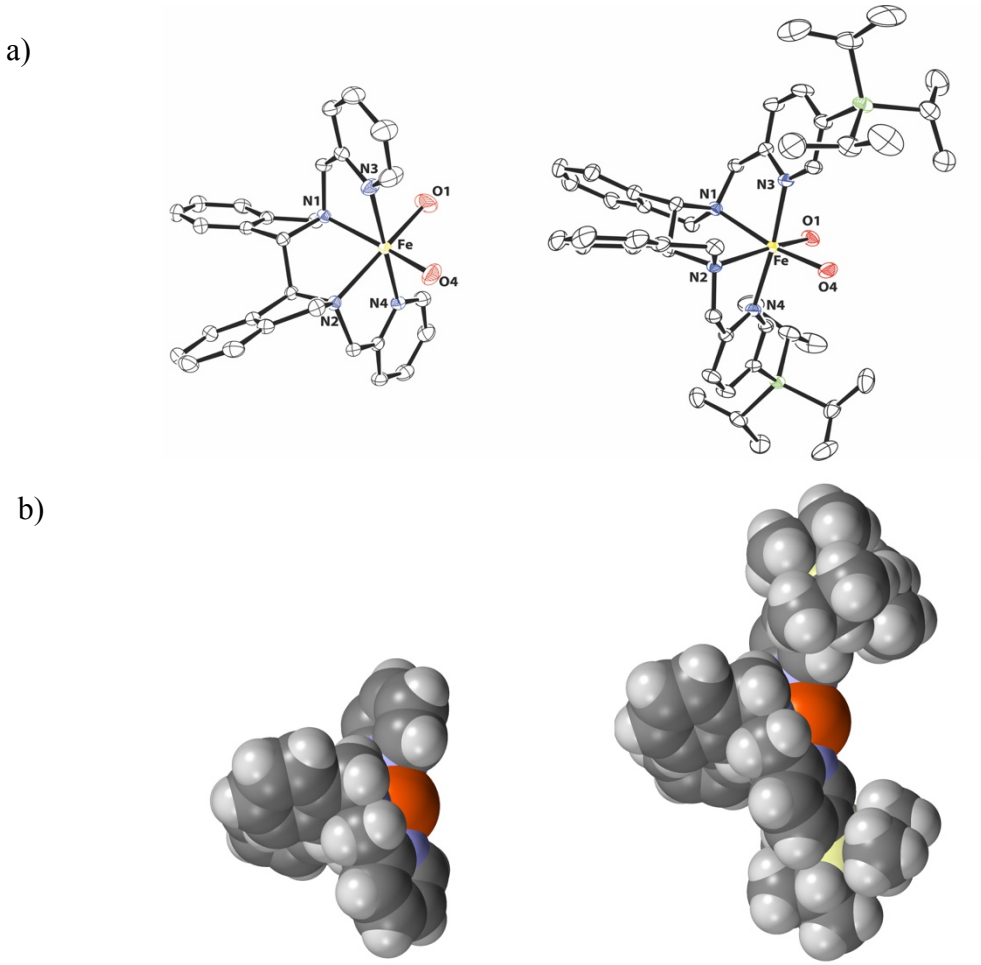

Figure 2. a) Molecular structures of **2** (left) and **3** (right) in the crystal, drawn at the 50% probability level.[33] Only the coordinated O atoms of the triflate groups are shown. Hydrogen atoms, solvent molecules and the second independent molecule of **3** are omitted for clarity. b) Space-filling models of complex **2** (left) and **3** (right). Only the iron centre and the coordinated ligand are shown.

Only slight differences are seen between the three complexes for the bond lengths and angles of the Fe coordination environment. Selected bond lengths and angles for (*R*,*R*)-**1**[34], (*S*,*S*)-**2** and (*S*,*S*)-**3** are listed in Table 1. As expected, the Fe-N(pyridine) distances (2.1390(4)-2.192(3) Å) are shorter than the Fe-N(amine) distances of 2.199(3)-2.2249(14) Å. This difference is more distinct in **2** and **3** compared to **1**. Overall, these long Fe-N distances are consistent with high-spin Fe(II) complexes.[30,35] The main differences in the crystal structures are found for the orientation of the triflate ligands. Slightly smaller O-Fe-O angles in **3** (100.17(6) and 100.56(6)°) are observed compared to **2** (102.49(15)°), which might be due to the larger steric demand of the ligand in **3**; the smallest O-Fe-O angle is found in **1**. A quaternion fit of **1** and **2** clearly shows that the BPBP and BPBI ligands provide a very similar steric environment around the iron center (Figure 3). Interestingly, ^{1}H NMR spectra of complex **2** and **3** show a single paramagnetic species, indicating that these complexes have a high-spin state in solution and that the C2 symmetric structure of the complexes is retained in solution. Cyclic voltammetry

measurements showed that **2** and **3** have very similar Fe(II)/Fe(III) potentials ($E_{1/2}$ = 0.82, 0.81 V, respectively). These values are somewhat more positive than that of **1** ($E_{1/2}$ = 0.70 V), which is likely due to the electron-withdrawing property of the benzene rings in the BPBI ligand.

Table 1. Selected bond lengths (Å) and angles (°) for (*R*,*R*)-**1**[34], (*S*,*S*)-**2** and (*S*,*S*)-**3**.

Distance(Å) /Angle (°)	(*R*, *R*)-**1**[a)]	(*S*,*S*)-**2**	(*S*,*S*)-**3**[b)]	
Fe-N1	2.203(3)	2.215(2)	2.2244(14)	2.2249(14)
Fe-N2	2.199(3)	2.206(2)	2.2152(14)	2.2243(14)
Fe-N3	2.192(3)	2.164(3)	2.1624(14)	2.1582(14)
Fe-N4	2.192(3)	2.156(3)	2.1390(14)	2.1511(14)
Fe-O1	2.110(3)	2.085(3)	2.1178(13)	2.0768(14)
Fe-O4	2.104(3)	2.102(3)	2.1001(13)	2.1136(13)
N1-Fe-N3	76.16(11)	77.26(9)	76.73(5)	77.09(5)
N2-Fe-N4	76.63(11)	77.95(9)	77.38(5)	76.80(5)
O1-Fe-O4	95.28(11)	102.49(15)	100.17(6)	100.65(6)

[a)] Crystallographic data for (*R*, *R*)-**1** was obtained from ref. 34. Structural data for (*S*,*S*)-**1** is not available. Structural parameters for [Fe(*S*,*S*-BPBP)$(CH_3CN)_2$]$(SbF_6)_2$ are very similar to those of (S,S)-**1**. [b)] Two independent molecules in the asymmetric unit.

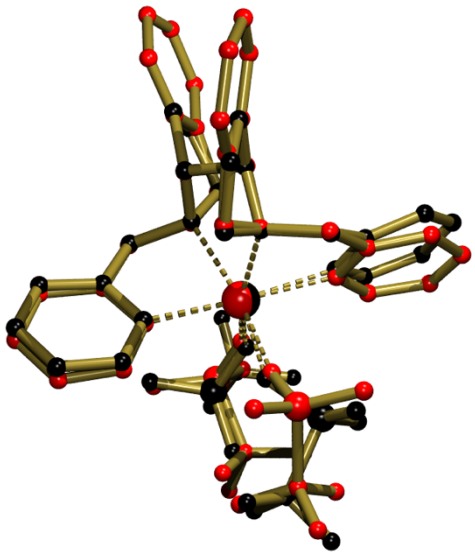

Figure 3. Quaternion fit of the molecular structures of (*R*, *R*)-**1** (black)[34] and **2** (red). The fit is based on the metal and its six coordinating atoms and performed with the PLATON program.[36] The overlay plot of these two molecules was made by overlapping the iron centers and the corresponding mirror symmetrical N and O atoms for each molecule, so that (*R*,*R*)-**1** and (*S*,*S*)-**2** can be overlapped with the same stereochemistry.

2.2.2 Catalytic performances in aliphatic C–H oxidation

With **2** and **3** in hand, their ability to catalyse the oxidation of aliphatic C–H bonds was investigated. To do so, a set of substrates consisting of cyclohexane (**4**), *cis*-1,2-dimethylcyclohexane (**7**), *trans*-1,2-dimethylcyclohexane (**11**), *trans*-decalin (**15**), adamantane (**19**), L-(−)-menthyl acetate (**23**) and methyl hexanoate (**26**) has been studied. For comparison purpose, complex **1** bearing the structurally related BPBP ligand was also tested.

Table 2. Cyclohexane Oxidation by **1**, **2** and **3**.[a)]

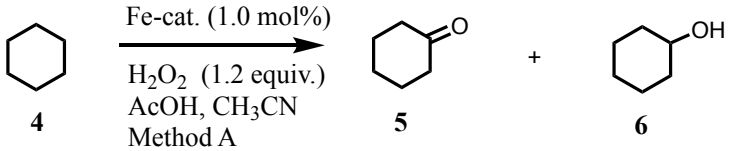

4 **5** **6**

Substrate	cat.	**5**, **6** (%)[b)]	Conv. (%)[b)]	K/A[c)]	Mass balance (%)
4	**1**	16.7, 2.4	45	7.0	42
4	**2**	8.8, 5.9	42	1.5	35
4	**3**	27, 6.8	64	4.0	53

[a)] Reaction conditions (method A): Fe-cat. : H_2O_2 : substrate : AcOH = 1 : 120 : 100 : 50, 0 °C, oxidant added by syringe pump over 6 min, and reaction mixture stirred for additional 10 min. [b)] Determined by GC analysis, average value of two runs. [c)] Ketone/alcohol ratio = **5**/**6**.

Using 1.0 mol% catalyst loading, cyclohexane (**4**) is oxidized to cyclohexanone (**5**) and cyclohexanol (**6**) in the presence of 1.2 equiv. H_2O_2 and 0.5 equiv. acetic acid in CH_3CN at 0 ^oC. For all three catalysts, **5** is formed as the major product (**5** is formed through oxidation of initially generated **6** due to the substrate limiting reaction conditions). Reaction with **1** gives a higher ketone to alcohol (K/A) ratio compared to **2** (7.0 over 1.5, Table 2). With **3** a medium K/A ratio (4.0) was observed, albeit with the highest substrate conversion and mass balance amongst the three complexes (64% and 53%, respectively).

The ability of these complexes to discriminate between tertiary and secondary C–H bonds is illustrated by the 3°/2° ratios in the oxidation of **7, 11, 15** and **19**, which have multiple secondary and tertiary C–H sites (Table 3). Oxidation of **7** catalyzed by **1** generates 3° oxidation product **8** as the major product with 2° oxidation products **9** and **10** as minor products, affording a 3°/2° ratio of 7.0. The corresponding 3°/2° ratio was found to increase to 8.8 when changing the catalyst to **2**, along with the decrease in conversion from 61% to 32% (Table 3). The oxidation of tertiary over secondary C–H bonds is less preferential when performing this reaction with **3**

Table 3. Oxidation of substrates **7, 11, 15** and **19**.[a)]

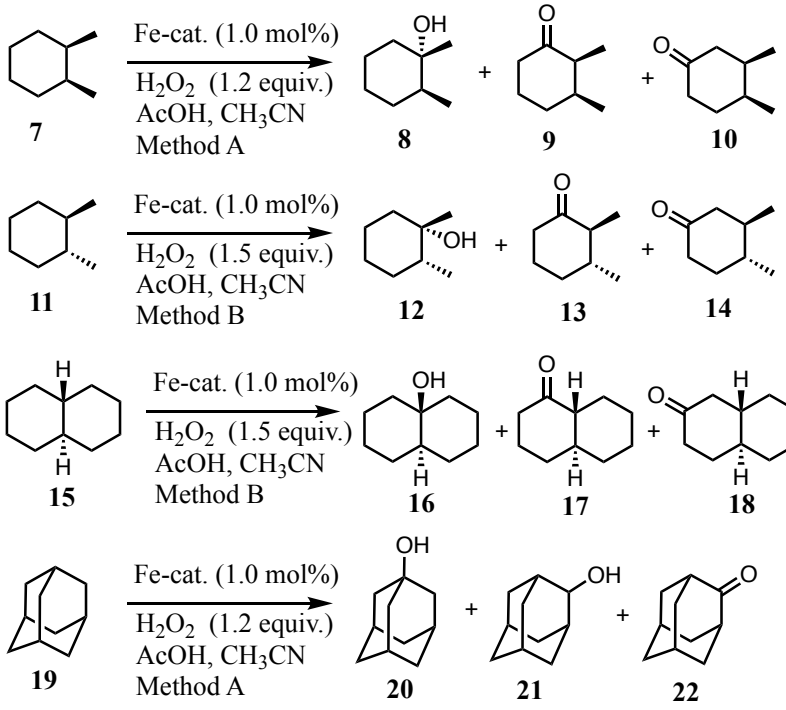

Alkane	cat.	**8**, **9**, **10** (%)[b)]	Conv. (%)[b)]	3°/2°[c)]	Mass balance (%)
7	**1**	39, 2.6, 3.0	61	7.0	73
7	**2**	22, 1.2, 1.3	32	8.8	77
7	**3**	37, 4.1, 3.9	65	4.6	69
Alkane	cat.	**12**, **13**, **14** (%)[b)]	Conv. (%)[b)]	3°/2°[d)]	Mass balance (%)
11	**1**	11, 3.7, 7.6	27	1.0	83
11	**2**	6.2, 1.6, 2.9	15	1.4	71
11	**3**	8.9, 7.5, 19	47	0.3	75
Alkane	cat.	**16**, **17**, **18** (%)[b)]	Conv. (%)[b)]	3°/2°[e)]	Mass balance (%)
15	**1**	5.5, 10.7, 17	53	0.2	62
15	**2**	5.6, 6.7, 9.2	36	0.35	60
15	**3**	2.2, 11.8, 21	60	0.07	59
Alkane	cat.	**20**, **21**, **22** (%)[b)]	Conv. (%)[b]	3°/2°[f)]	Mass balance (%)
19	**1**	14, 0.3, 1.6	38	21	42
19	**2**	24, 0.5, 1.7	40	33	66
19	**3**	24, 1.1, 3.3	53	16	54

[a)] For substrate **7** and **19**, method A is used. For substrate **11** and **15**, method B is used: Fe-cat. : H_2O_2 : substrate : AcOH = 1 : 150 : 100 : 50, 0 °C, oxidant added by syringe pump over 30 min, and reaction mixture stirred for additional 1.5 h. [b)] Determined by GC analysis, average value of two runs. [c)] 3°/2° = **8**/(**9** + **10**). [d)] 3°/2° = **12**/(**13** + **14**) [e)] 3°/2° = **16**/(**17** + **18**) [f)] 3°/2° = 3 x **20**/(**21** + **22**).

(with a value of 4.6, Table 3). This observation is consistent with a previous study, which showed that the introduction of bulky TIPS groups can lead to an enhanced 2°/3° C–H oxidation ratio, because oxidation of the sterically more congested tertiary C-H bond is disfavored.[27] Similarly, a slightly higher 3°/2° ratio (1.4) is found for **2** in the oxidation of **11** than for **1** (1.0). Much more secondary oxidized products are formed in the reaction catalyzed by **3**, giving a 3°/2° ratio of 0.3.

Similar catalytic outcomes were found in the oxidations of **15** and **19** in the presence of **1**-**3**. The tertiary C–H oxidation products are more preferentially formed in the reactions with **2** than in the cases of **1** and **3**, with a 3°/2° ratio of 0.35 in the case of **15** and 33 in the case of **19** (Table 3). Notably, the latter ratio is amongst the highest reported 3°/2° selectivities for non-heme Fe-catalyzed adamantane oxidation.[8,37,38] The lowest 3°/2° ratios (0.07 and 16, respectively) were observed for complex **3**, further supporting the enhanced ability of **3** to catalyze secondary C–H oxidations. For the reactivities of the reactions in Table 3, **3** stands out amongst these three complexes with highest conversions.

The oxidations of unfunctionalized aliphatic alkanes **4**, **7**, **11**, **15**, and **19** give different outcomes, responding to the structural changes in complexes **1**-**3**. The change in ligand backbone from bis-pyrrolidine in **1** to more rigid bis-isoindoline in **2** gives rise to a higher alcohol selectivity (Table 2) and improved 3°/2° ratios (Table 3). On the contrary, enhanced selectivities for methylene are achieved when **3** is applied. These observations stimulated the interest in the oxidation of functionalized aliphatic substrates.

To probe the steric effect on the oxidation site selectivity, the oxidation of L-(−)-menthyl acetate (**23**), containing two tertiary C–H bonds (both at a γ-position to the acetoxy group) with different steric environments, by complexes **1**-**3** was examined (Table 4). The lower steric hindrance hydroxylation product **24** was preferentially formed in the oxidation of **23** for all catalysts tested, indicating that these reactions in the presence of **1**-**3** are sensitive to steric factors. No difference in the preference of formation of **24** were observed, i.e., in all the cases, **24**/**25** ratios around 5.4 were found (Table 4). In terms of conversion and mass balance, **3** outperformed the other catalysts.

Table 4. Oxidation of substrate **23** and **26** by **1**, **2** and **3**.[a)]

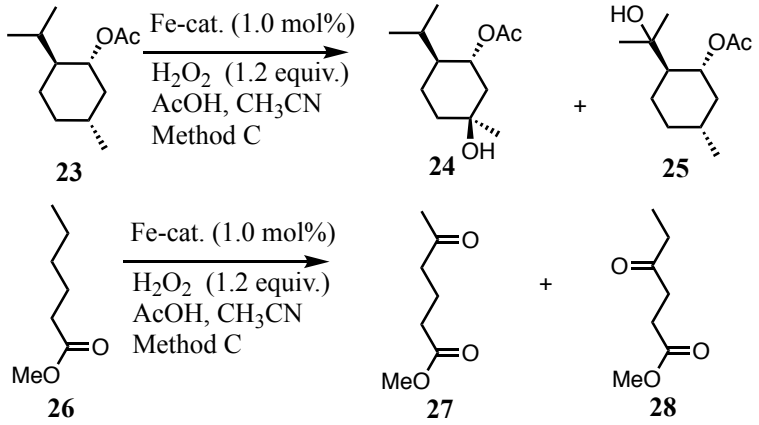

Substrate	cat.	**24**, **25** (%)[b)]	Conv. (%)[b)]	**24**/**25**	Mass balance (%)
23	**1**	28, 5.2	40	5.4	83
23	**2**	19, 3.6	30	5.3	75
23	**3**	30, 5.5	40	5.5	89
Substrate	cat.	**27**, **28** (%)[b)]	Conv. (%)[b]	**27**/**28**	Mass balance (%)
26	**1**	12.6,7.8	22	1.6	93
26	**2**	9.7, 5.7	16	1.7	96
26	**3**	13.3, 9.0	23	1.5	97

[a)] Reaction conditions (method C): Fe-cat. : H_2O_2 : substrate : AcOH = 1 : 120 : 100 : 50, 0 °C, oxidant added by syringe pump over 0.5 h, and reaction mixture stirred for additional 2 h. b) Determined by NMR analysis, average value of two runs.

Methyl hexanoate (**26**), containing an electron-withdrawing ester-group, was tested in order to look into electronic influences on site selectivity. It was found that the change in catalyst has nearly no effect on the ratios of δ-oxidized product (**27**) to γ-oxidized product (**28**) in the oxidation of **26** (all are around 1.6, Table 4). Notably, excellent mass balances were observed in all cases (93%–97%), with **3** again showing the highest product formation.

Next, the catalytic performance of **2** and **3** on elaborated steroidal substrates **29** and **30** was investigated (Scheme 1). These structurally complex compounds are ideal substrates to investigate site-selective C–H oxidation due to the multiple secondary and tertiary C–H groups. Steroids are of particular interest because of their importance in drug discovery[39] and their various physical and biological properties based on the different oxidation patterns.[40]

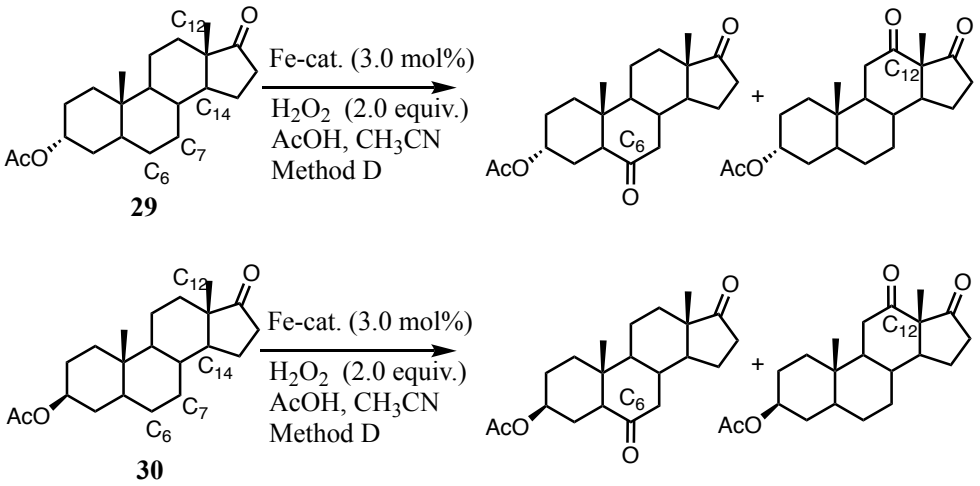

Scheme 1. Catalytic Oxidation of *cis*-acetylandrosterone acetate (**29**) and *trans*-acetylandrosterone acetate (**30**).

Oxidation of **29** and **30** was performed with 3 mol% Fe catalyst, 200 mol% H_2O_2 and 150 mol% AcOH at 0 °C. Poor yields and mass balances were obtained when **2** was employed in both reactions and no statistical site selectivities could be estimated in these cases (Table 5). Yields and mass balances increased responding to the steric bulk of catalyst **3**. For both substrates, the C6 oxidized ketone is preferentially formed (58% and 72% selectivity, respectively), with C7 and C12 oxidized ketones as minor products. Of note is that these observations support the importance of bulky silyl moieties on the ligand for achieving site-selective oxidations of acetylandrosterone derivatives.[27] In previous studies, **1** gave poor C6 over C12 selectivity,[41] while 49–82% selectivity for C6 oxidation was obtained in the cases of the corresponding TIPS-substituted **1**.[27]

Table 5. Oxidation of steroidal substrates by **2** and **3**.[a)]

Steroid	cat.	Conv. (%)[b)]	$C_6/C_7/C_{14}$ (%)[b)]	Norm. yield $C_6/C_7/C_{12}$ (%)
29	**2**	31	4/3/2	
29	**3**	31	11/5/3	58/26/18
Steroid	cat.	Conv. (%)[b)]	$C_6/C_7/C_{12}/C_{14}$ (%)[b)]	Norm. yield $C_6/C_7/C_{12}/C_{14}$ (%)
30	**2**	23	5/1/1/5	
30	**3**	38	23/4/4/1	72/13/13/2

[a)] Reaction conditions (method D): Fe-cat. : H_2O_2 : substrate : AcOH = 3 : 200 : 100 : 150, 0 °C, oxidant added by syringe pump over 30 min, and reaction mixture stirred for additional 10 min. [b)] Determined by GC analysis.

2.3 Conclusions

In conclusion, this chapter describes the use of bioinspired iron complexes based on an N2Py2 ligand platform bearing a bis-isoindoline backbone in selective aliphatic C–H oxidations. Compared to parent complex **1**, complex **2** shows preference for tertiary over secondary C–H bond oxidation for alkane substrates. The catalytic performance of **3** provides further experimental evidence that bulky TIPS groups on meta-positions of the pyridine moieties enhance secondary C–H bond oxidations and site-selective oxidations of acetylandrosterone derivatives.[27] It is believed that the incorporation of a bis-isoindoline backbone provides an additional means of modification of the popular BPBP ligand in oxidation catalysis. Further modification on the aromatic rings of the chiral BPBI backbone may offer a versatile and alternative strategy for ligand design in N2Py2-based iron complexes. Exploration of such ligand modifications in catalytic C–H bond oxidations and enantioselective epoxidation reactions is currently being carried out.

2.4 Experimental Section

2.4.1 General

The iron precursor $Fe(OTf)_2 \cdot 2CH_3CN$ was synthesized according to a reported procedure.[42] The solvents diethyl ether, tetrahydrofuran, acetonitrile, and hexane were dried with an MBraun MB SPS-800 solvent purification system. Tetrahydrofuran for complexation reactions, methanol and dichloromethane were dried with sodium, magnesium turnings and CaH_2, respectively, and distilled under nitrogen prior to use. Reference samples of alcohols and carbonyl compounds **8**-**10**, **12**-**14**, **16**-**18** were prepared using the known **1**/H_2O_2 system.[22,26] The substrates **29** and **30** and reference samples of corresponding oxidized products were synthetized following a reported procedure.[41] All other reagents, substrates and reaction products were obtained commercially and used without further purification. Column chromatography was performed using Merck silica gel (60–200 mesh). ^1H, ^{13}C NMR, and ^{19}F spectra were recorded with a 400 MHz Varian spectrometer at 25 °C, chemical shifts (δ) are given in ppm referenced to the residual solvent peak. IR spectra were recorded with a Perkin–Elmer Spectrum One FTIR spectrometer and ESI-MS measurements were performed with a Waters LCT Premier XE KE317. GC analyses of oxidation of **4**, **7**, **11**, **15**, and **19** were performed on a Perkin–Elmer Clarus 500 Gas Chromatograph equipped with a PE-17 column ((30 m × 0.23 mm × 0.25 μm), (50% phenyl)-(50% methyl)polysiloxane) and a flame-ionization detector. GC analyses of oxidation of **29** and **30** were performed on an Agilent 7820A Gas Chromatograph equipped with a HP-5 column (30m) or Cyclosil-B column (30 m) and a flame-ionization detector. CV measurements were performed on a Princeton 263A potentiostat/galvanostat, using a Pt counter electrode, a glassy carbon working electrode, and a $Ag/AgNO_3$ reference electrode. All data are referenced to ferrocene. Analyte concentrations were

typically between 0.5 and 5 mM in a 0.1 M NBu_4PF_6 in MeCN electrolyte. Elemental microanalyses were carried out by the Mikroanalytisches Laboratorium Kolbe, Germany.

2.4.2 Synthesis of ligands and iron complexes

Synthesis of (*S*,*S*)-bis-isoindoline

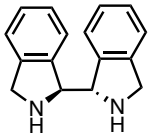

(*S*,*S*)-bis-isoindoline was prepared following a reported procedure.[28] ^{1}H NMR (400 MHz, $CDCl_3$): δ 7.34 – 7.36 (m, 2H), 7.30 – 7.25 (m, 6H), 4.96 (s, 2H), 4.23 (dd, *J* = 13.7 Hz, *J* = 33.1 Hz, 4H), 2.36 (s, 2H). ^{13}C NMR (100 MHz, $CDCl_3$) δ 142.32, 141.50, 127.34, 126.95, 122.60, 122.27, 66.26, 52.00. Spectral properties of the product are in agreement with the literature data.

Synthesis of pyridine synthons

$PyCH_2Cl{\cdot}HCl$ was purchased from Acros. **$^{TIPS}PyCH_2Cl$** was synthesized following the synthetic route described below starting from **$^{TIPS}PyCHO$**.

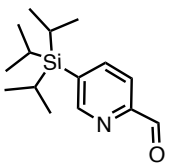

$^{TIPS}PyCHO$ was prepared following a reported procedure.[27] ^{1}H NMR (400 MHz, $CDCl_3$) δ 10.09 (s, 1H), 8.84 (s, 1H), 7.95 (ddd, J = 18.3, 7.6, 1.2 Hz, 2H), 1.53 – 1.40 (m, 3H), 1.08 (d, *J* = 7.4 Hz, 18H). ^{13}C NMR (100 MHz, $CDCl_3$) δ 193.90, 155.59, 152.42, 143.98, 137.05, 120.46, 18.34, 10.59. Spectral properties of the product are in agreement with the literature data.

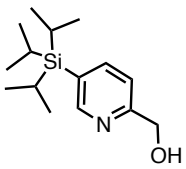

$^{TIPS}PyCH_2OH$ Dry methanol (10 mL) was added to $NaBH_4$ (160mg, 4 mmol) under N_2 and the resulting suspension was stirred for 3 min. A solution of **$^{TIPS}PyCHO$** (526 mg, 2 mmol) in dry methanol (10 mL) was added. The reaction was stirred at room temperature for 30 min. The solution was diluted with CH_2C1_2, washed with saturated $NaHCO_3$, and the aqueous layer was extracted with CH_2C1_2 (2x). The combined organic extracts were dried with $MgSO_4$ and concentrated to afford 524 mg of a yellow solid (99% yield), which was pure enough for the next step. ^{1}H NMR (400 MHz, $CDCl_3$) δ 8.61 (s, 1H), 7.76 (dd, *J* = 7.7, 1.8 Hz, 1H), 7.24 (d, *J* = 7.7 Hz, 1H), 4.75 (s, 2H), 1.47 – 1.35 (m, 6H), 1.07 (d, *J* = 7.5 Hz, 18H). ^{13}C NMR (101 MHz, $CDCl_3$) δ 158.93, 154.10, 143.57, 128.34, 119.93, 64.06, 18.38, 10.59. HRMS (ESI-MS) calcd. *m*/*z* for $C_{15}H_{28}NOSi$ ($[M+H]^+$): 266,1940, found 266,1922. IR ($\tilde{\nu}$, cm^{-1}): 3208, 2941, 2865, 1585, 1460, 1367, 1346, 1065, 993, 882, 681, 638.

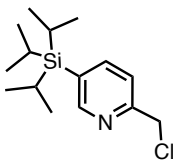

$^{TIPS}PyCH_2Cl$ Dry CH_2C1_2 (15 mL) was added to **$^{TIPS}PyCH_2OH$** (524mg, 2 mmol) under N_2 and the resulting mixture was cooled on an ice bath with stirring. Subsequently, thionyl chloride (219 μL, 3 mmol) was added dropwise. The reaction was stirred at 0 °C for 1.5 h. The solution was diluted with CH_2C1_2, washed with saturated $NaHCO_3$, and the aqueous layer was extracted with CH_2C1_2 (2x). The combined organic extracts were dried with $MgSO_4$ and concentrated to afford a light brown solid (540 mg, 95% yield),

which was pure enough for the next step. ^{1}H NMR (400 MHz, $CDCl_3$) δ 8.63 (s, 1H), 7.81 (d, J = 7.7 Hz, 1H), 7.45 (d, J = 7.7 Hz, 1H), 4.67 (s, 2H), 1.45 – 1.35 (m, 6H), 1.07 (d, J = 7.5 Hz, 18H). ^{13}C NMR (100 MHz, $CDCl_3$) δ 156.27, 154.91, 144.10, 129.63, 121.93, 46.68, 18.37, 10.59. HRMS (ESI-MS) calcd. m/z for $C_{15}H_{27}ClNSi$ ($[M+H]^+$): 284,1601, found 284,1595. IR ($\tilde{\nu}$, cm^{-1}): 2946, 2865, 1578, 1456, 1015, 1105, 991, 881, 662, 681.

Synthesis of ligands

(*S*,*S*)-BPBP was prepared following a reported procedure.[20]

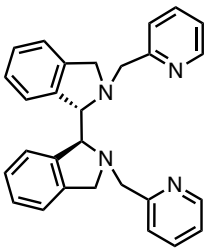

(*S*,*S*)-BPBI NaOH (320 mg, 8 mmol) was added to a round bottom flask charged with a stir bar and $PyCH_2Cl{\cdot}HCl$ (2-(chloromethyl)pyridine hydrochloride) (361 mg, 2.2 mmol) dissolved in CH_2Cl_2 (5 mL) and H_2O (5 mL). Subsequently, a solution containing (*S*,*S*)-bis-isoindoline (236 mg, 1.0 mmol) was added. The combined mixture was vigorously stirred overnight. At this point, the organic phase was separated and the aqueous phase was extracted with CH_2Cl_2 (3 x 6 mL). The combined organic extracts were dried over $MgSO_4$ and the solvent was eliminated under vacuum. The obtained brown oil was purified by silica column (petroleum ether:EtOAc 50:50 at first, then CH_2Cl_2:MeOH:NH_3 94:5:1) to provide 326 mg (0.78 mmol, yield 78%) of a brown oil. ^{1}H NMR (400 MHz, $CDCl_3$) δ 8.56 (s, 2H), 7.68 (t, J = 7.7 Hz, 2H), 7.56 – 7.52 (m, 2H), 7.34 (d, J = 7.6 Hz, 2H), 7.19 – 7.16 (m, 2H), 7.08 – 7.00 (m, 4H), 6.96 – 6.90 (m, 2H), 4.56 (s, 2H), 4.43 (d, J = 14.4 Hz, 2H), 4.38 (d, J = 13.2 Hz, 2H), 3.97 (d, J = 14.4 Hz, 2H), 3.85 (d, J = 13.2 Hz, 2H). ^{13}C NMR (100 MHz, $CDCl_3$) δ 160.02, 148.92, 140.70, 139.71, 136.62, 126.59, 126.27, 123.47, 122.78, 122.01, 121.59, 71.22, 61.10, 58.99. HRMS (ESI-MS) calcd. m/z for $C_{28}H_{27}N_4$ ($[M+H]^+$): 419.2236, found 419.2232. IR ($\tilde{\nu}$, cm^{-1}): 2940, 2922, 1710, 1550, 1440, 1342, 1320, 1110, 1021, 750, 695

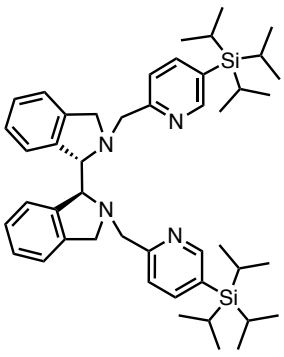

(*S*,*S*)-^{TIPS}BPBI was prepared in an analogous manner to **(*S*,*S*)-BPBI** starting from (*S*,*S*)-bis-isoindoline and $^{TIPS}PyCH_2Cl$. The brown residue was purified by silica column (petroleum ether:EtOAc 90:10 at first, then CH_2Cl_2:MeOH:NH_3 90:9:1) to provide a brown oil (48% yield). ^{1}H NMR (400 MHz, $CDCl_3$) δ 8.62 (s, 2H), 7.79 (dd, J = 7.8, 1.8 Hz, 2H), 7.55 (d, J = 7.7 Hz, 2H), 7.37 (d, J = 7.6 Hz, 2H), 7.09 – 7.02 (m, 4H), 6.94 (t, J = 7.4 Hz, 2H), 4.61 (s, 2H), 4.49 (d, J = 14.7 Hz, 2H), 4.42 (d, J = 13.2 Hz, 2H), 3.97 (d, J = 14.7 Hz, 2H), 3.86 (d, J = 13.2 Hz, 2H), 1.46 – 1.36 (m, 6H), 1.09 (dd, J = 7.5, 1.7 Hz, 36H). ^{13}C NMR (100 MHz, $CDCl_3$) δ 160.02, 154.61, 143.64, 140.75, 139.81, 127.73, 126.55, 126.23, 123.50, 121.85, 121.58, 71.18, 60.91, 59.01, 18.47, 10.64. HRMS (ESI-MS) calcd. m/z for $C_{46}H_{67}N_4Si_2$ ($[M+H]^+$): 731,4904, found 731.4984. IR ($\tilde{\nu}$, cm^{-1}): 2942, 2864, 2805, 1720, 1580, 1460, 1360, 1342, 1106, 1013, 881, 730, 677, 643.

Synthesis of iron complexes

[Fe(OTf)$_2$(*S,S*-BPBP)] (**1**) was prepared following a reported procedure.[34] ^{1}H NMR (400 MHz, CD_2Cl_2) δ 180.67, 114.48, 76.82, 51.50, 49.73, 32.54, 27.80, 15.62, 9.03, -2.07, -9.42, -21.01.

[Fe(OTf)$_2$(*S,S*-BPBI)] (**2**) Under a nitrogen atmosphere, a solution of (*S,S*)-BPBI (260 mg, 0.62 mmol) in THF (2 mL) was added to a vigorously stirred solution of Fe(OTf)$_2$·CH_3CN (270 mg, 0.62 mmol) in THF (2 mL) at room temperature. The reaction mixture turned brown slowly. After stirring overnight, the solvent was removed *in vacuo* to give a brown powder, which was recrystallized from CH_2Cl_2 and hexane to afford yellow crystals in 65% yield. ^{1}H NMR (400 MHz, CD_2Cl_2) δ 162.42 (s), 136.13 (s), 85.70 (s), 56.33 (s), 49.39 (s), 15.45 (s), 12.43 (s), 7.11 (s), 3.63 (s), 3.51 (s), 2.78 (s), 1.19 (s), -9.60 (s). ^{19}F NMR (376 MHz, CD_2Cl_2) δ -28.96. HRMS (ESI-MS) calcd. *m/z* for $C_{29}H_{26}F_3FeN_4O_3S$ ([M-OTf]$^+$): 623,1027, found 623,1033. Elemental analysis calcd. (%) for $C_{30}H_{26}F_6FeN_4O_6S_2$·1/2 CH_2Cl_2: C 44.95, H 3.34, N 6.87, found C 44.45, H 3.27, N 6.51. IR ($\tilde{\nu}$, cm^{-1}): 2962, 2924, 1607, 1445, 1302, 1259, 1235, 1214, 1156, 1051, 1020, 797, 760, 633.

[Fe(OTf)$_2$(*S,S*-^{TIPS}BPBI)] (**3**) Under a nitrogen atmosphere, a solution of (*S,S*)-BPBI (170 mg, 0.23 mmol) in THF (1 mL) was added to a vigorously stirred solution of Fe(OTf)$_2$·CH_3CN (101 mg, 0.23 mmol) in THF (1 mL) at room temperature. The reaction mixture turned brown slowly. After stirring overnight, 6 mL diethyl ether was layered to the reaction mixture carefully. In a few days, yellow crystals were obtained in 55% yield. ^{1}H NMR (400 MHz, CD_2Cl_2) δ 164.62 (s), 124.59(s), 83.54 (s), 47.07 (s), 14.05 (s), 11.62 (s), 8.27 (s), 7.93 (s), 4.01 (s), 3.70 (s), 1.21 (s), 0.53 (s), -10.67 (s). ^{19}F NMR (376 MHz, CD_2Cl_2) δ -38.05. HRMS (ESI-MS) calcd. *m/z* for $C_{47}H_{66}F_3FeN_4O_3SSi_2$ ([M-OTf]$^+$): 935,3696, found 935,3749. Elemental analysis calcd. (%) for $C_{48}H_{66}F_6FeN_4O_6S_2Si_2$: C 53.13, H 6.13, N 5.16, found C 52.79, H 6.17, N 5.08. IR ($\tilde{\nu}$, cm^{-1}): 2947, 2868, 1625, 1598, 1463, 1425, 1287, 1234, 1222, 1159, 1027, 851, 759, 729, 635.

2.4.3 X-ray crystal structure determination

X-ray crystal structure determination of 2

$C_{30}H_{26}F_6FeN_4O_6S_2 \cdot CH_2Cl_2$, Fw = 857.44, yellow plate, 0.30 × 0.21 × 0.04 mm^3, monoclinic, $P2_1$ (no. 4), a = 9.4763(3), b = 19.7106(6), c = 10.4929(7) Å, β = 116.646(3) °, V = 1751.74(14) Å^3, Z = 2, D_x = 1.626 g/cm^3, μ = 0.78 mm^{-1}. 41887 Reflections were measured on a Bruker Kappa ApexII diffractometer with sealed tube and Triumph monochromator (λ = 0.71073 Å) at a temperature of 150(2) K up to a resolution of $(\sin\theta/\lambda)_{max}$ = 0.65 Å^{-1}. The intensities were integrated using the Eval15 software.[43] A numerical absorption correction and scaling was performed with SADABS[44] (correction range 0.85-0.99). 8031 Reflections were unique (R_{int} = 0.021), of which 7728 were observed [I>2σ(I)]. The structure was solved with Patterson superposition methods using SHELXT.[45] Least-squares refinement was performed with SHELXL-2014[46] against F^2 of all reflections. Non-hydrogen atoms were refined freely with anisotropic displacement parameters. All hydrogen atoms were located in difference Fourier maps and refined with a riding model. 470 Parameters were refined with one restraint (shifting origin). R1/wR2 [I > 2σ(I)]: 0.0281 / 0.0669. R1/wR2 [all refl.]: 0.0299 / 0.0679. S = 1.040. Flack parameter x

= 0.010(4) from a refinement as inversion twin.[47] Residual electron density between -0.37 and 0.69 e/Å^3. Geometry calculations and checking for higher symmetry were performed with the PLATON program.[36]

X-ray crystal structure determination of 3

$C_{48}H_{66}F_6FeN_4O_6S_2Si_2$ + disordered solvent, Fw = 1085.19[48], yellow block, 0.44 × 0.41 × 0.22 mm^3, triclinic, P1 (no. 1), a = 10.8640(4), b = 12.7880(4), c = 23.6499(8) Å, α = 84.941(2), β = 81.667(2), γ = 67.060(1) °, V = 2992.07(18) Å^3, Z = 2, D_x = 1.205 g/cm^3[48], μ = 0.42 mm^{-1}[48]. 131341 Reflections were measured on a Bruker Kappa ApexII diffractometer with sealed tube and Triumph monochromator (λ = 0.71073 Å) at a temperature of 150(2) K up to a resolution of $(\sin\theta/\lambda)_{max}$ = 0.65 Å^{-1}. The intensities were integrated with the Eval15 software.[43] Multiscan absorption correction and scaling was performed with SADABS[44] (correction range 0.70-0.75). 27514 Reflections were unique (R_{int} = 0.016), of which 26959 were observed [I>2σ(I)]. The structure was solved with Patterson superposition methods using SHELXT.[45] Least-squares refinement was performed with SHELXL-2014[46] against F^2 of all reflections. The crystal structure contains large voids (481 Å^3 / unit cell) filled with disordered THF solvent molecules. Their contribution to the structure factors was secured by back-Fourier transformation using the SQUEEZE algorithm[49] resulting in 95 electrons / unit cell. Non-hydrogen atoms were refined freely with anisotropic displacement parameters. One of the coordinated triflate ligands was refined with a disorder model. Hydrogen atoms were introduced in calculated positions and refined with a riding model. 1322 Parameters were refined with 619 restraints (distances and angles of all triflate groups, displacement parameters of the disordered triflate ligand). R1/wR2 [I > 2σ(I)]: 0.0203 / 0.0546. R1/wR2 [all refl.]: 0.0210 / 0.0550. S = 0.991. Flack parameter x = 0.0052(13) from intensity quotients.[50] Residual electron density between -0.37 and 0.65 e/Å^3. Geometry calculations and checking for higher symmetry were performed with the PLATON program.[36]

2.4.4 Reaction protocol for catalytic studies

Catalytic oxidation of substrate 1, 7 and 19, Method A

A 20 mL vial was charged with: substrate (0.36 mmol, 1 equiv.), catalyst (3.6 μmol, 1 mol%), CH_3CN (1.5 mL). A 0.5 M CH_3CO_2H solution in CH_3CN was added (0.36 mL, 0.18 mmol, 50 mol%). The vial was cooled on an ice bath with stirring. Subsequently, a 1.0 M H_2O_2 solution in CH_3CN (0.43 mL, 0.43 mmol, 120 mol%, diluted from a 35% H_2O_2 aqueous solution) was delivered by syringe pump over 6 min. After the oxidant addition, the resulting mixture was stirred at 0 °C for another 10 min. At this point, a 1.0 M nitrobenzene solution in CH_3CN (0.36 mL, 0.36 mmol) was added as internal standard. The solution was diluted with Et_2O to precipitate the iron complex, passed through a cotton wool filter to remove the catalyst. Subsequently, a sample was submitted to GC analysis. GC analysis of the solution provided substrate conversions and product yields relative to the internal standard integration. Products were identified by comparison to the GC retention time of authentic samples.

Catalytic oxidation of substrate 11 and 15, Method B

A 20 mL vial was charged with: substrate (0.36 mmol, 1 equiv.), catalyst (3.6 μmol, 1 mol%), CH_3CN (1.5 mL). A 0.5 M CH_3CO_2H solution in CH_3CN was added (0.36 mL, 0.18 mmol, 50 mol%). The vial

was cooled on an ice bath with stirring. Subsequently, a 1.0 M H_2O_2 solution in CH_3CN (0.54 mL, 0.54 mmol, 150 mol%, diluted from a 35% H_2O_2 aqueous solution) was delivered by syringe pump over 30 min. After the oxidant addition, the resulting mixture was stirred at 0 °C for another 1.5 h. At this point, a 1.0 M nitrobenzene solution in CH_3CN (0.36 mL, 0.36 mmol) was added as internal standard. The solution was diluted with Et_2O to precipitate the iron complex, passed through a cotton wool filter to remove the catalyst. Subsequently, a sample was submitted to GC analysis. GC analysis of the solution provided substrate conversions and product yields relative to the internal standard integration. Products were identified by comparison to the GC retention time of authentic samples.

Catalytic oxidation of substrate 23 and 26, Method C

A 20 mL vial was charged with: substrate (0.36 mmol, 1 equiv.), catalyst (3.6 μmol, 1 mol%), CH_3CN (1.5 mL). A 0.5 M CH_3CO_2H solution in CH_3CN was added (0.36 mL, 0.18 mmol, 50 mol%). The vial was cooled on an ice bath with stirring. Subsequently, a 1.0 M H_2O_2 solution in CH_3CN (0.43 mL, 0.43 mmol, 120 mol%, diluted from a 35% H_2O_2 aqueous solution) was delivered by syringe pump over 30 min. After the oxidant addition, the resulting mixture was stirred at 0 °C for another 2 h. At this point, a 1.0 M nitrobenzene solution in CH_3CN (0.36 mL, 0.36 mmol) was added as internal standard. The solution was diluted with Et_2O to precipitate the iron complex, passed through a cotton wool filter to remove the catalyst. Solvent was removed *in vacuo* and a sample was submitted to ^{1}H NMR analysis. ^{1}H NMR analysis of oxidation of **23** was performed by comparison of the hydrogen α to the acetate group at 4.67 ppm (in **23**), 4.98 ppm (in **24**) and 4.81 ppm (in **25**).[51] ^{1}H NMR analysis of oxidation of **26** was performed by comparison of the hydrogen ε to the ester group at 0.93 ppm (in **26**), 2.13 ppm (in **27**) and 1.05 ppm (in **28**).[52]

Catalytic oxidation of substrate 29 and 30, Method D

A 5 mL vial was charged with: substrate (40 μmol, 1 equiv.), catalyst (1.2 μmol, 3 mol %), CH_3CN (0.8 mL) and a magnetic stir bar. A 1.74 M CH_3CO_2H solution in CH_3CN was added (35 μL, 60 μmol, 150 mol%). The vial was cooled on an ice bath with stirring. Subsequently, a 1.5 M H_2O_2 solution in CH_3CN (0.2 mL, 250 mol%, diluted from a 35% H_2O_2 aqueous solution) was delivered by syringe pump over 30 min. After the oxidant addition, the resulting mixture was stirred at 0 °C for another 10 min. Biphenyl (20 μmol) was added at this point as internal standard. The iron complex was removed by passing the solution through a short path of silica followed by elution with 2 mL of EtOAc. Finally, the solution was subjected to GC analysis. GC analysis of the solution provided substrate conversions and product yields relative to the internal standard integration. Products were identified by comparison to the GC retention time of authentic samples.

2.5 References

[1] C. Limberg, *Angew. Chem. Int. Ed.* **2003**, *42*, 5932–5954.

[2] M. Christmann, *Angew. Chem. Int. Ed.* **2008**, *47*, 2740–2742.

[3] L. Que, Jr., W. B. Tolman, *Nature* **2008**, *455*, 333–340.

[4] C.-L. Sun, B.-J. Li, Z.-J. Shi, *Chem. Rev.* **2011**, *111*, 1293–1314.

[5] M. Bordeaux, A. Galarneau, J. Drone, *Angew. Chem. Int. Ed.* **2012**, *51*, 10712–10723.

[6] E. I. Solomon, T. C. Brunold, M. I. Davis, J. N. Kemsley, S. K. Lee, N. Lehnert, F. Neese, a J. Skulan, Y. S. Yang, J. Zhou, *Chem. Rev.* **2000**, *100*, 235–350.

[7] M. Costas, M. P. Mehn, M. P. Jensen, L. Que, Jr., *Chem. Rev.* **2004**, *104*, 939–986.

[8] M. Costas, K. Chen, L. Que, Jr., *Coord. Chem. Rev.* **2000**, *200–202*, 517–544.

[9] W. Nam, *Acc. Chem. Res.* **2007**, *40*, 522–531.

[10] E. P. Talsi, K. P. Bryliakov, *Coord. Chem. Rev.* **2012**, *256*, 1418–1434.

[11] C. Kim, K. Chen, J. Kim, L. Que, Jr., *J. Am. Chem. Soc.* **1997**, *119*, 5964–5965.

[12] T. A. van den Berg, J. W. de Boer, W. R. Browne, G. Roelfes, B. L. Feringa, *Chem. Commun.* **2004**, 2550–2551.

[13] A. Company, L. Gómez, M. Güell, X. Ribas, J. M. Luis, L. Que, Jr., M. Costas, *J. Am Chem. Soc.* **2007**, *129*, 15766–15767.

[14] J. England, G. J. P. Britovsek, N. Rabadia, A. J. P. White, *Inorg. Chem.* **2007**, *46*, 3752–3767.

[15] J. England, C. R. Davies, M. Banaru, A. J. P. White, G. J. P. Britovseka, *Adv. Synth. Catal.* **2008**, *350*, 883–897.

[16] P. Liu, Y. Liu, E. L.-M. Wong, S. Xiang, C.-M. Che, *Chem. Sci.* **2011**, *2*, 2187–2195.

[17] Y. Hitomi, K. Arakawa, T. Funabiki, M. Kodera, *Angew. Chem. Int. Ed.* **2012**, *51*, 3448–3452.

[18] G. Olivo, O. Lanzalunga, S. Di Stefano, *Adv. Synth. Catal.* **2016**, *358*, 843–863.

[19] G. Olivo, O. Cussó, M. Costas, *Chem. Asian J.* **2016**, *11*, 3148–3158.

[20] M. S. Chen, M. C. White, *Science* **2007**, *318*, 783–787.

[21] E. A. Mikhalyova, O. V. Makhlynets, T. D. Palluccio, A. S. Filatov, E. V. Rybak-Akimova, *Chem. Commun.* **2012**, *48*, 687–689.

[22] L. Gómez, I. Garcia-Bosch, A. Company, J. Benet-Buchholz, A. Polo, X. Sala, X. Ribas, M. Costas, *Angew. Chem. Int. Ed.* **2009**, *48*, 5720–5723.

[23] I. Prat, L. Gómez, M. Canta, X. Ribas, M. Costas, *Chem. Eur. J.* **2013**, *19*, 1908–1913.

[24] G. Olivo, O. Lanzalunga, L. Mandolini, S. Di Stefano, *J. Org. Chem.* **2013**, *78*, 11508–11512.

[25] P. E. Gormisky, M. C. White, *J. Am. Chem. Soc.* **2013**, *135*, 14052–14055.

[26] L. Gómez, M. Canta, D. Font, I. Prat, X. Ribas, M. Costas, *J. Org. Chem.* **2013**, *78*, 1421–1433.

[27] D. Font, M. Canta, M. Milan, O. Cussó, X. Ribas, R. J. M. Klein Gebbink, M. Costas, *Angew. Chem. Int. Ed.* **2016**, *55*, 5776–5779.

[28] Q. Zhu, H. Huang, D. Shi, Z. Shen, C. Xia, *Org. Lett.* **2009**, *11*, 4536–4539.

[29] K. Chen, L. Que, Jr., *J. Am. Chem. Soc.* **2001**, *123*, 6327–6337.

[30] M. Costas, L. Que, Jr., *Angew. Chem. Int. Ed.* **2002**, *41*, 2179–2181.

[31] V. Yazerski, P. Spannring, D. Gatineau, C. H. M. Woerde, S. M. Wieclawska, M. Lutz, H. Kleijn, R. J. M. Klein Gebbink, *Org. Biomol. Chem.* **2014**, *12*, 2062–2070.

[32] J. Serrano-Plana, W. N. Oloo, L. Acosta-Rueda, K. K. Meier, B. Verdejo, E. García-España, M. G. Basallote, E. Münck, L. Que, A. Company, et al., *J. Am. Chem. Soc.* **2015**, *137*, 15833–15842.

[33] CCDC 1531774 (**2**) and 1531775 (**3**) contain the supplementary crystallographic data for this chapter. These data can be obtained free of charge from The Cambridge Crystallographic Data Centre *via* www.ccdc.cam.ac.uk/data_request/cif.

[34] K. Suzuki, P. D. Oldenburg, L. Que, Jr., *Angew. Chem. Int. Ed.* **2008**, *47*, 1887–1889.

[35] K. Chen, M. Costas, J. Kim, A. K. Tipton, L. Que, Jr., *J. Am. Chem. Soc.* **2002**, *124*, 3026–3035.

[36] A. L. Spek, *Acta Cryst.* **2009**, *D65*, 148–155.

[37] A. Company, L. Gómez, X. Fontrodona, X. Ribas, M. Costas, *Chem. Eur. J.* **2008**, *14*, 5727–5731.

[38] G. Olivo, M. Nardi, D. Vìdal, A. Barbieri, A. Lapi, L. Gómez, O. Lanzalunga, M. Costas, S. Di Stefano, *Inorg. Chem.* **2015**, *54*, 10141–10152.

[39] E. Vitaku, D. T. Smith, J. T. Njardarson, *J. Med. Chem.* **2014**, *57*, 10257–10274.

[40] J.-F. Biellmann, *Chem. Rev.* **2003**, *103*, 2019–2033.

[41] M. Canta, D. Font, L. Gõmez, X. Ribas, M. Costas, *Adv. Synth. Catal.* **2014**, *356*, 818–830.

[42] K. S. Hagen, *Inorg. Chem.* **2000**, *39*, 5867–5869.

[43] A. M. M. Schreurs, X. Xian, L. M. J. Kroon-Batenburg, *J. Appl. Crystallogr.* **2010**, *43*, 70–82.

[44] G. M. Sheldrick, **2008**, SADABS. Universität Göttingen, Germany.

[45] G. M. Sheldrick, *Acta Cryst.* **2015**, *A71*, 3–8.

[46] G. M. Sheldrick, *Acta Cryst.* **2015**, *C71*, 3–8.

[47] H. D. Flack, *Acta Cryst.* **1983**, *A39*, 876–881.

[48] Derived values do not contain the contribution of the disordered solvent.

[49] A. L. Spek, *Acta Cryst.* **2015**, *C71*, 9–18.

[50] S. Parsons, H. D. Flack, T. Wagner, *Acta Cryst.* **2013**, *B69*, 249–259.

[51] R. V Ottenbacher, D. G. Samsonenko, E. P. Talsi, K. P. Bryliakov, *Org. Lett.* **2012**, *14*, 4310–4313.

[52] S. A. Moteki, A. Usui, T. Zhang, C. R. S. Alvarado, K. Maruoka, *Angew. Chem. Int. Ed.* **2013**, *52*, 8657–8660.

Chapter 3

Epoxidation of Methyl Linoleate Catalyzed by Fe(N2Py2) Complexes with Hydrogen Peroxide as the Oxidant

Abstract

Epoxidized vegetable oils and poly-unsaturated acids (and esters) with different oxirane contents are industrially interesting products that can be used in different domains, based on their physicochemical properties. Although many efforts have been spent on the epoxidation of vegetable oils and their derivatives, the attention to selective epoxidation of poly-unsaturated fatty acids (and esters) in terms of partial and full epoxidation is still rather limited. In this chapter, an epoxidation method for methyl linoleate is described using various Fe(N2Py2) complexes as catalysts and H_2O_2 as the oxidant. Using 1 mol% of [Fe(OTf)$_2$(BPBI)] (**6**) or [Fe(OTf)$_2$(*mix*-BPBP)] (**5**), mono-epoxides (42%) or di-epoxides (92%) can be obtained as predominant products in very short reaction times of 1 h or 5 min, respectively. Catalytic protocols using these catalysts can accordingly be used when partial epoxides or full epoxides are preferably needed. In addition, the selectivities for epoxidation in both cases are very high (>90%) and the reaction temperatures are very mild (room temperature or 0 ºC). Further kinetic studies revealed a rather fast catalyst deactivation, and therefore, slow oxidant or catalyst addition protocols were explored to overcome this issue, and more importantly, to investigate the impacts on the mono-epoxides/di-epoxides (M/D) ratio. In general, slow oxidant addition suppresses di-epoxidation progression, while slow catalyst addition leads to increased formation of di-epoxides in this study. Finally, the O-transfer selectivity to different epoxide products for some Fe(N2Py2) catalysts has been studied, which reveals that these have a small, but significant preference for mono-epoxidation over di-epoxidation.

3.1 Introduction

In recent years, vegetable oils and their derivatives have attracted extensive attention as promising alternatives to replace fossil resources for the production of chemicals and fuels, because of their abundance from renewable resources, biodegradability, non-toxic natures, and high carbon content.[1–4] However, the current utilization of vegetable oils and their derivatives is rather limited due to their low oxidative stability, poor low-temperature properties, and narrow range of viscosity.[5–7] Epoxidizing the C=C bonds in unsaturated vegetable oils can largely improve the physicochemical properties of these oils.[5,8] In addition, epoxidized vegetable oils and their derivatives with different oxirane contents can be used in different areas, depending on their varying physicochemical properties.[9] Partial epoxidation of poly-unsaturated fatty acids and esters leads to relatively low viscosities and melting points of the epoxides, which makes them ideal for the production of reactive diluents.[10] On the contrary, fully epoxidized oils, fatty acids, or their esters show a high oxidative stability, and relatively high viscosities and melting points. In this context, they are widely used as building blocks for producing polyvinyl chloride (PVC) plasticizers and stabilizers,[9,11] surfactants, lubricants, and surface coatings formulations.[9,12,13]

Industrial epoxidation of vegetable oils is traditionally carried out with percarboxylic acids through the so-called Prilezhaev reaction, which uses formic (or acetic) acid and hydrogen peroxide to generate the peracid oxidant *in situ* by means of a mineral acid catalyst (e.g., sulfuric acid). This process is commonly used to perform full epoxidation of unsaturated compounds. Furthermore, the use of strong mineral acids results in a low selectivity because of undesirable epoxy ring-opening reactions and causes equipment corrosion problems. Thus, numerous catalytic epoxidation methods for the epoxidation of vegetable oils have been reported in order to avoid the drawbacks of the Prilezhaev process (see examples in Chapter 5 of this thesis). Nevertheless, only very limited studies have emphasized the selective epoxidation of vegetable oils and poly-unsaturated fatty acids in terms of partial and full epoxidation.[9] Some of the recent reports on catalytic (selective) epoxidation of a typical poly-unsaturated fatty acid ester, methyl linoleate (ML, Scheme 1), are discussed below.

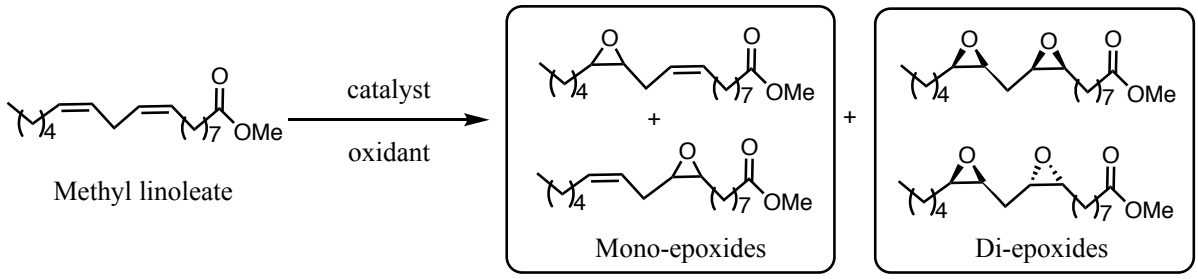

Scheme 1. Catalytic epoxidation of methyl linoleate.

In 2004, Woo and co-workers studied the catalytic epoxidation of ML with methyl-trioxorhenium (MTO)/H_2O_2/pyridine and manganese tetraphenylporphyrin chloride (Mn(TPP)Cl)/NaOCl/*n*-Bu_4NBr catalytic systems.[14] Full conversion of ML could be achieved with 1 mol% MTO in 6 h, with a roughly 1/1 mono-epoxides/di-epoxides (M/D) ratio. Mono-epoxides were found to be the major products (63%) when Mn(TPP)Cl (2 mol%) was used as catalyst, providing a M/D ratio of 3.5. Unfortunately, both cases required large excess amounts of oxidants (3.6 equiv. H_2O_2 and 4.8 equiv. NaOCl, respectively), and showed relatively low epoxidation selectivities (77% for MTO, 63% for Mn(TPP)Cl). Guidotti *et al.* reported that using niobium(V)-containing silica catalysts, mono-epoxides were preferably formed with a selectivity in the range of 80-93% in the presence of H_2O_2.[15] In this case a very high catalyst loading (100 mg for 1 mmol ML) and reflux temperature (MeCN) were used. Also using MTO as catalyst, Salimon *et al.* achieved mainly partial epoxidation of ML with a mono-epoxides yield of 46% at room temperature.[9] This method is not efficient for full epoxidation though. Full epoxidation was only obtained in this study by utilizing the conventional Prilezhaev method. Another example is the use of CoCuAl ternary layered double hydroxides (LDHs) as catalysts for the epoxidation of ethyl linoleate using *tert*-butyl hydroperoxide (TBHP) as the oxidant.[16] $Co_{30}Cu_{70}$Al-LDH was found to be the most efficient for di-epoxidation, providing a M/D ratio of 13/87 at 85% conversion. A high reaction temperature (110 ^oC) was essential for di-epoxidation, as a moderate 71/29 M/D ratio was obtained at room temperature, yet at a much lower conversion (44%). In 2016 Crucianelli and co-workers reported an oxovanadium(IV) complex for the catalytic epoxidation of ML, which gave a mixture of mono- and di-epoxides (M/D = 2) using up to 2.0 equiv. of TBHP per double bond in 8 h (Figure 1a).[17] Very recently, two catalytic systems based on molybdenum(VI) complexes have been reported for ML epoxidation by the Pillinger group, both resulting in a mixture of mono-epoxides and di-epoxides.[18,19] When an oxidomolybdenum(VI) complex bearing a bidentate 2-(2-pyridyl)-benzimidazole ligand was employed (Figure 1b), 46% mono-epoxides and 25% di-epoxides were obtained, albeit at 92% ML conversion.[18] In the reaction using an

oxodiperoxomolybdenum(VI) complex containing coordinated 4,4'-bipyridinium (Figure 1c), the yield of mono-epoxides and di-epoxides were 61% and 25% after 24 h, respectively.[19]

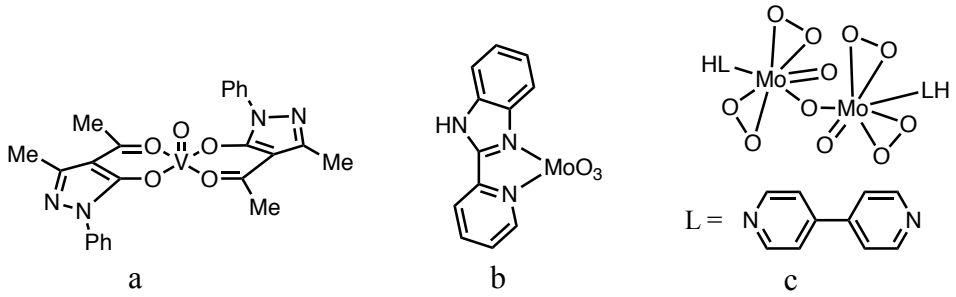

Figure 1. Structures of some complexes reported for ML epoxidation.

From the above literature examples and to the best of our knowledge, there are still no efficient catalytic systems reported for selective epoxidation of ML to generate either mono- or di-epoxides as the predominant products separately under mild reaction conditions. In our group's continuous investigations on oxidative transformations of unsaturated fatty acids and esters, molecular catalysts based on the abundant base metal iron were previously used for the one-pot oxidatively cleavage of mono-unsaturated fatty acids and esters.[20] This process was initiated by catalytic epoxidation of the substrate with $Fe/H_2O_2/AcOH$ catalytic systems, in which iron(II) complexes derived from tetradentate bis-alkylamine-bis-pyridine (N2Py2) ligands were used. In this study, these catalytic systems are further extended for the epoxidation of poly-unsaturated fatty acid esters, using ML as the model substrate. It was found that it is possible to obtain mono-epoxides or di-epoxides as predominant products in about 40 or 90% yield, respectively, depending on which Fe(N2Py2) catalyst is used. Additionally, the catalytic reactions were optimized for mild reaction conditions, *i.e.* low reaction temperature and short reaction time. This chapter furthermore details the investigations on the influence of various reaction parameters on the reaction progression and the M/D ratio and on the selectivity of O-distribution to either mono- or di-epoxides for some of the catalysts.

3.2 Results and Discussion

A series of non-heme Fe(N2Py2) complexes with modifications on both the alkylamine and pyridine moieties were chosen to catalyze the epoxidation of ML with H_2O_2 as the oxidant (Figure 2). Amongst them, $[Fe(OTf)_2(BPMEN)]$ (**1**),[21] $[Fe(OTf)_2(S,S\text{-BPBP})]$ (**2**),[22] and $[Fe(OTf)_2(S,S\text{-BPBI})]$ (**6**),[23] where BPMEN = *N*,*N*'-dimethyl-*N*,*N*'-bis(2-picolyl)ethylenediamine, BPBP = *N*,*N*'-bis(2-picolyl)-2,2'-bispyrrolidine, and BPBI = *N*,*N*'-bis(2-picolyl)-2,2'-bis-isoindoline, have alkylamine moieties with different rigidities in their

backbone. Specifically, more rigid pyrrolidine rings are present in **2** as opposed to the methylamines in **1**.[22] Complex **6** bears a rigid bis-isoindoline backbone *via* the formal introduction of benzene moieties on the pyrrolidine rings in **2**,[23] as discussed in Chapter 2 of this thesis. Based on BPBP-complex **2**, electronic ligand effects were investigated by the incorporation of electron-donating or electron-withdrawing groups on the appended pyridine rings ($[Fe(OTf)_2(S,S\text{-}^{dMM}BPBP)]$ (**3**)[24,25] or $[Fe(OTf)2(S,S\text{-}^{CO2Et}BPBP)]$[26] (**4**), respectively). $[Fe(OTf)_2(mix\text{-}BPBP)]$ (**5**) derived from a non-resolved mixture of racemic BPBP ligands, which showed retained overall reactivity and selectivity properties with respect to its optically pure components (for example **2**) in oxidation reactions (both epoxidation and C–H oxidation) in a previous study,[27] has also been tested in ML epoxidation. **5** represents a promising catalyst candidate as the costly and low yielding step of the resolution of the racemic mixture of the 2,2′-bipyrrolidine building block is not involved in the synthesis of **5**.[27] The influence of the steric properties of the catalyst was evaluated with $[Fe(OTf)_2(S,S\text{-}^{TIPS}BPBI)]$ (**7**, also see Chapter 2 of this thesis),[23,28] where bulky *tris*-(isopropyl)-silyl (TIPS) groups are present at one of the *meta*-positions of the pyridine rings.

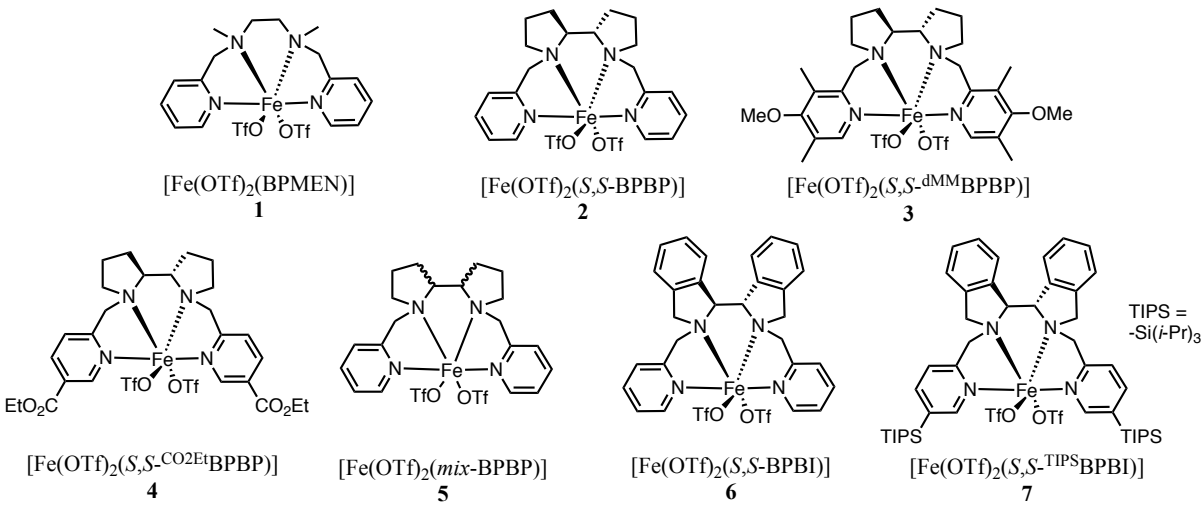

Figure 2. Non-heme iron complexes used in this study.

3.2.1 Catalytic properties of different Fe(N2Py2) complexes

The different catalysts were first evaluated for the epoxidation of ML (1 equiv.), with 1 mol% catalyst (*i.e.*, 0.5 mol% per double bond), 1.5 mol% AcOH, and 1.5 equiv. of H_2O_2 (*i.e.*, 0.75 equiv. per double bond) in MeCN at ambient temperature. When the simple iron salt $Fe(OTf)_2{\cdot}2CH_3CN$ (1 mol%) was used, no epoxide products were observed and only trace amounts (5%) of ML were converted (Table 1, entry 1). Subsequently, iron complexes **1**-**7** with

N2Py2 ligands, as detailed above, were employed for the epoxidation of ML. The formation of epoxides was observed in all cases (entries 2-8), showing that the use of Fe(N2Py2) complexes is crucial to achieve catalytic epoxidation of ML under the current conditions. The reaction with catalyst **1** yielded 20% of mono-epoxides, without the detection of di-epoxides by means of GC-analysis, at 40% ML conversion (entry 2). Iron complex **2,** with the more rigid bispyrrolidine ligand backbone, showed a significantly higher reactivity, giving rise to moderate yields of mono-epoxides and di-epoxides (47% and 32%, respectively) at 90% ML conversion (entry 3). Similarly, improved reactivities have also been found in previous studies in aliphatic C–H oxidation by increasing the rigidity of the alkylamino backbone from **1** to **2**.[22] In terms of the mono-epoxidation over di-epoxidation ratio, a value of 1.5 was obtained with **2**. Introducing electron-donating groups on the pyridine donors in **2** lead to a slight increase in catalyst activity and an increased yield of di-epoxides (entry 4, 39% with **3** vs. 32% with **2**), with the yield of mono-epoxides remaining nearly the same (46%). As a result, the M/D ratio was found to decrease from 1.5 to 1.2 (entry 4). On the contrary, upon introduction of electron-withdrawing groups to the pyridine rings, *i.e.*, catalyst **4** was employed, a significant drop in activity (73% ML conversion) and formation of di-epoxides was observed (11%), leading to a higher M/D ratio of 3.5 (entry 5). The electronic properties of the pyridines in the N2Py2 ligand have been previously reported to have strong and systematic impacts on epoxidation reactions, *i.e.*, electron-donating substituents were found to accelerate the epoxidation process, while electron-withdrawing ones have a negative impact on substrate conversion.[24] Therefore, in the epoxidation of ML, the over-epoxidized di-epoxide products are more preferably formed in the presence of **3**. In contrast, less double bonds are converted with **4**, leading to a higher M/D ratio and an overall lower conversion. As expected, catalyst **5** provided nearly the same catalytic outcome as **2**, with a slight erosion in conversion (85%) and a similar M/D ratio (1.7, entry 6). These observations are consistent with previous findings that **5** retains the reactivity and selectivity properties of **2** in epoxidation reactions.[27] Mono-epoxides were much more preferentially formed (42%) compared to di-epoxides, when performing the reaction in the presence of catalyst **6**, albeit at a much lower substrate conversion (52%, entry 7). In this case, only small amounts of di-epoxides (4.6%) were formed, giving rise to a very high M/D ratio of 9 (entry 7). Similarly, a general decrease in conversions in aliphatic C–H oxidation using **6** as catalyst compared to the use of **2** was found in Chapter 2.[23] Introduction of bulky TIPS groups at the *meta*-position of the pyridine rings as in **7** lead to a significant increase in conversion from 52% to 87% (entry 8), with much more di-epoxides formed, therefore, a much lower M/D ratio was obtained (1.4, entry 8). This result is in line with previous findings that complex **7** has a higher catalytic activity than **6** in C–H bond oxidations.[23,28]

Table 1. Epoxidation of ML catalyzed by different Fe(N2Py2) complexes. [a)]

Entry	Catalyst	Conv. (%)[b)]	Mono-epoxides (%)[b)]	Di-epoxies (%)[b)]	M/D[c)]	Epoxide selectivity (%)[d)]
1	$Fe(OTf)_2 \cdot 2CH_3CN$	5	0	0	-	0
2	**1**	40	20	-	-	50
3	**2**	90	47	32	1.5	88
4	**3**	92	46	39	1.2	92
5	**4**	73	39	11	3.5	68
6	**5**	85	48	28	1.7	89
7	**6**	52	42	4.6	9	90
8	**7**	87	43	30	1.4	84

[a)] General reaction conditions: ML (0.5 mmol), catalyst (1 mol %, w.r.t. ML), AcOH (1.5 mol% w.r.t. ML) and H_2O_2 (1.5 equiv., w.r.t. ML, added at once) were mixed in MeCN at room temperature (RT), and reaction mixture was stirred for 1 h. [b)] Conversion of ML and epoxides yields were determined by GC analysis. [c)] M/D = mono-epoxides yield / di-epoxides yield. [d)] Epoxide selectivity = {(mono-epoxides yield + di-epoxides yield) / ML conversion} x 100%

As can be seen in Table 1, BPBP-based iron complexes generally exhibited good reactivities in the epoxidation of ML (>85% ML conversion) and high epoxide selectivities (>85%) at 1 mol% catalyst loading (entries 3, 4, and 6). This general observation does not apply to complex **4**, which has electronically deactivating groups on the pyridine moieties (entry 5). Not surprisingly, the less reactive catalyst **6** gave the highest M/D ratio as di-epoxidation is largely attenuated. Nevertheless, **6** still provided an excellent epoxide selectivity of 90% (entry 7).

3.2.2 Influence of various reaction conditions

In the production of epoxidized fatty acids and esters for industrial uses, stereo-induction is not required (enantioselective epoxidation with the chiral catalysts was not investigated in this study either). Therefore, the less elaborated and less expensive, but reactivity-retained complex **5** was used as catalyst to examine solvent effects on the epoxidation of ML. Performing the reaction in other solvents than acetonitrile generally led to poor outcomes. 10%, 54%, and 7% conversion were found in CH_2Cl_2, MeOH, and DMF, respectively (entries 1-3, Table 2). Only the reaction using acetone as solvent provided a similar conversion as the reaction in MeCN, with a somewhat higher M/D ratio (83% vs. 85%, 2.1 vs. 1.7, respectively; entry 4). However,

in view of safety considerations, acetone is not an ideal solvent for large-scale reactions due to the formation of explosive acetone peroxides in the presence of H_2O_2. The set of catalysts tested here was found to be poorly soluble in some other solvents, including ethyl acetate, THF, and toluene.

Increasing the loading of AcOH (1.5 mol% to 500 mol%) or catalyst **5** (1 mol% to 2 mol%), both resulted in increased conversions of ML (95% and 90%, respectively) and yielded di-epoxidation products preferably, providing a M/D ratio of 0.5 in both cases (entries 5 and 6). It was also found that lowering the reaction temperature to 0 °C is beneficial for the epoxidation of double bonds (95% conversion and 0.5 M/D ratio, entry 7). On the basis of these findings, an optimized catalytic protocol was tested to obtain full epoxidation. To do so, the reaction was performed with 2.2 equiv. of H_2O_2 (excess H_2O_2 w.r.t. double bond), 1 mol% of **5**, and 100 mol% of AcOH at 0 °C, achieving an excellent yield of 92% of di-epoxides in only 5 min as monitored by GC, with full conversion of ML and without the detection of mono-epoxidized products (entry 8). Given the short reaction time, the H_2O_2 oxidant was added at once at the beginning of the reaction.

Table 2. Epoxidation of ML catalyzed by **5** with various reaction conditions.[a)]

Entry	**5** Loading (mol%)	AcOH loading (mol%)	solvent	Conv. (%)[b)]	Mono-epoxides (%)[b)]	Di-epoxies (%)[b)]	M/D[c)]	Epoxide selectivity (%)[f)]
1	1	1.5	CH_2Cl_2	10	5	0	-	50
2	1	1.5	MeOH	54	18	1.2	15	36
3	1	1.5	DMF	7	0	0	-	0
4	1	1.5	acetone	83	46	22	2.1	82
5	1	500	MeCN	95	30	60	0.5	95
6	2	1.5	MeCN	90	28	57	0.5	94
7[d)]	1	1.5	MeCN	95	29	61	0.5	95
8[e)]	1	100	MeCN	>99	0	92	-	92

[a)] General reaction conditions: ML (0.5 mmol), **5** (1 mol%, w.r.t. ML), AcOH (1.5 mol% w.r.t. ML) and H_2O_2 (1.5 equiv., w.r.t. ML, added at once) were mixed in the indicated solvent at room temperature (RT), and the reaction mixture was stirred for 1 h. [b)] Conversion of ML and epoxides yields were determined by GC analysis. [c)] M/D = mono-epoxides yield / di-epoxides yield. [d)] Reaction temperature was 0 °C. [e)] 2.2 equiv. of H_2O_2 were added, the reaction was carried out at 0 °C for 5 min. [f)] Epoxide selectivity = {(mono-epoxides yield + di-epoxides yield) / ML conversion} x 100%

3.2.3 Monitoring reaction over time; further protocol improvement

As illustrated in Tables 1 and 2, it is clear that the conversion of ML and M/D ratios are largely dependent of the reactivities of the catalysts and the loadings of reagents. Systematic increases in substrate conversion and di-epoxides yield have been observed in response to the improved catalytic activity of the iron complexes. Adding more catalyst, H_2O_2, or AcOH also leads to increased consumptions of double bonds in both the ML starting material and in intermediate mono-epoxide products. Di-epoxides can be obtained as the predominant product with 92% yield using **5** as catalyst under optimized reaction conditions (see entry 8, Table 2). In order to obtain insight into the influence of different reaction parameters on reaction progression as a function of time, which in turn provides information on the real-time formation of mono- and di-epoxide products, reaction time profiles were examined.

First, ML epoxidation using **2** as catalyst (1 mol%), with 2 equiv. of H_2O_2 (1 equiv. w.r.t. to double bond), and 1 equiv. of AcOH was monitored over time. Surprisingly, the conversion of ML was found to be nearly complete after 2 min, with only 7.7% of remaining starting material (rSM) in the reaction mixture (Figure 3, top). At the same point in time, the highest amount of mono-epoxides (47.4%) and 40% of di-epoxides was observed. Only 1.7% of ML was converted in the following 3 min, leaving 6% of remaining ML after 5 min of reaction time. At this point in time, the mono-epoxide yield slightly dropped to 45% and the formation of di-epoxides had increased to 44.8%, accordingly. Subsequently, all organic reaction components were found to be at close to constant concentrations, with only very slow conversion of mono-epoxides in to di-epoxides, ending up with 4.8% of rSM, 42.7% of mono-epoxides, and 47.8% of di-epoxides (0.9 M/D ratio) after 30 min (Figure 3, top). Because of the unexpectedly fast initial reaction progression using catalyst **2**, the reaction profile of ML epoxidation with another catalyst was also examined. Therefore, complex **6**, which showed a very different catalytic outcome than **2** in terms of substrate conversion and M/D ratio (see Table 1), was employed as catalyst. As clearly shown in the bottom diagram in Figure 3, very similar trends were observed for the reaction with **6** as for the reaction with **2**; *i.e.*, both mono-epoxide and di-epoxide formation nearly ceased around 2 min. Nevertheless, in accordance with the data in Table 1, a lower conversion of ML and higher M/D were found with **6** (76% and 3.1, respectively).

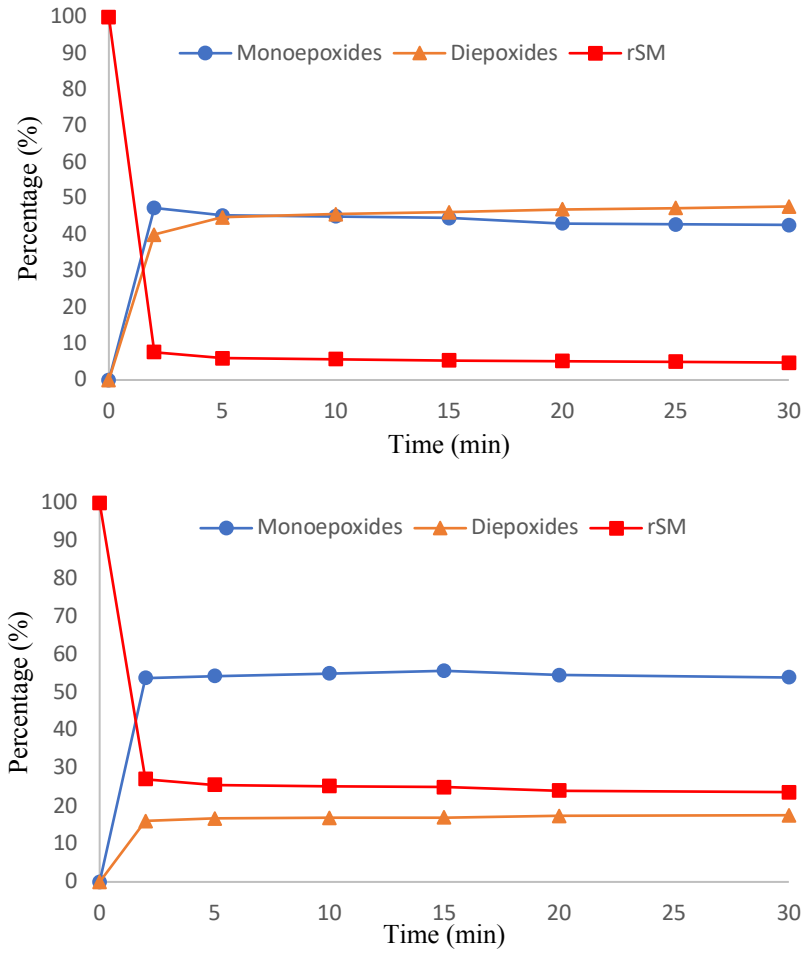

Figure 3. Reaction profiles of ML epoxidation with **2** (top) and **6** (bottom). Reaction conditions (standard conditions): ML (0.5 mmol), catalyst (1 mol%), AcOH (1 equiv.) and H_2O_2 (2 equiv.) in MeCN at RT. rSM = remaining starting material.

The results shown in Figure 3 indicate that the progression of the epoxidation reaction is very rapidly limited by a certain factor. It was first suspected that the depletion of H_2O_2 due to the catalytic disproportionation of H_2O_2 in the presence of an iron complex would hamper further reaction progression. In order to figure out if the actual oxidant concentration was the limiting factor, reactions involving an iterative addition of H_2O_2 were performed, *i.e.*, a second portion of H_2O_2 (1 equiv.) was added after 3 min, besides the first 2 equiv. of H_2O_2 added at the beginning of the reaction. However, as shown in Figure 4, no significant changes in the amounts of the ML starting material and epoxide products were observed after 5 min and beyond compared to the amounts present after 2 min, either using catalyst **2** (Figure 4, top) or **6** (Figure 4, bottom). These observations strongly suggest that the concentration of H_2O_2 is not the limiting factor in ML epoxidation.

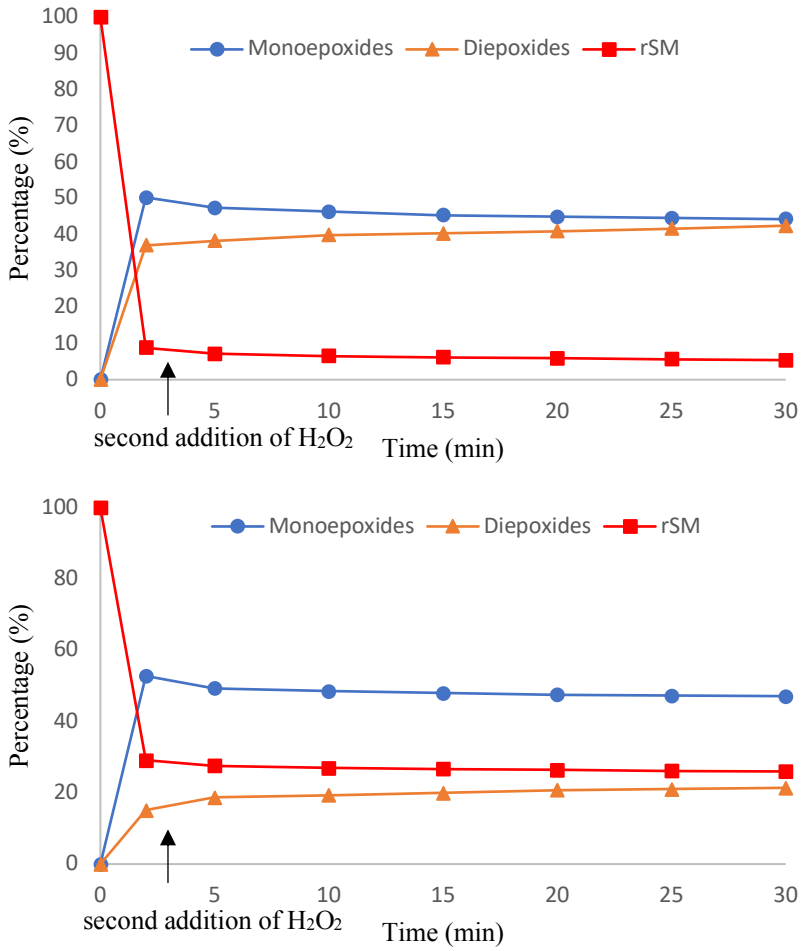

Figure 4. Reaction profiles of ML epoxidation using **2** (top) or **6** (bottom) with iterative addition of H_2O_2. Reaction conditions: ML (0.5 mmol), catalyst (1 mol %), AcOH (1 equiv.) and H_2O_2 (2 equiv.) in MeCN at RT. At 3 min, 1 additional equiv. of H_2O_2 was added.

Having found that no obvious catalytic activities occurred after addition of an excess H_2O_2 (Figure 4), it was considered that catalyst deactivation could be causing the rapid decay in catalytic activity. To prove this, reactions with iterative addition of catalyst **2** were carried out, as shown in Figure 5. This experiment was started with the standard reaction conditions as used to generate Figures 3 and 4. Again, a pseudo-steady-state phase was observed between 2 and 5 min of reaction time (Figure 5, top). At 6 min, an additional 1.0 mol% **2** was added to the reaction mixture, leading to an abrupt decrease of rSM and mono-epoxides, with a dramatic further increase in the formation of di-epoxide products. From this reaction profile, it can be clearly concluded that rapid catalyst deactivation takes place at a very early stage under the current conditions. It has been reported previously by the White group that catalytic aliphatic C–H bond oxidations using BPBP-based iron catalysts also benefit from iterative addition of catalyst (a solution of catalyst, H_2O_2, and AcOH was iteratively added in their case).[22,29–32] Steady-state concentrations of all the organic components were observed again after about 10

min (Figure 5, top). It is not clear though if catalyst deactivation had again taken place, as full conversion of ML and low amounts of mono-epoxides (ca. 5 %) were found, which can also lead to low catalytic activity. In order to figure out if this was the case, the same catalyst addition experiment was performed with **6**, which showed a lower activity in ML epoxidation (Table 1). The yield of di-epoxides was also found to be improved a lot when a second portion of 1.0 mol% **6** was used (Figure 5, bottom). However, the amount of ML and epoxide products stayed stable after 10 min also in this case, even though with 5% ML and 42% mono-epoxides still remaining, suggesting that catalyst deactivation had again taken place. Several studies have reported that non-heme iron catalysts are deactivated *via* oxidative dimerization in the presence of oxidants and acetic acid, forming inert binuclear oxo-bridged dimers.[27,32–36] More details on the deactivation of iron complexes with N2Py2 ligands will be discussed in Chapter 4 of this thesis.

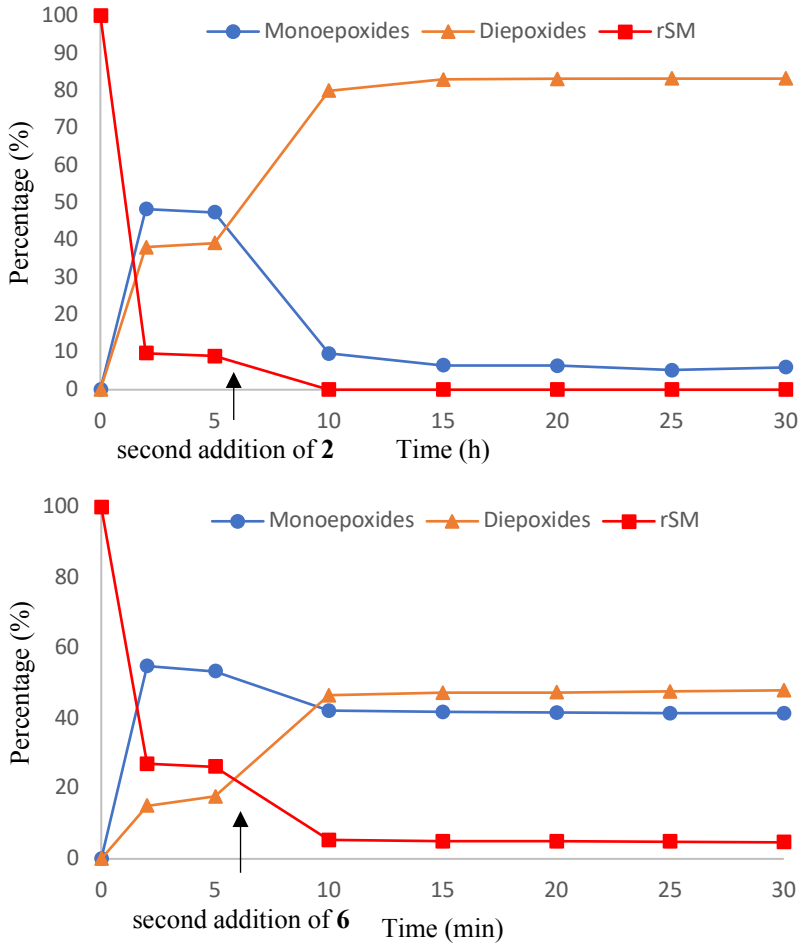

Figure 5. Reaction profiles of ML epoxidation with **2** (top) or **6** (bottom) with iterative addition of catalyst. Reaction conditions: ML (0.5 mmol), catalyst (1 mol%), AcOH (1 equiv.) and H_2O_2 (2 equiv.) in MeCN at RT. At 6 min, an additional 1 mol% of catalyst was added.

In fact, iterative addition protocols and slow addition of H_2O_2 are generally used in oxidation reactions catalyzed by non-heme iron complexes with tetradentate polyamine ligands. Significant decreases in yield have been observed if H_2O_2 was added rapidly,[22,29,32] which was explained as being due to catalyst decomposition. In order to investigate the influence of the addition rate of H_2O_2, the epoxidation reactions were performed using a slow H_2O_2 addition protocol. In the reaction with **2**, standard reaction conditions were utilized but delivery of H_2O_2 in the reaction mixture was extended *via* syringe pump over 30 min. As illustrated in the top time profile in Figure 6, the reaction proceeded much more slowly than the reaction under standard conditions (Figure 3, top). In fact, ML was continuously converted and the epoxidized products were generated accordingly along with the addition of H_2O_2 (0-30 min, Figure 6, top). Notably, the epoxidation reactions nearly ceased at the end of H_2O_2 addition as the ML and epoxide product concentration came to steady-state concentrations after 30 min. In addition, compared to the reaction with instant addition of H_2O_2 (Figure 3, top), a much lower conversion of ML and di-epoxides yield were noted (67% vs. 95%, 13% vs. 48%, respectively). Similar trends were also observed in the same experiment using catalyst **6** (Figure 6, bottom), *i.e.* conversion of ML and formation of epoxides proceeded slowly during 0-30 min. Again, less conversion of ML and terminal epoxidized products were provided than in the reaction with standard conditions (Figure 3, bottom). In this sense, it can be concluded that the slow H_2O_2 addition protocol seems to be a subtle factor in the catalytic epoxidation of ML. On the one hand it decreases the decomposition rate of catalyst, on the other hand it causes a lower concentration of H_2O_2 throughout the reaction. It has been reported that ML is a relatively less active substrate because of its relatively high unsaturation,[17,19,37,38] which means the concentration of H_2O_2 could be of importance to obtain high ML conversion. Additionally, catalyst reactivity was also deteriorating during the addition of H_2O_2. In both cases in Figure 6, only about 3% of ML was converted between 20 and 30 min, despite the fact that H_2O_2 was still being added. This indicates that the catalyst was nearly fully deactivated before complete addition of H_2O_2. These combined factors eventually lead to a halt of the epoxidation reactions.

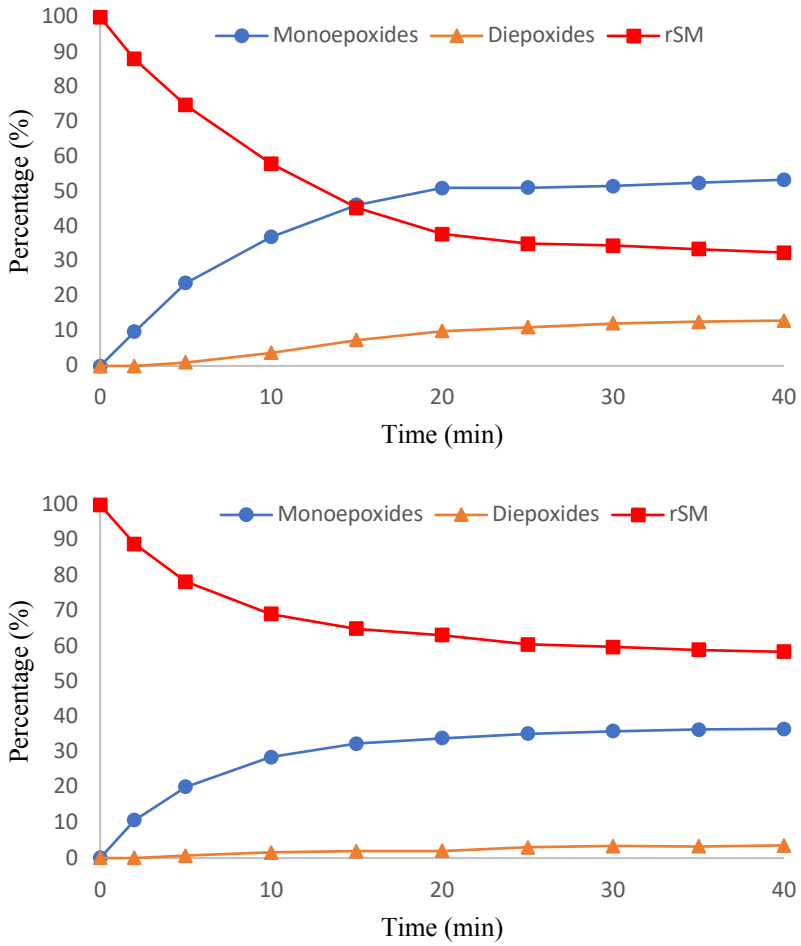

Figure 6. Reaction profiles of ML epoxidation with **2** (top) or **6** (bottom) with slow addition of H_2O_2. Reaction conditions: ML (0.5 mmol), catalyst (1 mol%) and AcOH (1 equiv.) were mixed in MeCN at RT, subsequently H_2O_2 (2 equiv.) was added dropwise over 30 min.

Next, the influence of slow addition of catalyst was examined. Using **2** as catalyst, the epoxidation of ML was monitored in time while adding 1 mol% **2** over 30 min (Figure 7, top). From 0 to 5 min, 32% of ML was converted, forming 28% of mono-epoxides. An initial lag phase was observed for di-epoxides formation in the very beginning, which is probably due to the low concentration of mono-epoxides. Upon progression of the reaction, the highest amount of mono-epoxides of 54% was detected around 10 min, after which the concentration of mono-epoxides consistently dropped with concomitant increase in di-epoxides yield until about 20 min. The reaction ceased after 20 min, even though fresh catalyst was still being added between 20 and 30 min, suggesting the depletion of H_2O_2. Indeed, it was found *via* iodometric titration that all of the H_2O_2 had been consumed at this point. Additionally, compared to the case of iterative addition of catalyst (Figure 5, top), a lower total yield of epoxy groups with respect to double bonds (mono-epoxides yield × 0.5 + di-epoxides yield) was noted in this reaction (78% vs. 98%), meaning that slow catalyst addition caused more (catalytic) H_2O_2 disproportionation

(ca. 22%), despite much higher initial catalyst concentration present in the case of iterative catalyst addition. It is assumed that H_2O_2 disproportionation is caused by 'active' iron species. In this regard, H_2O_2 disproportionation ceases when the catalyst is immediately deactivated in the reaction with instant catalyst addition (Figures 3 and 5). In contrast, in the case of slow catalyst addition, 'active' iron species are consistently added, leading to continuous disproportionation of H_2O_2, which then becomes an important factor that limits the epoxidation progression. However, this can be easily overcome by adding more H_2O_2.

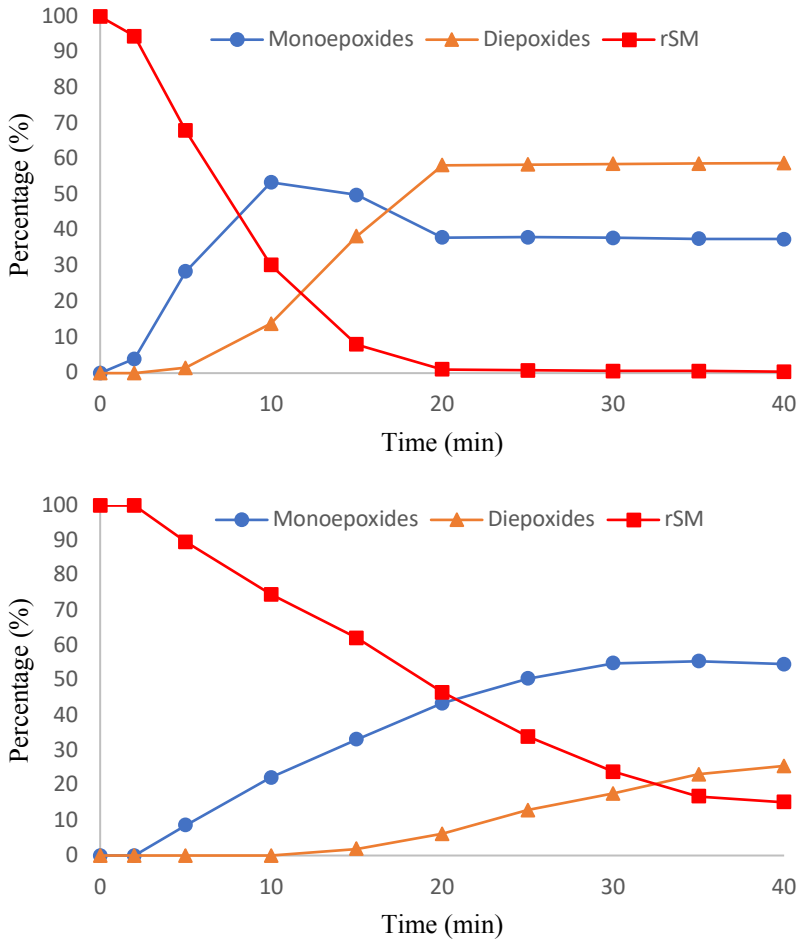

Figure 7. Reaction profiles of ML epoxidation with **2** (top) or **6** (bottom) using slow catalyst addition. Reaction conditions: ML (0.5 mmol), AcOH (1 equiv.) and H_2O_2 (2 equiv.). were mixed in MeCN at RT, subsequently catalyst (1 mol%, 0.5 mL 10 mM solution in MeCN) was added dropwise over 30 min.

In the case of **6**, a longer lag phase of di-epoxide formation was found from 0 to 15 min using slow catalyst addition (Figure 7, bottom). A similar 55% maximum yield of mono-epoxides was found in this case at 35 min. No remaining ML or 15% of ML was detected in the reaction at 40 min with **2** or **6**, respectively, which is less compared to the cases using standard reaction conditions (Figure 3). These observations are in agreement with a previous study in which the

slow catalyst addition protocol had a positive effect on substrate conversion.[29] More importantly, higher di-epoxides yields were obtained compared to the standard reaction conditions used in Figure 3 (59% vs. 48% for **2**, 26% vs. 18% for **6**), indicating that the production of di-epoxides could benefit from a slow catalyst addition protocol.

3.2.4 O-transfer selectivities: mono- vs. di-epoxidation

It is evident from Figure 7 that **2** and **6** show very different kinetic behaviors in the epoxidation of ML under similar reaction conditions. It was also noted that similar maximum yields of mono-epoxides of ca. 55% were obtained in these two cases. On the other hand, the reaction with **6** also gave a similar maximum mono-epoxides yield of 53% when iterative catalyst addition was used (Figure 5, bottom), instead of a slow catalyst addition protocol as in Figure 7. These observations suggest that **2** and **6** may have similar selectivities of O-transfer from H_2O_2 to mono-epoxidation or di-epoxidation products. Table 1, however, shows that **2** and **6** provide remarkably different M/D ratios (1.5 vs. 9) using initial reaction conditions. This is accompanied by very different ML conversions (90% and 52%, respectively), meaning that the difference in M/D ratio is probably due to the lower reactivity of **6** with respect to the starting material and, accordingly, a slower built-up of mono-epoxide concentration. Consequently, it is difficult to evaluate the ability of these catalysts to act as selective catalyst toward the formation of either mono- or di-epoxides on the basis of the above data.

In order to obtain insight into the mono- vs. di-epoxidation selectivity properties of the catalysts, a series of ML epoxidation reactions were performed using catalysts **2**, **3**, **4**, and **6**, with different H_2O_2 loadings in the range of 0.2-2.6 equiv. (see experimental section for reaction details). For each series of reactions, ML conversion and mono- and di-epoxides yields were plotted with respect to the total amount of oxygen atoms transferred from H_2O_2 to epoxide products. The amount of transferred oxygen atoms is described with respect to the amount of starting ML, and is calculated from the formula:

$$\text{O-transferred} = (\text{mono-epoxides yield} + \text{di-epoxides yield} \times 2) / 100\%$$

By doing so, correlations between epoxide yields, ML conversion (shown as rSM), and the number of transferred oxygen atoms could be obtained for each catalyst (Figure 8). For **2**, the maximum mono-epoxides yield of 52% was found when ca. 1 equiv. of O was transferred to products (Figure 8a); this percentage is similar to that observed in Figure 7. At the maximum amount of mono-epoxides, 26% of di-epoxides had formed and 19 % of rSM was present,

representing an M/D ratio of 2. It was found that ML was fully converted when 1.8 equiv. of oxygen atoms were transferred, yielding 8.7% of mono-epoxides and 87% of di-epoxides (0.1 M/D ratio). Very similar trends for each component have been obtained using **6** as catalyst (Figure 8b). Notably, the highest yield of mono-epoxides was also found to be 53% when about 1 equiv. of oxygen atoms was transferred to the products, with 23% of di-epoxides and 21% of rSM observed (M/D = 2.3). ML was fully consumed when 1.7 equiv. of oxygen atoms were transferred, giving rise to an M/D ratio of 0.19 (14.7% of mono-epoxides and 79% of di-epoxides). These data are nearly identical to those obtained in the reaction series with **2**.

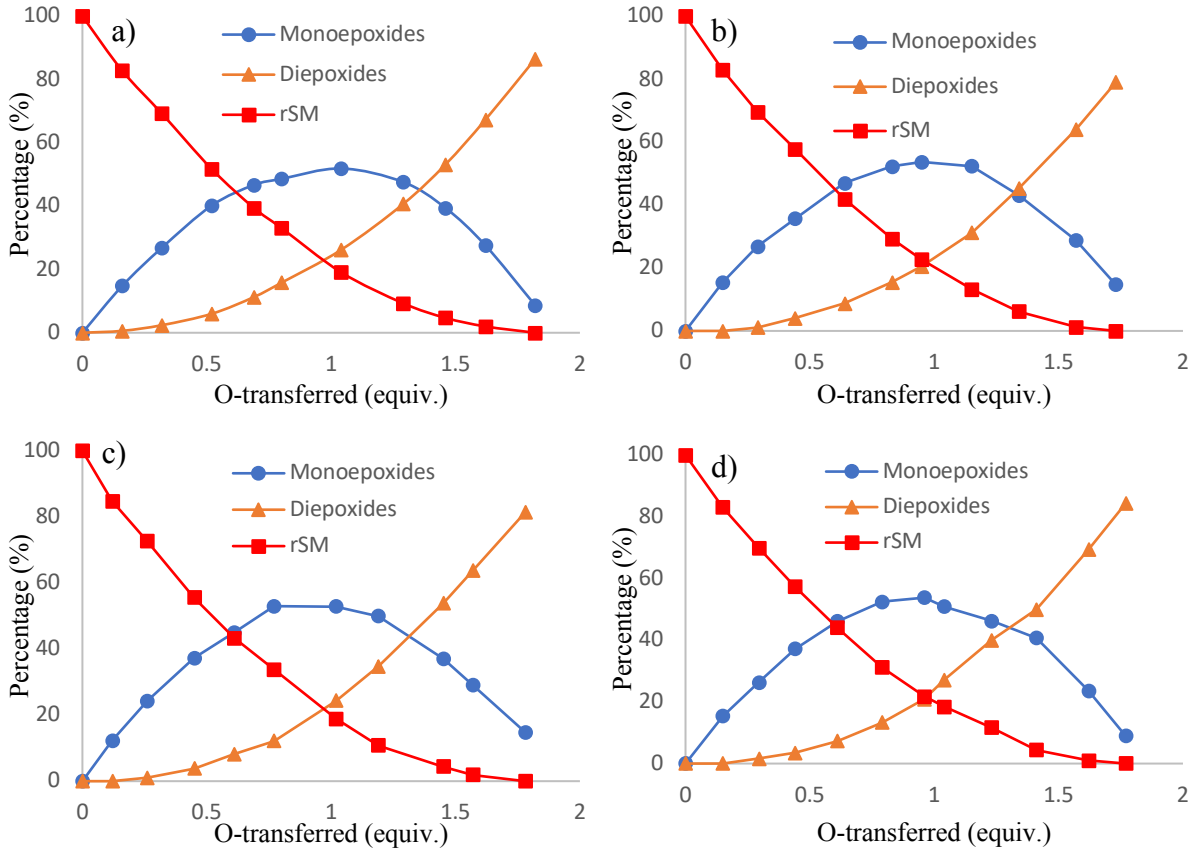

Figure 8. Correlations between mono-epoxides yield, di-epoxides yield, and rSM and the number of transferred oxygen atoms using **2** (a), **6** (b), **3** (c) or **4** (d) as catalyst. O-transferred = (mono-epoxides yield + di-epoxides yield × 2) / 100% (w.r.t. starting ML).

This comparison indicates that **2** and **6** have rather similar selectivity properties of O-distribution to epoxidation products. In order to find out if this similarity also holds for other catalysts, catalysts **3** and **4**, which showed different catalytic performances from **2** and **6** under the standard conditions (Table 1), were also tested. Figure 8c and 8d show that similar percentage trends were obtained using **3** and **4** with respect to **2** and **6**. Specifically, similar highest yields of mono-epoxides (53% for **3**, 54% for **4**) were observed with ca. 1 equiv. of

oxygen atoms transferred. Similarly, both for **3** and **4**, 1.8 equiv. of oxygen atoms were transferred to reach full conversion of ML, giving M/D ratios of 0.18 and 0.1 for **3** and **4**, respectively.

The O-distribution selectivity to epoxide products for different catalysts is depicted in Figure 9, which displays the correlation between M/D ratio and O-transferred using catalysts **2**, **3**, **4**, and **6**. This figure clearly shows that this set of catalysts provide rather similar M/D ratios when the same amount of oxygen atoms are transferred to form epoxides. It is difficult to compare M/D ratios when only small amounts of oxygen (<0.4) are transferred to epoxide products, since small errors in the GC-detection of low amounts of di-epoxides may cause significantly different M/D ratios. For instance, in the cases with ca. 0.3 equiv. of O-transferred, all the catalysts gave similar conversions of ML (~30%) and mono-epoxides yields (~26%), as shown in Figure 8. However, the di-epoxides yields varied between 1% and 2.4%, which lead to very different M/D ratios.

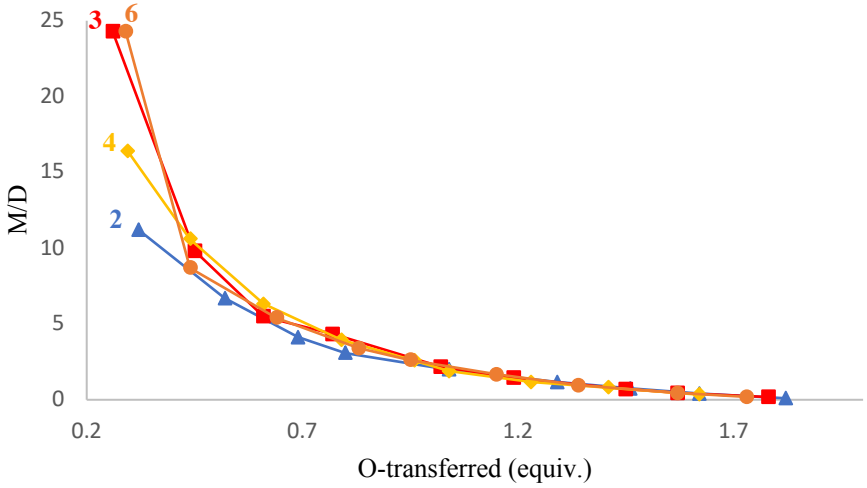

Figure 9. Correlation between M/D ratio and O-transferred using catalysts **2**, **3**, **4**, and **6**.

In a sequential reaction like the epoxidation of ML (Scheme 2), if the selectivities towards mono-epoxidation and di-epoxidation are identical, the reaction exhibits the same rate constants for mono-epoxidation (k_1) and di-epoxidation (k_2). Under these circumstances, kinetic simulations predict the upper limit for the yield of the intermediate product (mono-epoxides in this case) to be 36.8%, as previously reported by Blackmond *et al.*.[39] Whereas the current study has not provided clear indications for a preference for mono-epoxidation over di-epoxidation, or *vice versa*, all catalysts tested give similar maximum yields of mono-epoxides of ~55%. This value indicates that the Fe-catalysts do have a preference for mono-epoxidation over di-epoxidation, albeit that the difference between k_1 and k_2 may be small. The origin of

this difference is not clearly understood, but may be related to the increased steric hindrance around the remaining C=C double bond in ML-derived mono-epoxides, making di-epoxidation more difficult.

Scheme 2. Sequential formation of mono-epoxides and di-epoxides in epoxidation of ML.

3.3 Conclusions

In this chapter, the use of Fe(N2Py2) complexes in combination with H_2O_2 as the oxidant and AcOH as an additive for the epoxidation of methyl linoleate (ML), a typical poly-unsaturated fatty acid derivative, has been investigated and optimized. The catalytic activity of these catalyst systems, especially the mono-epoxides/di-epoxides product ratio (M/D), are highly dependent on the nature of the N2Py2 ligands. With 1 mol% [Fe(OTf)$_2$(BPBI)] (**6**), mono-epoxides are obtained with 42% yield at 52% ML conversion, with trace amounts of di-epoxides formed (4.7%). On the other hand, very high yields of di-epoxides (92%) at full ML conversion can be achieved using 1 mol% [Fe(OTf)$_2$(*mix*-BPBP)] (**5**) as catalyst in only 5 min, without the detection of mono-epoxides. In both cases, the selectivity for the formation epoxide products is very high (> 90%).

Using an optimized set of reaction conditions, the catalytic activity of [Fe(OTf)$_2$(*S,S*-BPBP)] (**2**) and **6** have been examined over time. This has led to the realization that upon full addition of the H_2O_2 oxidant at the beginning of the reaction very rapid catalyst deactivation takes place. Alternative catalytic protocols that include iterative or slow catalyst addition, or slow oxidant addition were found to overcome catalyst deactivation to a certain extent, and have an impact on, e.g., the M/D ratio. In general, slow oxidant addition suppresses di-epoxidation progression in this study, while slow catalyst addition is beneficial for the formation of di-epoxides. An investigation on the selectivity of oxygen atom transfer to epoxide products of a selected set of Fe(N2Py2) catalysts has shown a small, but significant preference for mono-epoxidation over di-epoxidation ($k_1 > k_2$).

Overall, the iron complexes presented here represent very potent catalysts for the epoxidation of ML and, accordingly, of fatty acid (esters) in general. High yields of epoxides can be obtained at high substrate conversion in short reaction times and at very mild conditions.

Changing the N2Py2 ligand in the complexes, as well as varying the overall catalytic protocol allows for facile modulation of the reaction outcome, *e.g.* in terms of the M/D ratio. Accordingly, it is envisioned that these catalysts, and in particular the readily accessible catalyst **5**, can be applied in fatty acid and plant valorization for the production of epoxidized products that may find use in various applications.

3.4 Experimental Section

3.4.1 General

The iron precursor $Fe(OTf)_2 \cdot 2CH_3CN$ was synthesized according to a reported procedure.[40] The solvents tetrahydrofuran, acetonitrile, and toluene used for catalysis were purified with an MBraun MB SPS-800 solvent purification system. Tetrahydrofuran for complexation reactions, methanol, and dichloromethane were dried with sodium, magnesium turnings, or CaH_2, respectively, and distilled under nitrogen prior to use. All other reagents and substrates were obtained commercially and used without further purification. Catalytic reactions were conducted under ambient conditions, unless noted otherwise. Column chromatography was performed using Merck silica gel (60–200 mesh). ^{1}H and ^{13}C NMR spectra were recorded with a 400 MHz Varian spectrometer at 25 °C, chemical shifts (δ) are given in ppm referenced to the residual solvent peak. Gas chromatography was performed on a Perkin–Elmer Clarus 500 Gas Chromatograph equipped with a PE-17 column ((30 m × 0.23 mm × 0.25 μm), (50% phenyl)-(50% methyl)polysiloxane) and a flame-ionization detector. Complexes **1**-**5** were synthesized according to literature procedures.[24,26,27,35,41] The synthesis and characterization of complexes **6** and **7** are described in Chapter 2 of this thesis.[23]

3.4.2 Large-scale synthesis of ML mono-epoxides and di-epoxides for GC reference samples

ML mono-epoxides and di-epoxides were prepared following a reported procedure.[42]
ML mono-epoxides (mixture of two isomers): ^{1}H NMR (400 MHz, $CDCl_3$): δ 5.55 – 5.38 (m, 2H), 3.66 (s, 3H), 2.94-2.89 (m, 2H), 2.40 – 2.14 (m, 2H), 2.30 (t, J = 7.5 Hz, 2H), 2.06 – 2.01 (m, 2H), 1.64 – 1.27 (m, 18), 0.89 (t, J = 6.9 Hz, 3H). ^{13}C NMR (100 MHz, $CDCl_3$) δ 174.20, 132.68, 132.52, 123.90, 123.75, 57.17, 57.11, 56.50, 51.44, 51.37, 34.03, 31.71, 31.46, 29.45, 29.32, 29.20, 29.14, 29.11, 29.06, 29.04, 29.00, 27.72, 27.38, 26.53, 26.25, 26.20, 24.90, 24.87, 22.56, 22.52, 14.02, 13.96. Spectral properties of the product are in agreement with the literature data.[43]
ML di-epoxides (mixture of two isomers): ^{1}H NMR (400 MHz, $CDCl_3$): δ 3.66 (s, 3H), 3.13 – 2.90 (m, 4H), 2.30 (t, J = 7.5 Hz, 2H), 1.78 – 1.32 (m, 22H), 0.90 (t, J = 6.9 Hz, 3H). ^{13}C NMR (100 MHz, $CDCl_3$) δ 174.15, 56.95, 56.90, 56.67, 56.61, 54.30, 54.28, 54.13, 51.37, 33.98, 31.62, 29.23, 29.09, 28.96, 27.83, 27.76, 27.16, 26.87, 26.47, 26.36, 26.19, 26.08, 24.83, 22.51, 13.92. Spectral properties of the product are in agreement with the literature data.[44]

3.4.3 Reaction procedures for catalytic reactions

General reaction procedure for the epoxidation of ML (Tables 1 and 2)

A 20 mL vial was charged with: ML (0.5 mmol, 1 equiv.), catalyst (5 μmol, 1 mol%), solvent (1.5 mL). A 0.5 M AcOH solution in CH_3CN was added (15 μL, 7.5 μmol, 1.5 mol%). Subsequently, a 1.0 M H_2O_2 solution in CH_3CN (0.75 mL, 0.75 mmol, 1.5 equiv., diluted from a 35% H_2O_2 aqueous solution) was added at once at RT. The resulting mixture was stirred at RT for 1 h. At this point, a 1.0 M nitrobenzene solution in CH_3CN (0.5 mL, 0.5 mmol, 1 equiv.) was added as internal standard. The solution was filtered through a silica gel plug, which was subsequently rinsed with 3 x 1 mL EtOAc. GC analysis of the solution provided substrate conversions and product yields relative to the internal standard integration. Products were identified by comparison to the GC retention time of authentic samples.

Time profiles of ML epoxidation using standard reaction conditions (Figure 3)

A 20 mL vial was charged with: ML (0.5 mmol, 1 equiv.), catalyst **2** or **6** (5 μmol, 1 mol%), AcOH (29 μL, 0.5 mmol, 100 mol%), solvent (1.5 mL). A 1.0 M nitrobenzene solution in CH_3CN (0.5 mL, 0.5 mmol, 1 equiv.) was added as internal standard. Subsequently, a 1.0 M H_2O_2 solution in CH_3CN (1 mL, 1 mmol, 2 equiv., diluted from a 35% H_2O_2 aqueous solution) was added at once at RT. After 2 min, the first sample (~ 50 μL) was submitted to GC analysis after filtration through a silica gel plug followed by rinsing with EtOAc. After 5 min and beyond, samples for GC analysis were taken every 5 min.

Iterative H_2O_2 addition protocol (Figure 4)

A 20 mL vial was charged with: ML (0.5 mmol, 1 equiv.), catalyst **2** or **6** (5 μmol, 1 mol%), AcOH (29 μL, 0.5 mmol, 100 mol%), solvent (1.5 mL). A 1.0 M nitrobenzene solution in CH_3CN (0.5 mL, 0.5 mmol, 1 equiv.) was added as internal standard. Subsequently, a 1.0 M H_2O_2 solution in CH_3CN (1 mL, 1 mmol, 2 equiv., diluted from a 35% H_2O_2 aqueous solution) was added at once at RT. After 2 min, the first sample (~ 50 μL) was submitted to GC analysis after filtration through a silica gel plug followed by rinsing with EtOAc. After 3 min, a second portion of H_2O_2 solution (1 equiv.) was added to the reaction mixture. After 5 min and beyond, samples for GC analysis were taken every 5 min.

Iterative catalyst addition protocol (Figure 5)

A 20 mL vial was charged with: ML (0.5 mmol, 1 equiv.), catalyst **2** or **6** (5 μmol, 1 mol%), AcOH (29 μL, 0.5 mmol, 100 mol%), solvent (1.5 mL). A 1.0 M nitrobenzene solution in CH_3CN (0.5 mL, 0.5 mmol, 1 equiv.) was added as internal standard. Subsequently, a 1.0 M H_2O_2 solution in CH_3CN (1 mL, 1 mmol, 2 equiv., diluted from a 35% H_2O_2 aqueous solution) was added at once at RT. After 2 min, the first sample (~ 50 μL) was submitted to GC analysis after filtration through a silica gel plug followed by rinsing with EtOAc. After 5 min and beyond, samples for GC analysis were taken every 5 min. After 6 min, a second portion of catalyst (1 mol%) was added to the reaction mixture.

Slow H_2O_2 addition protocol (Figure 6)

A 20 mL vial was charged with: ML (0.5 mmol, 1 equiv.), catalyst **2** or **6** (5 μmol, 1 mol%), AcOH (29 μL, 0.5 mmol, 100 mol%), solvent (1.5 mL). A 1.0 M nitrobenzene solution in CH_3CN (0.5 mL, 0.5

mmol, 1 equiv.) was added as internal standard. Subsequently, a 1.0 M H_2O_2 solution in CH_3CN (1 mL, 1 mmol, 2 equiv., diluted from a 35% H_2O_2 aqueous solution) was delivered by syringe pump over 30 min. After 2 min, the first sample (~50 μL) was submitted to GC analysis after filtration through a silica gel plug followed by rinsing with EtOAc. After 5 min and beyond, samples for GC analysis were taken every 5 min.

Slow catalyst addition protocol (Figure 7)

A 20 mL vial was charged with: ML (0.5 mmol, 1 equiv.), AcOH (29 μL, 0.5 mmol, 100 mol%), nitrobenzene (0.5 mmol, 1 equiv., internal standard) and solvent (2 mL). A 1.0 M H_2O_2 solution in CH_3CN (1 mL, 1 mmol, 2 equiv., diluted from a 35% H_2O_2 aqueous solution) was added. Subsequently, a solution of catalyst **2** or **6** (5 μmol, 1 mol%) in 0.5 mL CH_3CN was delivered by syringe pump over 30 min. After 2 min, the first sample (~50 μL) was submitted to GC analysis after filtration through a silica gel plug followed by rinsing with EtOAc. After 5 min and beyond, samples for GC analysis were taken every 5 min.

O-distribution experiments for ML epoxidation by 2 (Figure 8)

A set of 20 mL vials were all charged with: ML (0.5 mmol, 1 equiv.), catalyst **2** (5 μmol, 1 mol%), AcOH (29 μL, 0.5 mmol, 100 mol%), solvent (1.5 mL). A 1.0 M nitrobenzene solution in CH_3CN (0.5 mL, 0.5 mmol, 1 equiv.) was added to each vial as internal standard. Subsequently, different amounts of H_2O_2 (0.2, 0.4, 0.6, … 2.6 equiv., added as a 1.0 M solution in CH_3CN) were added dropwise to each reaction mixture. Once oxidant addition was completed, all reaction mixtures were stirred at RT for 10 min. At this point, for each reaction a sample was submitted to GC analysis after filtration through a silica gel plug followed by rinsing with EtOAc.

The O-distribution experiments with different catalyst (**3**, **4**, and **6**) were conducted in the same manner as the cases of **2**.

3.5 References

[1] S. G. Tan, W. S. Chow, *Polym. Plast. Technol. Eng.* **2010**, *49*, 1581–1590.

[2] A. K. R. Somidi, R. V. Sharma, A. K. Dalai, *Ind. Eng. Chem. Res.* **2014**, *53*, 18668–18677.

[3] S. M. Danov, O. A. Kazantsev, A. L. Esipovich, A. S. Belousov, A. E. Rogozhin, E. A. Kanakov, *Catal. Sci. Technol.* **2017**, *7*, 3659–3675.

[4] P. Spannring, P. C. A. Bruijnincx, B. M. Weckhuysen, R. J. M. Klein Gebbink, *Catal. Sci. Technol.* **2014**, *4*, 2182–2209.

[5] S. Z. Erhan, S. Asadauskas, *Ind. Crops Prod.* **2000**, *11*, 277–282.

[6] A. Adhvaryu, S. Z. Erhan, J. M. Perez, *Thermochim. Acta* **2002**, *395*, 191–200.

[7] N. J. Fox, G. W. Stachowiak, *Tribol. Int.* **2007**, *40*, 1035–1046.

[8] H.-S. Hwang, S. Z. Erhan, *J. Am. Oil Chem. Soc.* **2001**, *78*, 1179–1184.

[9] Y. N. Lye, J. Salimon, *J. Am. Oil Chem. Soc.* **2015**, *92*, 257–266.

[10] M. Rüsch gen. Klaas, S. Warwel, *Ind. Crops Prod.* **1999**, *9*, 125–132.

[11] L. H. Gan, K. S. Ooi, S. H. Goh, L. M. Gan, Y. C. Leong, *Eur. Polym. J.* **1995**, *31*, 719–724.

[12] K. M. Doll, S. Z. Erhan, *J. Surfactants Deterg.* **2006**, *9*, 377–383.

[13] J. Salimon, N. Salih, E. Yousif, *J. Saudi Chem. Soc.* **2011**, *15*, 195–201.

[14] G. Du, A. Tekin, E. G. Hammond, L. K. Woo, *J. Am. Oil Chem. Soc.* **2004**, *81*, 477–480.

[15] C. Tiozzo, C. Bisio, F. Carniato, L. Marchese, A. Gallo, N. Ravasio, R. Psaro, M. Guidotti, *Eur. J. Lipid Sci. Technol.* **2013**, *115*, 86–93.

[16] S. Sankaranarayanan, A. Sharma, K. Srinivasan, *Catal. Sci. Technol.* **2015**, *5*, 1187–1197.

[17] M. M. Cecchini, F. De Angelis, C. Iacobucci, S. Reale, M. Crucianelli, *Appl. Catal. A Gen.* **2016**, *517*, 120–128.

[18] P. Neves, L. S. Nogueira, A. C. Gomes, T. S. M. Oliveira, A. D. Lopes, A. A. Valente, I. S. Gonçalves, M. Pillinger, *Eur. J. Inorg. Chem.* **2017**, 2617–2627.

[19] P. Neves, A. C. Gomes, F. A. A. Paz, A. A. Valente, I. S. Gonçalves, M. Pillinger, *Mol. Catal.* **2017**, *432*, 104–114.

[20] P. Spannring, V. Yazerski, P. C. A. Bruijnincx, B. M. Weckhuysen, R. J. M. Klein Gebbink, *Chem. Eur. J.* **2013**, *19*, 15012–15018.

[21] K. Chen, L. Que, *Chem. Commun.* **1999**, 1375–1376.

[22] M. S. Chen, M. C. White, *Science* **2007**, *318*, 783–787.

[23] J. Chen, M. Lutz, M. Milan, M. Costas, M. Otte, R. J. M. Klein Gebbink, *Adv. Synth. Catal.* **2017**, *359*, 2590–2595.

[24] O. Cussó, I. Garcia-bosch, X. Ribas, J. Lloret-fillol, M. Costas, *J. Am. Chem. Soc.* **2013**, *135*, 14871−14878.

[25] O. Cussó, X. Ribas, J. Lloret-Fillol, M. Costas, *Angew. Chem. Int. Ed.* **2015**, *54*, 2729 –2733.

[26] V. A. Yazerski, D. Gatineau, R. J. M. Klein Gebbink, unpublished results.

[27] V. A. Yazerski, P. Spannring, D. Gatineau, C. H. M. Woerde, S. M. Wieclawska, M. Lutz, H. Kleijn, R. J. M. Klein Gebbink, *Org. Biomol. Chem.* **2014**, *12*, 2062–2070.

[28] D. Font, M. Canta, M. Milan, O. Cussó, X. Ribas, R. J. M. Klein Gebbink, M. Costas, *Angew. Chem. Int. Ed.* **2016**, *55*, 5776–5779.

[29] M. S. Chen, M. C. White, *Science* **2010**, *327*, 566–571.

[30] P. E. Gormisky, M. C. White, *J. Am. Chem. Soc.* **2013**, *135*, 14052–14055.

[31] J. M. Howell, K. Feng, J. R. Clark, L. J. Trzepkowski, M. C. White, *J. Am. Chem. Soc.* **2015**, *137*, 14590–14593.

[32] N. A. Vermeulen, M. S. Chen, M. C. White, *Tetrahedron* **2009**, *65*, 3078–3084.

[33] J. Y. Ryu, J. Kim, M. Costas, K. Chen, W. Nam, L. Que Jr., *Chem. Commun.* **2002**, *0*, 1288–1289.

[34] M. C. White, A. G. Doyle, E. N. Jacobsen, *J. Am. Chem. Soc.* **2001**, *123*, 7194–7195.

[35] L. Gómez, I. Garcia-Bosch, A. Company, J. Benet-Buchholz, A. Polo, X. Sala, X. Ribas, M. Costas, *Angew. Chem. Int. Ed.* **2009**, *48*, 5720–5723.

[36] L. Gómez, M. Canta, D. Font, I. Prat, X. Ribas, M. Costas, *J. Org. Chem.* **2013**, *78*, 1421–1433.

[37] E. Poli, J. M. Clacens, J. Barrault, Y. Pouilloux, *Catal. Today* **2009**, *140*, 19–22.

[38] A. E. Gerbase, J. R. Gregório, M. Martinelli, M. C. Brasil, A. N. F. Mendes, *J. Am. Oil Chem. Soc.* **2002**, *79*, 179–181.

[39] Q. Shi, M. P. Mower, D. G. Blackmond, J. Rebek, *Proc. Natl. Acad. Sci. U. S. A.* **2016**, *113*, 9199–9203.

[40] K. S. Hagen, *Inorg. Chem.* **2000**, *39*, 5867–5869.

[41] K. Suzuki, P. D. Oldenburg, L. Que, Jr., *Angew. Chem. Int. Ed.* **2008**, *47*, 1887–1889.

[42] H. a. J. Aerts, P. a. Jacobs, *J. Am. Oil Chem. Soc.* **2004**, *81*, 841–846.

[43] J. Samuelsson, M. Johansson, *J. Am. Oil Chem. Soc.* **2001**, *78*, 1191–1196.

[44] J. Langanke, L. Greiner, W. Leitner, *Green Chem.* **2013**, *15*, 1173–1182.

Chapter 4

Iron Complexes with N2Py2-D_4 Ligands: Towards More Robust Catalysts for Oxidation Reactions

Abstract

Fe(N2Py2)/H_2O_2/AcOH catalytic systems provide powerful tools for efficient C–H and C═C bond oxidations. Yet, the stability of the catalyst under the oxidizing conditions still remains a problem. The generally accepted catalyst decomposition pathway of Fe(N2Py2) complexes is through oxidative dimerization to form inactive oxo-bridged $Fe_2(\mu\text{-}O)(N2Py2)_2$ dimers. Detailed ESI-MS analysis has now shown a catalyst decomposition pathway of ligand oxidation *via* C–H oxidation on 2-pyridinylmethyl sites, followed by dissociation of the oxidized ligand from the iron center. By deuterating the 2-pyridinylmethyl sites of a series of N2Py2 ligands with variations on both alkylamine and pyridine fragments, providing access to the corresponding Fe(N2Py2-D_4) complexes, longer catalysts lifetimes are achieved in catalytic oxidation reactions with all complexes. As a consequence, improved substrate conversions and product yields were consistently observed in both aliphatic C–H oxidations and alkene epoxidations. Kinetic and catalytic studies revealed that deuteration does not change the intrinsic reactivity and product selectivity of Fe(N2Py2) complexes. In addition, different Fe(N2Py2-D_4) complexes provide different improvements in catalytic performances and lifetimes, responding to the differences in ligand rigidity and robustness of the corresponding non-deuterated N2Py2 ligands. Accordingly, these improvements are more pronounced for ligands with a more flexible bis-alkylamine backbone. These observations provide new insights and new routes for the further development of more robust ligands for homogeneous oxidation catalysis.

4.1 Introduction

C–H and C═C bond oxidations constitute essential transformations in organic synthesis and in many biological and industrial processes.[1–4] These oxidations are performed routinely in a very selective manner in nature by heme and non-heme iron-containing enzymes *via* activating of O_2. Yet, it is still challenging to perform such oxidations very selectively by means of synthetic iron coordination complexes outside the enzyme environment.[1] Taking inspiration from these iron enzymes (see Chapter 1 of this thesis), considerable efforts have been invested in the development of synthetic non-heme iron catalysts in the past two decades. These iron catalysts, especially the ones with tetradentate nitrogen (N4, generally aminopyridine) ligands, are able to oxidize substrates with high regio- and stereoselectivity utilizing H_2O_2 as the oxidant.[1,2] These selective oxidations are different from Fenton-like processes, which generally lead to unselective oxidations due to the involvement of highly reactive hydroxyl radicals. As also mentioned in Chapter 1 and 2, iron complexes with a *cis*-α topology derived from aminopyridine ligands with a linear bis-alkylamine-bis-pyridine (N2Py2) structure have been proven to be the most effective so far (Figure 1).[1] On the basis of this ligand platform, modifying the ligand in the bis-alkylamine backbone or the pyridine moieties allows for improving the reactivity and for fine-tuning the selectivity of the catalyst, providing powerful protocols for efficient C–H and C═C oxidations.[1]

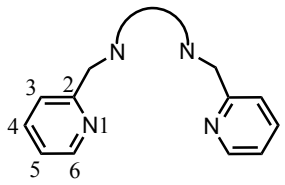

Figure 1. Generic structure of the linear N2Py2 ligand platform.

Nevertheless, the stability of such iron catalysts under the oxidizing conditions still remains a problem and attracts less attention, despite that it is an important factor that affects catalyst efficiency.[5,6] The commonly accepted catalyst decomposition pathway of non-heme iron complexes is through oxidatively dimerization to form inactive oxo-bridged $Fe^{III}_2(\mu\text{-}O)(L)_2$ dimers (L = ligand).[7] These decomposition species have been proposed for several N2Py2-based iron complexes, such as $[Fe(BPMEN)(CH_3CN)_2](ClO_4)_2$[8] and BPBP-based iron complexes,[9–12] as well as for other N4 complexes like TPA-based iron complexes[7] (BPMEN = *N*,*N*'-dimethyl-*N*,*N*'-bis(2-picolyl)ethylenediamine, BPBP = *N*,*N*'-bis(2-picolyl)-2,2'-bispyrrolidine, TPA = tris(2-pyridylmethyl)amine). In Chapter 3, rapid deactivation of

Fe(N2Py2) complexes was observed in the reaction profiles of catalytic epoxidations of methyl linoleate.

To suppress catalyst decomposition, a slow H_2O_2 addition protocol[11,13–18] or an iterative addition protocol of a solution of catalyst, H_2O_2, and acetic acid[19–24] have generally been adopted in reaction procedures. Modifications of the ligand by increasing the bulk of the pyridine fragments have also been reported to suppress the bimolecular self-decomposition pathway. Substituents at the 5-positions, as in 5-Et-TPEN developed by Banse *et al.*[25] or CF_3-BPBP developed by White *et al.*[21] (Figure 2), can shield the approach of another catalyst molecule towards the iron center, which in turn limits bimolecular self-decomposition (TPEN = *N*,*N*,*N*',*N*'-tetrakis(2-pyridylmethyl)ethane-1,2-diamine). In 2009, Costas *et al.* reported on the mcpp ligand in which bulky pinene moieties are placed at the 4- and 5-positions of the pyridine rings (mcpp = *N*,*N*'-dimethyl-*N*,*N*'-bis{[(*R*)-4,5-pinenepyridin-2-yl]-methyl}-cyclohexane-1,2-diamine, Figure 2), resulting in reduced bimolecular self-deactivation.[9] The incorporation of bulky *tris*-(isopropyl)silyl (TIPS) groups at the 5-positions of pyridines in [Fe(OTf)$_2$(*S,S*-^{TIPS}BPBP)] has been shown to translate into improved substrate conversions (Figure 2),[17] which is likely because of suppression of the formation of $Fe^{III}_2(\mu\text{-}O)(L)_2$ dimers. Similar observations were described for the catalytic performance of the iron complex derived from ^{TIPS}BPBI in Chapter 2 of this thesis.[26]

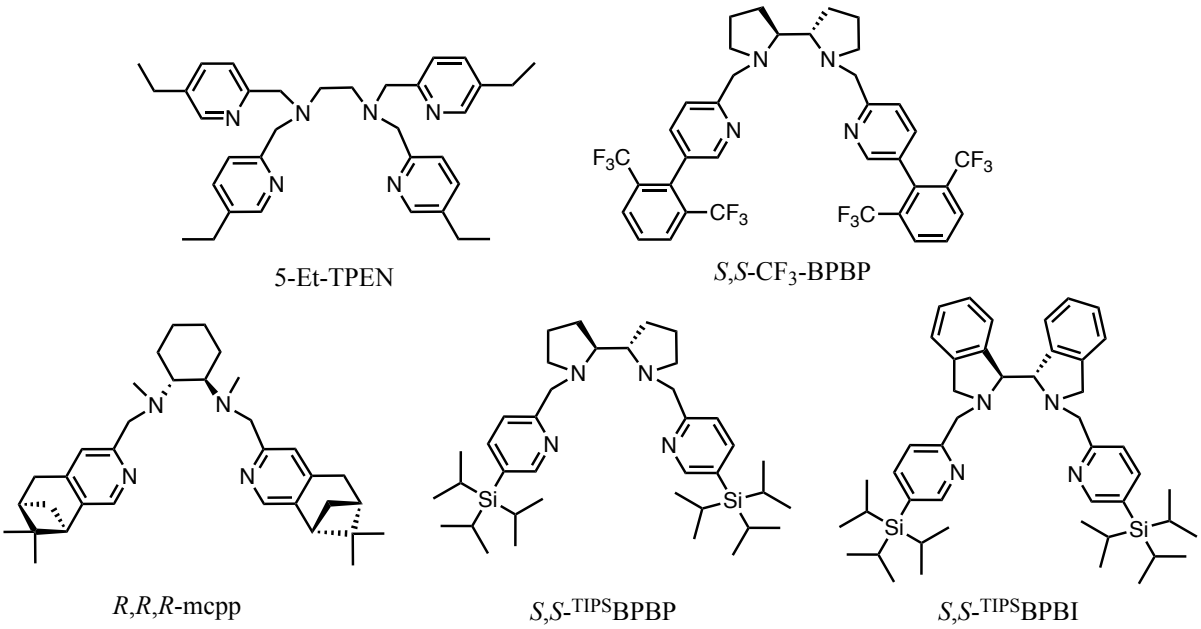

Figure 2. Some examples of N2Py2 ligands with increased steric bulk.

Another possible cause for catalyst decomposition is oxidative ligand degradation. For example, ligands bearing phenyl moieties are very reactive towards hydroxyl radicals, thus aryl C–H

bond oxidations can take place.[27–29] More importantly, 2-pyridinylmethyl sites adjacent to an amine are vulnerable to oxidative degradation. For instance, this 2-pyridinylmethyl site can undergo hydroxylation to form a hemiaminal compound when exposed to the oxidant.[30] One possible fate of this compound is C–N bond cleavage to form an aldehyde[25,31–36] and a secondary amine (Scheme 1, path A). Alternatively, the hemiaminal can be over-oxidized into an amide intermediate (path B),[30] which can potentially be hydrolyzed into a picolinic acid (path C), as reported by Browne[36] and others.[25,37,38] Efforts have been taken in order to prevent deleterious oxidations on 2-pyridinylmethyl sites in N2Py2 ligands. For example, Britovsek *et al.* proposed to introduce a methyl group or a carbonyl linkage at the 2-pyridinylmethyl positions in the BPMEN ligand.[6] However, these ligand modifications led to inferior catalytic efficiencies of the corresponding iron complexes in C–H bond oxidation, which was attributed to a change in ligand flexibility in the case of $–CH_3$ introduction leading to less-active coordination modes (*cis*-β and *trans*) or to the formation of inactive dinuclear complexes in the case of C═O introduction.[6]

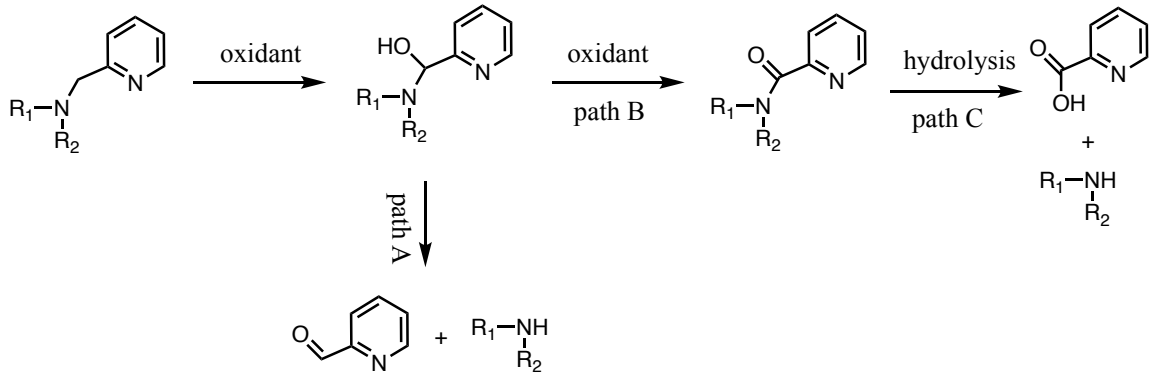

Scheme 1. Possible ligand oxidation pathways for amine-based non-heme iron complexes (the metal center is omitted for clarity).[6]

Other investigations on the stability of non-heme iron oxidation catalysts have either focused on recovering the ligands or on ESI-MS (electrospray ionization mass spectrometry) analyses after catalysis.[9,11,12] In a study by White and co-workers, 95% of non-oxidized BPBP ligand was recovered from a catalytic C–H oxidation experiment where $[Fe(BPBP)(CH_3CN)_2](SbF_6)_2$ was employed.[11] In contrast, the oxidized ligand was identified as a major species in ESI-MS traces of oxidation reactions using the catalytically inactive $[Fe(OTf)_2(R,S\text{-BPBP})]$ complex, which features a *cis*-β topological configuration.[12] All reported catalyst decomposition studies were performed after catalytic oxidations in the presence of substrate, meaning that the reaction conditions with respect to catalyst could be very different amongst these reports. To the best of our knowledge, there is so far no report on a dedicated investigation of the deactivation of

Fe(N2Py2) complexes under the oxidizing conditions used in catalytic reactions but in the absence of substrate.

This chapter describes the development of non-heme iron catalysts derived from N2Py2-D_4 ligands in which the 2-pyridinylmethyl positions in the ligand framework have been per-deuterated (see Scheme 2). The development of these ligands was inspired by the observation of significant ligand oxidation upon exposure of the parent, non-deuterated complexes to H_2O_2 in the absence of an organic substrate. This minor ligand alteration minimizes changes in the flexibility, steric, and electronic properties of the ligands. The corresponding deuterated iron complexes were found to outperform the non-deuterated complexes in terms of substrate conversion and product yield in all cases studied.

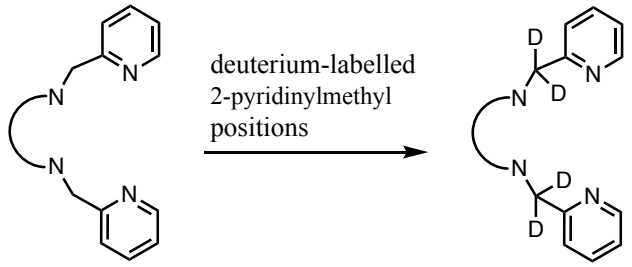

N2Py2 N2Py2-D_4

Scheme 2. Modification of N2Py2 ligands through the introduction of D atoms on 2-pyridinylmethyl positions.

4.2 Results and Discussion

4.2.1 Catalyst decomposition

The study was initiated by a simplified and dedicated decomposition experiment of [Fe(OTf)$_2$(*S*,*S*-BPBP)] under typical catalytic conditions but in the absence of an organic substrate, by mixing the complex (1 equiv.) with H_2O_2 (150 equiv.) and AcOH (50 equiv.) at 0 ^{o}C for 10 min. ESI-MS analysis of the resulting mixture revealed a predominant peak at *m/z* = 337.1954 (Figure 3a), with an isotopic pattern which is in agreement with an oxidized ligand carbonyl compound (BPBP)=O (calcd. *m*/z for $[(BPBP)=O+H]^+$ is 337.2029, Figure 3a, inset) resulting from aliphatic C–H oxidation of one of the methylene sites of the ligand. Of note is that no noticeable iron-containing species derived from the oxidized ligand product were found in the ESI-MS trace, suggesting that the oxidized ligand dissociates from the iron centre. In addition, no dimeric oxo-complexes of the type $Fe_2(\mu\text{-}O)(BPBP)_2$ were observed in this case.

These observations are significantly different from the notion that Fe(BPBP) decomposition occurs *via* dimerization reactions[9–12] and that no oxidized ligand was observed.[11,12] In the catalyst decomposition study described by White *et al.*,[11] 95% of the intact BPBP ligand was recovered. However, this analysis was conducted after a catalytic reaction in the presence of an alkane substrate and under distinctively different reaction conditions (substrate : cat. : H_2O_2 : AcOH = 100 : 15 : 360 : 0).

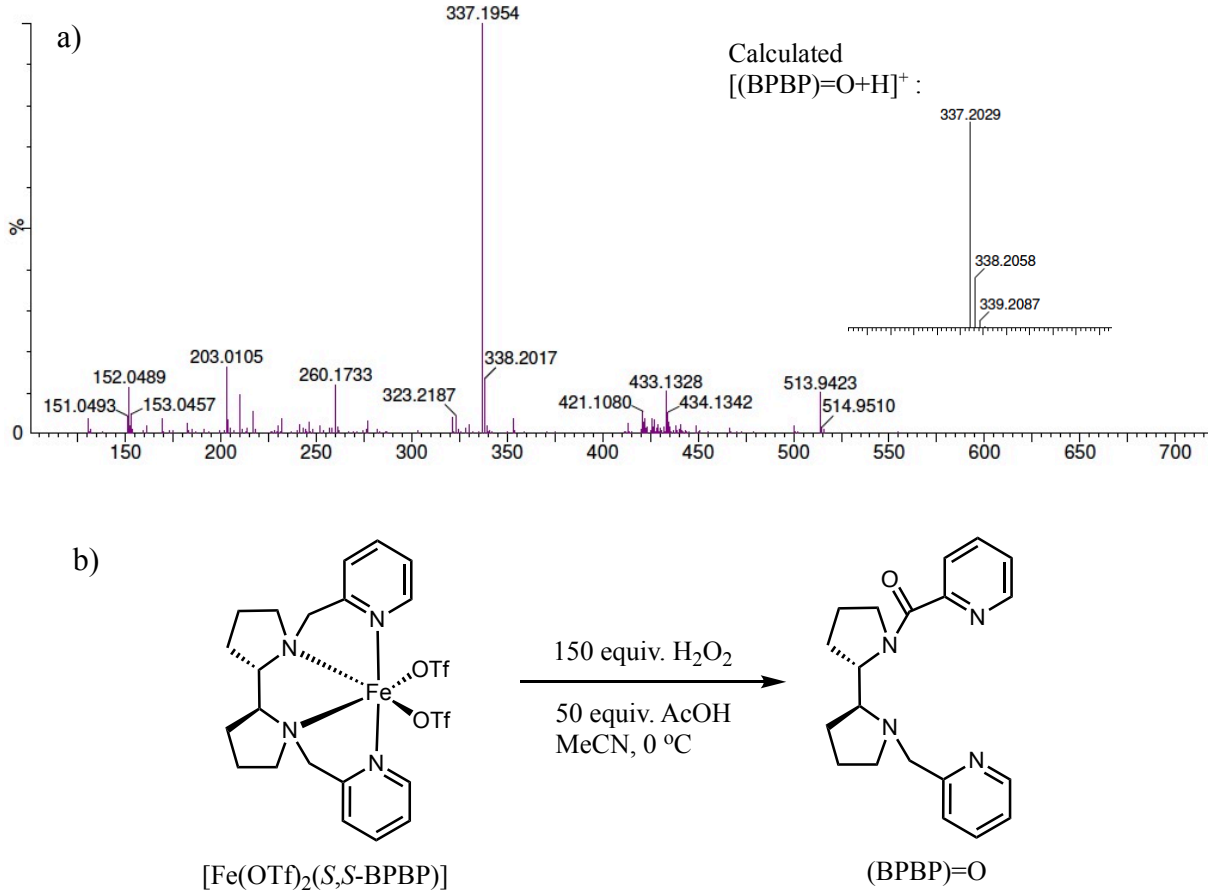

Figure 3. a) ESI-MS trace of the mixture from a reaction of [Fe(OTf)$_2$(*S*,*S*-BPBP)] (2mM) with H_2O_2 (150 equiv.) and AcOH (50 equiv.) in MeCN, stirred at 0 °C for 10 min. ESI-MS was directly measured for the reaction mixture without any work-up. The peak at *m/z* = 337.1946 corresponds to the decomposition compound (BPBP)=O, calcd. *m/z* for $C_{20}H_{27}N_4O$ ([M+H]$^+$): 337.2029 (inset). A minor peak corresponding to free BPBP ligand was also present, with a *m*/z value of 323.2189 (calcd. *m*/z for [BPBP+H]$^+$ is 323.2230). b) Proposed decomposition pathway of [Fe(OTf)$_2$(*S*,*S*-BPBP)] into amide compound (BPBP)=O with one 2-pyridinylmethyl position oxidized.

The observed ligand oxidation is likely to happen at one of the 2-pyridinylmethyl positions of the ligand (*vide supra*), since these represent the weakest of all C–H sites in the BPBP ligand (Figure 3b). Based on this observation and assumption, and according to the general concept of kinetic isotope effects, a stabilization of the 2-pyridinylmethyl positions in N2Py2 ligands in general could be achieved by replacing the 2-pyridinylmethyl H atoms by D atoms. This would

in turn make the corresponding Fe complexes more stable under the oxidizing conditions, leading to longer catalyst lifetimes and improved catalytic performances.

4.2.2 Synthesis of N2Py2-D_4 ligands and iron complexes

A series of deuterium-labelled N2Py2-D_4 ligands have been synthesized following the synthesis scheme developed for the non-deuterated ligands (Figure 4). Key to the synthesis is the reduction of alkyl picolinate analogues by $NaBD_4$,[39] followed by chlorination of the resulting hydroxymethylpyridine-D_2 derivatives,[40] to provide chloromethylpyridine-D_2 compounds. These were readily converted into N2Py2-D_4 ligands through alkylation of the appropriate alkylamine backbones. The first three ligands are derived from the well-known N2Py2 ligands BPBP,[19] BPMCN (*N*,*N*'-dimethyl-*N*,*N*'-bis(2-picolyl)-cyclohexane-*trans*-1,2-diamine),[41] and BPMEN,[42] which have different alkylamine backbones. Variation of the pyridine moieties has also been considered, *i.e.*, using isoquinoline rings as hetero-aromatic fragments instead of pyridines in the BQMEN ligand (BQMEN = *N*,*N*'-dimethyl-*N*,*N*'-bis(3-isoquinolyl)ethylenediamine). By doing so, the applicability of this catalyst design strategy can be properly evaluated based on variations in both the alkylamine and the pyridine fragments in the N2Py2 ligand platform. Ligands with non-fully deuterated 2-pyridinylmethyl cites (mainly N2Py2-D_3) have been found to be present in minor amounts in all N2Py2-D_4 ligands reported here, as confirmed by ^{1}H NMR and ESI-MS (see experimental section).

Using $Fe(OTf)_2 \cdot 2CH_3CN$ as iron precursor, iron complexes **1-D_4, 3-D_4**, and **4-D_4** were synthesized through complexation with the corresponding ligands in tetrahydrofuran (Figure 4). The synthesis of **2-D_4** was accomplished using $FeCl_2$ as iron precursor, followed by the treatment with Ag(OTf).[43] From ESI-MS, minor amounts of the [$Fe(OTf)_2$(N2Py2-D_3)] complexes were noted in each N2Py2-D_4 complex as a consequence of the N2Py2-D_3 impurity (see experimental section). For comparison purposes, the parent non-deuterated iron complexes **1** - **4** were also synthesized.

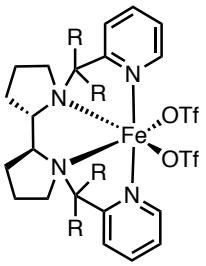

1, R = H, [Fe(OTf)$_2$(*S*,*S*-BPBP)]
1-D$_4$, R = D, [Fe(OTf)$_2$(*S*,*S*-BPBP-D$_4$)]

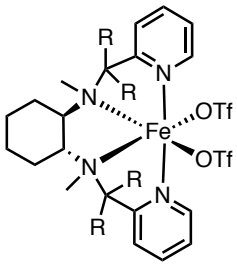

2, R = H, [Fe(OTf)$_2$(*R*,*R*-BPMCN)]
2-D$_4$, R = D, [Fe(OTf)$_2$(*R*,*R*-BPMCN-D$_4$)]

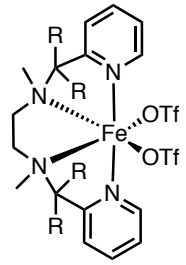

3, R = H, [Fe(OTf)$_2$(BPMEN)]
3-D$_4$, R = D, [Fe(OTf)$_2$(BPMEN-D$_4$)]

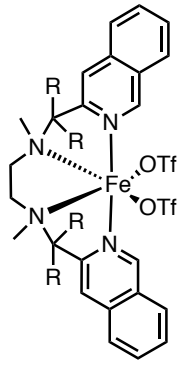

4, R = H, [Fe(OTf)$_2$(BQMEN)]
4-D$_4$, R = D, [Fe(OTf)$_2$(BQMEN-D$_4$)]

Figure 4. [Fe(OTf)$_2$(N2Py2)] and [Fe(OTf)$_2$(N2Py2-D$_4$)] complexes studied in this chapter.

4.2.3 Confirmation of the oxidized site and proposed ligand oxidation pathway

With the Fe(N2Py2-D$_4$) complexes in hand, the postulated site of ligand oxidation could be confirmed. To do so, the oxidation of **1-D$_4$** was performed using the same reaction conditions as in the oxidation of **1** (*vide supra*). ESI-MS analysis showed the presence of the oxidized ligand product at *m/z* = 339.2085 (Figure 5), which corresponds to a mass difference of 12 from the BPBP-D$_4$ ligand (calcd. *m/z* = 327.2481). This clearly indicates that C–H oxidation takes place on one of the deuterated 2-pyridinylmethyl positions to form (BPBP-D$_2$)=O (calcd. *m*/*z* for [M+H]$^+$ is 339.2185, Figure 5, inset). The small peak at *m/z* = 338 is due to the oxidation of the BPBP-D$_3$ ligand, which is present in small amounts in **1-D$_4$**. More importantly, no noticeable species were observed that represent ligand oxidation on non-deuterated methylene sites (calcd. *m/z* = 341.2274), meaning that ligand oxidation predominantly takes place on 2-pyridinylmethyl positions. Notably, in this case, binuclear oxo-bridged dimers resulting from bimolecular self-decomposition pathways were observed in high intensities. The two peaks at *m/z* = 279.7833 and 494.1451 are assigned to the binuclear species [Fe$_2$(μ-O)(BPBP-D$_4$)$_2$(OAc)]$^{3+}$ (calcd. *m*/z = 279.7861) and [Fe$_2$(μ-O)(BPBP-D$_4$)$_2$(OAc)(OTf)]$^{2+}$ (calcd. *m*/z = 494.1554), respectively. This clearly indicates that **1-D$_4$** more preferentially undergoes the aforementioned bimolecular self-decomposition pathway, which is assumed to be the

consequence of less favourable CD_2 oxidation. The peak at *m/z* = 493.6447 is again due to the presence of non-fully deuterated ligand. Similar to the ligand oxidation experiment of **1**, no noticeable iron-containing species containing the oxidized ligand were observed, meaning that the oxidized ligand dissociates from iron.

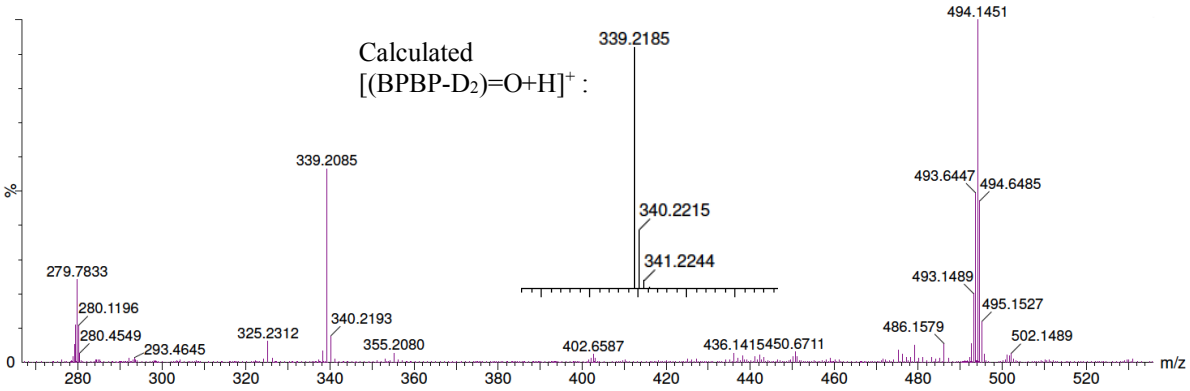

Figure 5. ESI-MS of the mixture from the reaction of **1-D$_4$** (2mM) with H_2O_2 (150 equiv.) and AcOH (50 equiv.) in MeCN, stirred at 0 °C for 10 min. ESI-MS was directly measured for the reaction mixture without any work-up. The peak at m/z = 339.2085 corresponds to the decomposition amide compound (BPBP-D_2)=O (inset: calcd. *m/z* for $C_{28}H_{27}N_4$ ($[M+H]^+$): 339.2185).

From the oxidation experiments using **1** and **1-D$_4$**, it was concluded that one of the oxidative decomposition compounds of **1** and **1-D$_4$** in the presence of H_2O_2 and AcOH is amide (BPBP)=O or (BPBP-D_2)=O, respectively, formed through C–H oxidation of one of the 2-pyridinylmethyl positions in the ligand. It is evident that this oxidation process includes at least two steps: ligand oxidation and dissociation from iron. Under catalytic conditions these events would lead to catalyst decomposition/deactivation and deterioration of catalytic activity over time.

In order to obtain insight into this ligand oxidation process, the oxidation of the free BPBP ligand was carried out in the presence of an equal amount of **1-D$_4$**, 150 equiv. of H_2O_2, and 50 equiv. of AcOH (Figure 6a). After stirring at 0 °C for 10 min, a sample of the reaction mixture was subjected to ESI-MS analysis, showing unreacted ligand BPBP (*m/z* = 323.2210) as the predominant species and no obvious formation of (BPBP)=O (Figure 6b, I). In addition, in a separate reaction of BPBP (1 equiv.), **1** (2 mol%), H_2O_2 (1.2 equiv.), and AcOH (50 mol%) for 30 min, only intact BPBP was observed both in ^{1}H NMR and ESI-MS. Combing these observations, it is clear that it is difficult for the free BPBP ligand to undergo C–H oxidation by the Fe(BPBP)/H_2O_2/AcOH catalytic system. In comparison, the deactivation of **1** produces (BPBP)=O as the major decomposition compound within 10 min (Figure 3a), which excludes

a scenario in which the BPBP ligand dissociates from iron first, followed by C–H oxidation of BPBP in the presence of the Fe(BPBP)/H_2O_2/AcOH catalytic system.

As expected, the decomposition compound (BPBP-D_2)=O (*m/z* = 339.2197, Figure 6b, I) derived from the oxidation of **1-D_4** was observed next to pristine BPBP ligand in the experiment in which BPBP and **1-D_4** were combined. A similar ESI-MS trace was obtained by allowing this reaction to continue for another 30 min, with BPBP as major species and (BPBP-D_2)=O as minor species (Figure 6b, II). After another hour at room temperature (RT), the C–H oxidation product of BPBP started to appear at *m/z* = 337.1917 (assigned to (BPBP)=O), along with low amounts of secondary hydroxylation products derived from the initial amide products (BPBP)=O and (BPBP-D_2)=O (*m/z* = 353.1915 for HO–(BPBP)=O and *m/z* = 355.2047 for HO–(BPBP-D_2)=O or DO–(BPBP-D)=O; Figure 6b, III). Nevertheless, unreacted BPBP still represented the predominant species in the reaction mixture after in total 100 min of reaction time (Figure 6b, III). Subsequently, the signal at *m/z* = 323 (BPBP) disappeared after stirring overnight at RT, and the concentration of the oxidized product (BPBP)=O was found to be increased accordingly (Figure 6b, IV). This means that the longer reaction time eventually leads to full conversion of BPBP into aliphatic oxidation products. At the same point in time, the amide product derived from the BPBP-D_4 ligand was also found at considerable concentration after the overnight reaction. As shown in Figure 6b, free BPBP is relatively stable in the presence of the Fe/H_2O_2/AcOH catalytic system at the early stage of the reaction. However, free BPBP was also found to be oxidized into oxidized compounds at the late stage of the reaction. It is speculated that as the dissociation of the oxidized BPBP-D_4 ligand from iron proceeds, free BPBP can subsequently bind to the released iron ions to form the (oxidatively) active species, which in turn can get involved in ligand oxidation leading to the oxidation of BPBP.

Based on these observations, BPBP ligand oxidation leading to ligand dissociation is proposed to take place in an intramolecular fashion, *i.e.* when the ligand is bound to an iron centre, and that intermolecular oxidation does not take place. This notion strengthens the hypothesis that enhancing the oxidative robustness of 2-pyridinylmethyl positions of the BPBP ligand would lead to an increased catalyst lifetime.

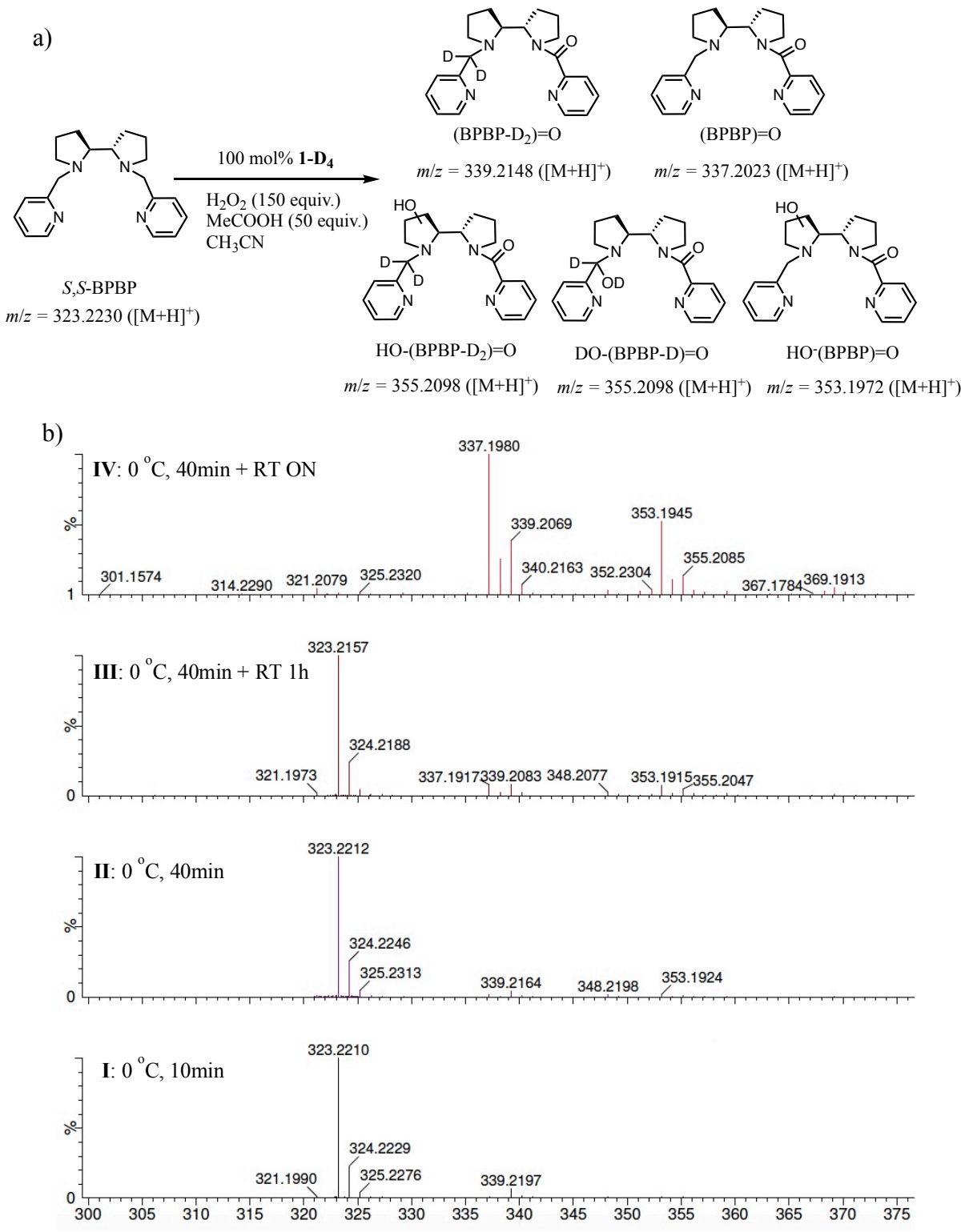

Figure 6. a) Reaction of *S*,*S*-BPBP in the presence of 100 mol% **1-D4**, 150 equiv. H_2O_2, and 50 equiv. AcOH. The oxidized ligand compounds from BPBP and BPBP-D_4 can be easily discriminated in ESI-MS due to deuterium labelling on 2-pyridinylmethyl carbons. b) ESI-MS of the reaction mixture of *S*,*S*-BPBP (1 equiv.), 100 mol% **1-D4**, 150 equiv. H_2O_2, and 50 equiv. AcOH over time. ESI-MS was directly measured for the reaction mixture without any work-up. The aldehyde compounds derived from amide compounds (BPBP)=O and (BPBP-D_2)=O as shown in Scheme 1 were also observed in IV (not shown in the figure).

4.2.4 Catalytic performances

To investigate the catalytic performances of the [Fe(OTf)$_2$(N2Py2-D_4)] complexes, several alkenes were chosen as benchmark substrates to examine catalytic epoxidation. For comparison purposes, for each catalyst a parallel experiment with the corresponding [Fe(OTf)$_2$(N2Py2)] complex was also carried out. The catalytic results are displayed in Table 1. *Cis*-cyclooctene (**5**) was epoxidized in the presence of **1** (0.25 mol%), H_2O_2 (100 mol%), and AcOH (1.5 mol%),[12] giving rise to 84% conversion and 75% yield of epoxide **6**. Under the same reaction conditions, the reaction with **1-D$_4$** gave a slightly higher conversion and yield of 89% and 80%, respectively. Despite these differences, these two reactions showed identical epoxide selectivities (89% for **1** and 90% for **1-D$_4$**). Interestingly, both conversion and yield increased with 14% when changing catalyst from **2** (73% conversion and 64% yield) to **2-D$_4$** (87% conversion and 78% yield). More significant differences were found in the cases of **3** and **3-D$_4$**. Cyclooctene epoxidation with **3-D$_4$** provides a more than 2-fold higher conversion and yield than the reaction carried out with **3** (70% vs. 34% conversion, and 57% vs. 27% yield, respectively). A remarkable improvement in catalytic performance was also found in the reaction catalyzed by **4-D$_4$**, with 43% conversion and 35% yield. In contrast, only 26% conversion and 20% yield were found in the case of **4** using the current conditions.

Table 1. Catalytic epoxidation of alkenes by Fe(N2Py2) vs. Fe(N2Py2-D_4) complexes

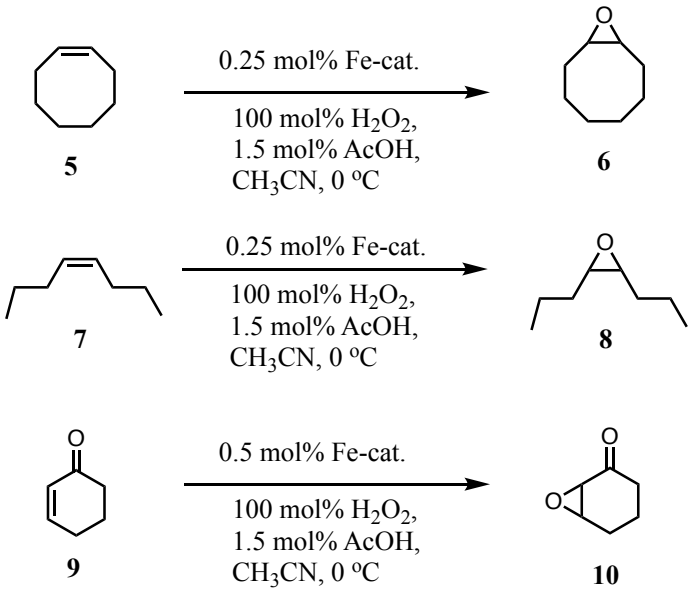

Alkene	cat.	Conv. (%)[b]	**6** (%)[b]	Selectivity (%)[c]
	1	84	75	89
	1-D4	89	80	90
	2	73	64	88
5	**2-D4**	87	78	90
	3	34	27	79
	3-D4	70	57	81
	4	26	20	77
	4-D4	43	35	81
Alkene	cat.	Conv. (%)[d]	**8** (%)[d]	Selectivity (%)[c]
	1	72	70	97
	1-D4	88	86	98
	2	70	65	93
7	**2-D4**	78	72	92
	3	55	51	93
	3-D4	73	70	96
	4	36	29	81
	4-D4	44	37	84
Alkene	cat.	Conv. (%)[d]	**10** (%)[d]	Selectivity (%)[c]
	1	54	45	83
	1-D4	63	55	87
	2	45	38	84
9	**2-D4**	53	44	83
	3	35	29	83
	3-D4	53	47	89
	4	34	29	85
	4-D4	39	34	87

[a] Reaction conditions: Fe-cat. : H_2O_2 : substrate : AcOH = 0.25 (or 0.5) : 100 : 100 : 1.5, 0 °C, oxidant added by syringe pump over 10 min, and reaction mixture stirred for additional 30 min. Reported analysis data represent the outcome of at least two independent catalysis experiments. [b] Determined by GC analysis. [c] Epoxide selectivity. [d] Determined by NMR analysis.

Two more alkene substrates, *cis*-4-octene and cyclohexanone, were tested next. Similar trends were found in all the reactions with the current set of catalysts, *i.e.* the reactions with Fe(N2Py2-D4) catalysts showed increased conversions and yields with respect to the reactions with

Fe(N2Py2) catalysts. In the epoxidation of *cis*-4-octene (**7**), catalysts **1-D_4**, **2-D_4**, **3-D_4**, and **4-D_4** performed the reaction with a 16%, 8%, 18% and 8% increase in conversion with respect to catalysts **1**, **2**, **3**, and **4**, respectively. Similarly, in the case of cyclohexenone (**9**) epoxidation, 9%, 8%, 18% and 5% more substrate was converted in the reactions with **1-D_4**, **2-D_4**, **3-D_4**, and **4-D_4**, compared to the reactions with **1**, **2**, **3**, and **4**, respectively. On the other hand, no major differences were observed in terms of epoxide selectivity between the parent and deuterated catalysts in these reactions, albeit that in most cases selectivities are slightly higher for the deuterated catalysts (Table 1).

Next to alkene epoxidation, the catalytic oxidation of aliphatic C–H bonds by [Fe(OTf)$_2$(N2Py2-D_4)] complexes was also examined (Table 2). Using 1.0 mol% catalyst loading, *cis*-1,2-dimethylcyclohexane (**11**) was oxidized in the presence of 120 mol% oxidant and 50 mol% AcOH,[26] generating 3° oxidation product **12** as the major product and 2° oxidation products **13** and **14** as minor products. When **1** was used as catalyst, 52% conversion, 30.1% total yield, and a 8.7 ratio of tertiary over secondary products (3°/2°) were obtained. **1-D_4** provided an improvement in catalytic performance, with 62% coversion and 37.9% total yield. Selectivity towards the oxidation of 3° over 2° sites remained the same though (3°/2° = 8.7). Complexes **2** and **2-D_4** showed a similar catalytic performance with respect to each other, albeit with higher conversions and product yields, and a lower $3^o/2^o$ product ratio compared to **1** and **1-D_4**. These results are in accordance with the previous observation by Costas *et al*. that the BPMCN-based iron catalyst is more active and shows a higher preference toward 2° oxidation than BPBP-based catalysts in C–H oxidations.[24] In contrast, a significant difference was noted between the reactions with **3** and **3-D_4**. The oxidation of **11** catalyzed by **3** gave rise to 41% conversion and 27.1% yield, while with **3-D_4** substrate conversion and yield increased to 56% and 38.7%, respectively. Similarly, **4-D_4** provided a noticeable increase in conversion and yield compared to **4**, with 22% conversion and 18.6% yield in the case of **4**, and 31% conversion and 27.6% yield in the case of **4-D_4**. Notably, similar 3°/2° ratios were obsvered in these two sets of reactions.

In the oxidation of adamantane (**15**), noticeably different catalytic results were only found between the reactions with **1** and **1-D_4**, with an improved conversion (from 73% to 82%) and yield (from 41.8% to 49.5%) for **1-D_4**. For the other three sets of reactions, slighly higher conversions and yields were found in the reactions with the Fe(N2Py2-D_4) catalyst than the ones with the Fe(N2Py2) catalyst (Table 2). In none of these reaction sets was a change in the $3^o/2^o$ product ratio observed.

Table 2. Catalytic C–H oxidation of alkanes by Fe(N2Py2) vs. Fe(N2Py2-D_4) complexes[a)]

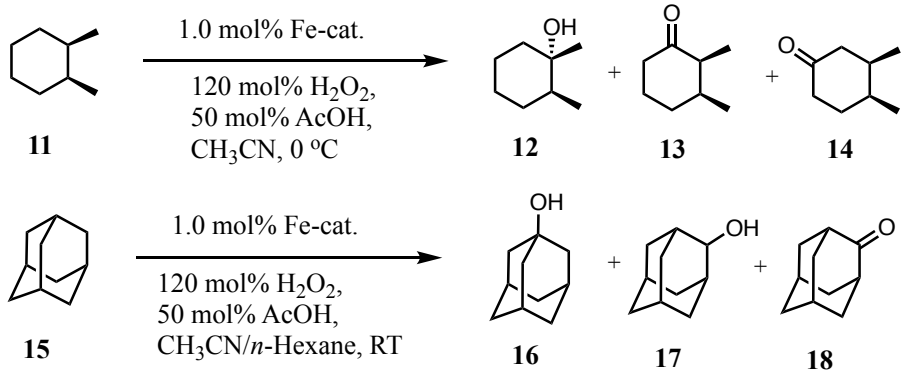

Alkane	cat.	Conv. (%)[b)]	**12**, **13**, **14** (%)[b)]	Total yield (%)[b)]	3°/2° [c)]
	1	52	27, 1.3, 1.8	30.1	8.7
	1-D_4	62	34, 1.8, 2.1	37.9	8.7
	2	67	40, 3.0, 4.0	47	5.7
11	**2-D_4**	70	42, 3.3, 4.3	49.6	5.5
	3	41	24, 1.5, 1.6	27.1	7.8
	3-D_4	56	34, 2.2, 2.5	38.7	7.3
	4	22	17, 0.7, 0.9	18.6	10.6
	4-D_4	31	25, 1.1, 1.5	27.6	9.6
Alkane	cat.	Conv. (%)[b)]	**16**, **17**, **18** (%)[b)]	Total yield (%)[b)]	3°/2° [d)]
	1	73	38, 1.3, 2.5	41.8	30
	1-D_4	82	45, 1.6, 2.9	49.5	30
	2	76	36, 1.5, 2.7	40.2	26
15	**2-D_4**	79	38, 1.6, 2.9	42.5	25
	3	71	31, 1.5, 1.9	34.4	27
	3-D_4	72	33, 1.6, 2.2	36.8	26
	4	70	41, 1.7, 2.6	45.3	29
	4-D_4	75	44, 1.9, 2.5	48.4	30

[a)] Reaction conditions: Fe-cat. : H_2O_2 : substrate : AcOH = 1 : 120 : 100 : 50, 0 °C or RT, oxidant added by syringe pump over 10 min, and reaction mixture stirred for additional 30 min. Reported analysis data represent the outcome of at least two independent catalysis experiments. [b)] Determined by GC analysis. [c)] 3°/2° = **12**/(**13** + **14**). [d)] 3°/2° = 3 ∗ **16**/(**17** + **18**).

4.2.5 Kinetic studies

In all the oxidative reactions tested, both alkene epoxidations and aliphatic C–H oxidations, the Fe(N2Py2-D_4) complexes generally showed improved catalytic performances with respect to the corresponding Fe(N2Py2) complexes, both in the sense of substrate conversion and of

product yield. Accordingly, the question arises whether the Fe(N2Py2-D_4) complexes have a higher reactivity or a longer lifetime compared to Fe(N2Py2) complexes. To obtain insight into their kinetic behaviours, the reaction progression was monitored over time for a number of reactions.

By using *cis*-cyclooctene (**5**) as the model substrate, catalytic epoxidation was carried out with 0.25 mol% of either **1** or **1-D4**, 1.5 mol% AcOH, and 1 equiv. of H_2O_2 (added at once). As shown in Figure 7a, **1-D4** consistently gave higher conversion and yield during the complete reaction duration to result in about 10% higher conversion and product yield. Interestingly, these two reactions showed a very similar initial reaction rate and took about the same time to complete (around 40 min). In a similar manner, **2-D4** showed a stronger catalytic ability than **2** from an early stage of the reaction (Figure 7b). More importantly, **2-D4** exhibited catalytic activity over a longer time frame. Consumption of **5** and formation of epoxide product **6** almost ceased around 50 min in the case of **2**, while the reaction still occurred after 60 min with **2-D4**. Furthermore, the kinetic behaviour of **3-D4** was found to be dramatically different from that of **3** (Figure 7c). While the reaction with **3** was observed to be complete after 30 min, the catalytic conversion with **3-D4** continued after the observation period of 1 h. This led to very different reaction results for **3** and **3-D4** at 60 min (33% vs. 71% conversion, and 25% vs. 63% yield, respectively). Since the reaction with **3-D4** seems to continue after 60 min, the differences between these two catalysts can be even larger. In addition, the initial rate of the reaction was significantly different between **3** and **3-D4**, the latter showing a higher initial rate. Finally, different durations of catalytic activity were also found in the reactions with **4** and **4-D4**. In the case of **4**, the reaction was found to be complete after 20 min, while catalytic conversion for the reaction with **4-D4** was observed for at least 30 min (Figure 7d). Like for the reactions with **2-D4** and **3-D4**, a significant increase in conversion and yield was found for **4-D4** with respect to **4**, confirming the observations listed in Table 1.

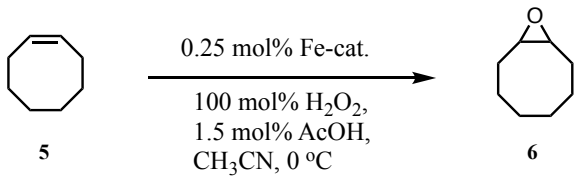

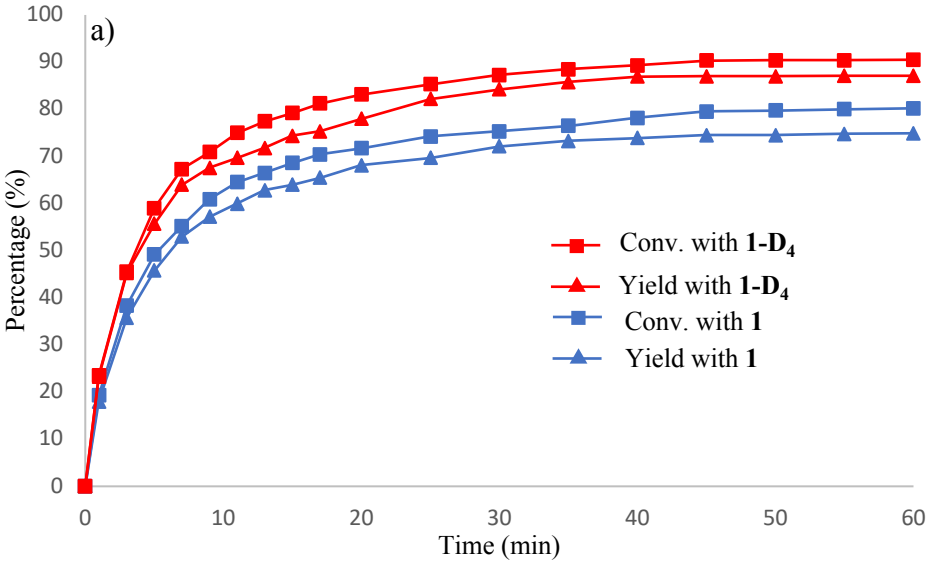
a)
Percentage (%)
Time (min)
Conv. with 1-D4
Yield with 1-D4
Conv. with 1
Yield with 1

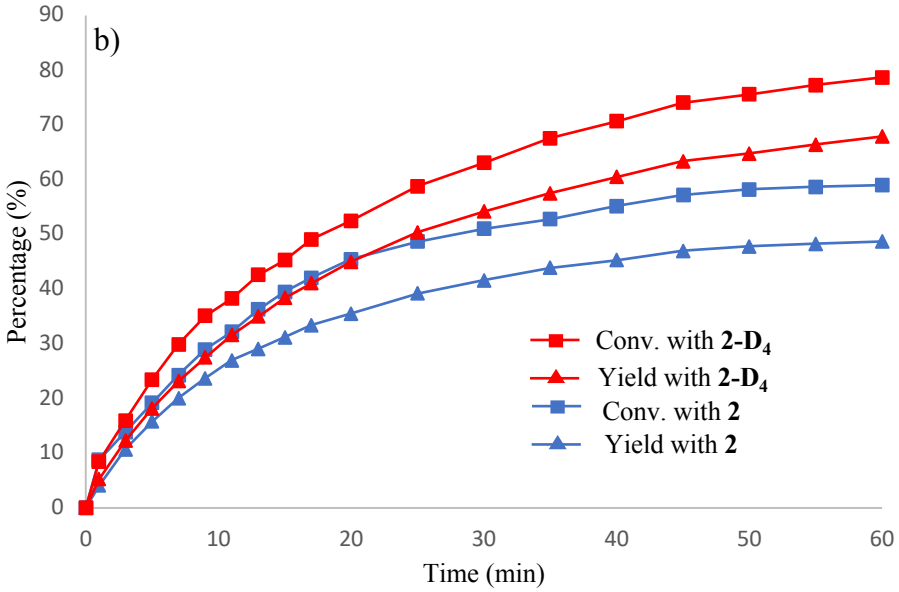
b)
Percentage (%)
Time (min)
Conv. with 2-D4
Yield with 2-D4
Conv. with 2
Yield with 2

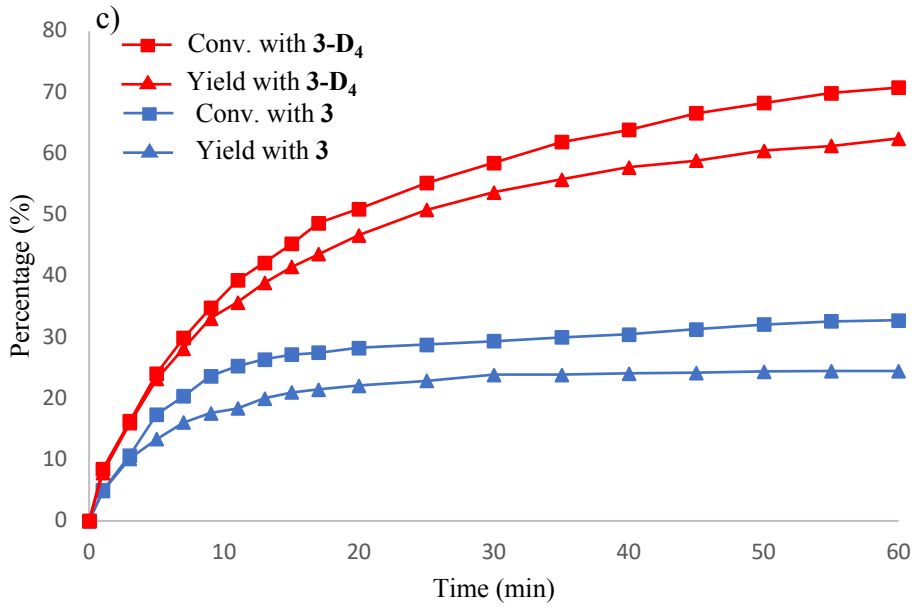
c)
Percentage (%)
Time (min)
Conv. with 3-D4
Yield with 3-D4
Conv. with 3
Yield with 3

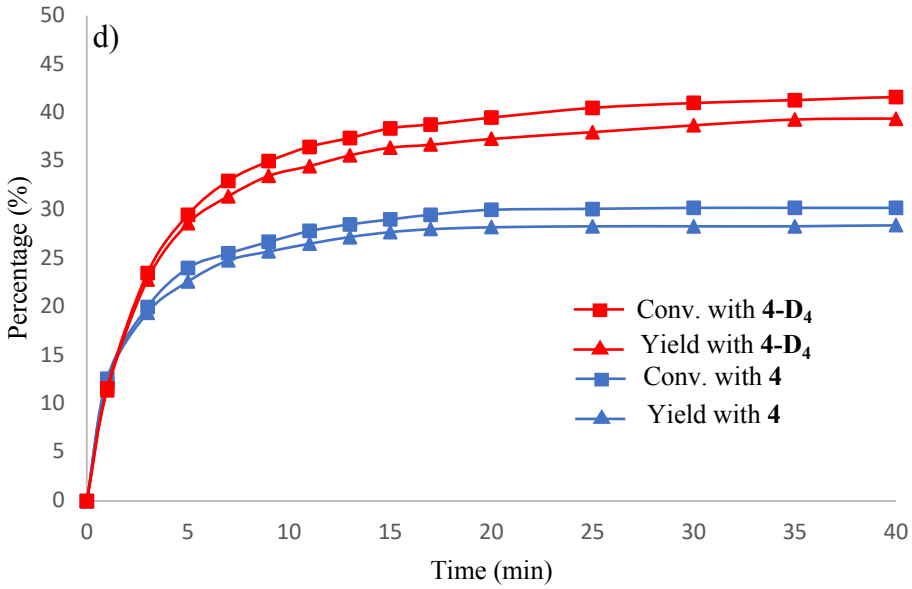

Figure 7. Time-dependent reaction profiles of the catalytic epoxidation of cis-cyclooctene (**5**) with catalysts **1** – **4** vs. catalysts **1-D4** – **4-D4**. Reaction conditions (a-c): Fe-cat. : H_2O_2 : substrate : AcOH = 0.25 : 100 : 100 : 1.5, 0 °C, the oxidant was added at once. Reaction conditions (d): Fe-cat. : H_2O_2 : substrate : AcOH = 0.5 : 100 : 100 : 1.5, 0 °C, the oxidant was added at once. Yields and conversions were determined by GC analysis.

In all these kinetic experiments, catalysts **1-D4** – **4-D4** showed enhanced catalytic abilities compared to catalysts **1** – **4**, which is in agreement with the observations described in Table 1 and 2. Noticeable longer duration of catalytic activity in *cis*-cyclooctene epoxidation was observed for catalysts **2-D4** – **4-D4**, suggesting that these Fe(N2Py2-D4) complexes have longer lifetimes than their Fe(N2Py2) counterparts under catalytic conditions. Considering that the oxidant was added at once, the large initial amount of H_2O_2 in the reaction mixture will cause catalyst deactivation through ligand oxidation at a (relatively) early stage during the reaction, leading to decreasing concentrations of active Fe(N2Py2) and Fe(N2Py2-D4) species in the reaction mixtures to different extents from the very beginning of the reaction.

In order to further evaluate the reactivities of these Fe(N2Py2) and Fe(N2Py2-D4) complexes, the reaction progression was monitored over time using a slow oxidant addition protocol typically used in non-heme oxidation catalysis (see above). Catalysts **3** and **3-D4** were used in this experiment since these showed the largest difference in catalytic results in the epoxidation of *cis*-cyclooctene. In these two experiments, 1.0 equiv. of H_2O_2 was delivered by syringe pump over 30 min. As clearly shown in Figure 8, **3** and **3-D4** provided nearly the same substrate conversions in the first 30 min of the reaction. Of note is that, during the addition of H_2O_2, conversions were always lower than the percentages of H_2O_2 added, meaning that the amount

of oxidant present was not the limiting factor. Beyond 30 min, the conversion rate for **3** clearly started to drop with respect to that of **3-D4** and at 55 min the reaction with **3** ceased; in contrast, *cis*-cyclooctene was still consumed until 70 min in the case of **3-D4** (Figure 8). This observation is consistent with previous observations, again showing that **3-D4** has a longer lifetime under catalytic conditions than **3**. This comparison indicates that the slow H_2O_2 addition protocol can indeed extend the lifetime of the catalyst, and more importantly, that Fe(N2Py2) and Fe(N2Py2-D4) complexes have the same reactivity towards external substrates. However, it is the greater longevity provided by the deuterated ligand in the Fe(N2Py2-D4) complexes that leads to higher substrate conversions and product yields. Because of the same reason, no obvious differences in product selectivities were found between the deuterated and non-deuterated catalysts (Table 1 and 2).

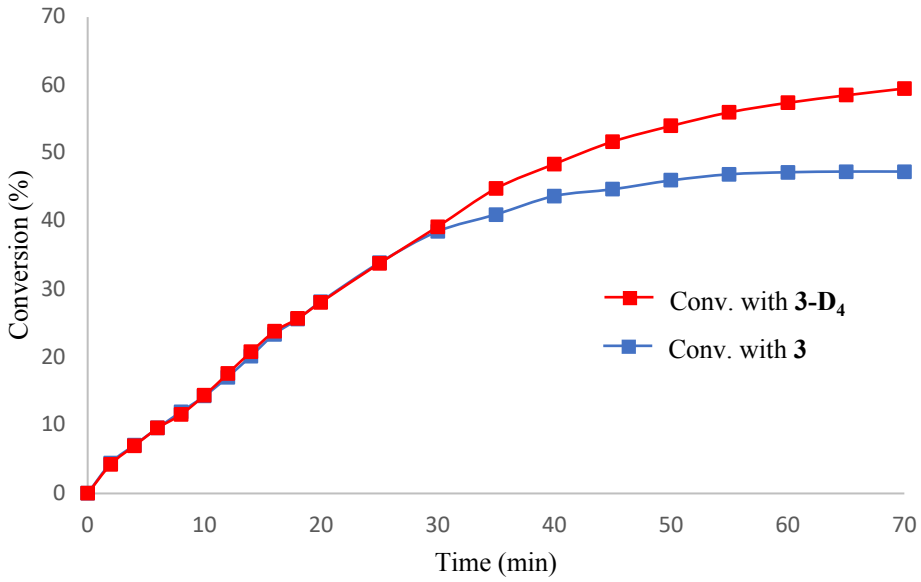

Figure 8. Reaction profiles of *cis*-cyclooctene (**5**) oxidation using catalyst **3** vs. catalyst **3-D4** with slow addition of the oxidant (30 min). Reaction conditions: Fe-cat. : H_2O_2 : substrate : AcOH = 0.25 : 100 : 100 : 1.5, 0 °C, the oxidant was added by syringe pump over 30 min. Conversions are determined by GC analysis.

Figure 7 clearly shows that the improvements in catalytic outcomes and the extended lifetimes provided by the deuterated catalysts are different from each other. **1-D4** showed a similar lifetime and a limited improvement in catalytic performance in comparison with **1**. Notably, the initial reaction rates observed for **1** and **1-D4** are also similar. As their reactivities towards substrate **5** are identical (*vide supra*), this indicates that **1** and **1-D4** have similar (oxidative) robustness under the present conditions. In sharp contrast, **3-D4** showed a much longer lifetime, a much higher initial reaction rate, and significantly improved catalytic outcomes than **3** in the

epoxidation of *cis*-cyclooctene. The difference in the effect of ligand deuteration is likely due to the relatively strong stability of the BPBP ligand under the oxidizing conditions, as a consequence of increased rigidity, with respect to the BPMEN ligand, which has a rather flexible bis-alkylamine backbone. In this regard, **1-D_4** with deuterated 2-pyridinylmethyl sites exhibits rather limited improvements compared to **1**. This finding is in line with previous notions that the stability of non-heme iron catalysts under the oxidizing conditions has a strong correlation with ligand rigidity.[5,6,19,44] It is believed that the enhanced robustness of the BPBP ligand is a key reason that (non-deuterated) BPBP-based iron complexes show better catalytic performances than their BPMEN-based counterparts. Deuteration of the BPMEN ligand results in catalytic performances of its iron complex **3-D_4** that are very similar to those of the non-deuterated BPBP-complex **1**, which illustrates the importance of oxidative ligand decomposition on catalytic activity.

4.2.6 Ligand oxidation of BPMEN-based iron complexes

These observations of evidently different catalytic performances between **3** and **3-D_4** triggered a more detailed investigation of the deactivation of BPMEN-based iron complexes. Similar to the decomposition test of BPBP-based iron complexes, **3** was mixed with 150 equiv. of H_2O_2 and 50 equiv. of AcOH in MeCN. After stirring at 0 °C for 10 min, similar to the observation for **1**, ESI-MS of the resulting mixture revealed a major peak at *m/z* = 285.1690, with an isotopic pattern that is in agreement with a carbonyl compound (BPMEN)=O (calcd. *m/z* = 285.1715) derived from aliphatic C–H oxidation of the ligand (Figure 9a). Interestingly, the same oxidation protocol applied to **3-D_4** gave two signals in this *m/z* region, *i.e.*, at *m/z* = 287.1843 and 289.1972 (Figure 9b), indicating that C–H oxidation happened both at one of the 2-pyridinylmethyl positions (calcd. *m/z* for $[(BPMEN\text{-}D_2)=O+H]^+$ is 287.1872, Figure 9b, inset) and at one of the methylene sites of the bis-alkylamine backbone (calcd. *m/z* for $[(BPMEN\text{-}D_4)=O+H]^+$ is 289.2029, Figure 9b, inset). This observation indicates that ligand oxidation in **3** and **3-D_4** is not restricted to the 2-pyridinylmethyl sites as observed for the other complexes discussed here, but may also occur on the bis-alkylamine backbone in the BPMEN ligand. Installation of deuterium atoms on the 2-pyridinylmethyl positions possibly shifts C–H oxidation more to methylene sites of the ligand backbone in **3-D_4**. However, the oxidation of these methylene sites seems to be more sluggish, leading to a slower deactivation process of **3-D_4** compared to **3**, and resulting in enhanced robustness and a much longer lifetime of **3-D_4**. In addition, oxidatively dimerized species were also found in both cases, *i.e.*, the signal at *m/z* = 242.4095 corresponds to $[Fe_2(\mu\text{-}O)(BPMEN)_2(OAc)]^{3+}$ (Figure 9a, calcd. 242.4151) and the

signal at *m/z* = 245.0943 corresponds to $[Fe_2(\mu\text{-}O)(BPMEN\text{-}D_4)_2(OAc)]^{3+}$ (Figure 9b, calcd. 245.0985).

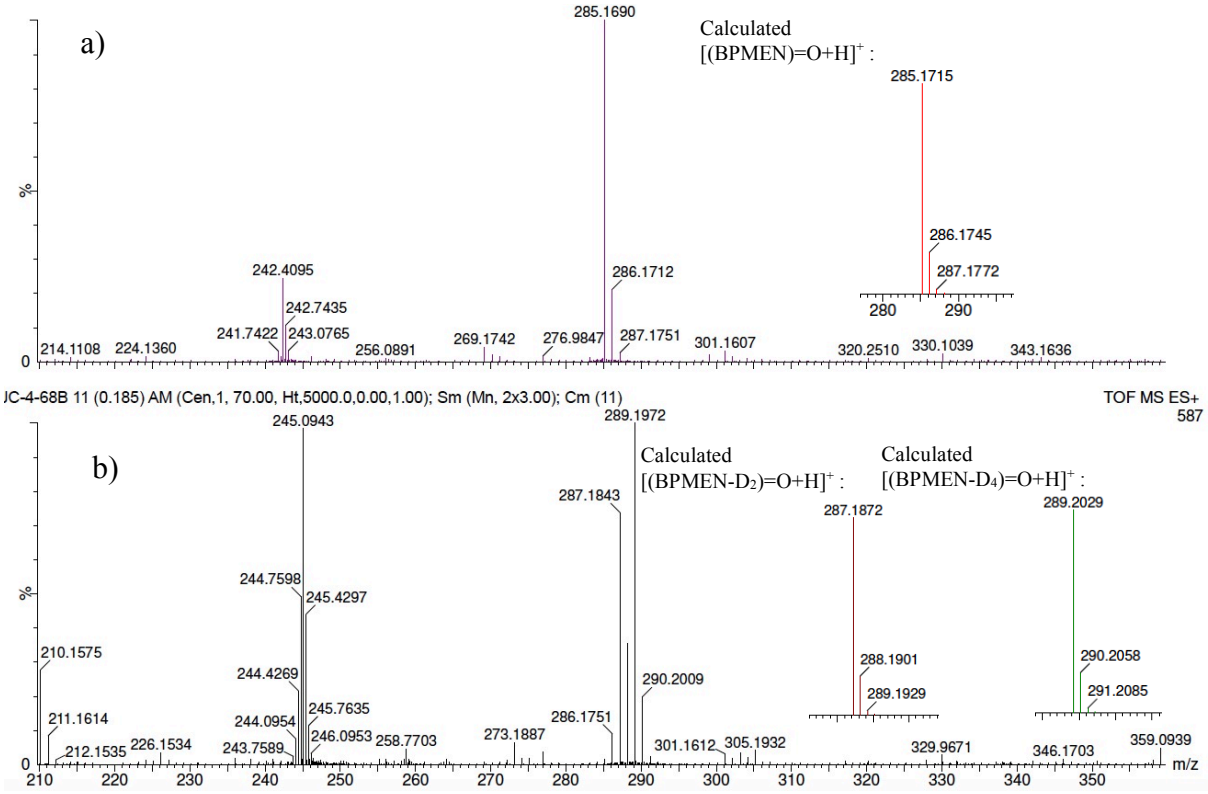

Figure 9. ESI-MS of the reaction of **3** (a) or **3-D$_4$** (b) (2mM) with H_2O_2 (150 equiv.) and AcOH (50 equiv.) in MeCN, stirred at 0 °C for 10 min. ESI-MS was directly measured from the reaction mixture without any work-up. a): The peak at *m/z* = 285.1690 corresponds to (BPMEN)=O. b): The peak at *m/z* = 287.1843 corresponds to (BPMEN-D_2)=O. The peak at *m/z* = 289.1972 corresponds to (BPMEN-D_4)=O. The peaks at *m/z* = 288 and 286 are due to the presence of non-fully deuterated complex **3-D$_3$**.

4.2.7 Lifetimes of active iron intermediates

The observation of longer lifetimes of Fe(N2Py2-D_4) complexes in catalytic oxidation reactions raised the interest in the inherent lifetimes of active intermediates formed under the oxidizing conditions. Generally, a well-characterized Fe^{III}–OOH intermediate[45,46] is generated upon reaction of the Fe^{II} complex with excess H_2O_2, which subsequently undergoes water-assisted O−O bond heterolysis to generate an Fe^{V}(O)–OH species[45,47,48] that is considered as the active oxidant in catalysis. In the presence of AcOH, the Fe/H_2O_2 catalytic systems have shown enhanced substrate conversion, as firstly reported by White.[8] In this case, an Fe^{V}(O)–OAc species[49] derived from a carboxylic acid-assisted pathway was postulated in early studies, which is analogous to the Fe^{V}(O)–OH oxidant. However, more recent DFT and spectroscopic studies favor the formation of an Fe^{III}–OOAc species, which subsequently decays to Fe^{IV}(O)–

AcO·,[50–52] representing an alternative electronic formulation of the Fe^{V}(O)–OAc species. Interestingly, the closely related Fe^{III}–OOH[53] and Fe^{III}–OOAc[51] species, generated with TPA-based ligands (TPA = tris(2-pyridylmethyl)-amine), both have been found to be correlated to the formation of product in epoxidations by Que and co-workers. That is, the formation of epoxide occurred only after the Fe^{III}–OOH or Fe^{III}–OOAc intermediate was formed, and ceased upon complete decay of these species. In this sense, it is of interest to obtain insight into the lifetimes of these species generated from corresponding Fe(N2Py2) and Fe(N2Py2-D_4) complexes.

Initial attempts to generate an Fe^{III}–OOAc intermediate, which has been reported to show an absorbance maximum at around 460 nm in UV-Vis,[51,52] by mixing of **1** (1 mM, 1 equiv.), AcOH (10 equiv.), and H_2O_2 (10 equiv.) at 0 °C unfortunately failed in our hands. The formation of the subsequent high-valent Fe-oxo species from the decay of Fe^{III}–OOAc, which has an absorbance maximum at around 740 nm,[51,52] was not successfully observed either. Next, generation of Fe^{III}–OOH species by simply mixing Fe^{II}-complexes with H_2O_2 only was successful.[53] Accordingly, the oxidation of the complexes **1** – **4** and **1-D_4** – **4-D_4** was carried with H_2O_2 (150 equiv.) in the absence of AcOH. Similar to the oxidation of these complexes using a combination of H_2O_2 and AcOH, ligand-based amide compounds derived from oxidation on 2-pyridinylmethyl sites were observed as the major products by ESI-MS analysis (e.g. (BPBP)=O (observed *m/z* =337.2019) in the case of **1**, Figure 10), indicating that active intermediates capable of C–H oxidation are formed also in the absence of AcOH. Accordingly, the lifetimes of Fe^{III}–OOH species generated from Fe(N2Py2-D_4) and Fe(N2Py2) complexes were explored.

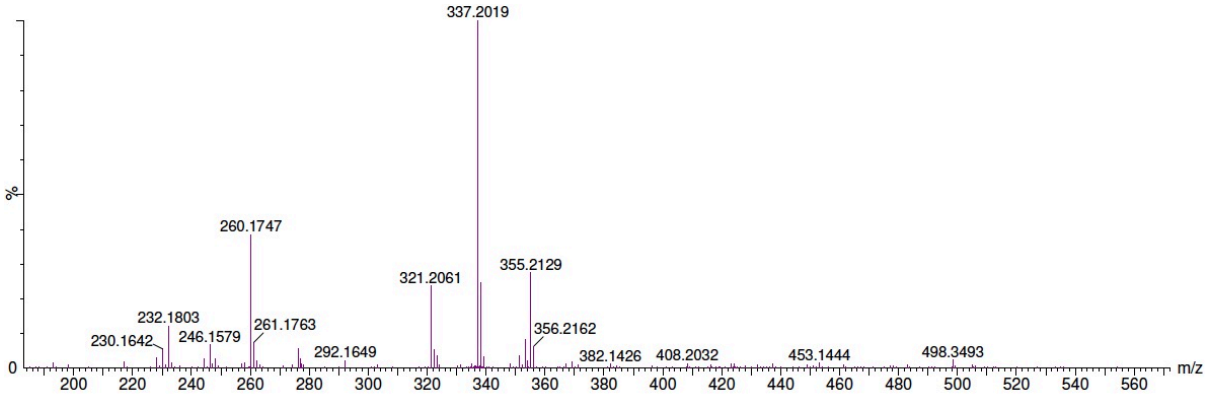

Figure 10. ESI-MS trace of the mixture from a reaction of **1** (2mM) with H_2O_2 (150 equiv.) in MeCN, stirred at 0 °C for 10 min. The peak at *m/z* = 337.2019 corresponds to the decomposition compound (BPBP)=O.

Using the reported conditions for generating Fe^{III}–OOH species,[52,53] H_2O_2 (10 equiv.) was added to a solution of **1** (1 mM) in MeCN at 0 °C. A purple chromophore appeared immediately at 560 nm in UV-Vis (Figure 11), which was assigned to the corresponding (BPBP)Fe^{III}–OOH species. By monitoring the intensity of the signal at 560 nm, this species was found to reach its maximum concentration after 60 s, then to decay completely within 300 s (Figure 12a). Subsequently, the same UV-Vis experiment was carried out with **1-D4**. The (BPBP-D4)Fe^{III}–OOH species generated in this experiment showed an almost identical concentration behaviour as (BPBP)Fe^{III}–OOH (Figure 12a), indicating that these species have rather similar lifetimes. These observations are in line with the similar catalytic activities of **1** and **1-D4** in *cis*-cyclooctene epoxidation (Figure 7a). Next, the same UV-Vis experiments were carried out to monitor the respective lifetimes of the Fe^{III}–OOH species generated from **2** and **2-D4**, and from **3** and **3-D4**, for which remarkably different kinetic behaviours were observed in catalysis (Figure 7b, 7c). However, also in these cases very similar lifetimes were observed for the (BPMCN)Fe^{III}–OOH and (BPMCN-D4)Fe^{III}–OOH (Figure 12b) species, and the (BPMEN)Fe^{III}–OOH and (BPMEN-D4)Fe^{III}–OOH species (Figure 12c).

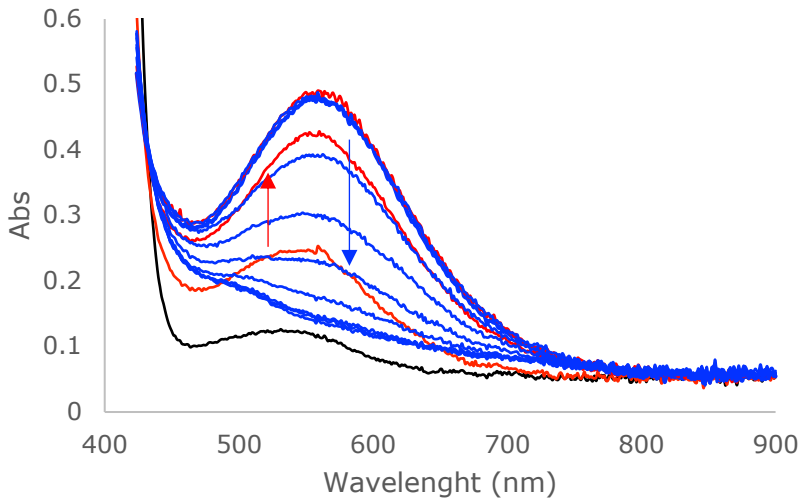

Figure 11. UV-Vis spectra for (BPBP)Fe^{III}-OOH formation (red lines) and decay (blue lines) upon mixing **1** (1 mM) with H_2O_2 (10 mM) at 0 °C in MeCN.

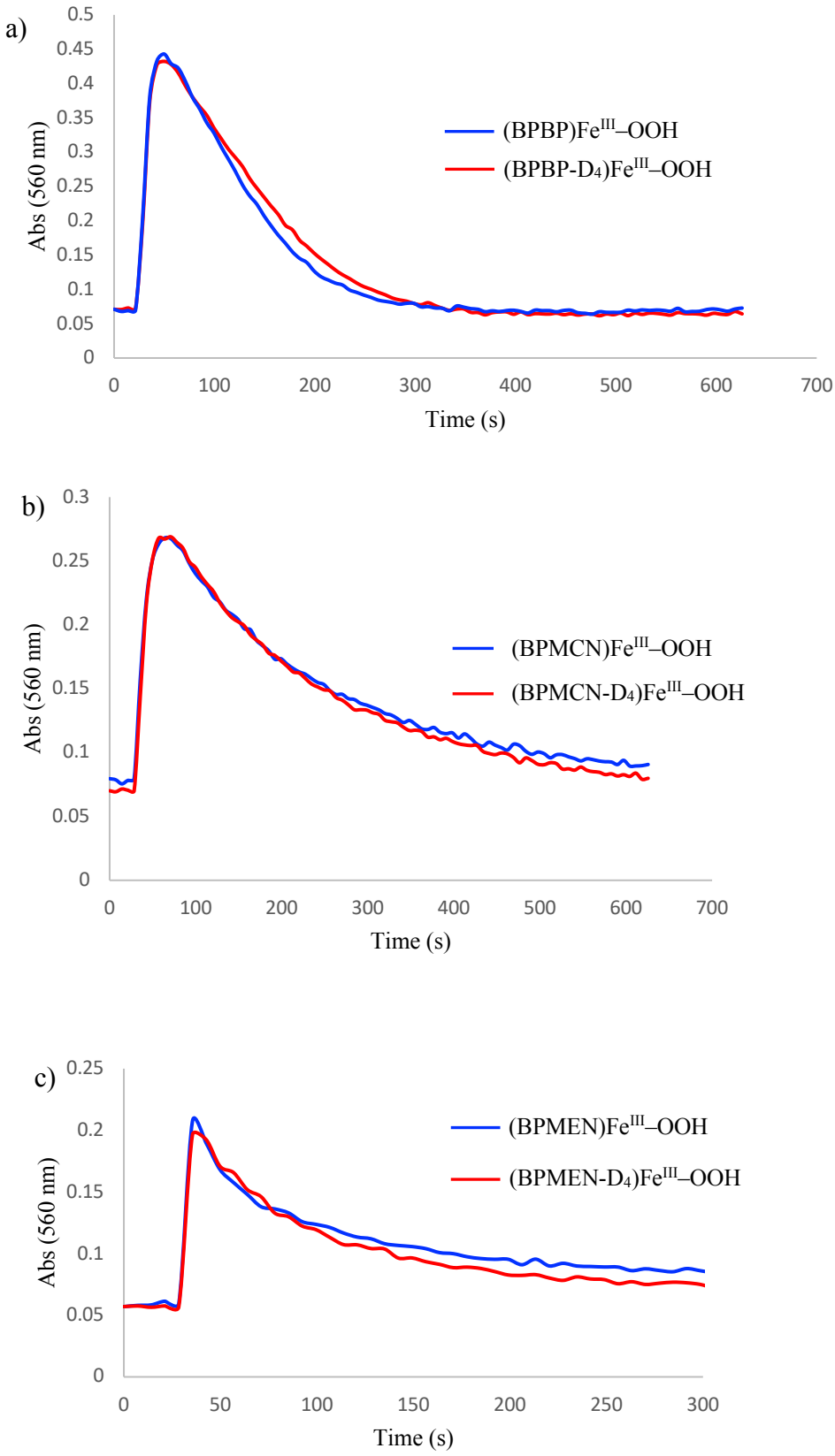

Figure 12. Time course of the formation and decay of Fe^{III}-OOH species monitored at 560 nm. The reactions were conducted with Fe(N2Py2) complexes (blue lines) or Fe(N2Py2-D_4) complexes (red lines).

ESI-MS analyses were carried out after the UV-Vis experiments to obtain insight into the speciation of the resulting mixtures. Typically, the starting Fe^{II} complex was observed as the most prominent species in the mixture. For instance, the signal at *m/z* = 527.1074 assigned to $[M\text{-}OTf]^+$ (calcd. 527.1022) represents the major species in the experiment using complex **1** (Figure 13). The amide compounds derived from ligand oxidation were found in trace amounts in these experiments (see signal at *m/z* = 337.2051 in Figure 13 for the experiment with **1**). These observations are very different from the dedicated catalyst decomposition experiments, where oxidized ligand was formed as the major product without the detection of the starting Fe^{II} complex (Figures 3 and 10). This suggests that the fates of the Fe^{II} complexes and the ligand oxidation progression depend on the reaction conditions (150 equiv. H_2O_2 was used in the dedicated catalyst decomposition experiments). Additionally, in kinetic experiments where longer lifetimes of Fe(N2Py2-D_4) complexes were observed, 400 equiv. of H_2O_2 with respect to iron complex was added.

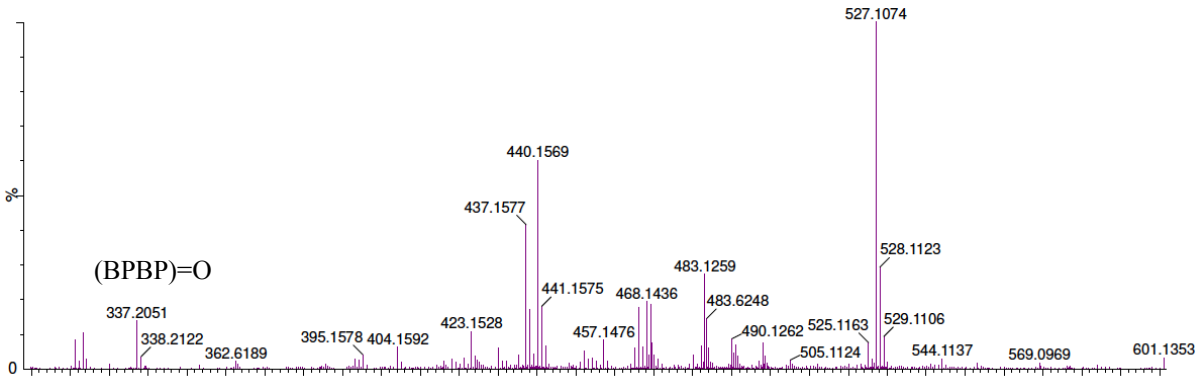

Figure 13. ESI-MS after the UV-Vis experiment with complex **1**. The peak at *m/z* = 337.2051 corresponds to the oxidized ligand (BPBP)=O. The peak at *m/z* = 527.1074 corresponds to **1** (calcd. *m/z* for $[M\text{-}OTf]^+$: 527.1022).

4.3 Conclusions

The present work demonstrates that the lifetimes of Fe(N2Py2)-based oxidation catalysts can be enhanced by replacing the H atoms with D atoms in the 2-pyridinylmethyl sites of the N2Py2 ligands. As a result, improved substrate conversions and product yields are consistently obtained in both catalytic aliphatic C–H oxidations and alkene epoxidations. This slight manipulation of the ligand is actually able to double the conversion and yield in particular catalytic reactions, and dramatically increase the lifetimes of the catalysts depending on the overall structure of the N2Py2 ligand. The Fe(N2Py2) and Fe(N2Py2-D_4) catalysts show identical reactivities (as illustrated in reaction kinetics) and similar product selectivities (as

shown in catalytic performance), which is attributed to unchanged electronic and steric properties of the deuterated and non-deuterated ligands. The overall effect of ligand deuteration on catalyst performance is exemplified by the similar catalytic performance of the deuterated BPMEN-catalyst **3-D_4** compared to non-deuterated BPBP-catalyst **1**.

This ligand design strategy has wide applicability as evaluated for a series of N2Py2 ligands with variations on both the bis-alkylamine and pyridine fragments. Yet, the improvements in catalytic performances and lifetimes provided by the deuterated ligands are different and are more pronounced for ligands with a more flexible bis-alkylamine backbone, which is likely due to differences in the inherent robustness of the parent N2Py2 ligands. The success of non-heme iron oxidation catalysts based on ligands comprizing more rigid bis-alkylamine backbones, with the BPBP ligand as a prominent example, have been explained in terms of these ligands providing a more rigid and strong chelate for iron which would prevent (oxidative) leaching of iron.[5,6] The current findings suggest that a more rigid ligand manifold attenuates intramolecular ligand oxidation, which would lead to catalyst decomposition, through a more restricted approach of 2-pyridinylmethyl C–H bonds to the intermediate iron-oxo moiety. Accordingly, deuteration of 2-pyridinylmethyl sites in more flexible ligands, such as BPMEN, results in a dramatic increase in overall catalytic performance because of less facile ligand oxidation and concomitant catalyst decomposition. Attempts to verify this hypothesis by monitoring the differences in lifetimes of pivotal oxygenated intermediates have so far not been successful. It is proposed that the present ligand design principle provides new insights and new routes for the further development of more robust ligands for homogeneous oxidation catalysts, giving rise to new and more powerful tools for practical catalytic oxidation reactions.

4.4 Experimental Section

4.4.1 General

The synthesis of iron complexes and other air- and moisture-sensitive reactions were performed under an inert nitrogen atmosphere using standard Schlenk line and glovebox techniques. Catalyst decomposition reactions and catalytic reactions were conducted under ambient conditions. The iron precursor $Fe(OTf)_2 \cdot 2CH_3CN$ was synthesized according to a reported procedure.[54] The solvents diethyl ether and acetonitrile were purified using an MBraun MB SPS-800 solvent purification system. Tetrahydrofuran for complexation reactions and methanol were dried with sodium and magnesium turnings, respectively, and distilled under nitrogen prior to use. HPLC grade anhydrous MeCN was used as solvent for UV-Vis measurements, which was stored in a glovebox. Reference samples of alcohols and carbonyl compounds **12-14** and **16-18** were prepared using the known **1**/H_2O_2 system.[9,10] Ligands

S,*S*-BPBP[19], *R*,*R*-BPMCN[43], and BPMEN[9,42], iron complexes **1**[15], **2**[43], and **3**[9,42] were synthesized according to literature procedures. All other reagents, substrates, and reaction products were obtained commercially and used without further purification. Column chromatography was performed using Merck silica gel (60–200 mesh). ^{1}H, ^{13}C NMR, and ^{19}F spectra were recorded with a 400 MHz Varian spectrometer at 25 °C, chemical shifts (δ) are given in ppm referenced to the residual solvent peak. ESI-MS measurements were performed with a Waters LCT Premier XE KE317 machine. GC analyses were performed on a Perkin–Elmer Clarus 500 Gas Chromatograph equipped with a PE-17 column ((30 m × 0.23 mm × 0.25 μm), (50% phenyl)-(50% methyl)polysiloxane) and a flame-ionization detector. UV-Vis spectra were recorded on an Agilent Cary 50 UV-Vis spectrometer equipped with a Hellma 661.202-UV 10 mm probe, wavelengths are reported in nm. Elemental microanalyses were carried out by the Mikroanalytisches Laboratorium Kolbe, Germany.

4.4.2 Synthesis of ligands and iron complexes

4.4.2.1 Synthesis of pyridine synthons

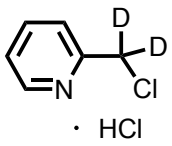

PyCD$_2$Cl·HCl This compound was prepared following reported procedures under modified reaction conditions for making PyCH$_2$Cl·HCl,[39,40] but using sodium borodeuteride as reductant. To a stirred solution of sodium borodeuteride ($NaBD_4$, 1.0 g, 24 mmol, 98 atom% D) in anhydrous methanol (10 mL) under a nitrogen atmosphere, ethyl picolinate (0.8 mL, 6 mmol) was added dropwise at 0 °C. Then the reaction was stirred at 0 °C for another hour and at ambient temperature for 2 h. The reaction mixture was poured into cold water and extracted with CH_2Cl_2 (10 mL). The aqueous phase was neutralized with 1 M HCl to pH 7 and extracted with CH_2Cl_2 (2 x 10 mL). The combined organic phase was then dried over $MgSO_4$, and concentrated to give the crude product, which was purified by column chromatography (CH_2Cl_2:MeOH:NH_3 20:1:0.1 (v/v) to 5:1:0.1 (v/v)) to provide 550 mg of 2-hydroxy-methylpyridine-D_2 as a yellow oil (5 mmol, 83% yield). Subsequently, it was treated with thionyl chloride (1.45 mL, 20 mmol) at 0 °C under a nitrogen atmosphere, which resulted in an initial color change to yellow, then to orange. The reaction was heated to 60 °C and allowed to stir for 3 h. The resulting dark-brown solution was concentrated to remove residual $SOCl_2$. The remaining brown oil was dissolved in 5 mL EtOH with gentle heating. After the solution was cooled to RT, anhydrous diethyl ether was added slowly until the solution turned cloudy. The suspension was allowed to settle and the resulting solid was filtrated, washed with diethyl ether several times, and dried in vacuo to obtain 637 mg of PyCD$_2$Cl·HCl as a light-brown solid (77% yield, 64% yield for two steps), which was of sufficient purity to be used in the next synthetic step. ^{1}H NMR (400 MHz, CD_3OD) δ 8.88 (d, J = 5.7 Hz, 1H), 8.65 (td, J = 7.9, 1.5 Hz, 1H), 8.18 (d, J = 7.9 Hz, 1H), 8.09 – 8.04 (m, 1H). A small singlet peak at 5.02 ppm was observed (with ca. 0.1 integration w.r.t. each H on pyridine), which corresponds to non-deuterated H on the 2-pyridinylmethyl position.[40] ^{13}C NMR (100 MHz, $CDCl_3$) δ 151.24, 147.49, 142.32, 127.25, 126.74, 39.34 (quint). HRMS (ESI-MS) calcd. m/z for $C_6H_5D_2ClN$ ([M-Cl]$^+$): 130.0387, found 130.0328. A small signal at m/z = 129 was observed, indicating the presence of PyCHDCl·HCl.

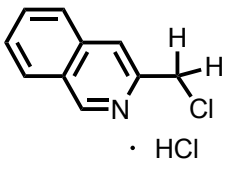

IQCH$_2$Cl·HCl This compound was prepared following reported procedures[40,55] under modified reaction conditions. To a suspension of anhydrous $CaCl_2$ (2 g, 18 mmol) in dry THF (20 mL) and absolute ethanol (20 mL) under a nitrogen atmosphere, $NaBH_4$ (1.25 g, 33 mmol) was added slowly at 0 °C. After stirring the mixture for 20 min at the same temperature, a solution of methyl 3-isoquinolinecarboxylate (1.12 g, 6 mmol) in dry THF (20 mL) was added and the mixture was stirred for another 60 min, giving a white suspension. At this point, the reaction was quenched carefully by addition of a saturated NH_4Cl aqueous solution. The resulting mixture was extracted with Et_2O (3 x 30 mL). The combined organic phase was then dried over $MgSO_4$, and concentrated to give the crude product, which was purified by silica column chromatography (first petroleum ether: EtOAc 1:3 to 1:5 (v/v), then CH_2Cl_2:MeOH 2:1 (v/v)) to provide 510 mg of a brown solid (isoquinolin-3-ylmethanol). Subsequently, this product was treated with thionyl chloride (1.3 mL, 18 mmol) at 0 °C under a nitrogen atmosphere. A white precipitate formed immediately then the mixture was heated to 60 °C and allowed to stir for 3 h. The resulting yellow suspension was concentrated to remove residual $SOCl_2$. The remaining yellow solid was dissolved in 5 mL EtOH with gentle heating. After the solution was cooled to RT, anhydrous diethyl ether was added slowly until the solution turned cloudy. The suspension was allowed to settle, and the resulting solid was filtrated, washed with diethyl ether several times and dried in vacuo. Finally, 680 mg of IQCH$_2$Cl·HCl was obtained as a white solid (53% yield for two steps), which was of sufficient purity to be used in the next synthetic step. ^{1}H NMR (400 MHz, CD_3OD) δ 9.84 (s, 1H), 8.54 (d, J = 5.1 Hz, 2H), 8.31– 8.24 (m, 2H), 8.06 (t, J = 7.3 Hz, 1H), 5.13 (s, 2H). ^{13}C NMR (100 MHz, $CDCl_3$) δ 148.70, 140.57, 139.10, 137.31, 131.29, 130.54, 127.61, 126.84, 124.89, 40.44. HRMS (ESI-MS) calcd. *m/z* for $C_{10}H_9ClN$ ([M-Cl]$^+$): 178.0418, found 178.0395.

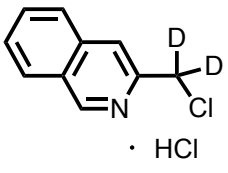

IQCD$_2$Cl·HCl This compound was prepared following the procedure for making IQCH$_2$Cl·HCl, but using $NaBD_4$ as reductant. 712 mg of a white solid was obtained in 55% overall yield. ^{1}H NMR (400 MHz, CD_3OD) δ 9.86 (s, 1H), 8.59 – 8.55 (m, 2H), 8.33 – 8.25 (m, 2H), 8.11 – 8.06 (m, 1H). A small singlet at 5.14 ppm was also observed (with ca. 0.2 integration w.r.t. each H on pyridine), which corresponds to non-deuterated H on the 3-isoquinolinylmethyl position.^{13}C NMR (100 MHz, $CDCl_3$) δ 148.60, 140.44, 139.10, 137.31, 131.28, 130.54, 127.57, 126.83, 124.91, 39.74 (quint). HRMS (ESI-MS) calcd. *m/z* for $C_{10}H_7D_2ClN$ ([M-Cl]$^+$): 180.0544, found 180.0495. Two small signals at *m/z* = 179 and 178 were also observed, indicating the presence of IQCHDCl·HCl and IQCH$_2$Cl·HCl.

4.4.2.2 Synthesis of ligands

***S,S*-BPBP-D$_4$** This compound was prepared in an analogous manner to BPBP,[19] but using PyCD$_2$Cl·HCl for constituting the pyridine fragment instead. To a solution of (*S*,*S*)-2,2′-bipyrrolidine D-tartrate trihydrate (510 mg, 1.5 mmol) and PyCD$_2$Cl·HCl (380 mg, 3 mmol) in CH_2Cl_2 (10 mL) and H_2O (10 mL), 480 mg of NaOH (12 mmol) was added. The combined mixture was vigorously stirred at RT overnight. Then the organic phase was separated and the aqueous phase was extracted with CH_2Cl_2 (3 × 10 mL). The combined organic phase was dried over $MgSO_4$ and the solvent was removed under vacuum. The obtained crude product was purified by silica column chromatography

(CH_2Cl_2:MeOH:NH_3 20:1:0.1 to 10:1:0.1 (v/v)). Then the fraction containing the desired product was washed with $NaHCO_3$ to remove remaining NH_3. Finally, BPBP-D_4 was obtained as a light-brown oil (372 mg, yield 76%). ^{1}H NMR (400 MHz, $CDCl_3$) δ 8.47–8.45 (m, 2 H), 7.55 (td, *J* = 7.8, 1.8 Hz, 2H), 7.36 (d, *J* = 7.8 Hz, 2H), 7.08–7.05 (m, 2 H), 2.98–2.94 (m, 2 H), 2.78–2.74 (m, 2 H), 2.21 (q, *J* = 8.2 Hz, 2H), 1.82–1.62 (m, 8 H). Two small singlet peaks at 4.13 and 3.45 ppm were also observed (with ca. 0.1 integration w.r.t. each H on pyridine), which correspond to ligands containing partially non-deuterated 2-pyridinylmethyl positions. ^{13}C NMR (100 MHz, $CDCl_3$) δ 160.22, 148.76, 136.22, 122.69, 121.62, 65.31, 60.51 (quint), 55.16, 25.95, 23.54. HRMS (ESI-MS) calcd. *m*/*z* for $C_{20}H_{23}D_4N_4$ ($[M+H]^+$): 327.2481, found 327.2492. A small signal at *m*/*z* = 326 was also observed, indicating the presence of *S*,*S*-BPBP-D_3.

***R*,*R*-BPMCN-D$_4$** This compound was prepared in an analogous manner to BPBP-D_4, starting from *R*,*R*-(−)-*N*, *N*′-dimethyl-1,2-cyclohexanediamine and $PyCD_2Cl$·HCl. Yellow oil, 54% yield. ^{1}H NMR (400 MHz, $CDCl_3$) δ 8.46–8.44 (m, 2 H), 7.57–7.52 (m, 4 H), 7.09–7.05 (m, 2 H), 2.62 (d, *J* = 9.8 Hz, 2H), 2.25 (s, 6H), 1.94 (d, *J* = 11.9 Hz, 2H), 1.72 (d, *J* = 8.9 Hz, 2H), 1.27–1.22 (m, 2 H), 1.15–1.09 (m, 2 H). Two small singlet peaks at 3.86 and 3.74 ppm were also observed (with ca. 0.1 integration w.r.t. each H on pyridine), which correspond to ligands containing partially non-deuterated 2-pyridinylmethyl positions. ^{13}C NMR (100 MHz, $CDCl_3$) δ 161.27, 148.56, 136.20, 122.86, 121.55, 64.42, 59.65 (quint), 36.56, 25.83, 25.76. HRMS (ESI-MS) calcd. *m*/*z* for $C_{20}H_{25}D_4N_4$ ($[M+H]^+$): 329.2638, found 329.2655. A small signal at *m*/*z* = 328 was also observed, indicating the presence of *R*,*R*-BPMCN-D_3.

BPMEN-D$_4$ This compound was prepared in an analogous manner to BPBP-D_4, starting from *N*, *N*′-dimethylethylenediamine and $PyCD_2Cl$·HCl. Yellow oil, 58% yield. ^{1}H NMR (400 MHz, $CDCl_3$) δ 8.49–8.47 (m, 2 H), 7.60 (td, *J* = 7.7, 1.8 Hz, 2H), 7.38 (d, *J* = 7.8 Hz, 2H), 7.10–7.07 (m, 2 H), 2.59 (s, 4H), 2.22 (s, 6H). A small singlet peak at 3.60 ppm was also observed (with ca. 0.2 integration w.r.t. each H on pyridine), which corresponds to ligands containing partially non-deuterated 2-pyridinylmethyl positions. ^{13}C NMR (100 MHz, $CDCl_3$) δ 159.25, 148.95, 136.22, 122.99, 121.81, 63.58 (quint), 55.39, 42.76. HRMS (ESI-MS) calcd. *m*/*z* for $C_{16}H_{19}D_4N_4$ ($[M+H]^+$): 275.2168, found 275.2143. A small signal at *m*/*z* = 274 was also observed, indicating the presence of BPMEN-D_3.

BQMEN This compound was prepared in an analogous manner to BPBP-D_4, starting from *N*, *N*′-dimethylethylenediamine and $IQCH_2Cl$·HCl. Yellow oil, 66% yield. ^{1}H NMR (400 MHz, $CDCl_3$) δ 9.15 (s, 2H), 7.87 (d, *J* = 8.1 Hz, 2H), 7.72 – 7.63 (m, 4H), 7.60 – 7.55 (m, 2H), 7.51 – 7.46 (m, 2H), 3.82 (s, 4H), 2.73 (s, 4H), 2.31 (s, 6H). ^{13}C NMR (100 MHz, $CDCl_3$) δ 152.47, 152.05, 136.29, 130.19, 127.59, 127.41, 126.65, 126.40, 118.94, 64.09, 55.57, 43.03. HRMS (ESI-MS) calcd. *m*/*z* for $C_{24}H_{27}N_4$ ($[M+H]^+$): 371.2230, found 371.2250.

BQMEN-D$_4$ This compound was prepared in analogous manner to BPBP-D_4, starting from *N*, *N*′-dimethylethylenediamine and $IQCD_2Cl$·HCl. Yellow oil, 66% yield. ^{1}H NMR (400 MHz, $CDCl_3$) δ 9.16 (s, 2H), 7.89 (d, *J* = 8.1 Hz, 2H), 7.70 – 7.67 (m, 4H), 7.61 – 7.57 (m, 2H), 7.52 – 7.48 (m, 2H), 2.73 (s, 4H), 2.32 (s, 6H). A small singlet peak at 3.80 ppm was also observed (with ca. 0.4 integration w.r.t. each H on pyridine), which corresponds to ligands containing partially non-deuterated 3-

isoquinolinylmethyl positions. ^{13}C NMR (100 MHz, $CDCl_3$) δ 152.37, 152.06, 136.28, 130.19, 127.61, 127.42, 126.66, 126.41, 119.00, 63.85 (quint), 55.50, 42.97. HRMS (ESI-MS) calcd. *m*/*z* for $C_{24}H_{23}D_4N_4$ ($[M+H]^+$): 375.2481, found 375.2504. Two small signals at *m*/*z* = 373 and 374 were also observed, indicating the presence of BQMEN-D_2 and BQMEN-D_3.

4.4.2.2 Synthesis of iron complexes

1-D_4 This complex was prepared in an analogous manner to **1**,[15] starting from *S*,*S*-BPBP-D_4. Under a nitrogen atmosphere, a solution of *S*,*S*-BPBP-D_4 (131 mg, 0.4 mmol) in dry THF (1 mL) was added to a vigorously stirred solution of $Fe(OTf)_2 \cdot CH_3CN$ (174 mg, 0.4 mmol) in dry THF (1 mL) at RT. After stirring overnight, a yellow precipitate had formed. The solid was filtrated, washed repetitively with dry THF and diethyl ether, and dried *in vacuo*. Finally, 177 mg of **1-D_4** (yellow solid, 65% yield) was obtained. ^{1}H NMR (400 MHz, CD_2Cl_2) δ 184.29, 108.28, 78.26, 52.34, 51.25, 35.68, 30.30, 9.34, 1.16, -7.12, -19.82. The 2-pyridinylmethyl H-signal was also found at 16 ppm with a weak intensity. ^{19}F NMR (376 MHz, CD_2Cl_2) δ -43.31. HRMS (ESI-MS) calcd. *m*/*z* for $C_{21}H_{22}D_4F_3FeN_4O_3S$ ($[M\text{-}OTf]^+$): 531.1278, found 531.1343. The intensity of the signal at *m*/*z* = 530 indicates the presence of **1-D_3**. Elemental analysis calcd. (%) for $C_{22}H_{22}D_4F_6FeN_4O_6S_2$: C 38.83, H 4.44, N 8.23, found C 38.20, H 4.71, N 8.11.

2-D_4 This complex was prepared in an analogous manner to **2**,[43] starting from *R*,*R*-BPMCN-D_4. Under a nitrogen atmosphere, a solution of *R*,*R*-BPMCN-D_4 (141 mg, 0.43 mmol) in dry MeCN (1 mL) was added to a vigorously stirred suspension of $FeCl_2$ (54 mg, 0.43 mmol) in dry MeCN (1 mL) at RT. The solution turned to a yellow-orange suspension immediately. After stirring overnight the yellow precipitate was filtrated, washed with dry MeCN, and dried *in vacuo*, to give 139 mg of *R*,*R*-[Fe(BPMCN-D_4)Cl_2] (0.3 mmol). Subsequently, the solid was dissolved in dry MeCN (2 mL) at RT, which was treated with AgOTf (157 mg, 0.6 mmol), immediately forming a white precipitate (AgCl). The reaction was stirred overnight, then AgCl was filtered off. The remaining brown filtrate was concentrated *in vacuo* to afford a yellow-brown semi-solid, which was recrystallized from CH_2Cl_2/diethyl ether to give **2-D_4** as a yellow solid (200 mg, 69% yield). ^{1}H NMR (400 MHz, CD_2Cl_2) δ 89.32, 28.47, 21.25, 17.02, 9.29, 7.75, 5.13, 2.17, 0.09. ^{19}F NMR (376 MHz, CD_2Cl_2) δ -79.11. HRMS (ESI-MS) calcd. *m*/*z* for $C_{21}H_{24}D_4F_3FeN_4O_3S$ ($[M\text{-}OTf]^+$): 533.1435, found 533.1332. The intensity of the signal at *m*/*z* = 532 indicates the presence of **2-D_3**. Elemental analysis calcd. (%) for $C_{22}H_{24}D_4F_6FeN_4O_6S_2$: C 38.72, H 4.73, N 8.21, found C 38.28, H 4.47, N 8.07.

3-D_4 This complex was prepared in an analogous manner to **1-D_4**, starting from BPMEN-D_4. Yellow solid, 63% yield. ^{1}H NMR (400 MHz, CD_2Cl_2) δ 169.61, 119.25, 96.50, 76.23, 53.18, 50.80, 12.28, 2.09, -13.34. The 2-pyridinylmethyl H-signal was also found at 28 ppm with a weak intensity. ^{19}F NMR (376 MHz, CD_2Cl_2) δ -30.04. HRMS (ESI-MS) calcd. *m*/*z* for $C_{17}H_{18}D_4F_3FeN_4O_3S$ ($[M\text{-}OTf]^+$): 479.0965, found 479.0931. The intensity of the signal at *m*/*z* = 478 indicates the presence of **3-D_3**. Elemental analysis calcd. (%) for $C_{18}H_{18}D_4F_6FeN_4O_6S_2$: C 34.41, H 4.17, N 8.92, found C 33.67, H 4.57, N 9.06.

4 This complex was prepared in an analogous manner to **1-D_4**, starting from BQMEN. Yellow solid, 71% yield. ^{1}H NMR (400 MHz, CD_2Cl_2) δ 177.67, 141.05, 97.65, 75.18, 49.04, 31.20, 13.34, 11.04, -9.54. ^{19}F NMR (376 MHz, CD_2Cl_2) δ -23.89. HRMS (ESI-MS) calcd. *m/z* for $C_{25}H_{26}F_3FeN_4O_3S$ ([M-OTf]$^+$): 575.1027, found 575.0964. Elemental analysis calcd. (%) for $C_{26}H_{26}F_6FeN_4O_6S_2$: C 43.11, H 3.62, N 7.73, found C 43.09, H 3.63, N 7.71.

4-D_4 This complex was prepared in an analogous manner to **1-D_4**, starting from BQMEN-D_4. Yellow solid, 74% yield. ^{1}H NMR (400 MHz, CD_2Cl_2) δ 178.54, 140.44, 97.59, 75.61, 49.05, 13.26, 10.94, -9.66. The 3-isoquinolinylmethyl H-signal was also found at 31 ppm with a weak intensity. ^{19}F NMR (376 MHz, CD_2Cl_2) δ -24.64. HRMS (ESI-MS) calcd. *m/z* for $C_{25}H_{22}D_4F_3FeN_4O_3S$ ([M-OTf]$^+$): 579.1278, found 579.1181. The intensities of signals at *m/z* = 578 and 577 and the presence of a signal at *m/z* = 576 indicate the presence of **3-D_3** and **3-D_2**. Elemental analysis calcd. (%) for $C_{26}H_{22}D_4F_6FeN_4O_6S_2 \cdot 2\ H_2O$: C 40.85, H 4.48, N 7.33, found C 40.35, H 4.55, N 7.49.

4.4.3 Catalyst decomposition experiments

A 20 mL vial was charged with: Fe-complex (4 μmol, 1 equiv.) and MeCN (2 mL). A 0.5 M CH_3CO_2H solution in MeCN was added (0.4 mL, 0.2 mmol, 50 equiv.). The vial was cooled on an ice bath with stirring. Subsequently, a 1.0 M H_2O_2 solution in MeCN (0.6 mL, 0.6 mmol, 150 mol%, diluted from a 35% H_2O_2 aqueous solution) was added in a dropwise manner. After stirring at 0 °C for 10 min, a sample of the reaction mixture was submitted to ESI-MS analysis directly.

4.4.4 Catalytic performance experiments

A 20 mL vial was charged with: substrate (1 equiv.) and the indicated loading of catalyst and MeCN. A 0.5 M CH_3CO_2H solution in MeCN was added with indicated loading. The vial was cooled on an ice bath with stirring. Subsequently, a 1.0 M H_2O_2 solution in MeCN (indicated loading, diluted from a 35% H_2O_2 aqueous solution) was delivered by syringe pump over 10 min. After the oxidant addition, the resulting mixture was stirred at 0 °C for another 30 min. At this point, a 1.0 M nitrobenzene solution in MeCN (1 equiv.) was added as internal standard. The solution was filtered through a silica gel plug, which was subsequently rinsed with 3 x 1 mL EtOAc. Then a sample was submitted to GC analysis or ^{1}H NMR analysis.

4.4.5 Kinetic study

A 20 mL vial was charged with: *cis*-cyclooctene (116 mg, 1 mmol, 1 equiv.), catalyst (0.25 or 0.5 mol%) and MeCN (5 mL). A 0.5 M CH_3CO_2H solution in MeCN (30 μL, 15 μmol, 1.5 mol%) and a 1.0 M nitrobenzene solution in MeCN (1 mL, 1 mmol) were added. The vial was cooled on an ice bath with stirring. Subsequently, a 1.0 M H_2O_2 solution in MeCN (1 mL, 1 mmol, 100 mol%, diluted from a 35% H_2O_2 aqueous solution) was added at once, or delivered by syringe pump over 30 min. At 1 min, the first sample was submitted to GC analysis after filtration through a silica gel plug followed by rinsing

with EtOAc. Then the GC samples were taken every 2 min . After 20 min GC samples were taken every 5 min.

4.4.6 In situ UV-Vis measurements

HPLC grade anhydrous MeCN was used as solvent for UV-Vis measurements, which was stored and taken into the glove box prior to use. A reactor equipped with a UV-Vis probe was charged with catalyst in MeCN (1 mM) under a nitrogen atmosphere, and was cooled on an ice bath with stirring. Subsequently, 10 equiv. of H_2O_2 was added to the reaction mixture, generating a purple chromophore immediately, which turned brown-yellow slowly over time.

4.5 References

[1] G. Olivo, O. Cussó, M. Costas, *Chem. Asian J.* **2016**, *11*, 3148–3158.

[2] W. N. Oloo, L. Que, Jr., *Acc. Chem. Res.* **2015**, *48*, 2612–2621.

[3] K. P. Bryliakov, E. P. Talsi, *Coord. Chem. Rev.* **2014**, *276*, 73–96.

[4] X. Engelmann, I. Monte-Pérez, K. Ray, *Angew. Chem. Int. Ed.* **2016**, *55*, 7632–7649.

[5] J. England, C. R. Davies, M. Banaru, A. J. P. White, G. J. P. Britovseka, *Adv. Synth. Catal.* **2008**, *350*, 883–897.

[6] M. Grau, A. Kyriacou, F. Cabedo Martinez, I. M. de Wispelaere, A. J. P. White, G. J. P. Britovsek, *Dalton Trans.* **2014**, *43*, 17108–17119.

[7] J. Y. Ryu, J. Kim, M. Costas, K. Chen, W. Nam, L. Que Jr., *Chem. Commun.* **2002**, *0*, 1288–1289.

[8] M. C. White, A. G. Doyle, E. N. Jacobsen, *J. Am. Chem. Soc.* **2001**, *123*, 7194–7195.

[9] L. Gómez, I. Garcia-Bosch, A. Company, J. Benet-Buchholz, A. Polo, X. Sala, X. Ribas, M. Costas, *Angew. Chem. Int. Ed.* **2009**, *48*, 5720–5723.

[10] L. Gómez, M. Canta, D. Font, I. Prat, X. Ribas, M. Costas, *J. Org. Chem.* **2013**, *78*, 1421–1433.

[11] N. A. Vermeulen, M. S. Chen, M. C. White, *Tetrahedron* **2009**, *65*, 3078–3084.

[12] V. Yazerski, P. Spannring, D. Gatineau, C. H. M. Woerde, S. M. Wieclawska, M. Lutz, H. Kleijn, R. J. M. Klein Gebbink, *Org. Biomol. Chem.* **2014**, *12*, 2062–2070.

[13] O. Cussó, I. Garcia-bosch, X. Ribas, J. Lloret-fillol, M. Costas, *J. Am. Chem. Soc.* **2013**, *135*, 14871−14878.

[14] O. Cussó, X. Ribas, J. Lloret-Fillol, M. Costas, *Angew. Chem. Int. Ed.* **2015**, *54*, 2729 –2733.

[15] K. Suzuki, P. D. Oldenburg, L. Que, Jr., *Angew. Chem. Int. Ed.* **2008**, *47*, 1887–1889.

[16] O. Cussó, M. Cianfanelli, X. Ribas, R. J. M. Klein Gebbink, M. Costas, *J. Am. Chem. Soc.* **2016**, *138*, 2732–2738.

[17] D. Font, M. Canta, M. Milan, O. Cussó, X. Ribas, R. J. M. Klein Gebbink, M. Costas, *Angew. Chem. Int. Ed.* **2016**, *55*, 5776–5779.

[18] A. M. Zima, O. Y. Lyakin, R. V. Ottenbacher, K. P. Bryliakov, E. P. Talsi, *ACS Catal.* **2016**, *6*, 5399–5404.

[19] M. S. Chen, M. C. White, *Science* **2007**, *318*, 783–787.

[20] M. S. Chen, M. C. White, *Science* **2010**, *327*, 566–571.
[21] P. E. Gormisky, M. C. White, *J. Am. Chem. Soc.* **2013**, *135*, 14052–14055.
[22] J. M. Howell, K. Feng, J. R. Clark, L. J. Trzepkowski, M. C. White, *J. Am. Chem. Soc.* **2015**, *137*, 14590–14593.
[23] T. J. Osberger, D. C. Rogness, J. T. Kohrt, A. F. Stepan, M. C. White, *Nature* **2016**, *537*, 214–219.
[24] M. Canta, D. Font, L. Gõmez, X. Ribas, M. Costas, *Adv. Synth. Catal.* **2014**, *356*, 818–830.
[25] A. Thibon, J.-F. Bartoli, S. Bourcier, F. Banse, *Dalton Trans.* **2009**, *0*, 9587–9594.
[26] J. Chen, M. Lutz, M. Milan, M. Costas, M. Otte, R. J. M. Klein Gebbink, *Adv. Synth. Catal.* **2017**, *359*, 2590–2595.
[27] S. J. Lange, H. Miyake, L. Que, Jr., *J. Am. Chem. Soc.* **1999**, *121*, 6330–6331.
[28] Y. Mekmouche, S. Ménage, C. Toia-Duboc, M. Fontecave, J.-B. Galey, C. Lebrun, J. Pécaut, *Angew. Chem. Int. Ed.* **2001**, *40*, 949–952.
[29] A. Nielsen, F. B. Larsen, A. D. Bond, C. J. McKenzie, *Angew. Chem. Int. Ed.* **2006**, *45*, 1602–1606.
[30] M. R. Bukowski, S. Zhu, K. D. Koehntop, W. W. Brennessel, L. Que, Jr., *J. Biol. Inorg. Chem.* **2004**, *9*, 39–48.
[31] L. You, S. R. Long, V. M. Lynch, E. V. Anslyn, *Chem. Eur. J.* **2011**, *17*, 11017–11023.
[32] D. Lee, S. J. Lippard, *J. Am. Chem. Soc.* **2001**, *123*, 4611–4612.
[33] D. Lee, S. J. Lippard, *Inorg. Chem.* **2002**, *41*, 827–837.
[34] E. C. Carson, S. J. Lippard, *J. Inorg. Biochem.* **2006**, *100*, 1109–1117.
[35] S. Groni, P. Dorlet, G. Blain, S. Bourcier, R. Guillot, E. Anxolabéhère-Mallart, *Inorg. Chem.* **2008**, *47*, 3166–3172.
[36] D. Pijper, P. Saisaha, J. W. De Boer, R. Hoen, C. Smit, A. Meetsma, R. Hage, R. P. Van Summeren, P. L. Alsters, B. L. Feringa, W. R. Browne, *Dalton Trans.* **2010**, *39*, 10375-10381.
[37] M. S. Vad, A. Nielsen, A. Lennartson, A. D. Bond, J. E. McGrady, C. J. McKenzie, *Dalton Trans.* **2011**, *40*, 10698–10707.
[38] D. G. Lonnon, D. C. Craig, S. B. Colbran, *Inorg. Chem. Commun.* **2003**, *6*, 1351–1353.
[39] I. V. Seregin, A. W. Schammel, V. Gevorgyan, *Org. Lett.* **2007**, *9*, 3433–3436.
[40] N. Rüger, M. Roatsch, T. Emmrich, H. Franz, R. Schüle, M. Jung, A. Link, *ChemMedChem* **2015**, *10*, 1875–1883.
[41] M. Costas, A. K. Tipton, K. Chen, D. H. Jo, L. Que, Jr., *J. Am. Chem. Soc.* **2001**, *123*, 6722–6723.
[42] K. Chen, L. Que, Jr., *Chem. Commun.* **1999**, 1375–1376.
[43] M. Costas, L. Que, Jr., *Angew. Chem. Int. Ed.* **2002**, *41*, 2179–2181.
[44] J. England, G. J. P. Britovsek, N. Rabadia, A. J. P. White, *Inorg. Chem.* **2007**, *46*, 3752–3767.
[45] K. Chen, L. Que, Jr., *J. Am. Chem. Soc.* **2001**, *123*, 6327–6337.
[46] A. Mairata I Payeras, R. Y. N. Ho, M. Fujita, L. Que, Jr., *Chem. Eur. J.* **2004**, *10*, 4944–4953.
[47] I. Prat, J. S. Mathieson, M. Güell, X. Ribas, J. M. Luis, L. Cronin, M. Costas, *Nat. Chem.* **2011**, *3*, 788–793.
[48] K. Chen, M. Costas, J. Kim, A. K. Tipton, L. Que, Jr., *J. Am. Chem. Soc.* **2002**, *124*, 3026–3035.
[49] R. Mas-Balleste, L. Que, Jr., *J. Am. Chem. Soc.* **2007**, *129*, 15964–15972.

[50] Y. Wang, D. Janardanan, D. Usharani, K. Han, L. Que, Jr., S. Shaik, *ACS Catal.* **2013**, *3*, 1334–1341.

[51] W. N. Oloo, K. K. Meier, Y. Wang, S. Shaik, E. Münck, L. Que, Jr., *Nat. Commun.* **2014**, *5*, 3046.

[52] O. V. Makhlynets, W. N. Oloo, Y. S. Moroz, I. G. Belaya, T. D. Palluccio, A. S. Filatov, P. Müller, M. A. Cranswick, L. Que, Jr., E. V. Rybak-Akimova, *Chem. Commun.* **2014**, *50*, 645–648.

[53] W. N. Oloo, A. J. Fielding, L. Que, Jr., *J. Am. Chem. Soc.* **2013**, *135*, 6438–6441.

[54] K. S. Hagen, *Inorg. Chem.* **2000**, *39*, 5867–5869.

[55] G. Guanti, R. Riva, *Tetrahedron Asymmetry* **2001**, *12*, 1185–1200.

Chapter 5

Highly Efficient Epoxidation of Vegetable Oils Catalyzed by [Mn(OTf)$_2$(*rac*-BPBP)] with Hydrogen Peroxide and Acetic Acid

Abstract

Vegetable oil is one of the most promising candidates as durable alternative raw material for chemical production. Epoxidized vegetable oils (EVOs) are versatile building blocks for lubricants, plastics plasticizers, polyvinyl chloride (PVC) stabilizers, and surface coating formulations. Therefore, many catalytic systems have been reported for producing EVOs. However, they generally involve at least one of the disadvantages of low product yield or selectivity, high catalyst loading, usage of high-cost catalyst, harsh reaction conditions, long reaction time, or the use of toxic organic solvent. In this chapter, a catalytic protocol for the efficient epoxidation of vegetable oils is presented that is based on a combination of a manganese catalyst, H_2O_2 as the oxidant, and acetic acid as additive. This protocol relies on the use of a homogeneous catalyst based on the non-noble metal manganese in combination with a racemic mixture of the *N*,*N*'-bis(2-picolyl)-2,2'-bispyrrolidine ligand (*rac*-BPBP). The optimized reaction conditions entail only 0.03 mol% of manganese catalyst with respect to the number of double bonds (ca. 0.1 wt% with respect to the oil) and ambient temperature. This epoxidation protocol is highly efficient, since it allows most of the investigated vegetable oils, including cheap waste cooking oil, to be fully epoxidized to EVOs in more than 90% yield with excellent epoxide selectivities (> 90%) within 2 h of reaction time. In addition, the protocol takes place in a biphasic reaction medium constituted by the vegetable oil itself and an aqueous acetic acid phase, from which the epoxidized product can be easily separated *via* simple extraction. In terms of efficiency and reaction conditions, including the limited use or exclusion of organic solvent (MeCN), the current epoxidation protocol outperforms previously reported catalytic protocols for plant oil epoxidation, representing a promising alternative method for EVO production.

5.1 Introduction

Nowadays, the decreasing supply of fossil resources and increasing environmental problems have triggered the search for durable alternative raw materials for chemical production. Renewable biomass has been identified world-wide as the prime candidate to replace fossil resources as the feedstock for the chemical industry.[1] Among various biomass resources, vegetable oils (VOs) represent one of the most promising candidates due to their wide availability, biodegradable properties, and low costs.[2–4] Common VOs are mixtures of triglycerides, which are composed of three fatty acid moieties connected by a glycerol backbone (Figure 1). These fatty acids, either saturated or unsaturated, normally have 14 to 22 carbons in each hydrocarbon chain, resulting is a relatively high overall carbon content.[5] More importantly, the fatty acids in VOs are mostly unsaturated with 0 to 3 double bonds per carbon chain. Modifications of these C=C bonds can produce new value-added chemicals or monomers for polymers, which has attracted research interests for many years.[6,7] Functionalizing the double bonds *via* epoxidation is one of the most common approaches to produce epoxidized vegetable oils (EVOs), which are versatile building blocks for lubricants,[8–10] plastics plasticizers,[11–13] polyvinyl chloride (PVC) stabilizers,[14–16] and surface coating formulations.[17–20]

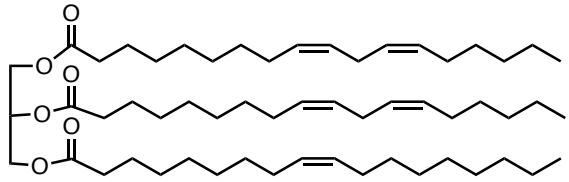

Figure 1. A typical triglyceride in sunflower oil, derived from the fatty acids linoleic acid (C18:2) and oleic acid (C18:1).

The Prilezhaev process is currently adopted in industry for the production of EVOs. In this process double bonds are converted with percarboxylic acids formed *in situ* from a carboxylic acid (e.g. acetic acid) and hydrogen peroxide in the presence of a mineral acid like H_2SO_4 or HCl (Scheme 1). This process has several drawbacks, such as low epoxide selectivity due to oxirane ring opening and corrosion issues, which are both caused by the strongly acidic reaction conditions. In the past decades, tremendous efforts have accordingly been spent on developing new catalytic systems, both homogeneous and heterogeneous, to form EVOs in a more selective and efficient manner.

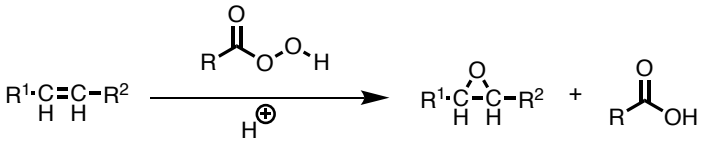

Scheme 1. Conventional vegetable oil epoxidation process (Prilezhaev reaction).

Some selected catalytic systems reported since 2000 for the epoxidation of VOs are listed in Table 1. Gerbase and co-workers reported a homogeneous $CH_3ReO_3/H_2O_2/CH_2Cl_2$ catalytic system, in which a very high yield of epoxide (95%) was obtained under mild reaction conditions (entry 1).[21] However, the use of an expensive noble metal (Re, 1 mol%) limits its application in a large-scale process. A cheaper metal (Mo) has been used by Farias *et al.* for the epoxidation of soybean oil.[22] However, a relatively high reaction temperature of 110 °C was needed, to give only a moderate yield (54%) of epoxide (entry 2). Lipases have also been used in the chemoenzymatic epoxidation of VOs. They have shown very high chemo-, regio-, and stereoselectivity without the formation of undesired ring-opening side-products.[23] Vlček and Petrović used lipase Candida antarctica (Novozyme 435) to epoxidize soybean oil with H_2O_2 in high yield (entry 3).[24] The protocol is sensitive to the reaction temperature; on one hand, a higher temperature is beneficial for double bond conversion, on the other hand this leads to deactivation of the lipase.[4] Some other drawbacks of the use of lipases are their high cost and their relatively low reactivity because of limited interaction between the catalytic center and the large triglyceride substrates due to steric hindrance.[4]

Entries 4-6 in Table 1 show examples of utilizing polyoxometalates as catalysts to epoxidize soybean oil with H_2O_2 as the oxidant. These epoxidation processes were carried out in a solvent-free medium, *i.e.*, using a mixture of aqueous H_2O_2 and the plant oil. A somewhat elevated reaction temperature (40-60 °C) and a high catalyst loading (5-33 wt%) were required in these examples. For instance, Cheng *et al.* used 5 wt% of $[\pi\text{-}C_5H_5N(CH_2)_{15}CH_3]_3[PW_4O_{16}]$ to obtain 90 % of epoxidized soybean oil at 60 °C reaction temperature.[25] Immobilization of polyoxometalates onto an inorganic solid support is mostly used in order to increase their stability and reusability,[4] nevertheless, this normally results in a lower catalytic activity. For example, Jiang *et al.* reported the use of the peroxophosphotungstate $[MeN(n\text{-}C_8H_{17})_3]\{PO_4[WO(O_2)_2]_4\}$ for the catalytic epoxidation of soybean oil, which provided 99% yield at very high catalyst loading (31 wt%, entry 5).[26] Supporting this catalyst on modified halloysite nanotubes resulted in a diminished yield of 12%.[26] Similarly, Chen *et al.* supported this complex on acid-activated palygorskite, giving rise to an epoxide yield of 79% (entry 6).[27]

Table 1. Selected catalytic systems for epoxidation of VOs.[4]

Entry	Oil	Oxidant	Catalyst (loading)	Solvent	Reaction conditions	Epoxide yield (%)
1[21]	Soybean oil	H_2O_2	CH_3ReO_3 (1 mol%)	CH_2Cl_2	30 °C, 2 h	95
2[22]	Soybean oil	TBHP	$[MoO_2(acac)_2]$ (1 mol%)	Toluene	110 °C, 2 h	54
3[24]	Soybean oil	H_2O_2	Novozym 435 (4.0 wt%)	Toluene	50 °C, 4 h	90
4[25]	Soybean oil	H_2O_2	$[\pi\text{-}C_5H_5N(CH_2)_{15}CH_3]_3\text{-}[PW_4O_{16}]$ (5.0 wt%)	-	60 °C, 4 h	90
5[26]	Soybean oil	H_2O_2	$[MeN(n\text{-}C_8H_{17})_3]\text{-}\{PO_4[WO(O_2)_2]_4\}$ (31 wt%)	-	40 °C, 3 h	99
6[27]	Soybean oil	H_2O_2	$[MeN(n\text{-}C_8H_{17})_3]\text{-}\{PO_4[WO(O_2)_2]_4\}$ supported on palygorskite (33 wt%)	-	50 °C, 2 h	79
7[28]	Soybean oil	H_2O_2	Amorphous Ti/SiO_2 (2.5 wt%)	*tert*-Butanol	90 °C, >54 h	88
8[29]	Soybean oil	TBHP[a]	Meso-Ti-HMS (2.5 wt%)	EtOAc	60 °C, 24 h	22
9[30]	Soybean oil	H_2O_2	Nb_2O_5–SiO_2 (12 wt%)	Et_2O	80 °C, 5 h	10
10[31]	Castor oil	H_2O_2	Amberlite IR-120 (15 wt%)	Benzene	50 °C, 10 h	78
11[32]	Soybean oil	TBHP[a]	MoO_3/Al_2O_3 (Mo/C═C = 1%)	Toluene	80 °C, 4 h	16
12[33]	Soybean oil	H_2O_2	γ-Al_2O_3 (12 wt%)	Et_2O	80 °C, 10 h	48

[a] TBHP = *tert*-butyl hydroperoxide.

Many heterogeneous catalytic systems have also been reported to be used in the epoxidation of VOs. Several representative examples are listed in Table 1, entries 7-12. As can been seen from

these examples, all reactions were performed at high temperatures (mostly > 80 °C), and in most of the cases relatively low reactivities were obtained (yields mostly < 70%). For instance, reaction temperatures between 60-80 °C were required in the reactions using meso-Ti-HMS, Nb_2O_5–SiO_2, MoO_3/Al_2O_3, or γ-Al_2O_3 as catalyst, giving rise to 10-48 % yields of epoxidized soybean oil (entries 8, 9, 11, 12). Fierro and co-workers have developed an amorphous $Ti/SiO_2/H_2O_2$/*tert*-butanol catalytic protocol for the epoxidation of soybean oil with relatively low catalyst loading (2.5 wt%), achieving relatively high epoxide yield (88%, entry 7).[28] However, a high reaction temperature (90 °C) and long reaction time (> 54 h) were used. Using Amberlite IR-120 as catalyst, 78% epoxidized castor oil can be obtained at relatively mild reaction conditions (50 °C, entry 10).[31] However, the toxic solvent benzene and a large amount of catalyst (15 wt%) were used in this case.

To sum up, the conventional Prilezhaev process and previously reported catalytic systems for the epoxidation of VOs generally entail at least one of the following disadvantages: low selectivity, low catalyst efficiency, usage of high-cost catalyst, harsh reaction conditions, long reaction time, or the use of a harmful organic solvent. In order to meet the increasing demand for the production of EVOs on a large-scale, the development of more efficient, practical catalytic systems for the selective epoxidation of VOs and their derivatives under mild reaction conditions is desirable. Ideally, such catalytic systems would conform to the principles of green chemistry in modern chemistry.[4]

Spannring *et al.* have reported on a one-pot oxidative cleavage protocol of unsaturated fatty acids (UFAs) and fatty acid methyl esters (FAMEs) to form aldehydes as primary products, with the catalytic epoxidation of double bonds as the first and key step.[34] This epoxidation step was carried out using the abundant, environmentally benign first-row transition metal iron, supported by a bis-alkylamine-bis-pyridine (N2Py2) ligand. In Chapter 3 of this thesis, similar Fe(N2Py2)/H_2O_2/AcOH catalytic protocols for the epoxidation of the fatty acid ester methyl linoleate were discussed. Even though these catalytic systems are relatively efficient, *i.e.*, full conversion of substrate can be achieved with 0.5 mol% catalyst per double bond, a further reduction of the catalyst loading seems necessary for the large-scale application of these protocols. Furthermore, these catalytic protocols make use of relatively toxic acetonitrile (MeCN) as the reaction solvent.

As a first-row transition metal, manganese has similar advantages as iron in terms of cost, availability, and low toxicity. In addition, several studies have reported that Mn(N2Py2) complexes generally demonstrate higher conversions and yields as compared to their Fe(N2Py2)

analogs in both aliphatic C–H oxidation and alkene epoxidation.[35–38] Based on this observation, the study presented in this chapter aimed to explore the use of Mn(N2Py2) type complexes in combination with H_2O_2 and acetic acid (AcOH) for the catalytic epoxidation of VOs and their derivatives. This study has resulted in the development of a highly efficient, Mn-based protocol that can be conducted at room temperature in only 2 h of reaction time, generally providing EVOs in more than 90% yield and with over 90% epoxy-group selectivity. In addition, the use of MeCN solvent could be strongly limited and even avoided through further optimization of the reaction conditions. Details on the use of this Mn-based epoxidation protocol for a series of different VOs will also be discussed.

5.2 Results and Discussion

A series of non-heme Mn-complexes bearing N2Py2 ligands have been synthesized to study the epoxidation of UFAs (FAMEs) and VOs (Figure 2). These N2Py2 ligands, including the well-known BPMEN[39], BPMCN,[40] and BPBP[41] (BPMEN = *N*,*N*'-dimethyl-*N*,*N*'-bis(2-picolyl)ethylenediamine, BPMCN = *N*,*N*'-dimethyl-*N*,*N*'-bis(2-picolyl)-cyclohexane-*trans*-1,2-diamine, BPBP = *N*,*N*'-bis(2-picolyl)-2,2'-bispyrrolidine), can be readily converted to the corresponding Mn complexes [Mn(OTf)$_2$(BPMEN)][42] (**1**), [Mn(OTf)$_2$(*R*,*R*-BPMCN)][42] (**2**) and [Mn(OTf)$_2$(BPBP)][43] (**3**), respectively, upon treatment with Mn(OTf)$_2$ in THF (Figure 2; see experimental section for details). Amongst the BPBP-based complexes, Mn-complexes derived from different BPBP stereoisomers,[44] *i.e.*, *S*,*S*-, *R*,*S*-, *rac*-, and *mix*-BPBP, were synthesized and tested for their epoxidation activity. In contrast to the enantiomerically pure versions of the ligand, less costly non-enantiomerically pure versions of the BPBP ligand (such as *rac*- and *mix*-BPBP) would be preferably used in the epoxidation of VOs, in which enantioselectivity issues are not at stake from a product application point of view. The development and application in Fe-catalyzed epoxidation reactions of *mix*-BPBP was earlier reported by Spannring *et al*.[34] *Mix*-BPBP constitutes a mixture of *R*,*R*-BPBP, *S*,*S*-BPBP, and (meso) *R*,*S*- BPBP. In the current study, *rac*-BPBP was also used, which constitutes a mixture of *R*,*R*- and *S*,*S*-BPBP (see experimental section for details). Another N2Py2 ligand used in this study is BPBI (*N*,*N*'-bis(2-picolyl)-2,2'-bis-isoindoline), which was discussed in Chapter 2 for the synthesis of the Fe(BPBI) complex employed in aliphatic C–H oxidations.[45] Recently, this ligand and its derivatives have also been reported for the synthesis of the corresponding Mn-complexes, for which good reactivities have been observed in alkene epoxidation.[46]

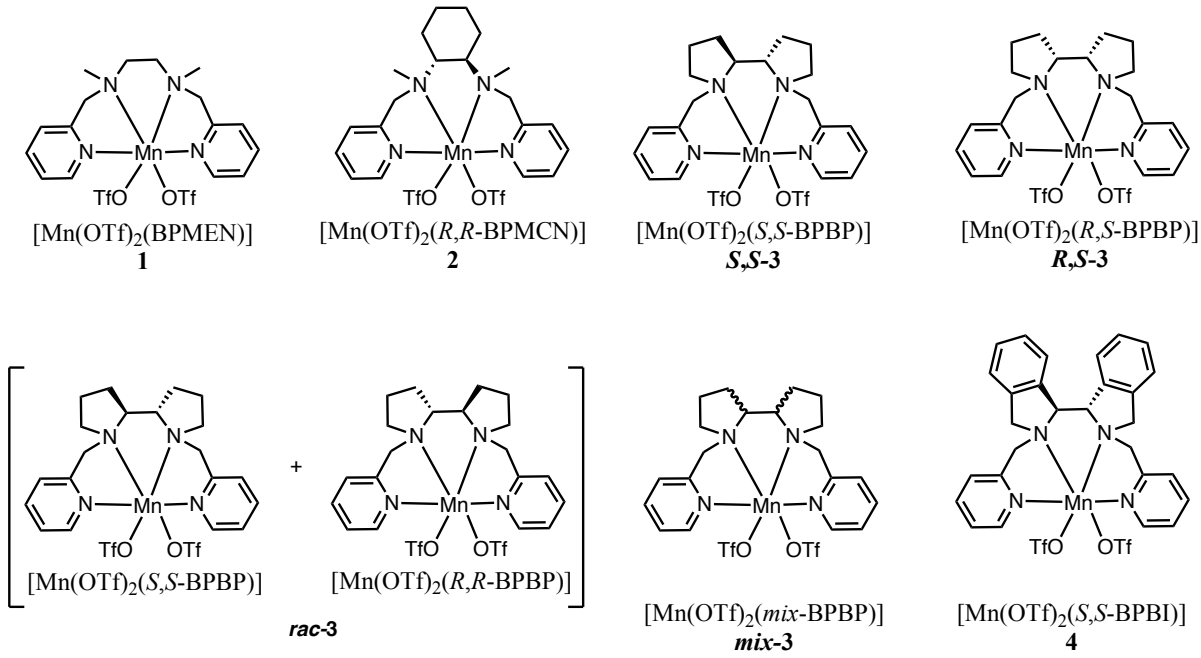

Figure 2. Non-heme Mn(II) complexes with N2Py2 ligands used in this study.

5.2.1 Epoxidation of UFAs and FAMEs

Oleic acid (C18:1) was chosen as the model substrate to optimize reactions conditions for the epoxidation of UFAs by the Mn-complexes in combination with H_2O_2 as the oxidant and AcOH as additive (Table 2). Initial experiments were carried out in the absence of Mn-complex to evaluate the crucial role of manganese in catalysis. Adding only oxidant, no substrate conversion was observed at all after 1 h, either using H_2O_2 (2 equiv.)/AcOH or *m*-chloroperoxybenzoic acid (*m*CPBA, 2 equiv.) (Table 2, entries 1 and 2). Similarly, when $Mn(OTf)_2$, the Mn salt used for the synthesis of the Mn complexes, together with H_2O_2 (2 equiv.) and AcOH (9 equiv., undiluted) was used, no conversion of oleic acid was detected (entry 3). Subsequently, using similar reaction conditions to the reported Fe(*mix*-BPBP)/H_2O_2/AcOH catalytic protocol for the epoxidation of UFAs,[34] catalytic experiments were performed with several Mn-complexes as catalyst (0.5 mol%). Complex **1** gave 40% conversion and yielded 32% of epoxidized oleic acid (entry 4). Similar to **1**, 32% of epoxide was found in the reaction with chiral complex **2**, albeit with a somewhat higher conversion (48%; entry 5). The epoxide yield was found to increase to 46% with ***S,S*-3**, even though substrate conversion did not further increase (48%, entry 6). Using complex **4**, a significant drop was found in both the conversion and yield (28% and 28%, respectively; entry7).

Since ***S,S*-3** outperforms the other Mn-catalysts in terms of epoxide yield, reaction condition optimization was carried out using BPBP-based Mn-complexes as catalyst. As reported

previously,[41,47] adding the oxidant slowly improves the substrate conversion in aliphatic C–H oxidations. A slow addition protocol, *i.e.*, dropwise addition of H_2O_2 over 30 min using a syringe pump, was therefore tested in oleic acid epoxidation. Considering that ***S,S*-3** shows very high epoxide selectivities and that N2Py2-based iron complexes were shown to decompose *via* ligand oxidation under catalytic conditions (see Chapter 4 of this thesis), the oxidant loading was lowered to 1.5 equiv. Using these conditions, substrate conversion and product yield both significantly increased to 99 % (entry 8). Further lowering of the catalyst loading to 0.1 mol% still gave quantitatively conversion of oleic acid into its epoxide product (entry 9). In comparison, using the same amount of ***S,S*-3-Fe** ([Fe(OTf)$_2$(*S*,*S*-BPBP)]), only 70% of conversion and yield were obtained (entry 10). This observation is consistent with previously reported results by Bryliakov and Talsi, that show that the Mn(N2Py2) complexes exhibit higher reactivities than the corresponding Fe(N2Py2) complexes in epoxidation reactions.[38,48] *Meso*-complex ***R,S*-3** turned out to be almost inactive in the epoxidation reaction, with only 10% substrate converted and product formed (entry 11), which is in line with the catalytic behavior of the corresponding iron complex [Fe(OTf)$_2$(*R*,*S*-BPBP)] in both alkene epoxidation and aliphatic C–H oxidation.[44] Furthermore, using 0.1 mol% of ***mix*-3** provided an identical reaction outcome to the reaction with ***S,S*-3** (quantitative yield, entry 12). This observation corroborates the notion that ***S,S*-3** and ***R,R*-3** are the catalytically active components in ***mix*-3** and that ***R,S*-3** does not contribute to the activity of ***mix*-3**. In accordance with this notion, the use of 0.1 mol% of ***rac*-3** in the reaction provided a quantitative yield of epoxide as well (entry 13). Since the *rac*-BPBP ligand mixture can be readily isolated from the *mix*-BPBP mixture *via* flash column chromatography and no ligand resolution is need, ***rac*-3** represents a much cheaper catalyst than an enantiopure Mn(BPBP) complex. In addition, the use of ***rac*-3** as opposed to ***mix*-3** could be advantageous for practical applications, since ***rac*-**3 is devoid of inactive metal-containing components which could facilitate regulatory registration and since a lower weight amount of catalyst could be used because ***rac*-3** contains more active catalyst per gram of catalyst material.

No drop in catalytic conversion and yield were found when further reducing the amount of catalyst by 50% (0.05 mol% ***rac*-3**, entry 14). Further lowering of the catalyst loading to 0.01 mol% ***rac*-3** gave 80% of substrate conversion and product yield within the standard reaction time of 1 h, providing a boundary of catalyst activity per time unit. Variation of the reaction parameters based on these combined observations finally led to a protocol that uses 0.02 mol% of ***rac*-3** catalyst loading, 45 min of H_2O_2 (1.5 equiv.) addition time, and an AcOH loading of 18 equiv., respectively; these reaction settings lead to full oleic acid conversion and quantitative formation of its epoxide (entry 16).

Table 2. Screening of reaction conditions for epoxidation of oleic acid using Mn-catalysts.[a)]

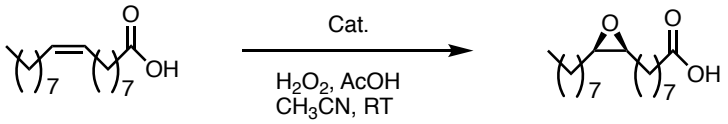

Entry	Cat. (mol%)	H_2O_2 equiv. (addition time)	AcOH (eq.)	Overall reaction time (h)	Conv. (%)[b)]	Yield (%)[b)]
1	-	2 (at once)	9	1	0	0
2[c)]	-	2 (at once)	9	1	0	0
3	$Mn(OTf)_2$ (0.5)	2 (at once)	9	1	0	0
4	**1** (0.5)	2 (at once)	9	1	40	32
5	**2** (0.5)	2 (at once)	9	1	48	32
6	***S,S*-3** (0.5)	2 (at once)	9	1	48	46
7	**4** (0.5)	2 (at once)	9	1	28	28
8	***S,S*-3** (0.5)	1.5 (30min)	9	1	>99	99
9	***S,S*-3** (0.1)	1.5 (30min)	9	1	>99	99
10[d)]	***S,S*-3-Fe** (0.1)	1.5 (30min)	9	1	70	70
11	***R,S*-3** (0.1)	1.5 (30min)	9	1	10	10
12	***mix*-3** (0.1)	1.5 (30min)	9	1	>99	99
13	***rac*-3** (0.1)	1.5 (30min)	9	1	>99	99
14	***rac*-3** (0.05)	1.5 (30min)	9	1	>99	99
15	***rac*-3** (0.01)	1.5 (30min)	9	1	80	80
16	***rac*-3** (0.02)	1.5 (45min)	18	1.25	>99	99

[a)] General reaction conditions: Oleic acid (0.5 mmol), catalyst, and AcOH were mixed and stirred in MeCN (2 mL) at room temperate (RT), subsequently H_2O_2 (1 M solution in MeCN) was added. [b)] Determined by NMR analysis. [c)] 2 equiv. of *m*CPBA was used as oxidant. [d)] [$Fe(OTf)_2$(*S,S*-BPBP)] was used as catalyst.

Using the catalytic protocol optimized for the epoxidation of oleic acid, the protocol was tested for the catalytic epoxidation of a series of other UFAs and FAMEs (Table 3). Elaidic acid, the *trans*-isomer of oleic acid, undergoes epoxidation quantitatively under the protocol conditions (entry 2). The same catalytic outcome was obtained when changing the carboxyl group in oleic acid to a carbomethoxy group as is methyl oleate (entry 3). Erucic acid (C22:1), on the other hand, seems more difficult to epoxidize using the current reaction conditions: only 36% of the substrate was converted in this case, yielding 36% yield of the epoxide (entry 4). Erucic acid is

a solid at room temperature (melting point = 34 °C) and not well soluble in MeCN. The resulting biphasic solid-liquid reaction medium is likely to limit catalytic activity, leading to poor catalytic results. Upon increase of reaction temperature to 36 °C, the resulting biphasic liquid-liquid reaction medium allowed for more effective catalysis to occur and, accordingly, erucic acid was fully converted to give 90% of the epoxide product under these conditions (entry 5). In turn, methyl erucate undergoes the epoxidation process smoothly using the standard protocol, forming the epoxide in quantitative yield (entry 6). For the small set of UFAs and FAMEs tested, excellent epoxide yields were obtained, meaning that the ***rac*-3**/H_2O_2/AcOH catalyst system is promising to be widely applied in the epoxidation of a wide range of UFAs and FAMEs.

Table 3. Epoxidation of UFAs (FAMEs) using the ***rac*-3**/H_2O_2/AcOH catalytic system.[a)]

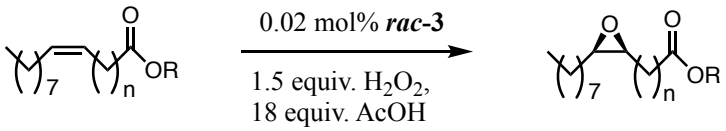

Entry	Substrate	n	Lipid number	R	Conv. (%)[b)]	Yield (%)[b)]
1	Oleic acid	7	C18:1 *cis*-9	H	>99	99
2	Elaidic acid	7	C18:1 *trans*-9	H	>99	99
3	Methyl oleate	7	C18:1 *cis*-9	Me	>99	99
4	Erucic acid	11	C22:1 *cis*-13	H	36	36
5[c)]	Erucic acid	11	C22:1 *cis*-13	H	>99	90
6	Methyl erucate	11	C22:1 *cis*-13	Me	>99	99

[a)] Unless stated otherwise, reaction conditions are substrate (0.5 mmol, 1 equiv.), ***rac*-3** (0.02 mol %, added as 10 mM solution in MeCN), H_2O_2 (1.5 equiv, 1 M solution in MeCN) and AcOH (18 equiv) in CH_3CN at room temperature, the oxidant was added over 45 min, and the reaction mixture stirred for additional 30 min. [b)] Determined by NMR analysis. [c)] Reaction temperature was 36 °C.

5.2.2 Epoxidation of VOs

Next, the Mn-catalyzed epoxidation of VOs was explored using the ***rac*-3**/H_2O_2/AcOH catalytic protocol (Table 4). In order to obtain the optimal reaction conditions, sunflower oil was chosen as the benchmark oil. The Wijs method[49] was used to determine the iodine value (I.V.) of sunflower oil, providing information on its C=C bond content (I.V. = 130). All reagent loadings listed in Table 4 are with respect to (w.r.t.) the amount of C=C bond in the oils. Iodine values were determined again after the epoxidation reaction in order to calculate the conversion of C=C bonds (see experimental section). The amount of epoxy-groups formed in the reaction is

described as the percentage of oxirane oxygen in the resulting oils, which was determined according to AOCS Official Method Cd 9-57.[50] The formal yields were calculated from the measured oxirane oxygen content and the theoretical maximum oxirane oxygen content (see experimental section).

Using similar reaction conditions to the optimized ones for epoxidation of UFAs and FAMEs, except for half the amount of AcOH used, the epoxidation of sunflower oil (100 mg) was performed with 0.02 mol% of ***rac*-3** (added as a 10 mM solution in MeCN), 1.5 equiv. of H_2O_2 (added as a 1 M solution in MeCN over 45 min), and 9 equiv. of AcOH in MeCN (2 mL) under vigorous stirring (1000 rpm) at ambient temperature. Full conversion of double bonds in the oil was obtained, with 95% of epoxy-group yield (Table 4, entry 1). When the reaction scale was increased to 1 g of sunflower oil (entry 2), both the conversion and yield dropped to 83% and 75%, respectively, albeit with a similar epoxide selectivity (95% for entry 1, 90% for entry 2). For 1 g scale reactions like this, H_2O_2 was added as a commercial 35% aqueous solution. With the aim of making the epoxidation protocol more environmentally friendly, the reaction conditions were further optimized not to use MeCN as the organic solvent. Of note is that in all the reactions in Table 4, the catalyst was added as a 10 mM stock solution in MeCN (ca. 100 – 200 μL), for the purpose of easy operation. As shown in entry 3, the epoxidation process performs very poorly in the absence of MeCN solvent: only 45% of the double bonds were converted, forming 25% of epoxide with an epoxide selectivity of 56%. Doubling the loading of Mn-catalyst to 0.04 mol% under these conditions increases both conversion (80%) and yield (45%) at the same epoxidation selectivity of 56% (entry 4).

In separate catalyst tests the Mn-catalyst was found to be insoluble in sunflower oil but slightly soluble in AcOH, whereas the oil is insoluble in AcOH. This results in a biphasic reaction medium (oil:AcOH = 1:2.4, v/v; 9 equiv. AcOH), with the Mn-catalyst residing in the AcOH layer. Addition of more AcOH (18 equiv., oil:AcOH = 1:4.8, v/v) was considered to increase the total liquid-liquid interface under vigorous stirring. Entry 5 clearly shows that the reaction benefited significantly from the additional amount of AcOH. Compared to entry 3, considerably more double bonds were converted (82% over 45%) and a moderate yield of epoxide was obtained (53%). Yet, the epoxide selectivity under these conditions is still relatively low (65%). In order to suppress the formation of side-products, H_2O_2 was delivered to the reaction mixture more slowly over a period of 90 min. This resulted in a significant improvement in epoxide selectivity to 87%, at almost the same conversion (84%, entry 6). A further increase in H_2O_2 delivery time (120 min) and extension of the overall reaction time to 3 h lead to a drop in epoxide selectivity (to 73%), even though a slightly increased conversion was observed (89%,

entry 7). ^{1}H NMR analysis of the resulting mixture obtained from extraction with diethyl ether and subsequent condensation showed the presence of a remarkable amount of diol compounds (~ 20%). Apparently, the longer overall reaction time (3 h) and the large amount of AcOH allows for a more pronounced ring-opening of the initially formed epoxides.

Table 4. Screening of reaction conditions for epoxidation of sunflower oil catalyzed by ***rac*-3**.[a)]

Sunflower oil —(***rac*-3**, H_2O_2 (1.5 equiv.), AcOH, RT)→ Epoxidized sunflower oil

Entry	MeCN	Catalyst loading (mol%)	H_2O_2 addition time (min)	AcOH (eq.)	Overall reaction time (h)	Conversion (%)	Epoxide yield (%)	Epoxide selectivity (%)
1[b)]	2 mL	0.02	45	9	1.75	>99	95	95
2	2 mL	0.02	45	9	1.75	83	75	90
3	-	0.02	45	9	1.75	45	25	56
4	-	0.04	45	9	1.75	80	45	56
5	-	0.02	45	18	1.75	82	53	65
6	-	0.02	90	18	2	84	73	87
7	-	0.02	120	18	3	89	65	73
8	-	0.03	90	18	2	>99	90	90
9	-	0.03	90	9	2	80	70	88
10[c)]	-	0.03	90	18	2	83	75	90

[a)] General reaction conditions: sunflower oil (1 g), ***rac*-3** (0.02-0.04 mol %, w.r.t. double bonds, added as 10 mM solution in MeCN, ca. 100 - 200 μL) and AcOH (2.6 mL for 9 equiv., 5.3 mL for 18 equiv.) were mixed in the absence or presence of MeCN (2 mL), and stirred vigorously (1000 rpm) at room temperature, H_2O_2 (1.5 equiv., w.r.t. double bonds, 35% aqueous solution) was added over 45-120 min, and the reaction mixture stirred for additional 30-60 min. [b)] 100 mg of sunflower oil was used, H_2O_2 was added as a 1 M solution in MeCN (0.8 mL) [c)] Stirring rate = 500 rpm.

To maximize the epoxide yield, the catalyst loading was slightly increased to 0.03 mol% and the delivery time of H_2O_2 brought back to 90 min. In this case, the double bonds were fully converted and an excellent epoxide yield (90%) was found (entry 8). Considering the potential

epoxide ring-opening side reaction under acidic condition, using these altered conditions but at a lower AcOH loading (9 equiv.) lead to a decrease of both the conversion and yield (80% and 70%, respectively, entry 9). Finally, the impact of vigorous stirring was examined by bringing down the stirring rate to 500 rpm, which resulted in a decrease of the conversion from 99% to 83% (entry 10). The necessity of using a larger amount of AcOH and a high stirring speed indicates that the epoxidation reaction is enhanced with more pronounced mixing, which suggests that the catalytic reaction takes place at the biphasic liquid-liquid interface.

Overall, the reaction conditions described in entry 8 provide an optimized reaction parameter set for the epoxidation of sunflower oil in the absence of an organic solvent (other than acetic acid) and lead to full conversion of all double bonds in the oil and to 90% of epoxide formation with the corresponding diols as likely byproducts. These conditions even provide a better reaction outcome than the original conditions using acetonitrile as a solvent (compare entries 2 and 8 for 1 g scale reactions).

To further investigate the substrate tolerance and validation of this epoxidation strategy, the epoxidation of various VOs was examined using this optimized ***rac*-3**/H_2O_2/AcOH catalytic system (Table 4, entry 8). All reactions were done without using MeCN as solvent. Of note is that in the cases of 1-gram scale reactions, the catalyst was added as a 10 mM stock solution in MeCN for the purpose of easy operation. In addition, a fixed amount of AcOH (5.3 mL) was used for all 1-gram scale reactions, regardless of the different iodine values of the oils. As shown in entries 1-7 in Table 5, most of the VOs can be epoxidized using these standard reaction conditions with full conversions and excellent yields (up to 99%). For olive oil a somewhat lower reactivity was observed (90% conversion and 85% yield, entry 6). Notably, amongst these VOs rapeseed oil, linseed oil, and soybean oil are promising feedstocks to produce epoxidized VOs in industry, because of their wide availabilities and low prices.[4] The present epoxidation protocol provides an excellent tool to produce EVOs from these three VOs, with nearly quantitative epoxide yields in all cases (98%, 99% and 99%, respectively, entry 4, 5, 7).

Full epoxidation of the double bonds in rice oil could also be achieved using a small increase in catalyst loading to 0.04 mol% (entry 8). At 0.03 mol% catalyst, only 81% conversion was found for rice oil. However, under these conditions some 20% of double bonds remain in sesame oil, with 75% epoxides being formed (entry 9). Overall, entries 1-9 show that the performance of this catalyst system is independent of the iodine values of the starting VOs. Not only vegetable oils with a low iodine number (like peanut oil, I.V. = 91), but also the ones with

a high iodine number (like linseed oil, I.V. = 165) give full conversion and very high epoxide yields (90% for peanut oil, 99% for linseed oil).

Table 5. Epoxidation of VOs using the ***rac*-3**/H_2O_2/AcOH catalyst system.[a)]

Vegetable oil —(0.03 mol% ***rac*-3**, H_2O_2 (1.5 equiv.), AcOH, RT)→ Epoxidized vagetable oil

Entry	Oil	Iodine value	Catalyst loading (mol%)	Conversion (%)	Epoxide yield (%)	Epoxide selectivity (%)
1	Sunflower oil	130	0.03	>99	90	90
2	Walnut oil	144	0.03	>99	96	96
3	Peanut oil	91	0.03	>99	90	90
4	Rapeseed oil	121	0.03	>99	98	98
5	Linseed oil	165	0.03	>99	99	99
6	Olive oil	88	0.03	90	85	94
7	Soybean oil	128	0.03	>99	99	99
8	Rice oil	105	0.04	>99	92	92
9	Sesame oil	115	0.04	80	75	94
10	Cooked sunflower oil	118	0.03	>99	98	98
11 [b, c)]	Sunflower oil	130	0.03	>99	90	90

[a)] Unless stated otherwise, reaction conditions are: oil (1 g), ***rac*-3** (0.03 mol % w.r.t. double bonds, added as 10 mM solution in MeCN, ca. 100 - 180 µL), and AcOH (5.3 mL) at room temperature; H_2O_2 (1.5 equiv. w.r.t. double bonds) was added over 90 min, and the reaction mixture was stirred for additional 30 min, stirring rate = 1000 rpm. [b)] 5 g of oil was used, 26.5 mL of AcOH was added. [c)] Solid catalyst was added.

From a cost point of view, waste cooking oils are potentially promising feedstocks for the production of EVOs since they are generally 30-60% cheaper than regular vegetables oils.[6] Applying the current epoxidation protocol to cooked sunflower oil gave full conversion of double bonds and 98% epoxide yield (entry 10). Next, a scale-up experiment with 5 grams of sunflower oil was carried out (entry 11). No drop in conversion and yield were observed in

comparison with the 1-gram scale experiment (entry 1 vs. entry 11). Notably, the Mn-catalyst was added as a solid in this case, meaning that the reaction can be performed with the same efficiency in the complete absence of MeCN. Furthermore, separation of the resulting epoxidized sunflower oil was conducted straightforwardly by simple extraction of the reaction mixture with Et_2O and follow-up removal of the organic solvents. The obtained epoxidized sunflower oil showed high purity according to ^1H NMR analysis.

It can be concluded from Table 5 that the Mn-based catalytic protocol is capable of epoxidizing a variety of VOs, mostly leading to epoxide yields of 90% or higher (only sesame oils showed a 75% yield). In addition, the system provides very high selectivities for the epoxide products in the range of 90-99% for all oils tested in this study.

5.2.3 One-pot oxidative cleavage of UFAs and FAMEs

As mentioned earlier, epoxidized UFAs, their ester derivatives, and EVOs can be further transferred into other industrially valuable compounds.[4] One example is through the oxidative cleavage of the C–C bond in the oxirane ring to yield a monofunctional aldehyde and an α,ω-aldehyde fatty acid (or methyl ester) as the primary products (Scheme 2).[5] The primary aldehyde product, *e.g.* nonanal in the case of oleic acid, can be used as a direct, yet renewable replacement for petrochemically-derived nonanal in plasticizer production.[5] On the other hand, the aldehyde moiety in an α,ω-aldehyde fatty acid (ester) can readily be converted to either an acid, hydroxy, or amino group. These bifunctional fatty acids (or esters) can be used for the production of nylons and polyesters, both large volume and high value products.[5] Spannring *et al.* have previously developed the Fe-catalyzed one-pot oxidative cleavage of UFAs and FAMEs into aldehydes with H_2O_2 and sodium periodate.[34] This protocol comprizes consecutive reaction steps involving double bond epoxidation catalyzed by the [Fe(OTf)$_2$(*mix*-BPBP)]/H_2O_2/AcOH catalyst system (in which 0.5 mol% of Fe-catalyst was employed), hydrolysis of the epoxide in the presence of H_2SO_4 to form a vicinal diol, and cleavage of the diol to give the two aldehydes with $NaIO_4$ as the oxidant (Scheme 2).[34]

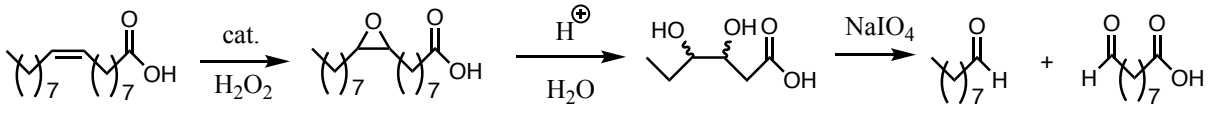

Scheme 2. Oxidative cleavage of oleic acid into aldehyde products.[34]

Similarly, the Mn-based epoxidation protocol developed in this chapter was used in the one-pot cleavage of a number of UFAs and FAMEs. The cleavage reaction followed the same

procedure as before: 1) epoxidation of the double bond using the optimized reaction conditions with the ***rac*-3**/H_2O_2/AcOH (0.02 mol%, 1.5 equiv. and 18 equiv., respectively) catalyst system as used in Table 3; 2) hydrolysis of the oxirane ring by addition of 0.5 equiv. of H_2SO_4 (1 equiv. of H^+); and 3) cleavage of the diol with 1 equiv. of $NaHCO_3$ and 1 equiv. of $NaIO_4$. GC analyses were conducted after the one-pot procedure to determine the amount of nonanal and detect the formation of nonanoic acid (over-oxidized product from nonanal). Of note is that only the formation of nonanal was quantified by GC, and that the formation of the α,ω-aldehyde fatty acid (ester) was considered to have taken place in equal amounts.

Table 6. One-pot oxidative cleavage of UFAs and FAMEs initiated by ***rac*-3**.[a)]

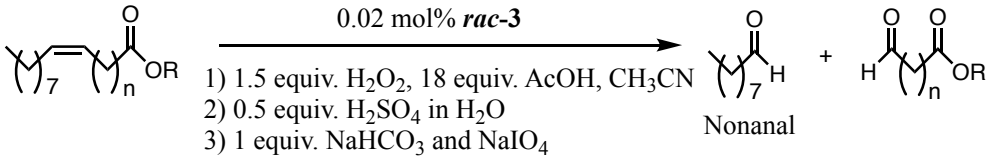

Entry	Substrate	n	R	Conv. (%)[b)]	Nonanal yield (%)[c)]
1	Oleic acid	7	H	>99	98
2[d)]	Elaidic acid	7	H	>99	70
3[d)]	Methyl oleate	7	Me	>99	94
4[e)]	Erucic acid	11	H	>99	55
5[d)]	Methyl erucate	11	Me	>99	91

[a)] General reaction conditions at ambient temperature: step 1: substrate (0.5 mmol), ***rac*-3** (0.02 mol%), AcOH (9 mmol), and H_2O_2 (0.75 mmol, added in 45 min) in CH_3CN (2 mL), 1.25 h reaction time; step 2: 1 mL of CH_3CN and 1 mL of H_2SO_4 (0.25 M) in water were added, 3 h reaction time; step 3: 0.5 mmol of $NaHCO_3$ and 0.5 mmol of $NaIO_4$ were added, 1.5 h reaction time. [b)] Determined by NMR analysis. [c)] Determined by GC analysis. [d)] The reaction time for step 3 was 3 h. [e)] Same as d), in addition the reaction in step 1 was heated to 36 ^{0}C.

Table 6 shows that all reactions gave full substrate conversion with 0.02 mol% of ***rac*-3** in a total reaction time of 5.75 - 7.25 h. In the cases of oleic acid, methyl oleate, and methyl erucate, very high nonanal yields were achieved (98%, 94% and 91%, respectively, entries 1, 3, 5). A moderate nonanal yield of 70% was observed in the oxidative cleavage of elaidic acid (entry 2). ^{1}H-NMR analysis of the resulting reaction mixture showed that in this case there was still ca. 20% of intermediate epoxide remained, which is likely due to the fact that a *trans*-epoxide, formed from epoxidation of the *trans* double bond in elaidic acid, is harder to hydrolyze than a *cis*-epoxide.[51] Oxidative cleavage of erucic acid yielded only 55% of nonanal (entry 4), whereas neither over-oxidized nonanoic acid nor unreacted intermediates (epoxide and diol)

were detected by GC or NMR analyses. In all these reactions, no formation of nonanoic acid was observed, indicating that this one-pot cleavage methodology is highly selective for aldehyde products. In general, this Mn-initiated protocol for one-pot oxidative cleavage of UFAs and FAMEs outperforms the reported Fe-based catalytic system in terms of catalytic efficiency. In the later protocol, 0.5 mol% of [Fe(OTf)$_2$(*mix*-BPBP)] was used to yield 69-96 % of nonanal in a general reaction time of 20-72 h.[34]

5.3 Conclusions

A highly efficient catalytic protocol has been developed for the epoxidation of UFAs, FAMEs, and VOs based on the use of the abundant first-row transition metal manganese in combination with aqueous H_2O_2 as the oxidant. Using [Mn(OTf)$_2$(*rac*-BPBP)] (***rac*-3**) as catalyst, the double bonds in most of the vegetable oils tested can be fully converted with a very low catalyst loading: 0.03 mol% w.r.t double bonds or ca. 0.1 wt% w.r.t oil. In all the VOs tested, this catalytic system is highly selective for epoxides (>90%), and most of the EVOs were obtained in more than 90% yield within 2 h of reaction time at ambient temperature. Therefore, this protocol has a wide applicability for a variety of VOs, with a range of iodine values from 88 to 165. In the cases of walnut oil, linseed oil, rapeseed oil, cooked sunflower oil, and soybean oil, (nearly) quantitative epoxide yields can be achieved under standard reaction conditions. By increasing the addition time of the H_2O_2 oxidant to 90 min and the volume ratio of oil:AcOH to ca. 1:4.8, it is possible to perform the reaction without the use of an organic solvent, *i.e.*, a minor amount of MeCN was only used as a delivery medium of the catalyst solution rather than a solvent in 1-gram scale reactions. Notably, the high catalytic efficiency was retained in a scale-up experiment with 5 g of sunflower oil in which the use of MeCN could be completely omitted. The volume of AcOH and the stirring rate are essential as the reaction medium is biphasic due to the absence of MeCN. In addition, the resulting EVOs can be obtained straightforwardly from the reaction crude *via* simple extraction with Et_2O. Further transformation of epoxidized UFAs and FAMEs have also been carried out *via* an oxidative cleavage procedure, providing nonanal and an α,ω-aldehyde fatty acid (ester) with moderate to excellent yields (55-98%). This process is performed in a one-pot manner, initiated by the ***rac*-3**/H_2O_2/AcOH catalytic system in the first epoxidation step.

Overall, the present homogeneous Mn-catalyzed epoxidation protocol provides a highly efficient and practical tool for the production of EVOs under very mild reaction conditions in short reaction times, and can be carried out using only minute amounts of MeCN as solubilizing agent or even in the complete absence of an organic solvent, allowing for facile product

isolation. This protocol is expected to represent a promising alternative to conventional epoxidation methods and outperforms previously reported catalytic protocols for EVO production in terms of efficiency and reaction conditions, which largely conforms to the principles of green chemistry in modern chemistry.

5.4 Experimental Section

5.4.1 General

All the complexation reactions were performed under a nitrogen atmosphere using standard Schlenk techniques and all other reactions including catalytic reactions were conducted under ambient conditions. The solvents diethyl ether and MeCN were purified with an MBraun MB SPS-800 solvent purification system. Demineralized water and technical grade CH_2Cl_2 were used for reactions. Tetrahydrofuran for complexation reactions was dried with sodium, and distilled under nitrogen prior to use. Vegetable oils were obtained from local supermarkets. All other reagents, substrates, and reaction products were obtained commercially and used without further purification. Column chromatography was performed using neutral alumina. ^{1}H and ^{13}C NMR spectra were recorded with a 400 MHz Varian spectrometer at 25 °C, chemical shifts (δ) are given in ppm referenced to the residual solvent peak. Gas chromatography (GC) was performed on a Perkin–Elmer Clarus 500 Gas Chromatograph equipped with an Agilent HP 5 column with a 5%phenyl-95%methylpolysilaxane ratio and a flame-ionization detector. ESI-MS measurements were performed with a Waters LCT Premier XE KE317. The ligands *R*,*S*-BPBP,[44] *mix*-BPBP,[44] and *S*,*S*-BPBI[45] and Mn complexes **1**,[42] **2**,[42] and ***S*,*S*-3**[43] were synthetized following reported procedures. Elemental microanalyses were carried out by the Mikroanalytisches Laboratorium Kolbe, Germany.

5.4.2 Synthesis of ligands and Mn complexes

***Rac*-BPBP** To a vigorously stirred 10 mL mixture of water and CH_2Cl_2 (1/1, v/v) containing 320 mg of crude dl/meso-2,2'-bipyrrolidine[52] (2.2 mmol) at room temperature (RT), sodium hydroxide (572 mg, 14 mmol) was added. Subsequently, 2-picolyl chloride hydrochloride salt (750 mg, 4.5 mmol) was added at once, turning the mixture red. After stirring overnight, another 10 mL of water and CH_2Cl_2 (1/1, v/v) was added, and the yellowish organic phase was separated and the aqueous phase was extracted with CH_2Cl_2 (3 × 10 mL). Organic extracts were combined, dried over $MgSO_4$ and the solvent was removed under vacuum. The crude product was purified by neutral alumina column chromatography (petroleum ether/ EtOAc, 3/1 to 1/1 (v/v)) to provide 352 mg of *rac*-BPBP (50% yield). ^{1}H NMR (400 MHz, $CDCl_3$) δ 8.47–8.45 (m, 2 H), 7.56 (td, J = 7.7, 1.8 Hz, 2H), 7.37 (d, J = 7.8 Hz, 2H), 7.10–7.05 (m, 2 H), 4.16 (d, J = 14.3 Hz, 2H), 3.48 (d, J = 14.3 Hz, 2H), 2.99–2.94 (m, 2 H), 2.79–2.74 (m, 2 H), 2.20 (q, J = 8.6 Hz, 2H), 1.83–1.62 (m, 8 H). ^{13}C NMR (100 MHz, $CDCl_3$) δ 160.62, 148.84, 136.45, 122.51, 121.67, 65.46, 61.25, 55.34, 25.92, 23.67. HRMS (ESI-MS) calcd. *m*/*z* for $C_{20}H_{27}N_4$ ($[M+H]^+$): 323.2230, found 323.2235.

[Mn(OTf)$_2$(*R*,*S*-BPBP)] (***R*,*S*-3**) To a vigorously stirred solution of Mn(OTf)$_2$ (107 mg, 0.3 mmol) in dry MeCN (1 mL) under a nitrogen atmosphere, a solution of *R*,*S*-BPBP (104 mg, 0.32 mmol) in dry MeCN (1 mL) was added. The resulting mixture was stirred at RT overnight, providing a light brown/white precipitate. The precipitate was allowed to settle and the supernatant was removed. The remaining precipitate was washed with diethyl ether twice then dissolved in dry MeCN. The resulting solution contained some black impurities, which was removed *via* filtration through a filter paper. Subsequently, diethyl ether was layered carefully to the remaining solution, which was left to crystalize. In a few days, yellow crystals were obtained in 65% yield. HRMS (ESI-MS) calcd. *m*/*z* for $C_{21}H_{26}F_3MnN_4O_3S$ ([M-OTf]$^+$): 526.1058, found 526.1108. Elemental analysis calcd. (%) for $C_{22}H_{26}F_6MnN_4O_6S_2 \cdot 2H_2O$: C 37.14, H 4.25, N 7.87, found C 37.45, H 4.43, N 8.06.

[Mn(OTf)$_2$(*Rac*-BPBP)] (***rac*-3**) This complex was prepared in an analogous manner to ***R*,*S*-3** starting from *rac*-BPBP. Yellow-white solid (55% yield). HRMS (ESI-MS) calcd. *m*/*z* for $C_{21}H_{26}F_3MnN_4O_3S$ ([M-OTf]$^+$): 526.1058, found 526.1129. Elemental analysis calcd. (%) for $C_{22}H_{26}F_6MnN_4O_6S_2$: C 39.12, H 3.88, N 8.29, found C 39.71, H 3.75, N 8.36.

[Mn(OTf)$_2$(m*ix*-BPBP)] (***mix*-3**) This complex was prepared in an analogous manner to ***R*,*S*-3** starting from *mix*-BPBP. Yellow-white solid (51% yield). HRMS (ESI-MS) calcd. *m*/*z* for $C_{21}H_{26}F_3MnN_4O_3S$ ([M-OTf]$^+$): 526.1058, found 526.1187. Elemental analysis calcd. (%) for $C_{22}H_{26}F_6MnN_4O_6S_2 \cdot H_2O$: C 38.10, H 4.07, N 8.08, found C 38.31, H 4.15, N 8.26.

[Mn(OTf)$_2$(*S*,*S*-BPBI)] (**4**) This complex was prepared in an analogous manner to ***R*,*S*-3** starting from *S*,*S*-BPBI. Light yellow solid (42% yield). HRMS (ESI-MS) calcd. *m*/*z* for $C_{29}H_{26}F_3MnN_4O_3S$ ([M-OTf]$^+$): 622,1058 found: 622,1052. Elemental analysis calcd. (%) for $C_{30}H_{26}F_6MnN_4O_6S_2 \cdot 2H_2O$: C 44.62, H 3.74, N 6.94, found C 46.12, H 3.91, N 6.87.

5.4.3 Catalysis

General procedure for optimization of the epoxidation of oleic acid (Table 2).
A 20 mL vial was charged with: oleic acid (0.5 mmol, 1 equiv.), catalyst, AcOH (9 or 18 equiv.), and MeCN (2 mL). Subsequently, a 1.0 M H_2O_2 solution in CH_3CN (2 or 1.5 equiv., diluted from a 35% H_2O_2 aqueous solution) was added over the indicated time at RT. Next, the resulting mixture was allowed to stir at RT for the indicated time. At this point, a 1.0 M nitrobenzene solution in CH_3CN (0.5 mL, 0.5 mmol, 1 equiv.) was added as internal standard. The solution was diluted with Et_2O to precipitate the Mn-complex and passed through a cotton wool filter to remove residual complex. Solvent was removed *in vacuo* and a sample was submitted to ^{1}H NMR analysis. Conversion of oleic acid was determined by comparison of the olefinic hydrogen signals at 5.3 ppm. Epoxide yield was determined by comparison of the oxirane hydrogen signals at 2.9 ppm.

Epoxidation of UFAs (FAMEs) by *rac*-3 (Table 3).
A 20 mL vial was charged with: substrate (0.5 mmol, 1 equiv.), ***rac*-3** (10 μL of a 10 mM solution in MeCN, 0.02 mol%), AcOH (0.5 mL, 9 mmol, 18 equiv.), and MeCN (2 mL). Subsequently, a 1.0 M

H_2O_2 solution in CH_3CN (0.75mL, 1.5 equiv., diluted from a 35% H_2O_2 aqueous solution) was added over 45 min, and the reaction mixture stirred for additional 30 min. At this point, a 1.0 M nitrobenzene solution in CH_3CN (0.5 mL, 0.5 mmol, 1 equiv.) was added as internal standard. The solution was diluted with Et_2O to precipitate the Mn-complex, passed through a cotton wool filter to remove residual complex. Solvent was removed *in vacuo* and a sample was submitted to ^{1}H NMR analysis. Conversion of oleic acid was determined by comparison of the olefinic hydrogens at 5.3-5.4 ppm. Epoxide yield was determined by comparison of the oxirane hydrogens at 2.7-2.9 ppm.

General procedure for optimization of the epoxidation of sunflower oil by *rac*-3 (Table 4).
Sunflower oil (1 g), ***rac*-3** (0.02-0.04 mol %, w.r.t. double bonds in the starting oil, added as a 10 mM solution in MeCN), and AcOH (2.6 mL for 9 equiv., 5.3 mL for 18 equiv.) were mixed in the absence or presence of MeCN (2 mL). The resulting mixture was stirred vigorously (1000 rpm) at RT. Subsequently, 1.5 equiv. of H_2O_2 w.r.t. double bonds in the starting oil (35% H_2O_2 aqueous solution) was added over 45-120 min, then the reaction mixture was allowed to stir for additional 30-60 min. Upon completion of the reaction, H_2O (20 mL) was added to the reaction mixture, followed by extraction with Et_2O (3 ×20 mL). Organic extracts were combined and dried over $MgSO_4$ and the solvent was removed under vacuum. The residue was separated into two portions. One portion was used to determine conversion by measuring the iodine value (IV) according to the Wijs method.[49] The other portion was used to determine the yield of oxirane oxygens (OO) formed *via* the AOCS Official Method Cd 9-57.[50]

The conversion of substrate was determined as follows:

$$\text{Conversion} = \frac{IV_o - IV_p}{IV_o} \times 100\%$$

Where IV_o is the initial iodine value of starting vegetable oil, IV_p is the iodine value of epoxidized vegetable oil after epoxidation.

The yield of epoxidized products was determined as follows:

$$\text{Yield} = \frac{OO_p}{OO_{the}} \times 100\%$$

Where OO_p is the measured percentage of oxirane oxygen in epoxidized products, OO_{the} is the theoretical maximum percentage of oxirane oxygen, which is calculated as follows:

$$OO_{the} = \frac{(IV_o/253.8) \times 16}{100 + (IV_o/253.8) \times 16} \times 100\%$$

Epoxidation of vegetable oils by *rac*-3 (Table 5).
A 20 mL vial was charged with: oil (1 or 5 g), ***rac*-3** (0.03 mol%, w.r.t. double bonds in the starting oil, added as a 10 mM solution in MeCN for 1 g scale reactions, and as a solid for 5 g scale reactions), and AcOH (5.3 mL for 1 g scale, 26.5 mL for 5 g scale). The resulting mixture was stirred vigorously (1000 rpm) at RT. Subsequently, 1.5 equiv. of H_2O_2 w.r.t. double bonds in the starting oil (35% H_2O_2 aqueous

solution) was added over 90 min, then the reaction mixture was allowed to stir for additional 30 min. Upon completion of the reaction, H_2O (20 mL) was added to the reaction mixture, followed by extraction with Et_2O (3 × 20 mL). Organic extracts were combined and dried over $MgSO_4$ and the solvent was removed under vacuum. The residue was separated into two portions. One portion was used to determine conversion and the other portion was used to determine the yield of oxirane oxygens (OO) formed (see above). In the case of 5-gram scale reaction with sunflower oil, the obtained product after work-up was also characterized by ^{1}H NMR.

One-pot oxidative cleavage of UFAs and FAMEs (Table 6).[34]

Substrate (0,5 mmol, 1 equiv.), ***rac*-3** (10 μL of a 10 mM solution in MeCN, 0.02 mol%), and AcOH (0.5 mL, 9 mmol, 18 equiv.) were dissolved in CH_3CN (2 mL) at RT (36 ºC for erucic acid). Subsequently, a 1.0 M H_2O_2 solution in CH_3CN (0.75 mL, 1.5 equiv., diluted from a 35% H_2O_2 aqueous solution) was added over 45 min. The resulting mixture was allowed to stir for another 30 min. At this point, 1 mL MeCN and 1 mL 0.25 M H_2SO_4 aqueous solution (0.5 equiv.) were added (thus MeCN/H_2O = 3/1, v/v). After stirring for 3 h, 42 mg of $NaHCO_3$ (0.5mmol, 1 equiv.) and 107 mg of $NaIO_4$ (0.5mmol, 1 equiv.) were added, after which the reaction was stirred for 1.5 or 3 h. Upon completion of the reaction, 0.5 mmol biphenyl was added as internal standard. The solution was diluted with Et_2O to precipitate the catalyst, passed through a cotton wool filter to remove residual catalyst. Subsequently, samples were submitted to ^{1}H NMR and GC analysis. ^{1}H NMR analysis provided substrate conversions and GC analysis provided nonanal yields by comparison with authentic samples.

5.5 References

[1] T. E. Bull;, *Science* **1999**, *285*, 1209b–1209.

[2] S. G. Tan, W. S. Chow, *Polym. Plast. Technol. Eng.* **2010**, *49*, 1581–1590.

[3] A. K. R. Somidi, R. V. Sharma, A. K. Dalai, *Ind. Eng. Chem. Res.* **2014**, *53*, 18668–18677.

[4] S. M. Danov, O. A. Kazantsev, A. L. Esipovich, A. S. Belousov, A. E. Rogozhin, E. A. Kanakov, *Catal. Sci. Technol.* **2017**, *7*, 3659–3675.

[5] P. Spannring, P. C. A. Bruijnincx, B. M. Weckhuysen, R. J. M. Klein Gebbink, *Catal. Sci. Technol.* **2014**, *4*, 2182–2209.

[6] J. McNutt, Q. S. He, *J. Ind. Eng. Chem.* **2016**, *36*, 1–12.

[7] Y. B. Huang, M. Y. Yao, P. P. Xin, M. C. Zhou, T. Yang, H. Pan, *RSC Adv.* **2015**, *5*, 74783–74789.

[8] A. Adhvaryu, S. Z. Erhan, *Ind. Crops Prod.* **2002**, *15*, 247–254.

[9] A. Campanella, E. Rustoy, A. Baldessari, M. A. Baltanás, *Bioresour. Technol.* **2010**, *101*, 245–254.

[10] L. Fantoni, C. Simoneau, *Food Addit. Contam.* **2003**, *20*, 1087–1096.

[11] H. Schuster, L. A. Rios, P. P. Weckes, W. F. Hoelderich, *Appl. Catal. A Gen.* **2008**, *348*, 266–270.

[12] J. Salimon, N. Salih, E. Yousif, *Eur. J. Lipid Sci. Technol.* **2010**, *112*, 519–530.

[13] J. O. Metzger, *Eur. J. Lipid Sci. Technol.* **2009**, *111*, 865–876.

[14] H.-S. Hwang, A. Adhvaryu, S. Z. Erhan, *J. Am. Oil Chem. Soc.* **2003**, *80*, 811–815.
[15] H.-S. Hwang, S. Z. Erhan, *J. Am. Oil Chem. Soc.* **2001**, *78*, 1179–1184.
[16] X. Wu, X. Zhang, S. Yang, H. Chen, D. Wang, *J. Am. Oil Chem. Soc.* **2000**, *77*, 561–563.
[17] M. D. Soucek, A. H. Johnson, J. M. Wegner, *Prog. Org. Coatings* **2004**, *51*, 300–311.
[18] W. D. Wan Rosli, R. N. Kumar, S. Mek Zah, M. M. Hilmi, *Eur. Polym. J.* **2003**, *39*, 593–600.
[19] N. O. Shaker, E. M. Kandeel, E. E. Badr, M. M. El-Sawy, *J. Dispers. Sci. Technol.* **2008**, *29*, 421–425.
[20] S. F. Thames, H. Yu, *Surf. Coatings Technol.* **1999**, *115*, 208–214.
[21] A. E. Gerbase, J. R. Gregório, M. Martinelli, M. C. Brasil, A. N. F. Mendes, *J. Am. Oil Chem. Soc.* **2002**, *79*, 179–181.
[22] M. Farias, M. Martinelli, D. P. Bottega, *Appl. Catal. A Gen.* **2010**, *384*, 213–219.
[23] J. O. Metzger, U. Bornscheuer, *Appl. Microbiol. Biotechnol.* **2006**, *71*, 13–22.
[24] T. Vlček, Z. S. Petrović, *J. Am. Oil Chem. Soc.* **2014**, *83*, 247–252.
[25] W. Cheng, G. Liu, X. Wang, X. Liu, L. Jing, *Eur. J. Lipid Sci. Technol.* **2015**, *117*, 1185–1191.
[26] J. Jiang, Y. Zhang, L. Yan, P. Jiang, *Appl. Surf. Sci.* **2012**, *258*, 6637–6642.
[27] H. Zhang, H. Yang, H. Guo, J. Yang, L. Xiong, C. Huang, X. Chen, L. Ma, Y. Chen, *Appl. Clay Sci.* **2014**, *90*, 175–180.
[28] A. Campanella, M. A. Baltanás, M. C. Capel-Sánchez, J. M. Campos-Martín, J. L. G. Fierro, *Green Chem.* **2004**, *6*, 330–334.
[29] X. Ye, P. Jiang, P. Zhang, Y. Dong, C. Jia, X. Zhang, H. Xu, *Catal. Letters* **2010**, *137*, 88–93.
[30] M. Di Serio, R. Turco, P. Pernice, A. Aronne, F. Sannino, E. Santacesaria, *Catal. Today* **2012**, *192*, 112–116.
[31] M. R. Janković, S. V. Sinadinović-Fišer, O. M. Govedarica, *Ind. Eng. Chem. Res.* **2014**, *53*, 9357–9364.
[32] Y. X. Miao, J. P. Liu, *Adv. Mater. Res.* **2014**, *881–883*, 140–143.
[33] R. Turco, C. Pischetola, R. Tesser, S. Andini, M. Di Serio, *RSC Adv.* **2016**, *6*, 31647–31652.
[34] P. Spannring, V. Yazerski, P. C. A. Bruijnincx, B. M. Weckhuysen, R. J. M. Klein Gebbink, *Chem. Eur. J.* **2013**, *19*, 15012–15018.
[35] R. V. Ottenbacher, E. P. Talsi, K. P. Bryliakov, *Molecules* **2016**, *21*, 1454.
[36] D. Shen, C. Miao, D. Xu, C. Xia, W. Sun, *Org. Lett.* **2015**, *17*, 54–57.
[37] R. V Ottenbacher, D. G. Samsonenko, E. P. Talsi, K. P. Bryliakov, *Org. Lett.* **2012**, *14*, 4310–4313.
[38] O. Y. Lyakin, R. V. Ottenbacher, K. P. Bryliakov, E. P. Talsi, *ACS Catal.* **2012**, *2*, 1196–1202.
[39] K. Chen, L. Que, Jr., *Chem. Commun.* **1999**, 1375–1376.
[40] M. Costas, A. K. Tipton, K. Chen, D. H. Jo, L. Que, Jr., *J. Am. Chem. Soc.* **2001**, *123*, 6722–6723.
[41] M. S. Chen, M. C. White, *Science* **2007**, *318*, 783–787.
[42] A. Murphy, G. Dubois, T. D. P. Stack, *J. Am. Chem. Soc.* **2003**, *125*, 5250–5251.
[43] R. V Ottenbacher, K. P. Bryliakov, E. P. Talsi, *Adv. Synth. Catal.* **2011**, *353*, 885–889.
[44] V. Yazerski, P. Spannring, D. Gatineau, C. H. M. Woerde, S. M. Wieclawska, M. Lutz, H. Kleijn, R. J. M. Klein Gebbink, *Org. Biomol. Chem.* **2014**, *12*, 2062–2070.
[45] J. Chen, M. Lutz, M. Milan, M. Costas, M. Otte, R. J. M. Klein Gebbink, *Adv. Synth. Catal.*

2017, *359*, 2590–2595.

[46] X. Chen, B. Gao, Y. Su, H. Huang, *Adv. Synth. Catal.* **2017**, *359*, 2535–2541.

[47] N. A. Vermeulen, M. S. Chen, M. C. White, *Tetrahedron* **2009**, *65*, 3078–3084.

[48] R. V. Ottenbacher, D. G. Samsonenko, E. P. Talsi, K. P. Bryliakov, *Org. Lett.* **2012**, *14*, 4310–4313.

[49] C. Paquot, *Stand. Methods Anal. Oils, Fats Deriv.* **1979**, 66–70.

[50] C. Paquot, *Stand. Methods Anal. Oils, Fats Deriv.* **1979**, 92–93.

[51] R. E. Parker, N. S. Isaacs, *Chem. Rev.* **1959**, *59*, 737–799.

[52] S. E. Denmark, J. Fu, M. J. Lawler, *Org. Synth.* **2006**, *83*, 121–130.

Summary

C–H and C═C bond oxidations constitute essential transformations in organic synthesis and in many biological and industrial processes. In the past decades numerous non-heme iron enzymes have been discovered and identified, that are able to conduct biological C–H and C═C bond oxidations *via* O_2 activation in a very selective manner. In **Chapter 1**, three typical non-heme iron enzymes, mono-nuclear Rieskes dioxygenases and α-ketoglutarate-(α-KG)-dependent enzymes, as well as soluble methane monooxygenase (sMMO), are detailed to provide insight into the structures of their iron active sites and their reaction mechanisms. Inspired by these enzymes, many efforts have been spent on modelling catalytic iron sites and active intermediates involved in catalysis, in order to achieve these oxidation reactions by molecular catalysts outside the enzyme environment. Depending on the ligand, the coordination chemistry and reactivity of synthetic non-heme iron complexes may be drastically different; accordingly, the development of ligands is of pivotal importance to the field. So far, iron complexes with tetradentate nitrogen (N4, generally aminopyridine) ligands have shown to be most successful in achieving highly regio- and stereoselective oxidation reactions utilizing H_2O_2 as the oxidant. Amongst them, iron complexes with a *cis*-α topology derived from linear bis-alkylamine-bis-pyridine (N2Py2) ligands have been proven to be most effective so far (Figure 1). This ligand platform has two pyridine moieties linked to a bis-alkylamine backbone, wrapping around the iron center in a *cis*-α manner. In this coordination topology, two labile sites (X) are *cis* to each other and *trans* to the alkylamine nitrogen donors, causing them to be chemically equivalent.

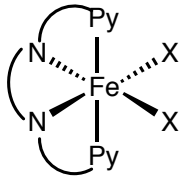

Figure 1. Generic structure of Fe(N2Py2) complexes adopting a *cis*-α topological configuration.

This ligand platform enables modifications on both the bis-alkylamine backbone and pyridine moieties, which allows for a systematic improvement of the reactivity and for fine-tuning of the selectivity of non-heme iron catalysts, providing powerful protocols for efficient C–H and C═C oxidations. Next to the iron complexes, the interest in structurally related manganese complexes has increased in recent years. In addition, these Mn-complexes seem to follow similar reaction mechanisms and may provide (much) higher reactivities as compared to their

Fe analogs in both C–H and C═C bond oxidations. The research described in this thesis not only focuses on the modification of the N2Py2 ligand platform, but also on the practical use of the corresponding iron and manganese complexes in (selective) catalytic oxidations using H_2O_2 as the oxidant and acetic acid (AcOH) as additive.

It has been reported previously that the increase in ligand rigidity is beneficial for achieving improved catalytic efficiencies and product selectivities in aliphatic C–H oxidations. Based on the design of the well-known BPBP ligand, **Chapter 2** describes the development of the BPBI ligand with a further rigidified bis-alkylamine backbone through the incorporation of benzene moieties on the pyrrolidines (BPBP = *N*,*N*'-bis(2-picolyl)-2,2'-bispyrrolidine, and BPBI = *N*,*N*'-bis(2-picolyl)-2,2'-bis-isoindoline, Scheme 1). Additionally, a more bulky analog ^{TIPS}BPBI was also synthesized, where a TIPS substituent was introduced at the 5-position of each pyridine ring. Steric congestion at the pyridine moieties has previously been shown to play an important role in site-selective C–H oxidations.

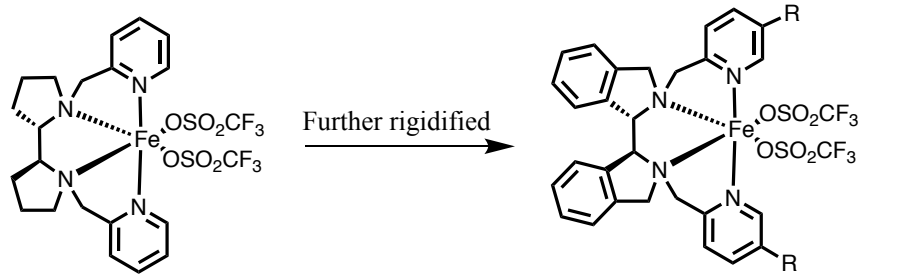

[Fe(OTf)$_2$(*S*,*S*-BPBP)]

R = H, [Fe(OTf)$_2$(*S*,*S*-BPBI)]
R = TIPS, [Fe(OTf)$_2$(*S*,*S*-^{TIPS}BPBI)]

Scheme 1. Ligand modification described in Chapter 2.

It was found that [Fe(OTf)$_2$(*S*,*S*-BPBI)] consistently shows a higher preference for the oxidation of tertiary over secondary (3°/2°) C–H bonds in alkane substrates compared to [Fe(OTf)$_2$(*S*,*S*-BPBP)]. Substrate conversions and product yields tend to be lower though, which is likely due to the electron-withdrawing property of the benzene moieties in the BPBI ligand. Notably, [Fe(OTf)$_2$(*S*,*S*-BPBI)] provides a 3°/2° ratio of 33 in the oxidation of adamantane, which is amongst the highest reported 3°/2° selectivities for non-heme Fe catalyzed adamantane oxidation, and, additionally, without a drop in substrate conversion compared to the reaction catalyzed by [Fe(OTf)$_2$(*S*,*S*-BPBP)]. The introduction of bulky TIPS-groups in [Fe(OTf)$_2$(*S*,*S*-^{TIPS}BPBI)] brings about a higher reactivity and enhances the preference for secondary C–H bond oxidations, allowing for site-selective oxidations of biologically interesting acetylandrosterone derivatives. In terms of steric and electronic effects of substrates on site selectivity, no obvious differences in product distribution were observed for these three complexes.

Next, **Chapter 3** describes the use of the Fe(BPBP) and Fe(BPBI) and other Fe(N2Py2) complexes in the catalytic epoxidation of poly-unsaturated fatty acids and esters, using methyl linoleate (ML) as the model substrate (Scheme 2). This study has a specific focus on the selectivity between mono-epoxidation and di-epoxidation, as the resulting mono-epoxides and di-epoxides represent different industrial uses due to their different physicochemical properties.

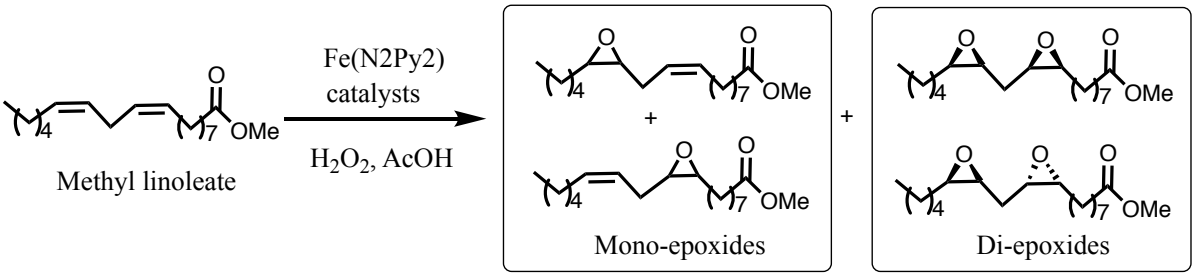

Scheme 2. Epoxidation of methyl linoleate catalyzed by Fe(N2Py2) complexes.

Catalytic studies revealed that a more active catalyst, elevated catalyst or AcOH loadings, or a lower reaction temperature give higher ML conversion and favor the formation of di-epoxides, leading to a lower mono-epoxides/di-epoxides (M/D) ratio. Mono-epoxides or di-epoxides thus can be obtained as primary products, respectively, using different reaction conditions. 42% of mono-epoxides and 4.7% of di-epoxides can be obtained at 52% ML conversion using 1 mol% of [Fe(OTf)$_2$(*S*,*S*-BPBI)], 1.5 equiv. of H_2O_2, and 1.5 mol% of AcOH, in contrast to 92% of di-epoxides at full ML conversion without the formation of mono-epoxides when conducting the reaction with 1 mol% of [Fe(OTf)$_2$(*mix*-BPBP)] (*mix*-BPBP = mixture of *S*,*S*-, *R*,*R*- and *R*,*S*-isomers of BPBP), 2.2 equiv. of H_2O_2, and 100 mol% of AcOH. Notably, both reactions are performed under very mild reaction conditions (room temperature or 0 ^oC, respectively), in short reaction times (1 h or 5 min, respectively), and with excellent epoxide selectivity (> 90%). Kinetic studies showed that the Fe(N2Py2) complexes are deactivated rather quickly in the epoxidation of ML (within 2 min). A slow catalyst addition protocol was found to improve the epoxidation progression and to favor the formation of di-epoxides. A higher M/D ratio can be obtained by using a slow oxidant addition protocol, albeit at lower ML conversion. A detailed study of the O-transfer selectivity showed a small but significant kinetic preference for mono-epoxidation over di-epoxidation for Fe(N2Py2) complexes in general.

The stability of the Fe(N2Py2) complexes under the oxidizing conditions seems to be an important factor that limits the epoxidation of ML in **Chapter 3**. In fact, catalyst deactivation is a common but less investigated issue in non-heme iron oxidation catalysis. **Chapter 4** describes the development of Fe(N2Py2-D$_4$) complexes with deuterated 2-pyridinylmethyl sites

in the ligands (Figure 2a), which is based on the observation of significant intramolecular C–H oxidation of one of the 2-pyridinylmethyl sites in the ligand and subsequent dissociation of the oxidized ligand upon exposure of the parent Fe(N2Py2) complexes to H_2O_2 in the absence of an organic substrate.

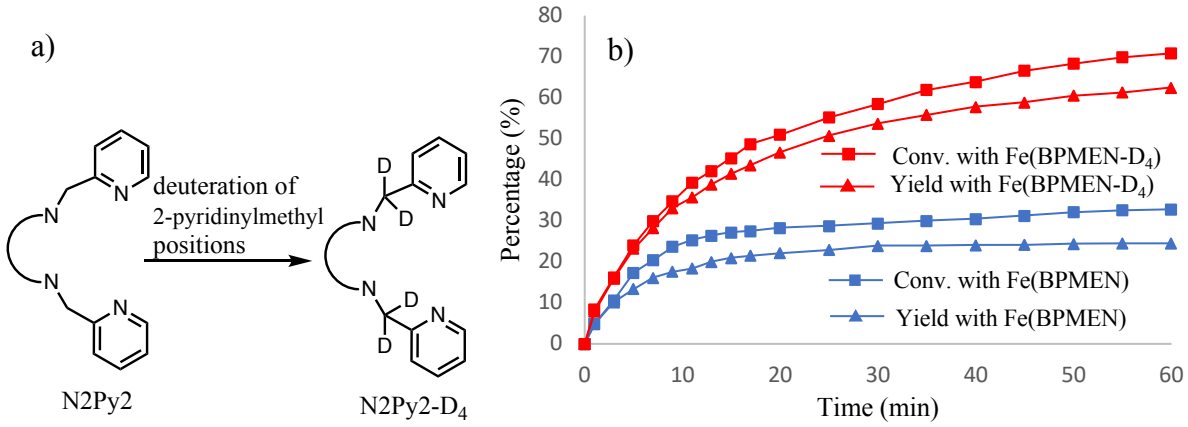

Figure 2. a) Ligand modification of N2Py2 through the introduction of D atoms on 2-pyridinylmethyl positions. b) Time-dependent reaction profiles of the catalytic epoxidation of *cis*-cyclooctene with catalyst [Fe(OTf)$_2$(BPMEN)] vs. catalyst [Fe(OTf)$_2$(BPMEN-D$_4$)].

Improved conversions and yields are consistently obtained in both aliphatic C–H oxidations and alkene epoxidations employing the Fe(N2Py2-D$_4$) catalysts compared to reactions with the non-deuterated Fe(N2Py2) catalysts. Kinetic studies revealed that this is attributed to an extended lifetime of the Fe(N2Py2-D$_4$) complexes; their inherent reactivity remains the same as that of the parent, non-deuterated complexes. Additionally, the improvements in catalytic performances and lifetimes provided by deuterated complexes depend on the rigidity of the parent N2Py2 ligands. That is, applying the deuteration approach to ligands with more rigid bis-alkylamine backbones, e.g. BPBP, leads to a limited extension of catalyst lifetime. In contrast, the improvements in catalytic performances and lifetimes are more pronounced for Fe(N2Py2-D$_4$) complexes derived from relatively flexible N2Py2 ligands. For instance, [Fe(OTf)$_2$(BPMEN-D$_4$)] shows a much longer lifetime and gives a more than 2-fold higher conversion and epoxide yield in the epoxidation of *cis*-cyclooctene, in comparison with its counterpart [Fe(OTf)$_2$(BPMEN)] (Figure 2b, BPMEN = *N*,*N*'-dimethyl-*N*,*N*'-bis(2-picolyl)-ethylene-diamine). Deuteration of the more flexible BPMEN ligand, actually leads to a catalytic performance of the [Fe(OTf)$_2$(BPMEN-D$_4$)] complex that resembles the performance of the non-deuterated [Fe(OTf)$_2$(BPBP)] complex. These observations suggest that the enhanced catalytic abilities of more rigid ligands (like BPBP) are attributed to attenuated catalyst decomposition, through a more restricted approach of 2-pyridinylmethyl C–H bonds to the intermediate iron-oxo moiety.

The N2Py2 ligands were further explored in **Chapter 5** for the use of Mn(N2Py2) type complexes in the catalytic epoxidation of vegetable oils (VOs). An optimized catalytic protocol relies on the use of the non-noble metal manganese in combination with a racemic mixture of the BPBP ligand (*rac*-BPBP, Figure 3), using H_2O_2 as the oxidant and acetic acid as additive.

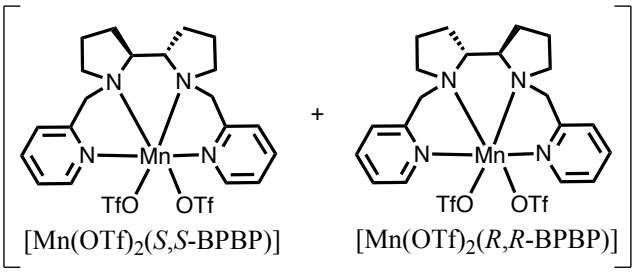

Figure 3. Structure of [Mn(OTf)$_2$(*rac*-BPBP)].

The protocol is highly efficient and highly selective for the epoxide products: most of the investigated VOs, including cheap waste cooking oil, can be fully converted to epoxidized vegetable oils (EVOs) in more than 90% yield with excellent epoxide selectivities (> 90%) within 2 h of reaction time at ambient temperature, using only 0.03 mol% of [Mn(OTf)$_2$(*rac*-BPBP)] catalyst with respect to the number of double bonds (ca. 0.1 wt% with respect to oil). Furthermore, in 1-gram scale reactions the use of MeCN can be largely limited to its use as a delivery medium of the catalyst solution (100 - 180 μL) rather than as the reaction solvent, by increasing the addition time of the H_2O_2 oxidant and the oil:AcOH volume ratio. Notably, the high catalytic efficiency is retained in a scale-up experiment with 5 g of sunflower oil, in which the catalyst was added as a solid. Therefore, the reactions can be performed in a completely MeCN-free medium and EVOs can be obtained from the reaction crude *via* simple extraction with Et_2O. Finally, one-pot oxidative cleavage of unsaturated fatty acids (and esters) into nonanal and an α,ω-aldehyde fatty acid (ester) has been carried out using the current Mn-catalyzed epoxidation protocol as the first and key step, which outperforms the reported Fe-based catalytic system in terms of catalytic efficiency.

In conclusion, this thesis describes several ligand modifications of the N2Py2 ligand platform, with the aim of either improving C–H oxidation selectivities or enhancing the lifetimes of Fe(N2Py2) complexes in oxidation catalysis. Furthermore, the practical use of the Fe(N2Py2) and Mn(N2Py2) complexes in the oxidation of a number of biologically or industrially relevant compounds, like steroidal derivatives, unsaturated fatty acids and their esters, and vegetable oils, is also investigated in this thesis.

Samenvatting

Oxidaties van C–H en C═C bindingen zijn essentieel in de organische synthese en in vele biologische en industriële processen. In de afgelopen decennia zijn tal van niet-heem-ijzerenzymen ontdekt en geïdentificeerd die in staat zijn om op een biologische wijze C–H en C═C bindingen te oxideren *via* O_2-activering met een zeer hoge selectiviteit. In **Hoofdstuk 1** worden drie typische niet-heem-ijzerenzymen gedetailleerd omschreven; mononucleaire Rieske dioxygenasen en α-ketoglutaraat-(α-KG)-afhankelijke enzymen, evenals oplosbare methaan mono-oxygenasen (sMMO). Hiermee wordt inzicht verkregen in de structuren van hun actieve centra en hun reactiemechanismen. Geïnspireerd door deze enzymen is er veel aandacht besteed aan het modelleren van katalytische ijzercentra en actieve intermediairen die betrokken zijn bij katalyse, om deze oxidatiereacties uit te kunnen voeren met behulp van moleculaire katalysatoren buiten een enzymomgeving. Afhankelijk van het ligand kunnen de coördinatiechemie en reactiviteit van synthetische non-heemijzer complexen drastisch variëren; de ontwikkeling van liganden is dus van cruciaal belang voor het veld. Tot dusverre zijn ijzercomplexen met tetradentate stikstofliganden (N4, over het algemeen aminopyridines) het meest succesvol gebleken in regio- en stereoselectieve oxidatiereacties, waarbij waterstofperoxide wordt gebruikt als oxidant. IJzercomplexen met een *cis*-α-topologie afgeleid van lineaire bis-alkylamine-bis-pyridine (N2Py2) liganden laten tot nu toe de hoogste reactiviteit zien (Figuur 1). Dit ligandplatform omvat twee pyridine groepen gebonden aan een bis-alkylamine hoofdketen en wikkelt zich op een *cis*-α-wijze rond het ijzercentrum. In deze coördinatietopologie bevinden zich twee labiele posities (X) *cis* ten opzichte van elkaar en *trans* ten opzichte van de alkylamine-stikstofdonoren, waardoor ze chemisch equivalent zijn.

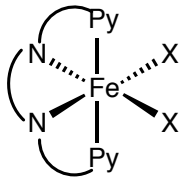

Figuur 1. Algemene structuur van Fe(N2Py2) complexen met een *cis*-α-topologie.

Modificaties aan dit ligandplatform zijn mogelijk op zowel de bis-alkylamine hoofdketen als op de pyridinegroepen, wat een systematische verbetering van de reactiviteit en een nauwkeurige fine-tuning van de selectiviteit van non-heem-ijzerkatalysatoren mogelijk maakt.

Dit levert krachtige katalytische protocollen voor efficiënte C–H en C═C oxidaties op. Naast de ijzercomplexen is de belangstelling voor de structureel verwante mangaancomplexen de laatste jaren toegenomen. Bovendien lijken deze Mn-complexen vergelijkbare reactiemechanismen te volgen en kunnen ze over een (veel) hogere reactiviteit beschikken ten opzichte van vergelijkbare Fe-complexen in oxidaties van zowel C–H- als C═C-bindingen. Het onderzoek beschreven in dit proefschrift richt zich niet alleen op de modificatie van het N2Py2 ligandplatform, maar ook op het praktische gebruik van de overeenkomstige ijzer- en mangaancomplexen in (selectieve) katalytische oxidaties met waterstofperoxide als oxidator en azijnzuur als additief .

Er is eerder beschreven dat de toename in de rigiditeit van het N2Py2ligand gunstig is voor een verbeterde katalytische efficiëntie en selectiviteit in alifatische C–H-oxidaties. Gebaseerd op het ontwerp van het welbekende BPBP-ligand, beschrijft **Hoofdstuk 2** de ontwikkeling van het BPBI-ligand met een verdere verhoging van de rigiditeit van het bis-alkylamine skelet door de functionalisering van de pyrrolidinen met benzeen (BPBP = *N*,*N*'-bis (2-picolyl)-2,2'-bispyrrolidine en BPBI = *N*,*N*'-bis(2-picolyl)-2,2'-bis-isoindoline, Schema 1). Bovendien werd een meer 'bulky' analoog ^{TIPS}BPBI gesynthetiseerd, waarbij een TIPS-substituent werd geïntroduceerd op de 5-positie van elke pyridine-ring. Er is eerder aangetoond dat sterische congestie rond de pyridinegroepen een belangrijke rol speelt bij regio-selectieve C–H-oxidaties.

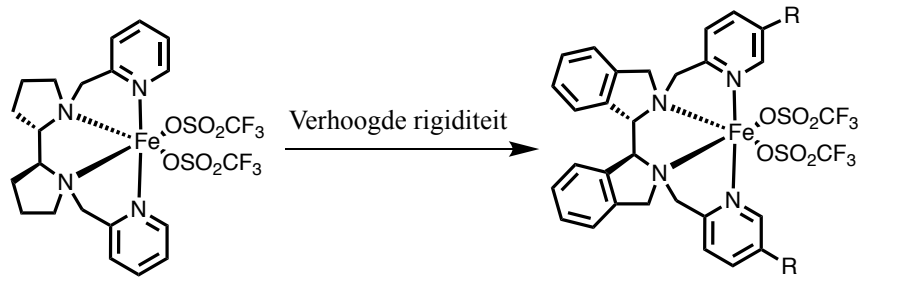

[Fe(OTf)$_2$(*S*,*S*-BPBP)]

R = H, [Fe(OTf)$_2$(*S*,*S*-BPBI)]
R = TIPS, [Fe(OTf)$_2$(*S*,*S*-^{TIPS}BPBI)]

Schema 1. Ligandmodificatie beschreven in Hoofdstuk 2.

[Fe(OTf)$_2$(*S*,*S*-BPBI)] blijkt een consequent hogere voorkeur te hebben voor de oxidatie van tertiaire (3°) tem opzichte van secundaire (2°) C–H-bindingen in alkaansubstraten in vergelijking met [Fe(OTf)$_2$(*S*,*S*-BPBP)]. Substraatomzettingen en productopbrengsten zijn echter meestal lager, wat waarschijnlijk te wijten is aan de elektronen-zuigende eigenschap van de benzeengroepen in het BPBI-ligand. Met name [Fe(OTf)$_2$(*S*,*S*-BPBI)] geeft een bijzonder hoge 3°/2°-ratio van 33 in de oxidatie van adamantaan, zonder een afname in substraatconversie

vergeleken met de reactie gekatalyseerd door [Fe(OTf)$_2$(*S,S*-BPBP)]. De introductie van grote TIPS-groepen in [Fe(OTf)$_2$(*S,S*-^{TIPS}BPBI)] zorgt voor een hogere reactiviteit en verhoogt de voorkeur voor de oxidatie van secundaire C–H-bindingen, waardoor regio-selectieve oxidaties van biologisch interessante acetylandrosteron-derivaten mogelijk worden. Met betrekking tot sterische en elektronische effecten van substraten op de selectiviteit van de site werden er geen duidelijke verschillen in productverdeling waargenomen voor deze drie complexen.

Hoofdstuk 3 beschrijft het gebruik van Fe(BPBP), Fe(BPBI) en andere Fe(N2Py2) complexen in de katalytische epoxidatie van meervoudig onverzadigde vetzuren en esters met methyl linoleaat (ML) als modelsubstraat (Schema 2). Deze studie focust zich specifiek op de selectiviteit tussen mono-epoxidatie en di-epoxidatie, daar de resulterende mono-epoxiden en di-epoxiden verschillende industriële toepassingen hebben vanwege hun verschil in fysisch-chemische eigenschappen.

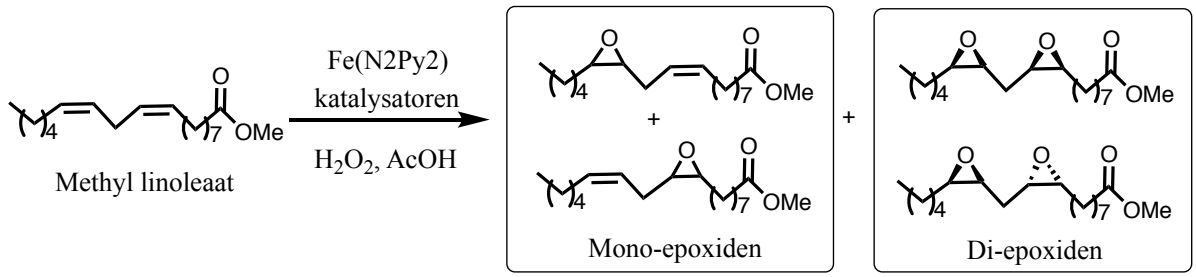

Schema 2. Epoxidatie van methyl linoleaat gekatalyseerd door Fe(N2Py2) complexen.

Katalytische studies hebben aangetoond dat een actievere katalysator, verhoogde katalysator- of AcOH-belading of een lagere reactietemperatuur een hogere ML-omzetting geven en de vorming van di-epoxiden bevorderen, wat een lagere mono-epoxide/di-epoxide (M/D) ratio geeft. Mono-epoxiden of di-epoxiden kunnen dus worden verkregen als hoofdproducten, respectievelijk, door variatie van de reactie-omstandigheden. 42% Mono-epoxiden en 4,7% di-epoxiden worden verkregen bij een 52% ML-omzetting met 1 mol% [Fe(OTf)$_2$(*S,S*-BPBI)], 1.5 equivalent H_2O_2 en 1.5 mol% AcOH, in tegenstelling tot 92% di-epoxiden bij volledige ML-omzetting zonder de vorming van mono-epoxiden bij het uitvoeren van de reactie met 1 mol% [Fe(OTf)$_2$(mix-BPBP)] (mix-BPBP = mengsel van *S,S*-, *R,R*- en *R,S*-isomeren van BPBP), 2,2 equivalenten H_2O_2 en 100 mol% AcOH. Belangrijk is dat beide reacties worden uitgevoerd onder zeer milde reactieomstandigheden (kamertemperatuur of 0 °C), korte reactietijden (1 uur of 5 minuten) en met uitstekende epoxideselectiviteit (> 90%). Kinetische studies toonden aan dat de Fe(N2Py2)-complexen vrij snel gedeactiveerd worden in de epoxidatie van ML (binnen 2 minuten). Een protocol waarbij de katalysator langzaam wordt toegevoegd aan het

reactiemengsel bleek de epoxidatiereactie te verbeteren en de vorming van di-epoxiden te bevorderen. Een hogere M/D-verhouding kan worden verkregen door waterstofperoxide langzaam toe te voegen, met als nadeel een lagere ML-omzetting. Een gedetailleerde studie van de O-transfer selectiviteit toonde een kleine maar significante kinetische voorkeur voor mono-epoxidatie ten opzichte van di-epoxidatie voor Fe(N2Py2)-complexen in het algemeen.

De stabiliteit van de Fe(N2Py2)-complexen onder de oxiderende omstandigheden lijkt een belangrijke factor te zijn die de epoxidatie van ML in **Hoofdstuk 3** beperkt. In feite is deactivering van de katalysator een veel voorkomend maar minder onderzocht probleem bij niet-heem-ijzer oxidatiekatalyse. **Hoofdstuk 4** beschrijft de ontwikkeling van Fe(N2Py2-D_4)-complexen met gedeutereerde 2-pyridinylmethyl posities in de liganden (Figuur 2a). Deze studie is gebaseerd op de significante intramoleculaire C–H-oxidatie van één van de 2-pyridinylmethyl posities in het ligand en de daaropvolgende dissociatie van het geoxideerde ligand bij blootstelling van de Fe(N2Py2)-complexen aan H_2O_2 bij afwezigheid van een organisch substraat.

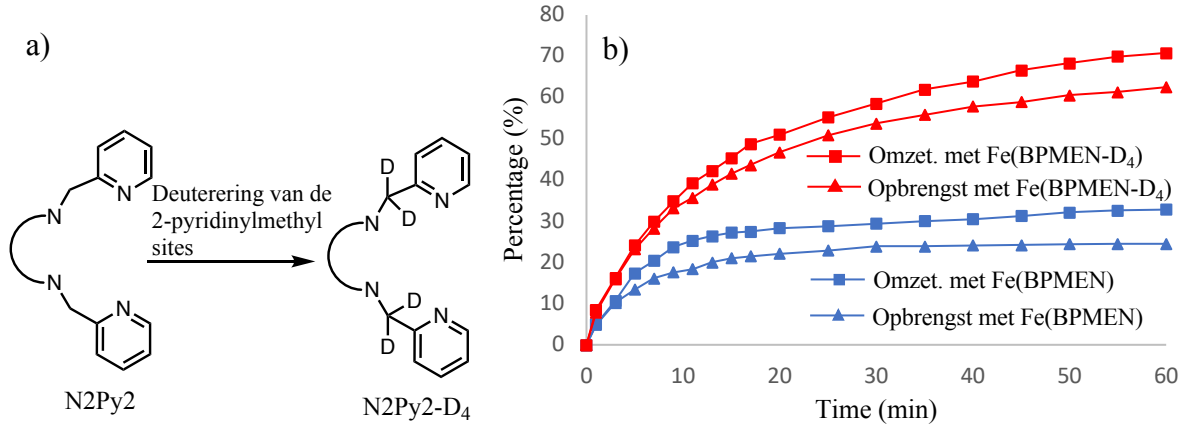

Figuur 2. a) Ligandmodificatie van N2Py2 door de introductie van D-atomen op de 2-pyridinylmethyl posities. b) Tijdsafhankelijke reactieprofielen van de katalytische epoxidatie van *cis*-cyclo-octeen met [$Fe(OTf)_2$(BPMEN)] vs. [$Fe(OTf)_2$(BPMEN-D_4)].

Verbeterde omzettingen en opbrengsten worden consequent verkregen in zowel alifatische C–H-oxidaties als alkeenepoxidaties waarbij de Fe(N2Py2-D_4) -katalysatoren worden gebruikt in vergelijking met reacties met de niet-gedeutereerde Fe(N2Py2)-katalysatoren. Kinetische studies onthulden dat dit wordt veroorzaakt door een verlengde levensduur van de Fe(N2Py2-D_4)-complexen; hun inherente reactiviteit blijft echter hetzelfde als die van de vergelijkbare, niet-gedeutereerde complexen. Bovendien hangen de verbeteringen in katalytische activiteit en levensduur van gedeutereerde complexen af van de rigiditeit van de oorspronkelijke N2Py2-liganden. Het deutereren van meer rigide bis-alkylaminehoofdketens, bijvoorbeeld BPBP, leidt tot een beperkte verlenging van de levensduur van de katalysator. Daarentegen zijn de

verbeteringen in katalytische activiteit en levensduur duidelijker voor Fe(N2Py2-D_4)-complexen die zijn afgeleid van de relatief flexibele N2Py2-liganden. Zo vertoont bijvoorbeeld [Fe$(OTf)_2$(BPMEN-D_4)] een veel langere levensduur en geeft een meer dan verdubbelde conversie en epoxide-opbrengst in de epoxidatie van *cis*-cyclo-octeen, in vergelijking met zijn tegenhanger [Fe$(OTf)_2$(BPMEN)] (Figuur 2b, BPMEN = *N*,*N*'-dimethyl-*N*,*N*'-bis(2-picolyl)-ethyleendiamine). Deuterering van het meer flexibele BPMEN-ligand leidt zelfs tot een katalytische activiteit van het [Fe$(OTf)_2$(BPMEN-D_4)] complex dat lijkt op de activiteit van het niet-gedeutereerde [Fe$(OTf)_2$(BPBP)] complex. Deze waarnemingen suggereren dat de verhoogde katalytische activiteit van meer rigide liganden (zoals BPBP) kan worden toegeschreven aan een verminderde katalysatordeactivering vanwege een verminderde intramoleculaire toenadering van 2-pyridinylmethyl C–H-bindingen tot het katalytische ijzercentrum.

De N2Py2-liganden werden verder onderzocht in **Hoofdstuk 5** voor het gebruik van Mn (N2Py2)-type complexen in de katalytische epoxidatie van plantaardige oliën (PO's). Een geoptimaliseerd katalytisch protocol op basis van het niet-edelmetaal mangaan in combinatie met een racemisch mengsel van het BPBP-ligand (*rac*-BPBP, figuur 3), H_2O_2 als het oxidatiemiddel en azijnzuur als additief.

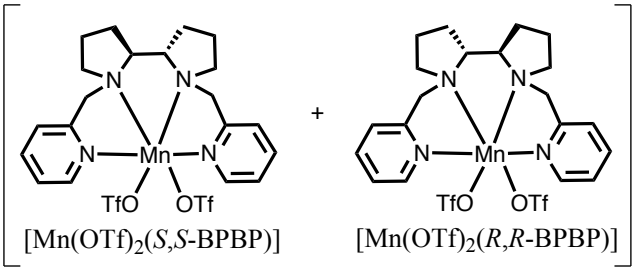

[Mn$(OTf)_2$(*S*,*S*-BPBP)] [Mn$(OTf)_2$(*R*,*R*-BPBP)]

Figuur 3. Samenstelling van [Mn$(OTf)_2$(*rac*-BPBP)].

Het protocol is zeer efficiënt en zeer selectief voor de epoxideproducten: de meeste van de onderzochte PO's, onder meer goedkope gebruikte bakolie, kunnen volledig worden omgezet in geëpoxideerde plantaardige oliën (EPO's). Een opbrengst van meer dan 90% werd verkregen met uitstekende epoxideselectiviteit (> 90%) binnen 2 uur reactietijd bij kamertemperatuur, met gebruikmaking van slechts 0.03 mol% [Mn$(OTf)_2$(*rac*-BPBP)] katalysator in verhouding tot het aantal dubbele bindingen (ongeveer 0.1 gew.% in verhouding tot olie). Verder kan bij 1-gram schaal reacties het gebruik van acetonitril grotendeels worden beperkt tot het gebruik als toedieningsmedium van de katalysatoroplossing (100-180 μL) in plaats van als het oplosmiddel voor de reactie, door een langzamere toevoeging van H_2O_2 en een verhoogde olie:azijnzuur volume ratio. Opmerkelijk is dat de hoge katalytische efficiëntie wordt behouden in een

opgeschaald experiment met 5 g zonnebloemolie, waarbij de katalysator als een vaste stof werd toegevoegd. Daarmee kunnen de reacties worden uitgevoerd in een volledig acetonitril-vrij medium en kunnen EPO's worden verkregen uit het ruwe reactiemengsel via een eenvoudige extractie met diethylether. Tenslotte is een één-pots oxidatieve splitsing van onverzadigde vetzuren (en esters) tot nonanal en een α,ω-aldehyde vetzuur (ester) uitgevoerd met behulp van dit Mn-gekatalyseerde epoxidatieprotocol als de eerste en belangrijkste stap, waarbij betere opbrengsten verkregen werd dan met het eerder beschreven op ijzer gebaseerde katalytische protocol.

In conclusie beschrijft dit proefschrift verschillende ligandmodificaties van het N2Py2-ligandplatform, met als doel ofwel verbetering van de C–H-oxidatieselectiviteit of verbetering van de levensduur van Fe(N2Py2)-complexen in oxidatiekatalyse. Verder wordt ook het praktische gebruik van de Fe(N2Py2) en Mn(N2Py2) complexen bij de oxidatie van een aantal biologisch of industrieel relevante verbindingen, zoals steroïde-derivaten, onverzadigde vetzuren en hun esters, en plantaardige oliën onderzocht in dit proefschrift.

Acknowledgements

A lot of great help and contributions from many people have made this thesis possible, which also made my stay in Utrecht an enjoyable journey. Herein, it is a great moment for me to look back at my around 4-year PhD life and it is a pleasure for me to convey my sincere acknowledgements to these people.

First and foremost, I would like to give my deepest gratitude to my promoter, prof. dr. Klein Gebbink. Dear **Bert**, thank you for giving me this wonderful opportunity to perform my PhD study in the OCC group at Utrecht; for helping me prepare the application for the CSC scholarship; for telling me 'don't feel too bad' after I burned the microwave reactor; for motivating me to come up with my own ideas of my research and allowing me to carry out these ideas in the lab, from which I was trained efficiently towards an independent junior scientist; for giving me tremendous inputs and support during my writing stage of this thesis, so that I can tell the stories as nicely as possible; for your care about my personal life in the Netherlands. I enjoyed our meetings and discussions a lot, although they were a little bit tough to me at the beginning when I was still new to this project. They were of special importance to my whole PhD project, as you shared your precious experiences and knowledges in the field of chemistry, and gave me your guidance to make things go in the right direction. All in all, thank you, **Bert**, for everything!

My co-promoter, dr. Matthias Otte, also deserves my sincere thanks, of course. Dear **Matthias**, your input at the early stage of my PhD was of great help for me to get familiar with the group and the lab, and to get started with my project. I was lucky to have you involved in my PhD project, especially in the first half. I greatly acknowledge your care and suggestions in many aspects of my research, and your contributions to the preparation and correlations of some of the thesis chapters. I wish you a very successful career in Göttingen!

Marc-Etienne, your wide knowledge in many fields, critical views on my research, and instant discovery of the problems are inspiring, which resulted in many nice suggestions at both the work discussions and my research presentations. Some of them are already reflected in this thesis, for instance, the O-distribution selectivity experiments in Chapter 3. I greatly appreciate all your help on my PhD project.

Of course, I have received a lot of help and support from the OCC group during my PhD. **Johann**, thank you for your instruction of NMR measurements and your help on my computer issues. Undoubtedly, chemicals are the bases to make my chemistry happen, thank you **Jord**, for ordering them and for keeping the lab running regularly; and later on **Thomas**, you are bringing not only the chemicals, but also beers into the OCC group, thank you for organizing those incredible Friday borrels! **Henk**, thank you for your help with ESI-MS measurements and GC instructions. You were always passionate during those instructions, which was impressive. **Milka**, your dedication and input for my visa preparation and my residential issues in the Netherlands were essential at my start-up stage. It always comforted me a lot when you were saying 'everything is going to be fine' to me. Also thank you for your help at the last moments of my PhD. **Danny**, you just joined the group, but you already showed your care to my research in a couple of conversations, which I appreciate.

My collaborators both inside and outside Utrecht have contributed to this thesis as well. Dr. **Martin Lutz**, thank you for providing me some beautiful crystal structures, and for your discussions and input for the X-ray structural analysis part. Dr. **Miquel Costas** and **Michela** from Girona, you performed the experiments of the oxidation of steroidal substrates in Chapter 2, thank you so much for that, and for your contributions to the manuscript preparation.

I was fortunate to have several motivated bachelor and master students involved in some chapters of this thesis, who had dedicated themselves to some experimental work and provided some very nice results! **Laurens** and **Yannick**, you made the first batch of bis-isoindoline, which is the key backbone for the synthesis of BPBI-based ligands in Chapter 2. **Laurens**, I am glad that you continue doing your master research project in our group, I wish you the best for that. **Joren**, **Marc** and **Lucas**, you have done some beautiful manganese chemistry in Chapter 5! First, **Joren**, you started the reaction condition screening for the Mn-catalyzed epoxidation of oleic acid, which established a good foundation for Chapter 5. Then **Marc** continued further optimizing the reaction conditions, and completed the experimental work of oxidative cleavage of unsaturated fatty acids (esters). Later on, **Lucas** joined the team to start investigating this manganese catalytic system in the epoxidation of sunflower oil. All of your contributions were very helpful to shape a nice story of Chapter 5, which you should be proud of!

My awesome OCC colleagues, it is my fortune to work with you in this group. It is you building up a wonderful group atmosphere, in which I have been helped in many occasions, and have learned a lot in the perspective of both the professional and employability skills.

To the former OCC members: **Pradip**, you were such a good listener and a wonderful friend with whom I could share my successes and failures in my research. You felt happy for me whenever I had some achievements. And your professionalism, your experiences and your

advices were greatly helpful and encouraging for me to overcome many hard times. I was so lucky to have you around for more than two years, and thanks for your concern about my research and thesis writing progress after you left the group. I wish you all the best for your current work in Hamburg and your future career! **Emma**, thanks for your help on my accommodation in Utrecht when I still didn't arrive here yet, and for your experiences on iron chemistry. **Yuxing**, thank you for giving me the privilege to be one of your paranymphs and your care about my PhD progress and my future career. **Suresh**, thank you for sharing your experiences in the lab when we worked in the same lab aisle. **Manuel**, thanks for organizing the unbelievable 90's NOW parties. **Bas**, my former neighbor in the office, thank you for translating the Dutch letters for me. **Dide**, thank you for organizing those fantastic camping trips, they constructed some of my best memories in the group. **Léon**, thank you for helping me with some occasional problems in the laboratory. **Richard**, we were neighbors in the laboratory, thank you for all the wonderful conversations when either you or me stopped by each other's fume hood. **Peter S**, thank you for asking about my research at the parties. Also thanks to **Sipeng**, **Stefan** and **Adri** for the presence at the earlier stage of my PhD. **Marco** and **Valeria**, we had some nice discussions on our similar research fields during your stays in Utrecht, thank you for your constructive suggestions. **Federica**, it was my pleasure to chat with you on the UV-Vis measurements. **Massi**, thank you for being willing to learn some Mandarin and the kind conversations on our projects.

To current OCC members: **Peter J**, we started and finished with our PhDs nearly at the same time, although you were not in OCC group that often in the second half of your PhD. Thank you for sharing your "adventures" in China, for chatting with me with your "spectacular" Chinese and for the "delicious" hotpot in your basement. **Alessio**, my paranymph, my always-roommate at the conferences. We have the closest phases in our PhDs in the group who do catalysis, and have the closest desks in the office area as well. You are such a cool guy who can start up a funny chat at any moment. Massive thanks to you for all the conversations we had about our projects and writing issues, for your "disappearance" to allow me to "practice" my presentation in the hotel room, for being a such good friend. I wish you the best for the rest of your PhD and hope you can defend your thesis at your age of "25". **Emily**, thank you for always being willing to organize the group events; for your help in many occasions both in the lab and office; for recommending me Tripel Karmeliet, which is my favorite Belgian beer so far! **Eduard**, we are neighbors in the office area and are both doing oxidation catalysis. Thank you for sharing your experimental results and your ideas with me, for all the nice conversations about our projects, and for giving your likes to my photos in Instagram. **Jing**, you are one of my paranymphs and the one I can always speak Mandarin to in the group. Thank you for sharing your thoughts, your happiness and your concerns in many aspects with me. I wish you all the best for your PhD! **Jacco**, thank you for your kindness and for writing the Dutch summary of this thesis. **Charl**, you are a very nice guy! Thanks to you for the help on the EPR measurements.

Pablo, you showed us the drunk and the other "Pablo" in your first weeks in Utrecht, amazing! **Serhii**, thank you for the interesting stuff you sent to the WhatsApp groups. **Martine**, thank you for keeping reminding people to bring the cookies on Thursdays, which is incredibly important! **Sander**, your birthday party at your place was awesome! **Maria**, thank you for those very funny Mexican references. **Pamela** and **Fanshi**, I hope you will have an enjoyable time in the group and I wish you all the good luck with your projects.

Many thanks to the bachelor and master students in the group: **Cody** (the upcoming OCC PhD!), **D-J**, **Raoul**, **Roel**, **Daniel**, **Bram**, **Errikos**, **Yoni**, **Arthur**, **Elena**, **Sam**, **Hidde**, **Stella**, **Maxime**, **Richt**, **Bart**, **Annet**, **Yuri**, **Jelle**, **Camille** and **Nora**, for those beautiful memories at the coffee corner, camping trips, group outings, Christmas dinners and many other group events!

I was lucky to meet many people outside the group, whom I have the fortunate to live with, to get a lot of help from, and to build some beautiful friendships with. **Gerard** and **Nelleke**, thank you for offering me a home in the Netherlands, which is located at one of the most gorgeous spots in Utrecht! I will never forget the stunning view outside my window. My housemates, **Jinbao** and **Lin**, thank you for your companion in the house and those get-together dinners. **Gao Shan**, **Haozi**, **Li Yan**, **Ahua** and **Tangtang**, we had travelled to many places together, and had many wonderful parties and beautiful memories, thank you all for that! Also thanks to my Chinese friends in Utrecht: **Xin Y**, **Jie S**, **Hao Z**, **Wenjing**, **Minglong**, **Lifeng**, **Yanyan**, **Dushen**, **Donglong**, **Xianke**, **Guangyun**, **Lemeng**, **Xuan W**, **Yanna**, **Haili**, **Fang L**, **Yulong**, **Shuqiong**, **Jie Z**, **Jie H**, **Na C**, **Yuxi** and **Jie G**, for your companion at the lunches and for those memorable get-together parties. Special thanks to **Sara C**, for your support and encouragement throughout.

Last but not least, I would like to give my immense thanks to my family. 最后，我要把我最衷心的感谢献给我的家人，我的爷爷、爸爸、妈妈、大姐、二姐以及哥哥。爸、妈，是你们含辛茹苦的养育、自始至终的支持与非比寻常的理解，才有了我的今天。孩儿不孝，快到而立之年却还没能够尽到为人子的义务。这篇博士毕业论文，是我远渡重洋四年留学生涯的总结，也是献给你们的一份礼物。有你们作为我的家人，是我这辈子的幸运。

About the Author

The author of this thesis was born on June 18, 1989, in Longyan City, Fujian Province, China. He was raised up, and received primary and secondary education in the same city. After graduating from high school in 2007, he started to study chemistry at Jilin University in the same year, major in material chemistry. He obtained his Bachelor's degree in 2011, after which he continued with his Master's program in organic chemistry at the same university, under the supervision of prof. dr. W. Liao. After finishing his Master's thesis on Metal-Free Synthesis of Allylic α-Aminonitrile and Intramolecular Carbocyanation of Alkenes, he obtained his MSc (honors, *cum laude*) in 2014. From October in that same year, he moved to the Netherlands and started as a PhD student in the Organic Chemistry and Catalysis group at Utrecht University, under the supervision of prof. dr. R. J. M. Klein Gebbink and dr. M. Otte. The project was financially supported by the China Scholarship Council (CSC) Scholarship and the most important results of this project are presented in this thesis. Parts of this thesis have been presented at national and international conferences including the Netherlands' Catalysis and Chemistry Conferences (NCCC), the Dutch Chemistry Conferences (CHAINS), the 17th International Symposium on Relations between Homogeneous and Heterogeneous Catalysis (ISHHC-17, Utrecht, The Netherlands), the 42nd International Conference on Coordination Chemistry (ICCC-42, Brest, France), the 9th Workshop on Fats and Oils as Renewable Feedstock for the Chemical Industry (Karlsruhe, Germany), the 22nd EuCheMS International Organometallic Conference (EuCOMC-22, Amsterdam, The Netherlands) and the 21st International Symposium on Homogeneous Catalysis (ISHC-21, Amsterdam, The Netherlands).

List of Publications

Regioselective Cleavage of Electron-Rich Double Bonds in Dienes to Carbonyl Compounds with [Fe(OTf)$_2$(mix-BPBP)] and a Combination of H_2O_2 and $NaIO_4$.
P. Spannring, V. A. Yazerski, **J. Chen**, M. Otte, B. M. Weckhuysen, P. C. A. Bruijnincx, and R. J. M. Klein Gebbink. *Eur. J. Inorg. Chem.*, **2015**, 3462.

Non-Heme Iron Catalysts with a Rigid Bis-isoindoline Backbone and Their Use in Selective Aliphatic C−H Oxidation.
J. Chen, M. Lutz, M. Milan, M. Costas, M. Otte, and R. J. M. Klein Gebbink. *Adv. Synth. Catal.*, **2017**, *359*, 2590. (Chapter 2)

Non-Heme Iron Oxidation Chemistry and Biochemistry. (Book chapter in *Iron Complexes in Catalysis - from Coordination and Spectroscopy to Applications.* ed. B. Plietker, Wiley-VCH).
J. Chen, M. Otte, and R. J. M. Klein Gebbink, in publication. (Chapter 1)

Deuterated N2Py2 Ligands: Building More Robust Non-Heme Iron Oxidation Catalysts.
J. Chen, and R. J. M. Klein Gebbink. *ACS. Catal.* revision in progress. (Chapter 4)

Highly Efficient Epoxidation of Vegetable Oils Catalyzed by a Manganese Complex with Hydrogen Peroxide and Acetic Acid.
J. Chen, M. de Liedekerke Beaufort, L. Gyurik, J. Dorresteijn, M. Otte and R. J. M. Klein Gebbink, to be submitted. (Chapter 5)

Epoxidation of Methyl Linoleate Catalyzed by Non-Heme Iron Complexes with Hydrogen Peroxide as the Oxidant.
J. Chen, M. Otte and R. J. M. Klein Gebbink, to be submitted. (Chapter 3)

Previous publications:

Metal-Free Intramolecular Carbocyanation of Alkenes: Catalytic Stereoselective Construction of Pyrrolo[2,1-*a*]isoquinolines with Multiple Substituents.
J. Chen, Q. Xu, and W. Liao, *Chem. Eur. J.*, **2014**, *20*, 13876.

Metal-Free Intramolecular Carbocyanation of Activated Alkenes: Functionalized Nitriles Bearing β-Quaternary Carbon Centers
J. Chen, G. Zou, and W. Liao, *Angew. Chem. Int. Ed.*, **2013***, 52*, 9296. (Hot Paper)

A Novel Multicomponent Tandem Phosphine-Catalyzed Umpolung Reaction: Facile Access to Highly Functionalized α- Aminonitriles.
J.-M. Chen, Y.-Z. Fang, Z.-L. Wei, and W.-W. Liao, *Synthesis*, **2012**, *44*, 1849. (An invited contribution to the special issue on tandem reaction)

Controllable Regioselective Construction of Both Functional α-Methylene-β- and -γ-amino Acid Derivatives Through an Organocatalyzed Tandem Allylic Alkylation and Amination.
F. Pan, **J.-M. Chen**, T.-Y. Qin, Sean X.-A. Zhang, and W.-W. Liao, *Eur. J. Org. Chem.,* **2012**, 5324.

Lewis Base Promoted Intramolecular Acylcyanation of α-Substituted Activated Alkenes: Construction of Ketones Bearing β-Quaternary Carbon Centers.
Z. Zhuang, **J.-M. Chen**, F. Pan, and W.-W. Liao, *Org. Lett.*, **2012**, *14*, 2354.

Construction of Highly Functional α-Amino Nitriles *via* a Novel Multicomponent Tandem Organocatalytic Reaction: a Facile Access to α-Methylene γ-Lactams.
F. Pan, **J.-M. Chen**, Z. Zhuang, Y.-Z. Fang, Sean X.-A. Zhang and W.-W. Liao, *Org. Biomol. Chem.*, **2012,** *10*, 2214.

Construction of Highly Functional Quaternary Carbon Stereocenters *via* an Organocatalytic Tandem Cyanation-Allylic Alkylation Reaction.
Z. Zhuang, F. Pan, J.-G. Fu, **J.-M. Chen**, and W.-W. Liao, *Org. Lett.*, **2011**, *13*, 6164.